



UNIVERSITAT DE
BARCELONA

Exposure characterisation and sources of nanoparticles in workplace environments

Ana Sofia Godinho da Fonseca

ADVERTIMENT. La consulta d'aquesta tesi queda condicionada a l'acceptació de les següents condicions d'ús: La difusió d'aquesta tesi per mitjà del servei TDX (www.tdx.cat) i a través del Dipòsit Digital de la UB (diposit.ub.edu) ha estat autoritzada pels titulars dels drets de propietat intel·lectual únicament per a usos privats emmarcats en activitats d'investigació i docència. No s'autoritza la seva reproducció amb finalitats de lucre ni la seva difusió i posada a disposició des d'un lloc aliè al servei TDX ni al Dipòsit Digital de la UB. No s'autoritza la presentació del seu contingut en una finestra o marc aliè a TDX o al Dipòsit Digital de la UB (framing). Aquesta reserva de drets afecta tant al resum de presentació de la tesi com als seus continguts. En la utilització o cita de parts de la tesi és obligat indicar el nom de la persona autora.

ADVERTENCIA. La consulta de esta tesis queda condicionada a la aceptación de las siguientes condiciones de uso: La difusión de esta tesis por medio del servicio TDR (www.tdx.cat) y a través del Repositorio Digital de la UB (diposit.ub.edu) ha sido autorizada por los titulares de los derechos de propiedad intelectual únicamente para usos privados enmarcados en actividades de investigación y docencia. No se autoriza su reproducción con finalidades de lucro ni su difusión y puesta a disposición desde un sitio ajeno al servicio TDR o al Repositorio Digital de la UB. No se autoriza la presentación de su contenido en una ventana o marco ajeno a TDR o al Repositorio Digital de la UB (framing). Esta reserva de derechos afecta tanto al resumen de presentación de la tesis como a sus contenidos. En la utilización o cita de partes de la tesis es obligado indicar el nombre de la persona autora.

WARNING. On having consulted this thesis you're accepting the following use conditions: Spreading this thesis by the TDX (www.tdx.cat) service and by the UB Digital Repository (diposit.ub.edu) has been authorized by the titular of the intellectual property rights only for private uses placed in investigation and teaching activities. Reproduction with lucrative aims is not authorized nor its spreading and availability from a site foreign to the TDX service or to the UB Digital Repository. Introducing its content in a window or frame foreign to the TDX service or to the UB Digital Repository is not authorized (framing). Those rights affect to the presentation summary of the thesis as well as to its contents. In the using or citation of parts of the thesis it's obliged to indicate the name of the author.



Programa de Doctorat “*Química Analítica i Medi Ambient*”

EXPOSURE CHARACTERISATION AND SOURCES OF NANOPARTICLES IN WORKPLACE ENVIRONMENTS

Ana Sofia Godinho da Fonseca

PhD Thesis

Barcelona, April 2016

Supervisors:

Dr. María del Mar Viana Rodríguez
(IDÆA-CSIC)

Dr. Xavier Querol Carceller
(IDÆA-CSIC)

Tutor:

Dr. María Teresa Galceran Huguet
(Barcelona University, Faculty of Chemistry)



*To everyone who has been there to support my
journey towards the finished thesis.*

“Science never solves a problem without creating ten more.”

George Bernard Shaw (1856-1950), Irish playwright

SUMMARY

Exposure to micro- and nano-scaled particles has been widely linked to adverse health effects including pulmonary, cardiovascular and nervous system disease leading to increased mortality and morbidity rates. In urban environments, outdoor air quality is impacted by atmospheric aerosols which originate mostly from anthropogenic sources, mainly traffic and other combustion-related sources. With regard to population exposure, indoor microenvironments constitute a particularly vulnerable source given that adults spend on average 60 - 80% of their time indoors, and approximately 50% of it in the workplace. However, due to the multiplicity of microenvironments and the complexity and heterogeneity of indoor sources, indoor air quality has been in comparison less studied than outdoor air. Specifically for workplaces, the European and American agencies for occupational health and safety consider nanoparticles as one of the major current emerging risks in workplace microenvironments.

The fast development and spread of innovative technologies and processes used in many industrial sectors (with and without relation to nanotechnology) have benefited from advances but new risks and uncertainties related to possible exposure to unknown nanoparticle types and concentrations may arise. In the workplace, workers may be exposed to nanoscale particles while dealing with engineered nanoparticles (ENP) or process-generated nanoparticles (PGNP) during specific industrial processes involving unintentional nanoparticle release or the formation of nanoparticles from gaseous precursors. Due to the relative novelty of "*nanosafety*" as a field of research, relevant studies about ENP and PGNP release and exposure under real-world conditions are relatively scarce. Furthermore, adequate analytical techniques and monitoring instrumentation have only recently become available. To date, specific online instrumentation for the targeted detection of nanoparticles in real-time is lacking.

The goals of this PhD thesis were to (i) assess the performance of novel instrumentation for nanoscale aerosol measurements, and (ii) to carry out exposure assessments to nanoparticles emitted in workplaces under real-world operating conditions, focusing on ENP and PGNP. The scenarios selected for exposure characterisation were single-walled carbon nanotubes (SWCNT) manufacturing and application processes (ENP), and tile ablation and sintering with laser technologies used in the ceramic industry (PGNP). In addition to emissions and potential particle

transformations in workplace air, the potential for particle release to the outdoor environment, and the effectiveness of control measures were assessed in both types of exposure scenarios. A multi-instrument approach was used to characterise source-specific worker exposure, aiming to cover the most relevant nanoparticle metrics and physicochemical properties. The results obtained are presented in the form of five research articles.

Two of the research articles deal with the evaluation of the performance of specific nanoparticle instrumentation: a portable scanning mobility particle sizer (NanoScan SMPS; Article IV), and cascade impactors for nanoparticle sampling (Article V). Results regarding the assessment of the NanoScan SMPS in terms of its application in workplace exposure studies revealed that mobility particle sizers using unipolar and bipolar charging may be affected differently by particle size, morphologies, particle composition and concentration. While the sizing accuracy of the NanoScan SMPS was mostly within $\pm 25\%$, results evidence that it may miscount total particle number concentration by more than 50% (especially for agglomerated particles). Thus, whereas the use of this instrument may be recommended for Tier 1 and Tier 2 exposure assessment studies, for Tier 3 conventional and stationary SMPS instruments would be the preferred choice. The NanoScan SMPS was seen to be a useful instrument to obtain estimates of the aerosol size distribution in indoor and workplace air, and also for outdoor air. With regard to the assessment of the performance of cascade impactors for nanoparticle sampling and analysis, results revealed that particle volatilisation and particle bounce play a major role in the collection efficiency and in the aerosol size distribution of each impactor. Attention should be paid to volatilisation issues during aerosol transport inside the impactors especially with regard to temperature increases associated with internal rotating mechanisms in some impactors.

Based on the instrumental limitations encountered during the course of this PhD thesis, it was concluded that only through the combination of diverse monitoring techniques and parameters does it become possible to obtain a detailed characterisation of nanoparticle exposure routes and scenarios.

The remaining three research articles in this thesis describe nanoparticle exposure scenarios in industrial settings, one of them dealing with ENP (Article I) and two with PGNP (Articles II and III). In the study where workers' quantitative exposure to ENP (SWCNT while manufacturing conductive thin films, Article I), results evidenced non-significant nanoparticle exposure concentrations ($SWCNT < Background + 3 \cdot \sigma_{background}$ in terms of particle number and mass concentration) during all of the activities

assessed where SWCNT may have been potentially released. However, these exposures may have been underestimated given that results suggested that online instruments did not seem able to accurately detect SWCNT, probably due to the irregular shapes and high aspect ratios (length/width > 500) of these nanofibers. The analysis of transmission electron microscopy (TEM) images was the only direct method to confirm the presence of SWCNT in workplace air. Despite this, counting of SWCNT with TEM micrographs was challenging due to their high aspect ratio and branching. The highest SWCNT counts (ranging from 1.7×10^{-3} - $5.6 \text{ SWCNT cm}^{-3}$) and exceedance of the available occupational exposure limits were seen during the worst case scenario corresponding to a failure of the local exhaust ventilation (LEV) system corresponding to the reactor. The correct application of LEV to the collection chambers in the SWCNT manufacturing facility was found to reduce CO and SWCNT emissions by approximately 95% and 98%, respectively. The main recommendation extracted was that the operation of the LEV should be systematically verified. To overcome the problem of fibres counting and discrimination from background concentrations, the development of new methods to detect and quantify nanofibers in real-time would be strongly advisable.

In Articles II and III, dealing with PGNP, major nanoparticle exposures ($>1.0 \times 10^5 \text{ cm}^{-3}$) were identified in the worker breathing zone during high-energy laser processes such as tile sintering and ablation, which were in addition statistically significant ($>\text{Background}+3.\sigma_{\text{background}}$). Tile sintering generated statistically significant exposure concentrations in terms of particle number (up to $5.5 \times 10^5 \text{ cm}^{-3}$) and with significantly low particle diameters ($< 24 \text{ nm}$), which were markedly smaller than background air particles (34 nm as particle average diameter) originating from the infiltration of vehicular traffic diesel emissions (Articles II and III). The high particle number concentrations with lower particle sizes detected during the thermal treatment of ceramic tiles suggested the occurrence of new particle formation mechanisms by nucleation (nanoparticles $\leq 30 \text{ nm}$ in diameter being formed), which were probably induced by the cooling down of exhaust gases containing SO_2 emitted from the thermal decomposition of S-bearing minerals present in the ceramic tiles. Finally, during the tile ablation experiments (Article II), worker exposure was assessed using particle mass concentration (as opposed to particle number concentration) as a more effective due to the coarser diameter of the particles emitted. Laser engraving induces phase transitions, causing catastrophic break down of the original material which results in coarser particles (80 nm). Because the toxicity of PGNP is not necessarily different from the assumed toxicity of ENP, the comparison of particle exposure concentrations with the available nano reference values (NRV) was

deemed to be advisable. Since workers were exposed to concentrations above the nano-reference values (NRV; $4 \times 10^4 \text{ cm}^{-3}$) during the industrial processes under study, there was clear evidence of health risk of occupational exposure to nanoparticles. In terms of mass, current regulations set a 3 mg m^{-3} threshold limit value (TLV; ACGIH, 2013) for the total respirable fraction which would not have been exceeded during any process condition. Based on the statistically significant exposures registered in the worker breathing zone during the thermal treatment of ceramic tiles and the clear exceedance of the NRV, industrial control measures should be proposed and tested specifically for this environment, tailored to its needs. The effectiveness of the mitigation measures in place in the environments assessed during this PhD thesis were tested and results showed that the use of appropriate strategies may reduce worker exposure to nanoparticles (ENP and PGNP) by up to 98%.

Overall, this PhD thesis provides recommendations regarding the use and applicability of specific nanoparticle monitoring and sampling instrumentation, and characterises real-world exposure scenarios affected by unintentional release of ENP and PGNP. Further research on both of these topics is advisable in order to better understand the processes and mechanisms determining occupational exposure to nanoparticles in workplace environments.

ACKNOWLEDGEMENTS

I am aware that this PhD thesis is a result of the many experiences I have encountered during the last three years with countless and outstanding people that I had honour to meet who taught and helped me every step. There is not enough space, nor time, to acknowledge everyone to the extent they deserve. I hope people understand the brevity of this part.

Firstly, I would like to express my sincere gratitude to my supervisors Dr. Mar Viana and Dr. Xavier Querol from Institute of Environmental Assessment and Water Research (IDÆA-CSIC) to make my PhD experience productive and stimulating. I really appreciate their continuous support, patience, and their shared immense knowledge. Their joy and enthusiasm for research was contagious and an incentive for me to widen my research from various perspectives. With sincerity, thank you! I would like to thank also my tutor Dr. Maria Teresa Galceran Huguet from Barcelona University (Faculty of Chemistry), for her kind support, advice and interest in my research work.

I want to express my gratitude to all my co-authors, for their contributions to the articles comprised in this thesis.

This thesis is also a result of fruitful collaborations which I would like to thank each one individually. To the people from the University of Helsinki and the Finnish Institute of Occupational Health (FIOH), thank you for the great four-months period that I spent there, especially to Dr. Joonas Koivisto, Dr. Anna-Kaisa Viitanen and Professor Kaarle Hämeri. I learned a lot from you and I really appreciated your guidance and selfless help.

I express also my gratitude to Instituto de Ciencia de Materiales de Aragón (ICMA - Universidad de Zaragoza) for providing the facilities (both laboratory and pilot-plant scale) for the intensive campaigns aiming to study the nanoparticle emissions released during ceramic industrial activities. I praise the enormous amount of help, support and the enlightened discussions with Professor Germán de la Fuente, Dr. Isabel de Francisco, Dr. Vassili Lennikov, Mr. Carlos Estepa and Mr. Carlos Borrell. During the experiments done in the pilot-plant scale furnace, I especially recognize the significant contributions from the PhD student Androniki Maragkidou (belonged to the HEXACOMM project). It would not have been possible without her intensive dedication during the sampling campaign and time spent in the lab afterwards. I

sincerely thank you for all the chemical digestions of the filter samples and for providing such nice collaborating in its processing and data interpretation. Besides all this, I thank you for your true friendship, and for all the fun we have had in the last three years that I will never forget.

It was given to me the chance to participate in an intensive intercomparison study of cascade impactors in collaboration with Institute of Chemical Process Fundamentals of the ASCR, v.v.i. (ICPF) and University of Birmingham. To all the people from ICPF I very much appreciated your hospitality during my one-month period of stay in Prague. Especial thanks go to Nick Talbot, Tuan Vu and Jana Kozáková. Without your valuable collaboration in data acquisition, processing and its interpretation, this work would not have been possible. For the helpful and inspirational discussions regarding the results I especially thank the following people: Dr. Vladimír Ždímal, Dr. Jaroslav Schwarz, Dr. Jakub Ondráček and Professor Roy Harrison.

I express also my gratitude to Coordinator of the nanoIndEx project, Dr. Christof Asbach, for have given me the opportunity to participate in an intercomparison study of a portable and two stationary SMPS at the NanoTest-Center of the Institute for the Research on Hazardous Substances (IGF) in Dortmund, Germany. It was a pleasure to cooperate with all of your team and I wish to thank especially you and Dr. Ana Maria Todea for your precious support.

My experience at IDÆA-CSIC has been nothing short of amazing. Since my first day on 1st March 2013 I have felt at home, for which I am eternally grateful. I really have enjoyed the possibility to work in our Institute with such an incredible colleagues which are listed below (random order): Viana, M., Querol, X., Alastuey, A., Karanasiou, A., Moreno, T., Pérez, N., Amato, F., Minguillón, M. C., Pandolfi, M., Moreno, N., Font, O., Tobias, A., Reche, C., Ealo, M., Martins, V., Silva, C., Cabañas, M., Bartrolí, R., Martínez, S., Vázquez, R., Castro, I., Muñoz, C., Sosa, G., Vasconcelos, C., Parga, J., Gil, J., and anyone that I may have forgotten). All of you have been a source of friendships as well as valuable advices and collaborations that I will be grateful forever. In particular, I would like to thank Andrés Alastuey, and Angeliki Karanasiou for their professional and personal support. Thank you for being always available for my queries.

A special acknowledgement goes also to my office mate: Noemí Pérez. Thank you for your willingness to help me since we began to share the office in 2013. Thank you for being such an amazing person, always with a smile put on the face. I will remember you every time I will eat "*Palmolitas*". To my ex office mate: Mariola Brines, thank you for cheer me up in all my hardship moments. My Spanish would be

catastrophic without yours and Noemi's lessons. And I also thank Roy, my other great office mate for the nice chats and for have spoiled us with gifts every time he traveled around the world.

To my colleague and friend Garay Sosa who is always spreading good vibes and always ready to help me and give me an advice whenever I need, thank you very much for everything. To Cristina Vasconcelos, thank you for your outpourings of support during all these three years. I am thankful to all my colleagues from HEXACOMM project with whom I was able to exchange scientific knowledge as well as enjoy joyful moments.

To all my friends, both from Portugal and the new ones that I had a pleasure to meet along this journey from many places around Europe, thank you for being part of my life and have shared experiences with me which have contributed to shape the person I am today. A very special thanks goes out to my Professor and friend Dr. Isabel Nunes, who was though her that I completed my MSc. degree and I was encouraged to apply for this PhD. I doubt that I will ever be able to convey my fully appreciation, but I owe her my eternal gratitude.

A special thanks goes to all my family for all their love, encouragement and belief in me. In particular, I must acknowledge my parents who raised me and supported me unconditionally in all my pursuits through my entire life. To my sister Luísa Fonseca, I would like to express my thanks for have helped and supported me when I needed it the most. I love you and I thank you for everything.

Lastly, for my loving, and patient boyfriend Emil Sierda who was always my support during the final stages of this PhD and a motivation to strive towards my goal. Thank you, you are the best!!

Ana Sofia Fonseca

University of Barcelona/Spanish Research Council

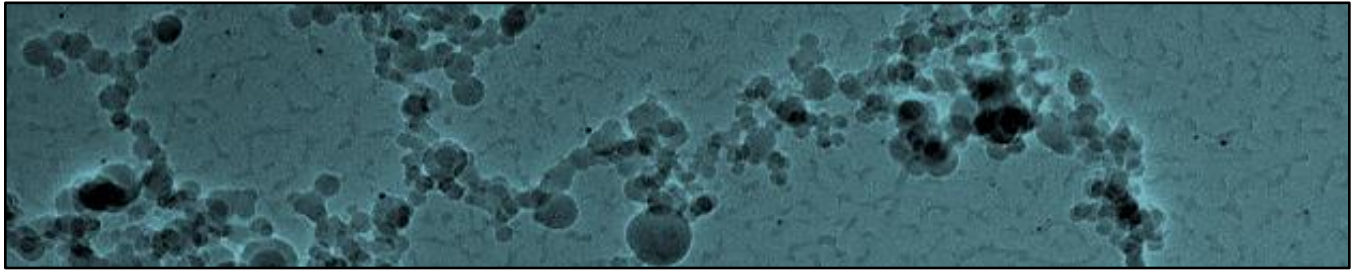
April 2016

CONTENTS

	Page
SUMMARY	vii
ACKNOWLEDGEMENTS	xi
CONTENTS	xv
1. INTRODUCTION	1
1.1 <i>Nanoparticles in occupational settings</i>	4
1.1.1 Particle formation and/or transformation processes.....	4
1.1.2 Sources of nanoparticles.....	5
1.1.3 Nano-related workplaces: from release to exposure.....	8
1.1.4 Evidences of workers exposure to nanoparticles.....	9
1.1.5 Potential health and environmental concerns.....	11
1.2 <i>Exposure assessment and characterisation</i>	14
1.2.1 Exposure metrics.....	15
1.2.2 Measurement instrumentation.....	16
1.2.3 Exposure assessment strategies.....	19
1.2.4 Control measures to mitigate occupational exposure.....	24
1.3 <i>Regulatory background</i>	25
2. SCOPE, OBJECTIVES AND STRUCTURE	31
2.1 <i>Scope and Objectives</i>	31
2.2 <i>Structure of the thesis</i>	32
3. METHODOLOGY	37
3.1 <i>Monitoring sites and exposure scenarios</i>	37
3.1.1 SWCNT manufacturing.....	37
3.1.2 Ceramic tile sintering and ablation.....	38
3.2 <i>Measurement instrumentation and techniques</i>	39
3.2.1 Nanoparticle monitoring.....	40
3.2.2 Nanoparticle collection on filter substrates.....	44
3.2.3 Chemical characterisation of collected particles.....	45
3.2.4 Electron microscopy.....	46
3.2.5 Instrumental and technical limitations.....	46
3.3 <i>Instrument intercomparisons</i>	47
3.4 <i>Measurement strategy</i>	49
3.4.1 Personal task-based vs. full shift exposure assessment.....	49
3.4.2 Multi-instrument approach.....	50

3.4.3	Sampling locations	50
3.4.4	Background distinction.....	50
3.4.5	Worker exposure concentrations	51
4.	RESULTS	55
4.1	<i>Article I: Characterisation of exposure to carbon nanotubes in an industrial setting..</i>	<i>57</i>
4.2	<i>Article II: Ultrafine and nanoparticle formation and emission mechanisms during laser processing of ceramic materials</i>	<i>75</i>
4.3	<i>Article III: Process-generated nanoparticles from ceramic tile sintering: emissions, exposure and environmental release</i>	<i>93</i>
4.4	<i>Article IV: Intercomparison of a portable and two stationary mobility particle sizers for nanoscale aerosol measurements</i>	<i>111</i>
4.5	<i>Article V: Intercomparison of four different cascade impactors for fine and ultrafine particle sampling in indoor and outdoor air</i>	<i>147</i>
5.	DISCUSSION	179
5.1	<i>Performance of nanoparticle monitoring and sampling instrumentation</i>	<i>180</i>
5.1.1	Intercomparison studies.....	180
5.1.2	Instrumental limitations during field measurements	183
5.2	<i>Nanoparticle exposure scenarios.....</i>	<i>186</i>
5.2.1	Exposure to particles in the worker breathing zone.....	187
5.2.2	Comparison of worker exposure concentrations with exposure limits ..	192
5.3	<i>Mitigation strategies.....</i>	<i>194</i>
6.	CONCLUSIONS	199
7.	LIMITATIONS AND FUTURE RESEARCH NEEDS	205
	FUNDING SOURCES	209
	REFERENCES.....	211
	ANNEX A: LIST OF ABBREVIATIONS, ACRONYMS AND SYMBOLS	235

Chapter 1. INTRODUCTION



1. INTRODUCTION

Atmospheric pollution is recognised as a major contributor to the global burden of disease (Lim *et al.*, 2012). Both gaseous and particulate pollutants are emitted to the atmosphere from natural and anthropogenic sources (Bozlaker *et al.*, 2013; Gieré and Querol, 2010; Wagstrom and Pandis, 2011), the latter been growing since the Industrial Revolution in the 18th century, especially from internal combustion engines, power plants, and other industrial sources (Karagulian *et al.*, 2015; Streets *et al.*, 2011). Atmospheric particulate matter (PM) is commonly referred as aerosol which is found suspended in the atmosphere in liquid and/or solid phase ranging from few nanometers (nm) to tenth of micrometers (μm) in size diameter (Mészáros, 1999). In the field of aerosol science, particles with an aerodynamic diameter ≤ 100 nm are usually referred to as ultrafine particles, and those ≤ 50 nm, as nanoparticles (Hirano, 2009). Conversely, in the nanotechnology field, particles with at least one dimension ≤ 100 nm are referred to as nanoparticles (COM, 2011; ISO, 2015). For the sake of clarity, in the framework of this PhD thesis, the terminology of the nanotechnology field will be followed.

Nanoparticles may be classified in two types:

- **Engineered nanoparticles (ENP):** Nanoparticles intentionally manufactured with specific physical and chemical properties and having at least one, and usually two dimensions ≤ 100 nm (COM, 2011; ISO, 2015).
- **Non-engineered nanoparticles (N-ENP):**
 - (i) *Process-generated nanoparticles (PGNP):* Nanoparticles generated from industrial sources and processes with or without relation to nanotechnology.
 - (ii) *Background nanoparticles:* Nanoparticles that may have a natural and anthropogenic origin and are emitted to the atmosphere directly or newly formed into the atmosphere as a result of atmospheric processes and mechanisms.

In the International System of Units (SI), the prefix "*nano*" is one-billionth of a meter (10^{-9} m) or about the width of an atom. To further illustrate differences in size, a strand of human antibody has a diameter of 10 nm, a cancer cell has a diameter of 10^4 nm, and a human hair is of the order of 7.5×10^4 to 10^5 nm wide (Figure 1.1).

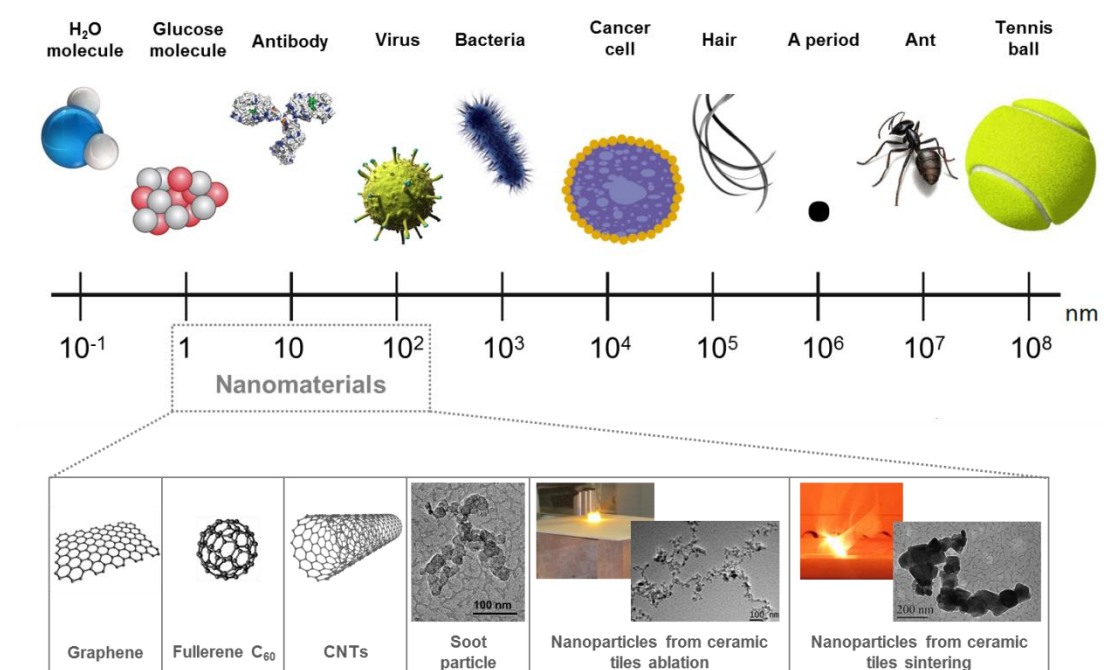


Figure 1.1 Comparative scheme of the objects size in a nanometer scale. Source: modified from Savolainen *et al.* (2013).

The direct link between exposure to particles and adverse health outcomes has been widely proven in the literature (Atkinson *et al.*, 2015; Lelieveld *et al.*, 2015; Lim *et al.*, 2012). Several studies have highlighted that particles of low solubility with aerodynamic diameters <100 nm, are the fractions with higher potential for adverse health effects (Donaldson *et al.*, 2001; Nel, 2005; Oberdörster, 2001; Oberdörster *et al.*, 2005; Oberdörster *et al.*, 2002; Peters *et al.*, 1997a; Politis *et al.*, 2008; Seaton *et al.*, 1995). This is because of their ability to penetrate deeper into the respiratory tract in human lungs, and to translocate to the blood circulatory system and arrive to other organs via a variety of pathways and mechanisms (Geiser and Kreyling, 2010; Oberdörster, 2010; Oberdörster *et al.*, 2005) or even be transported directly to the brain through the olfactory epithelium (Oberdorster *et al.*, 2004).

Within urban environments, where the largest fraction of the population in Europe is exposed to atmospheric pollutants regulations have been developed by the European Commission (Directives 2004/107/EC and 2008/50/EC) which establish limit and target values for a number of ambient air pollutants (EC, 2004, 2008). As a result, air contaminants are monitored at central outdoor locations in air quality monitoring networks (see AirBase; the European air quality database by the European Environment Agency - EEA; www.eea.europa.eu). However, in modern societies, population exposure mainly takes place in indoor environments, where adults spend on average 60-80% of their time and approximately 50% of it at the workplace (Klepeis *et al.*, 2001). Consequently, indoor occupational exposure

constitutes a significant fraction of total exposure to atmospheric pollutants. However, indoor air quality has been in comparison less studied than outdoor air (Weschler, 2011). This can be attributed to the multiplicity of microenvironments (industrial facilities, office spaces, homes, schools, restaurants, among others) and the complexity and heterogeneity of indoor sources (Viana *et al.*, 2011). Contrary to outdoor air quality, for which limit values are stringent and subject to being revised and reduced, regulations and guidance for workplace air are scarce. The only limits available are those established by the American Conference of Governmental Industrial Hygienists (ACGIH, 2013) and the Occupational Safety and Health Administration (OSHA, 2006). These institutions set a permissible exposure limit (PEL) for 8-hour time weighted average concentrations (8-h TWA) of 5 mg m^{-3} (OSHA, 2006) and of 3 mg m^{-3} threshold limit value (TLV) for respirable particles (PM_{10}) (ACGIH, 2013), which are easily attained. With regard to nanoparticles in industrial workplaces, regulations are even scarce (see regulatory background in section 1.3).

Numerous studies evaluate nanoparticle concentrations in different types of indoor microenvironments: (i) residential environments (Bhangar *et al.*, 2011; Bordado *et al.*, 2012; Géhin *et al.*, 2008; Hussein *et al.*, 2005; Isaxon *et al.*, 2015; Kearney *et al.*, 2011); (ii) offices (He *et al.*, 2007; Koivisto *et al.*, 2010; Koponen *et al.*, 2001; McGarry *et al.*, 2011); (iii) restaurants (Buonanno *et al.*, 2010); (iv) schools (Almeida *et al.*, 2011; Braniš and Šafránek, 2011; Buonanno *et al.*, 2013a; Dorizas *et al.*, 2015; Fromme *et al.*, 2007; Reche *et al.*, 2014; Rivas *et al.*, 2015; Rivas *et al.*, 2014; Viana *et al.*, 2014); (v) nanotechnology-related industries (Brouwer, 2010; Dahm *et al.*, 2013; Fonseca *et al.*, 2015c; Gomez *et al.*, 2014b; Jensen *et al.*, 2015; Kaminski *et al.*, 2015; Kim *et al.*, 2014; Koivisto *et al.*, 2012; Koponen *et al.*, 2015; Tsai *et al.*, 2011; van Broekhuizen *et al.*, 2011, 2012a; Vaquero *et al.*, 2015); and, (vi) non-nanotechnology related industries (Azarmi *et al.*, 2014; Buonanno *et al.*, 2011; Fonseca *et al.*, 2016; Fonseca *et al.*, 2015a; Gomes *et al.*, 2012; Kumar *et al.*, 2012; Voliotis *et al.*, 2014).

The variety of processes and the diversity of pollutant sources that can be found in indoor microenvironments render the topic of indoor exposure very complex and highlight the need for further research. The focus of this PhD thesis is on occupational microenvironments, specifically, on industrial settings.

1.1 Nanoparticles in occupational settings

1.1.1 Particle formation and/or transformation processes

Once emitted, nanoparticle behaviour in indoor and outdoor air is affected by formation and/or transformation processes such as diffusion, dilution, coagulation, condensation and deposition, which influence the mass, the number and the size distribution (Figure 1.2).

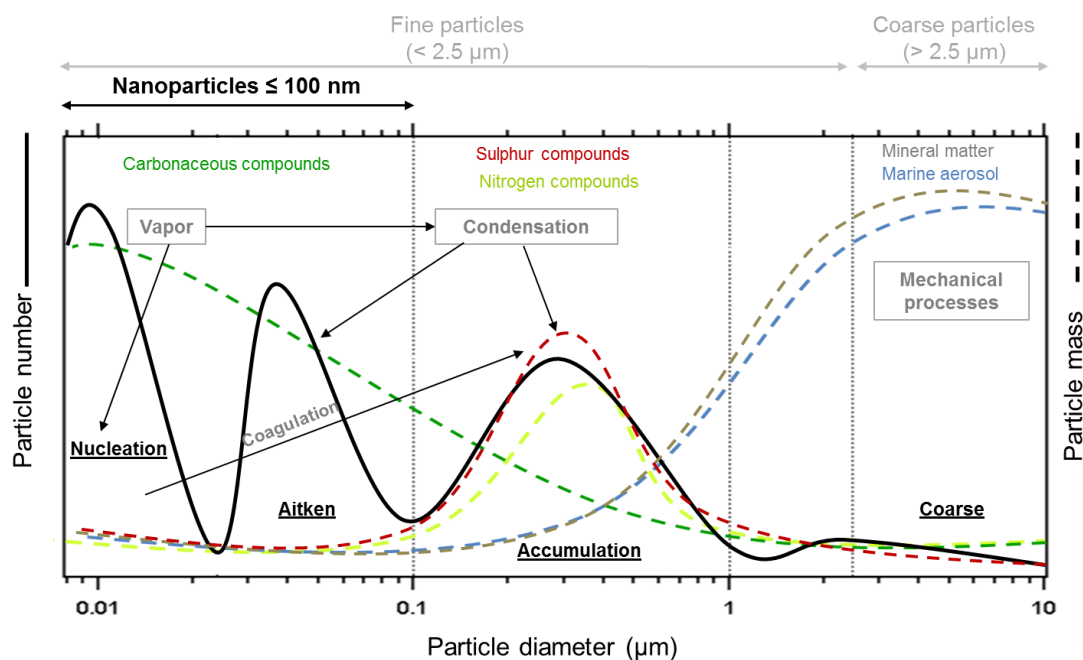


Figure 1.2 Schematic illustration of the relationship between particle size, number distribution and mass, chemical composition and particle formation and transformation processes. Source: modified from Harrison and van Grieken (1998) and Warneck (1988).

Aerosol sizes cover five orders of magnitude (1 nm - 10^5 nm) and reflect their formation mechanisms. Nanoparticles (≤ 100 nm) have been divided into two subgroups (Seinfeld and Pandis, 2006):

- **Nucleation mode (<20 nm):** This mode is dominated by newly formed particles from gaseous precursors (mainly NO_x , H_2SO_4 , NH_3 and VOCs; Kulmala, 2003). These nanoparticles are very abundant in number but have an almost insignificant contribution to aerosol mass (Harrison and Yin, 2000). They quickly tend to coagulate with other particles or grow by condensation, resulting in coarser particles (Charron and Harrison, 2003; Rodríguez *et al.*, 2005; Zhu *et al.*, 2002).
- **Aitken mode (20 - 100 nm):** This mode includes nanoparticles emitted directly or those which evolve by coagulation and condensation processes on pre-existing particles (Kerminen *et al.*, 2007; Lingard *et al.*, 2006; Wehner *et al.*, 2002).

The accumulation mode particles (0.1 - 1 μm) link nanoparticles with fine (<2.5 μm) and coarse (>2.5 μm) particles (Seinfeld and Pandis, 2006).

Seipenbusch *et al.* (2008) demonstrated in experimental studies a rapid coagulation of the ENP after release in a well-mixed chamber. During transport and aging nanoparticles may be found in coarser-sized particles. Two different coagulation processes were observed: the major coagulation was the attachment of the nanoparticles to larger sized background particles, and the second mechanism was the mutual coagulation or agglomeration of the nanoparticles. A concentration dependency was also observed: the higher the concentrations the more rapid the coagulation.

1.1.2 Sources of nanoparticles

In industrial settings, nanoparticles may be primary when they are emitted during mechanical processes like raw material sanding, grinding, demolition, cutting or polishing (Azarmi *et al.*, 2014; Gomez *et al.*, 2014b; Koponen *et al.*, 2009; Kumar *et al.*, 2012; Zimmer and Maynard, 2002). In specific industries such as nanotechnology-related ones, generation of direct or fugitive emissions of ENP may also occur (carbon nanotubes, nano-oxides, nanoclays, graphene, etc.) (Brouwer, 2010; Demou *et al.*, 2008a; Fonseca *et al.*, 2015c; Kaminski *et al.*, 2015; Lee *et al.*, 2012; Park *et al.*, 2009). In addition, nanoparticles may be secondary in nature produced by nucleation, from combustion by products, or from vapours arising from processes involving heat such as materials sintering (Fonseca *et al.*, 2016; Fonseca *et al.*, 2015a), welding (Buonanno *et al.*, 2011; Gomes *et al.*, 2012), firing (Voliotis *et al.*, 2014), thermal spraying (Bémer *et al.*, 2010; Wake *et al.*, 2002), soldering (Gomez *et al.*, 2013), among others. In many of the later cases, these nanoparticles are not voluntarily produced and explaining why those are known as N-ENP. Hence, occupational settings in industrial facilities will present inherently different characteristics with regard to particle emissions in comparison to other types of microenvironments.

The use of the term “*nanoparticle*” in this PhD thesis reflects only particle size and not chemical composition and includes all engineered, and non-engineered nano-sized particles ≤ 100 nm that may or may not be produced in a controlled, engineered way.

1.1.2.1 Engineered nanoparticles

The ENP exhibit technologically interesting properties that are distinctively different from the same non-nanoscale materials and can affect their physical, chemical, and

biological behaviour (Feynman, 1959; Kaluza *et al.*, 2009). These nanoscale particles can be presented as nanotubes, spherical, irregularly shaped, and may also exist in aggregated formations (Kaluza *et al.*, 2009).

Examples of ENP include zinc oxide - ZnO (Figure 1.3a), synthetic amorphous silica - SiO₂, titanium dioxide - TiO₂ (Figure 1.3b), aluminium oxide - Al₂O₃, iron oxides as hematite - Fe₂O₃, nanogold - Au, nanosilver - Ag, carbon-based nanomaterials (e.g. fullerenes, carbon nanofibers, graphene, carbon black, carbon nanotubes (Figure 1.3c), nanopolymers and dendrimers, quantum dots and nanoclays (COM, 2012).

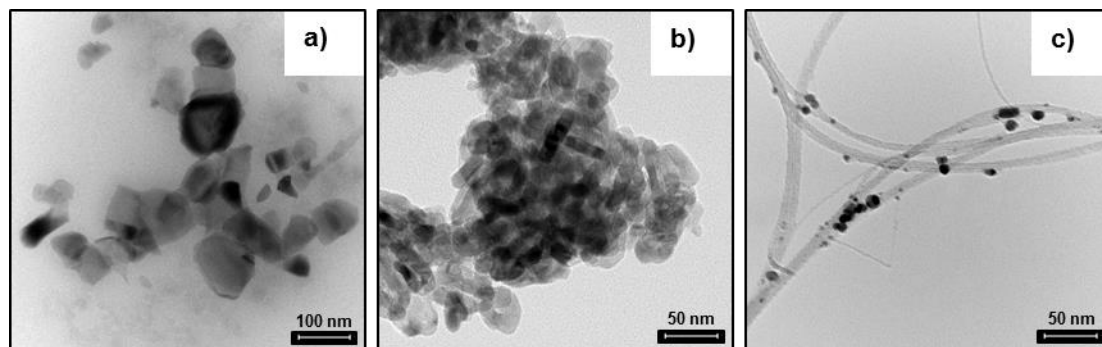


Figure 1.3 Transmission electron microscopic images of: a) zinc oxide; b) aggregated titanium dioxide; c) single-walled carbon nanotubes with iron particles attached.

Emissions of ENP are more likely to occur in case of leaks during the manufacturing processes, when the reaction chamber is opened or the product is dried, or during the handling and use of products after their production, during the reactor cleaning activity or during end of life activities such as re-use or recycling, waste treatment (e.g., incineration) and disposal (e.g., landfill) (Brouwer, 2010; Fujitani *et al.*, 2008; Gomez *et al.*, 2014a; Ham *et al.*, 2012; Kim *et al.*, 2014; Mazzuckelli *et al.*, 2007). However, emissions into the atmosphere (outdoor) may occur through diffusive emissions (e.g., if flue gas of the process is not properly treated to retain nanoparticles).

1.1.2.2 Non-engineered nanoparticles

- Process-generated nanoparticles (PGNP)

Industrial sources and processes with or without relation to nanotechnology may also generate secondary and primary particles which have dimensions in the nano-sized range that may contribute substantially to nanoparticle pollution in workplace air (Kaluza *et al.*, 2009; van Broekhuizen *et al.*, 2012a). They are usually termed incidental nanoparticles or PGNP (van Broekhuizen, 2012).



Figure 1.4 Industrial processes with potential to generate nanoparticles in workplace air: a) ceramic milling processes; b) atmospheric plasma spraying; c) use of vacuum cleaner.

Examples of sources with the potential to give rise to PGNP emissions in workplaces are thermal treatments (Bémer *et al.*, 2010; Evans *et al.*, 2010; Fonseca *et al.*, 2016; Fonseca *et al.*, 2015a; Voliotis *et al.*, 2014), melting and combustion processes (Donaldson *et al.*, 2005; Evans *et al.*, 2008; Ono-Ogasawara *et al.*, 2009), laser ablation (Barcikowski *et al.*, 2007; Fonseca *et al.*, 2015a), soldering (Gomez *et al.*, 2013), welding (Buonanno *et al.*, 2011; Gomes *et al.*, 2012), metal grinding, fracturing and abrasion activities (e.g. sanding, milling and drilling) (Azarmi *et al.*, 2014; Evans *et al.*, 2008; Göhler *et al.*, 2010; Gomez *et al.*, 2014b; Koponen *et al.*, 2009; Peters *et al.*, 2009; Pfefferkorn *et al.*, 2010; Wohleben *et al.*, 2011), and the use of electrical equipment like compressors, universal motors, drilling machines, vacuum cleaners and by diesel engines (Szymczak *et al.*, 2007; van Broekhuizen *et al.*, 2011, 2012a) (Figure 1.4). High temperature, low relative humidity, available SO₂ and low pre-existing particle surface area are common features that enhance new particle formation events (Kulmala and Kerminen, 2008). Additionally, there are processes in which conventional materials are used which contain a fraction of particles at the nano scale that may contribute to nanoparticle emissions in the workplace air. Examples of these may occur in ceramic industries (such as the cases of firing processes where the painting and glazing of ceramics occur) and paint manufacturing facilities, with emission of nanoparticles from conventional materials (van Broekhuizen *et al.*, 2012a; Voliotis *et al.*, 2014).

- Background nanoparticles

Primary nanoparticles in background air, originating mainly from diesel exhaust (soot particles with prevailing mode 20 - 30 nm; Gramsch *et al.*, 2009), show a distinct morphology and chemical composition (Charron and Harrison, 2003; Gillies and Gertler, 2000; Janssen *et al.*, 2012; Kaminski *et al.*, 2013; Matti Maricq, 2007). Conversely, secondary particles are mainly formed by nucleation from gaseous

precursors (Kulmala and Kerminen, 2008) and rapidly increase in diameter by processes as coagulation and agglomeration (Seinfeld and Pandis, 2006). In workplace air, the presence of both types of particles is dependent on infiltration processes, which in turn depends on particle size (Alzona *et al.*, 1979; Bennett and Koutrakis, 2006; Kearney *et al.*, 2014; Kearney *et al.*, 2011; Long and Sarnat, 2004; MacNeill *et al.*, 2012; Viana *et al.*, 2011; Viana *et al.*, 2014).

The term “*background particles*” is also used to refer to particles emitted by indoor sources (e.g. diesel engines, vacuum cleaners and thermal or mechanic processes) located inside the workplace, but unrelated to the specific industrial process under study (Szymczak *et al.*, 2007; van Broekhuizen *et al.*, 2011, 2012a; Zimmer and Maynard, 2002). Hence, the background particle concentrations are highly dependent on diurnal and seasonal variations, proximity to roadways, and workplace activities.

1.1.3 Nano-related workplaces: from release to exposure

At the end of the 20th century, a remarkable number of new technologies were introduced in the industrial sector offering substantial possibilities for improving the competitive position of the European Union (EU) and for responding to key societal challenges. In particular, a novel field of science called “*nanotechnology*” was developed and envisaged to become a promising industry (Adlakha-Hutcheon *et al.*, 2009; Kuhlbusch *et al.*, 2009). Feynman (1959) was one of the first to recognise the potential of nanomaterials for our industrial society when he stated that there was “*plenty of room at the bottom*”. The term “*nanotechnology*” was later introduced by Taniguchi (1974), while the basic idea of this technology was explored in greater detail by Drexler (1986) in his book “*Engines of Creation - The Coming Era of Nanotechnology*”. Nanotechnology is based on controlling matter at an atomic and molecular level where material properties may be adjusted and enhanced. Applications of nanomaterials have shown promise in advancing the fields on everyday life for example by providing means for medical treatment (gene therapy and targeted drug delivery), environmental remediation technology (such as savings in raw materials, the consumption of natural resources and a reduced environmental pollution by clean energy and pure water), and the production of light and strong materials (Adlakha-Hutcheon *et al.*, 2009; Kuhlbusch *et al.*, 2009; Ostraat *et al.*, 2015; Savolainen *et al.*, 2013).

Today, ENP can be found in more than 800 consumer products including electronic components, cosmetics and personal care products, lubricants and fuel additives, cigarette filters, paints and coatings, food processing and packaging, agrochemicals,

antimicrobial and stain-resistant fabrics and sprays, textiles and clothing, plastics, construction materials, cleaning products, ski waxes, among others (Savolainen *et al.*, 2010; WHO, 2013; Wijnhoven *et al.*, 2011; Zhang *et al.*, 2015). Nanotechnology has been identified as one of the key enabling technologies (KET) in Horizon 2020 thus underlining the significance of this field for Europe's competitiveness (Savolainen *et al.*, 2013).

The growing market, fast development and spread of novel technologies and processes used in many industrial sectors (with and without relation to nanotechnology) have on the one hand offered new properties of materials and opportunities and on the other hand brought new risks and uncertainties. Recently, the European Agency for Safety and Health at Work (EU-OSHA, 2009) considered nanoparticles as one of the major current emerging risks in workplaces. The concern is that the novel industrial technologies and production rate of ENP is growing exponentially (Aitken *et al.*, 2006). Consequently, the risk of possible exposure of humans and the environment to unknown nanoparticle types and concentrations may increase dramatically in the near future compared with the exposure to particles originating from more conventional sources. Therefore, industries which have benefited from advances made available through nanotechnology and through innovative industrial processes, are identified as a workplaces suffering from potential of nanoparticle releases. During their life-cycle, nanoparticles may end up in different environmental compartments such as: (i) air; (ii) water; or (iii) soil. Consequently this may lead to exposures in the environment, and also human exposure through these environmental compartments and possibly adverse health effects (Borm *et al.*, 2006; Handy and Shaw, 2007; Maynard *et al.*, 2006; van Broekhuizen, 2012; Yokel and MacPhail, 2011).

1.1.4 Evidences of workers exposure to nanoparticles

A variety of exposure pathways are possible (Kaluza *et al.*, 2009). Because higher concentrations of nanoparticles and higher frequency of exposure to them are more likely to happen in workplace settings, occupational exposures assessments require special attention in this kind of settings (Aitken *et al.*, 2004; Hristozov *et al.*, 2012). In the workplace, workers may be exposed to nanoscale particles while manufacturing ENP (research or industrial scale), formulating them into products, transporting, bagging, handling them in the storage facilities, during cleaning operations (Balas *et al.*, 2010; Brouwer, 2010), and even during unexpected system failure such the local exhaust ventilation (Fonseca *et al.*, 2015c). This is also possible during specific industrial processes involving N-ENP from unintentional nanoparticle release or the formation of nanoparticles from gaseous precursors (Aitken *et al.*, 2004; Kuhlbusch

and Fissan, 2006; van Broekhuizen, 2012). The predominant route of exposure for workers who are in contact with nanoscale particles is inhalation and/or dermal contact (Hansen, 2009; Schmoll *et al.*, 2009).

1.1.4.1 Engineered nanoparticles

The net exposure to ENP may vary depending on the type of nanomaterials used (powder, paste, liquid), the process, and the control measures applied to mitigate worker exposure (Brouwer, 2010; Jensen *et al.*, 2015; Methner, 2010; Plitzko, 2009). Worker exposure is somewhat less likely to occur during the manufacturing process, since most ENP manufacturing processes are performed in closed reaction chambers (Hansen, 2009). Release and exposure to ENP is especially likely to happen while handling and bagging the nanomaterials (Kaminski *et al.*, 2015), during cleaning operations (Fonseca *et al.*, 2015c; Plitzko, 2009). A review by Kuhlbusch *et al.* (2011b), aimed at identifying potential exposure scenarios at nanotechnology workplaces, related to the manufacture and use of ENP (fullerenes, carbon nanotubes, carbon black, carbon nanofibers, metals and metal oxides).

Several studies have already been carried out regarding carbon nanotubes (CNT), carbon nanofibers (CNF) and fullerenes (Bello *et al.*, 2008a; Bello *et al.*, 2008b; Bello *et al.*, 2010; Dahm *et al.*, 2013; Dahm *et al.*, 2012; Evans *et al.*, 2010; Fujitani *et al.*, 2008; Maynard *et al.*, 2004). For instance, Dahm *et al.* (2012) investigated the airborne exposures generated in six representative sites identified as CNT/CNF primary or secondary manufacturers and concluded that there was visual and microscopy-based evidence of CNT/CNF at all sampling sites, with the highest CNT and CNF structure counts being found in samples collected at secondary manufacturing sites. However inconsistent results were obtained by Dahm *et al.* (2013) concerning monitored data from different online instruments.

Biswas and Wu (2005) concluded that there is linear dependence between the operations in production and exposure to ENP in the workplace. Several other authors suggested that the influences of background concentration as well as the spatio-temporal variations of exposure are very relevant (Evans *et al.*, 2010; Kling *et al.*, 2016; Mazzuckelli *et al.*, 2007; Peters *et al.*, 2009).

Koponen *et al.* (2009), Göhler *et al.* (2010), Wohlleben *et al.* (2011), van Broekhuizen *et al.* (2012a) and Gomez *et al.* (2014b), showed that during the abrasion of surfaces coated with nano-enabled coatings workers may be exposed to nanoparticles but mainly due to the use of electrical equipment since no differences in particle number concentration (N) can be detected with the same process with conventional coatings (without nanoparticle additives).

1.1.4.2 Non-engineered nanoparticles

- Process-generated nanoparticles

Industrial processes (high-energy processes, mainly thermal or mechanical) may have a high potential for nanoparticle formation and release, and thus for worker exposure. Worker exposure is dependent on the materials processed, the way of processing, machinery used, temperature, etc. (van Broekhuizen, 2012). For example, Voliotis *et al.* (2014) revealed that nanoparticle emissions and subsequent exposures may reach up to N of $1 \times 10^6 \text{ cm}^{-3}$ during firing processes where the painting and glazing of ceramics occur. Also Gomez *et al.* (2013) evidenced that metal-containing nanoparticles may reach high exposure concentrations in the same order of magnitude ($1 \times 10^6 \text{ cm}^{-3}$), with initial size distributions centred at 35 - 60 nm, during a low power soldering activity. Nanoparticle exposure concentrations $>1 \times 10^8 \text{ cm}^{-3}$ (mean particle size diameter $\geq 28 \text{ nm}$) were recorded by Bémer *et al.* (2010) inside ventilated cabins, in which thermal spraying of metals using electric arc processes were performed.

According to Szymczak *et al.* (2007), van Broekhuizen *et al.* (2011) and van Broekhuizen *et al.* (2012a), exposure to nanoparticle concentrations from electrical equipment like compressors, universal motors, drilling machines, vacuum cleaners and diesel engines may exceed several $0.1 \times 10^6 \text{ cm}^{-3}$ up to $9 \times 10^6 \text{ cm}^{-3}$.

- Background particles

In industrial workplaces environments in moderately polluted urban areas, an average background in the range $10^3 - 10^4 \text{ cm}^{-3}$ is common (Gomez *et al.*, 2014a; Koivisto, 2013). In comparison to the exposure concentrations described in previous sections, these concentrations may be considered relatively low. However, the discrimination of background concentrations is essential in order to accurately identify and quantify exposures to ENP or PGNP. Therefore, it is highly important to understand the different particle sources and background characteristics to be able to distinguish the target nanoparticles from the background.

1.1.5 Potential health and environmental concerns

As shown in previous section 1.1.4, evidences about workers exposure to ENP and PGNP are clear. Hence, possibilities for unexpected effects of nanoparticles on human health, safety and environmental burden should not be neglected (Maynard *et al.*, 2006; Oberdörster *et al.*, 2005).

Nanoparticles are found in a variety of forms, based on physico-chemical properties and should not be considered as a uniform group of substances (Borm *et al.*, 2006;

GAO, 2014; Savolainen *et al.*, 2010). The environmental, health, and safety risks of a nanomaterial may differ by characteristics (Borm *et al.*, 2006; GAO, 2014; Maynard *et al.*, 2004; Nel, 2005) such as: (i) mean particle size; (ii) particle size distributions; (iii) morphology; (iv) particle surface area; (v) agglomeration state; and (vi) surface chemistry including chemical reactivity, surface composition or particle shape (see Figure 1.5).

As the particle size is reduced, the proportion of atoms found at the surface related to the atoms in the interior of the particle increases and as consequence, the nanoscale particles are more reactive (Kaluza *et al.*, 2009). Major differences between unintentional and intentional nanoparticles are the polydispersity and chemically complex nature of the former, in contrast to the monodisperse and precise chemically engineered characteristics and particle morphology of the latter (Oberdörster *et al.*, 2005). However, despite these differences, the same toxicological principles are likely to apply to all nanoparticles, because not only size but also a number of other particle parameters determine their biological activity.

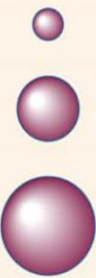
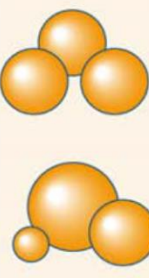
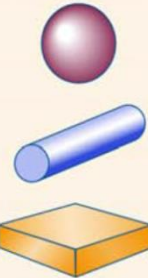
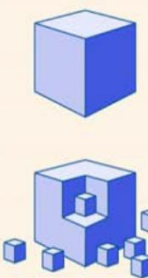
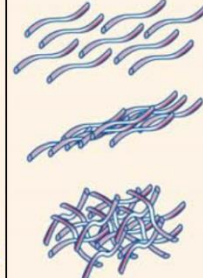
Size	Size distribution	Morphology	Surface area	Agglomeration state	Surface chemistry
					

Figure 1.5 Characteristics of a nanomaterial that could affect the environmental, health, and safety risks. Source: GAO (2014).

The inhalation pathway is considered the major route of nanoparticle exposure and the lungs and pleura the major primary targets for adverse effects (Donaldson and Seaton, 2012; Oberdörster *et al.*, 2005). However ingestion and dermal exposures also need to be considered especially during manufacture, use, and disposal of ENP (Oberdörster *et al.*, 2005).

As particles reach smaller diameters they can travel deeper into the lungs (Heal *et al.*, 2012; Hoet *et al.*, 2004; Oberdörster, 2001; Weichenthal, 2012). The main deposition mechanism of inhaled nanoparticles (≤ 100 nm) in the respiratory tract is diffusion. Other relevant mechanisms for coarser particles, such as inertial impaction, gravitational settling, and interception, do not contribute to nanoparticles deposition, and electrostatic precipitation may occur only in cases where nanoparticles carry significant electric charges (Oberdörster *et al.*, 2005). Figure 1.6 shows the inhalation deposition probability of particulates in different regions of the human respiratory tract

during nose breathing at rest from an adult based on a predictive mathematical model from International Commission on Radiological Protection (ICRP, 1994).

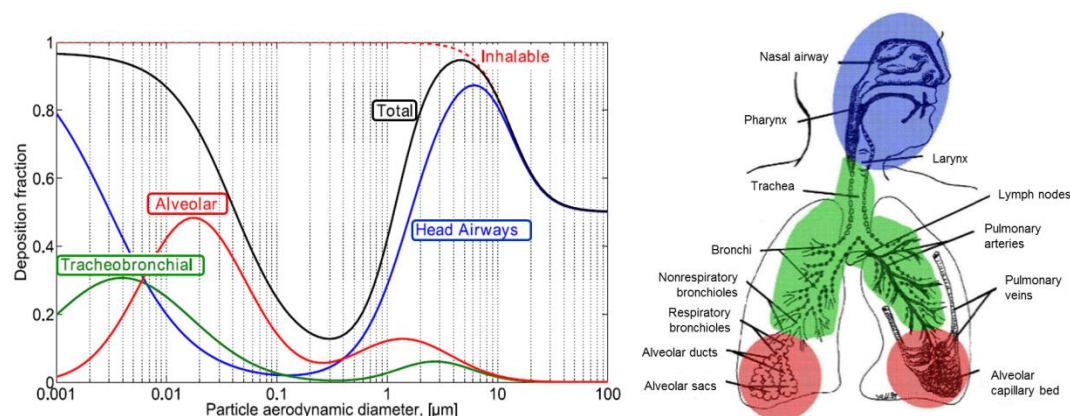


Figure 1.6 Fractional deposition of inhaled particles in the nasopharyngeal, tracheobronchial, and alveolar regions of the human respiratory tract under conditions of nose breathing during rest from an adult according to the ICRP deposition model. Source: Koivisto (2013).

As shown in Figure 1.6, the larger particles deposit higher up in the nose and upper respiratory tract, while only the smaller size particles deposit in the more peripheral bronchioles and proximal alveolar region (Donaldson and Seaton, 2012). Nanoparticles with the size between 10-100 nm deposit primarily in the alveolar region (red line of Figure 1.6), while smaller and larger particles may deposit in the tracheobronchial region (green line of Figure 1.6) or in the head airways (blue line of Figure 1.6). There is increasing scientific evidence that removal of particles in the lung is size-related (Kim *et al.*, 2015; Salma *et al.*, 2015).

These different deposition efficiencies should have consequences for potential effects induced by inhaled nanoparticles of different sizes as well as for their translocation into the blood and lymph circulation and disposition to extrapulmonary region (Choi *et al.*, 2010; Geiser and Kreyling, 2010; Oberdörster, 2010).

The available information about the effects of nanoparticles in general on human health is still limited. Toxicological animal studies conducted to date cannot be considered conclusive and the epidemiological data related to the toxicological effects of the nanomaterials in real conditions are scarce. Oxidative stress is considered the main cytotoxicity mechanism developed by nanoparticles of different properties which can give rise to an ongoing inflammation or genotoxic effects of reactive nanoparticles which can even lead to lung fibrosis or cancer (Donaldson and Poland, 2012; Guo *et al.*, 2012; NIOSH, 2011; Shvedova *et al.*, 2012). In addition, *in vivo* studies indicate that some nanomaterials can be translocated from the lung to the blood circulatory system and reach other organs and tissues (such as the liver,

kidneys, heart, bone and in the soft tissue) or even be taken up directly to the brain through the olfactory epithelium (Elder *et al.*, 2006; Kreyling *et al.*, 2009; Oberdorster *et al.*, 2002) and give rise to several health effects. Exposure to nanoparticles has been associated with a number of health effects including pulmonary inflammation (Rossi *et al.*, 2010; Shvedova *et al.*, 2012; Shvedova *et al.*, 2008), genotoxicity (Chen *et al.*, 2014; Falck *et al.*, 2009; Guichard *et al.*, 2012; Karlsson *et al.*, 2009), carcinogenicity (Sakamoto *et al.*, 2009; Takagi *et al.*, 2008; Tsuda *et al.*, 2009), and circulatory effects (Nurkiewicz *et al.*, 2008; Nurkiewicz *et al.*, 2009). Some nanomaterials, among which are carbon black and titanium dioxide have been classified based on in vivo studies as "*possibly carcinogenic to humans*" (Group 2B) by the International Agency for Research on Cancer (IARC) (WHO, 2015). It has been shown that rigid, chemically/biologically persistent free nanofibers, rods and tubes with a high aspect ratio (length > 20 µm), can induce similar effects to those of asbestos such as acute inflammation leading to progressive fibrosis of the pleura (Murphy *et al.*, 2011; Poland *et al.*, 2008; Takagi *et al.*, 2008).

1.2 Exposure assessment and characterisation

Although some nanoparticles have shown to be potentially hazardous for human health, systematic studies on hazards or exposure to nanoparticles are still lacking (see for example reviews by Borm *et al.* (2006), Yokel and MacPhail (2011) and Savolainen *et al.* (2013)). The implementation of standards for appropriate safety control systems may still take several years, in spite of recent progresses (e.g. ongoing SIINN Eranet projects nanoIndEx and nanOximet, EU FP7 project NanoDiode, MARINA or German BMBF projects nanoGEM and nanoCare). Industrial settings should adopt responsible risk assessment, as well as risk management strategies, in order to guarantee a safe work environment (Hameri *et al.*, 2009) and obtain products with no health threats at any point of their lifecycle (Friedrichs and Schulte, 2007).

Mathematically, risk can be expressed as the multiplication of exposure and hazard (Krug and Klug, 2010), i.e., risk assessment always requires both determination of exposure and toxicity. Risk assessment requires detailed knowledge of worker exposure during processes with potential to release nanoparticles to workplace air, which will firstly require the understanding of exposure scenarios. Once the potential release scenarios are understood, worker exposure needs to be characterised following clearly defined protocols.

The assessment of exposure to nanomaterials provides particular challenges such as the following (Brouwer, 2010; Brouwer *et al.*, 2009):

- Discrimination from background particles.
- Collection and analysis of size information.
- Effective high spatial and temporal variability.
- Choice of exposure metrics and measurement instruments.
- Measurement of high aspect ratio nanoparticles.

Furthermore, the identification and chemical composition characterisation appear to be more challenging when dealing with PGNP its particle nature are unknown and more complex due to non-specificity of nanoparticle types and sources.

1.2.1 Exposure metrics

The metric that should be used to assess exposure to nanoparticles should be that which most closely links to any potential health effects. Three main aerosol metrics can be differentiated (Abbott and Maynard, 2010; Maynard and Aitken, 2007; Ramachandran *et al.*, 2011):

- Mass concentration (M ; $\mu\text{g m}^{-3}$): workplace exposure limits for hazardous materials and chemicals are mostly based on mass concentration, typically expressed as mg m^{-3} of air (Pietrojusti and Magrini, 2014).
- Particle number concentration (N ; cm^{-3}): as discussed in earlier sections, due to their small diameter, nanoparticles contribute strongly to particle number concentrations, and almost insignificantly to particle mass concentration. However, existing guidelines do not include limit values in terms of particle number concentration.
- Surface area concentration (SA; $\mu\text{m}^2 \text{cm}^{-3}$): studies have indicated that particle surface area concentration is associated with biological response (Abbott and Maynard, 2010; Oberdörster *et al.*, 2005; Oberdorster *et al.*, 2007; Ramachandran *et al.*, 2011) and thus, the best metric for predicting health effects of nanoparticles in humans (Pietrojusti and Magrini, 2014). Heitbrink *et al.* (2008) suggested that the active surface area concentrations can largely be explained by particles smaller than 100 nm. Reche *et al.* (2015) conclude that particles up to 200 nm may contribute significantly to surface area concentrations. By assuming a spherical size for these nanoparticles the surface area can be related to the number concentration (Ramachandran *et al.*, 2011).

Additionally, it is acknowledged that particle size distribution is a relevant metric to indicate the efficacy of particle intake into the respiratory tract and the location of particle deposition and interaction with the biological system. Particle size distribution

can also be used to calculate other (health-relevant) metrics like surface area of the particles assuming smooth, compact spherical particles; however, errors in surface area estimates arise when the assumptions are not valid (Brouwer *et al.*, 2012).

Given that there is no conclusive agreement on the most relevant dose-metric(s) to express human exposure to nanoparticles, it is recommended that measurements of particle number, surface area and mass concentration metrics should be undertaken simultaneously, whenever possible (Brouwer *et al.*, 2012; Park *et al.*, 2010).

1.2.2 Measurement instrumentation

A number of instruments are available for workplace exposure characterisation, regarding physical and chemical properties of airborne nanoparticles (Ostraat *et al.*, 2015). The measurement instruments can be classified as online (size resolved/integrated and time resolved) and offline (size and time integrated). Physical characterisation of airborne nanoparticles, most commonly particle size, surface area, size distributions, and/or number concentration measurements, are typically conducted using online (real-time) instruments. Offline instruments (e.g. electron microscopy, filter samples) additionally allow for the characterisation of the morphology as well as chemical composition of collected nanoparticles. This section provides an overview of the type of instruments currently available. The specific instruments used in this PhD are described in detail in chapter 3, and also in each of the research articles presented in chapter 4.

1.2.2.1 Online (real-time) instrumentation

This type of instrumentation provides information of the metrics under study (particle mass, number, size distribution, etc.) independently on the chemical composition or morphology of the material. Therefore, these instruments are generally unable to differentiate between ENP and PGNP or background nanoparticles. For practical purposes, online instrumentation may be classified into two types: (i) stationary instrumentation, and (ii) handheld instrumentation.

Stationary instruments are complex instrumentation in terms of use, size and weight, and they are commonly used in comprehensive studies aiming to characterise nanoparticles and worker exposure in workplace environments. Examples of the most frequently used stationary instruments, discussed in detail in chapters 3 and 4, are stationary scanning mobility particle sizers (SMPS; Figure 1.7a), condensation particle counters (CPC; Figure 1.7b), electrical low pressure impactors (ELPI™; Figure 1.7c), optical particle sizers (Grimm; Figure 1.7d) and aerosol photometers

(DustTrak™; Figure 1.7e). With regard to optical particle sizers and aerosol photometers, although their particle size range is outside the nanoscale, they can be used for agglomerates or aggregates of larger particle sizes.

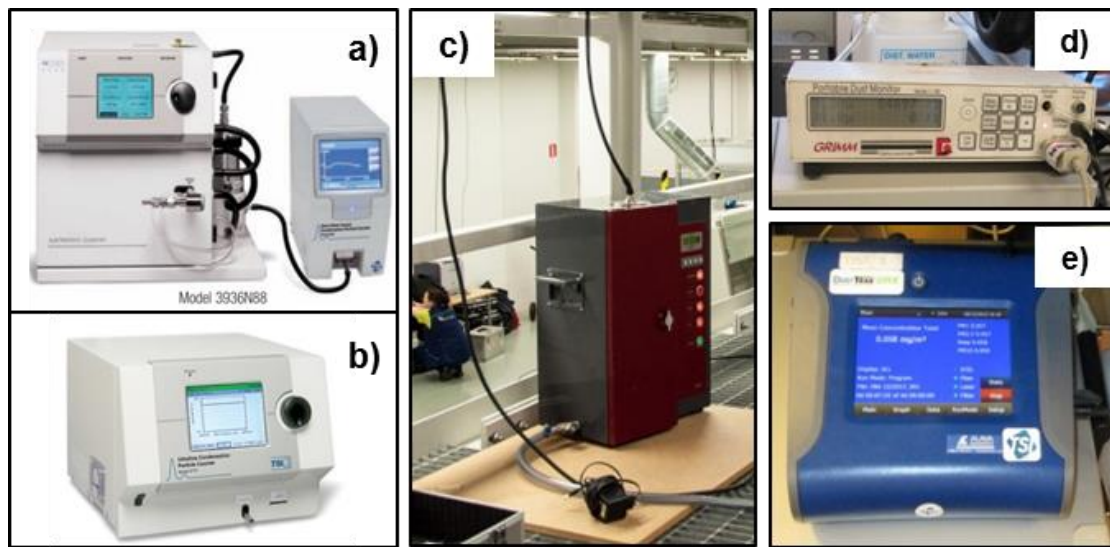


Figure 1.7 Example of stationary online instruments: a) SMPS, TSI Model 3936N88 consisting of a nano DMA, TSI Model 3085 and a water CPC, TSI Model 3788; b) UCPC, TSI Model 3776; c) ELPI™, Dekati Ltd.; d) optical particle sizer (Grimm Model 1.108); e) laser photometer (DustTrak™ DRX aerosol monitor, TSI Model 8533).

With regard to portable monitors, these instruments are generally useful for the detection of nanoparticle emission sources (e.g. leaks), for determining concentrations of the metrics of interest, and to test the effectiveness of preventive measures. Examples of frequently used instruments, discussed in further detail in chapters 3 and 4 as in the case of stationary instruments, are handheld CPC (Figure 1.8a), diffusion chargers (DC; Figure 1.8b), micro-aethlometers (Figure 1.8c), portable NanoScan SMPS, and portable aerosol photometers (Figure 1.8d).

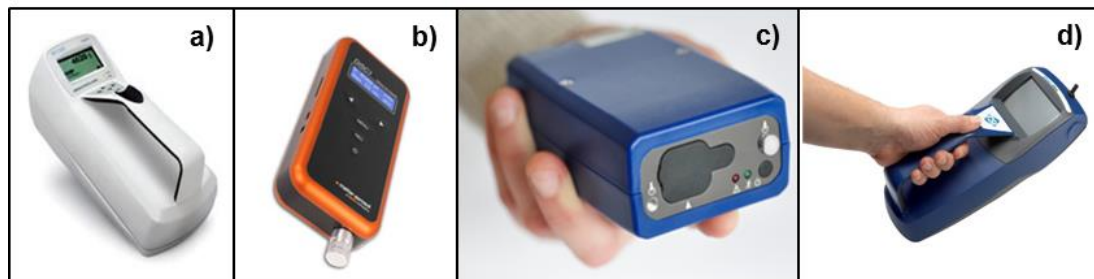


Figure 1.8 Example of portable online instruments: a) CPC, TSI Model 3007; b) DC, DiSCmini Matter Aerosol; c) Micro-aethlometer, Micro-aethlometer, microAeth®, Model AE51; and d) laser photometer (DustTrak™ DRX aerosol monitor, TSI Model 8534).

1.2.2.2 Offline instrumentation (sample collection and analysis)

Offline instruments, besides allowing for the determination of particle mass concentration by gravimetric methods, also allow for the physical and chemical characterisation of particles. Examples of offline techniques are open-face sampling (e.g. by 3-piece conductive polypropylene air sampling cassettes SKC Inc.), filtration, electrostatic or thermal precipitation (e.g., by nanometer aerosol sampler - NAS, TSI Model 3089; Li *et al.*, 2010; TSI, 2013b; Dixkens and Fissan, 1999), elutriation, size-selective collection by cascade impaction such as Berner low-pressure impactor (BLPI or nano-BLPI) (Berner and Luerzer, 1980; Berner *et al.*, 1979; Hering *et al.*, 1978; Hillamo and Kauppinen, 1991; Preining and Berner, 1979), micro-orifice uniform deposit impactor (Moudi or nano-Moudi) (Marple *et al.*, 2014; Marple *et al.*, 1991) or personal cascade impactor sampler (PCIS) (Misra *et al.*, 2002).

Collected samples can be analysed gravimetrically or by other analytical techniques such as ion chromatography (IC), inductively coupled plasma by atomic emission spectrometry (ICP-AES) or by mass spectrometry (ICP-MS), which provide information about the chemical composition of the nanoparticles collected.

The identification, e.g. morphology and geometry of single particles and agglomerates and determination of optical diameters can be accomplished by electron microscopy techniques such as high resolution transmission electron microscopy (TEM) or scanning electron microscopy (SEM). In addition, samples can be used for further elemental composition identification, e.g. energy dispersive X-ray (EDX) analysis, often coupled with SEM or TEM devices (ECHA, 2015b).

To sum up, the lack of specificity of the online instruments and the intrinsic limitations of the instruments and techniques preclude the idea of a single exposure metric. Therefore, exposure is determined by multiple exposure characteristics (physical, chemical, and physicochemical characteristics and workplace factors) and thus should be described by a set of metrics/information (e.g. direct reading data, additional offline analysis, and observations). However, for initial screenings (e.g. during workplace inspection of the potential worker exposure to nanoparticles), one of these metrics may be consider sufficient (Brouwer *et al.*, 2012). Detailed assessments necessarily require an integrated approach combining different tools and metrics.

1.2.3 Exposure assessment strategies

Understanding the relationship between airborne nano-sized particles and exposure, under different environmental conditions, is of great importance for developing efficient control measures and for establishing, evaluating and improving regulations and legislation aiming to guarantee environmental health and safety of industrial processes. Several assessment strategies have been developed for the determination of exposure to nanoparticles in workplaces (e.g., BSI, 2010, Methner *et al.*, 2010; Ramachandran *et al.*, 2011; Asbach *et al.*, 2012b; Brouwer *et al.*, 2012; Ostraat *et al.*, 2015). All of them identify the need for a tiered approach to facilitate assessments that should be easy to pursue, cost effective, based on established measurement methods, able to discriminate and quantify target nanoparticles from background particles, and deliver comparable results independent from the workplaces under investigation.

1.2.3.1 Tiered approach for exposure assessment

An example of a flow chart of a tiered approach for exposure assessment is shown in Figure 1.9 which contains 3 hierarchical tiers (Ostraat *et al.*, 2015): (i) initial assessment; (ii) basic exposure assessment; and (iii) expert exposure assessment. Each tier uses different devices and generates different degrees of detail and specificity of the resulting data. Sections below provide a detailed description of each tier.

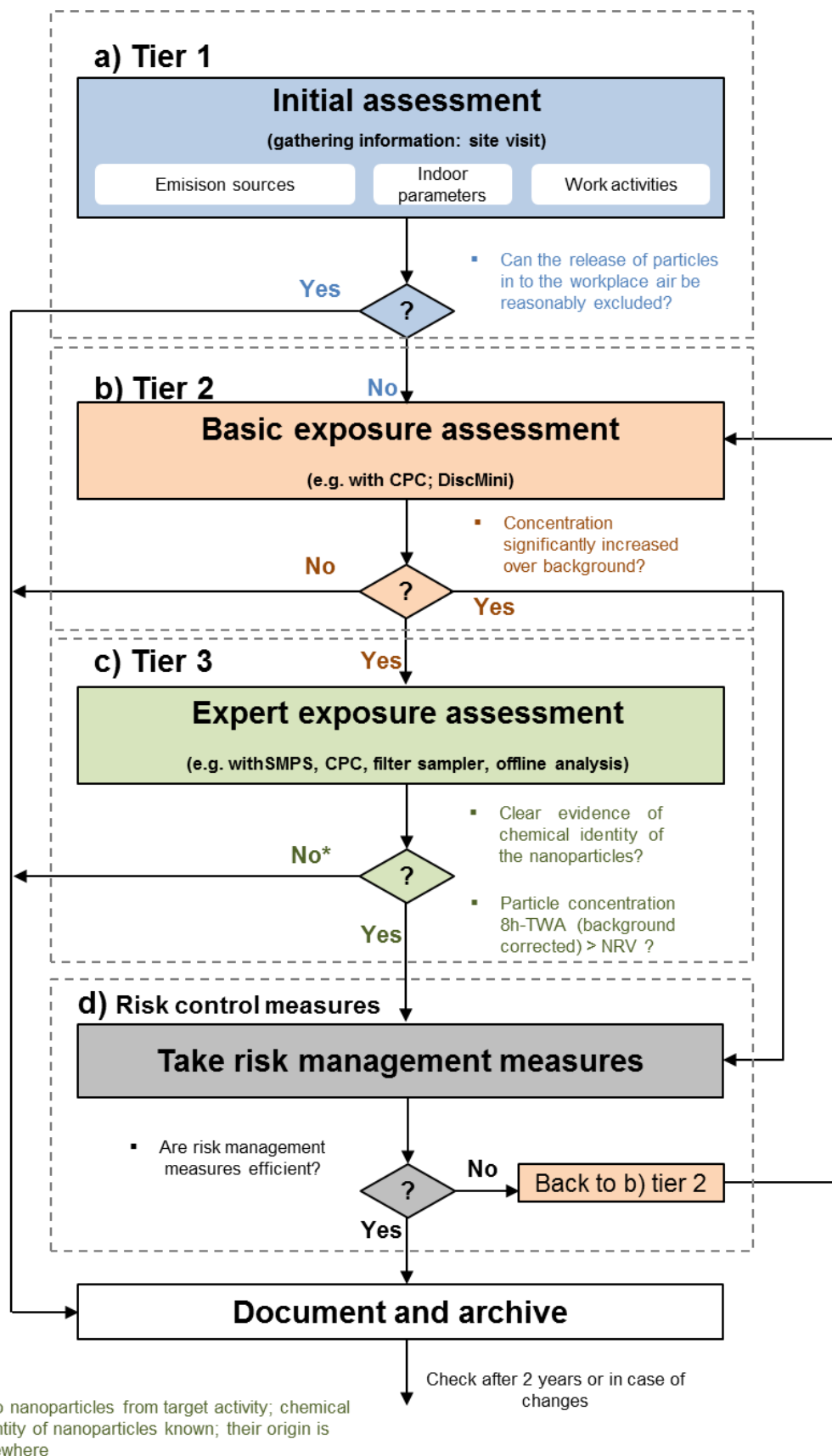


Figure 1.9 Flow chart of the tiered approach for exposure assessment. Source: modified from Ostraat et al. (2015). Dashed boxes indicate the basic steps of the exposure assessment process in workplaces and the arrows show how the exposure assessment proceeds.

- Tier 1: Initial assessment

Tier 1 (Figure 1.9a) is a qualitative assessment focused on gathering information prior to laboratory or field assessment in order to identify potential nanoparticle emission mechanisms and worker exposure (e.g. through on-site inspection of potential locations where nanoparticles may be released into workplace air). Examples of exposure and risk assessment tools that contain information gathering guidance include the precautionary matrix for synthetic nanomaterials and risk or control banding tools, e.g. control Banding Nanotool, NanoSafer, and Stoffenmanager Nano (Brouwer, 2012; Cornelissen *et al.*, 2011; Höck *et al.*, 2008; Paik *et al.*, 2008; Riediker *et al.*, 2012; Schneider *et al.*, 2011; Van Duuren-Stuurman *et al.*, 2012a; Van Duuren-Stuurman *et al.*, 2012b; Zalk *et al.*, 2009). These are qualitative nanoparticle release models based exclusively on inventory data.

If nanoparticle emissions and occupational exposure cannot be excluded during Tier 1 analysis, the potential exposure has to be determined in Tier 2.

- Tier 2: Basic exposure assessment

The focus of Tier 2 (Figure 1.9b) is to determine whether exposure to nanoparticles may occur by utilizing particle size-integrating, easy-to-use portable online instruments. Simple particle number or surface concentration measurements are usually sufficient in this Tier (Kaminski *et al.*, 2015). Typical instruments are portable CPC and diffusion charger based devices (e.g. DiSCmini, nanoTracer, Aerotrak 9000). In addition, offline analyses, such as SEM-EDX or TEM-EDX, may be useful, especially if the source of elevated concentrations and the corresponding particle characteristics are unknown. To determine realistic exposure levels, the particle concentrations should be measured near potential release locations and in the breathing zone of workers and compared with the background concentration. If the particle concentration is significantly increased over the background, a potential exposure exists and has to be assessed in Tier 3 measurements (Figure 1.9c). The level of significance of emission or exposure concentrations is described by comparison with background concentrations. Net-emission particle concentrations deriving from industrial processes are corrected by subtraction of the average background concentration (Asbach *et al.*, 2012b; Kaminski *et al.*, 2015):

$$\text{Particle release} = WA - BG \quad \text{Eq (1)}$$

where *WA* is the measured particle concentrations at the breathing zone or emission source during the work activity, and *BG* is the average background registered concentrations.

This approach is only acceptable if background concentrations remain relatively stable throughout the measurement period and particle emissions from the process under study are sufficiently higher than background.

According to Asbach *et al.* (2012b), the resulting concentration difference between the activity under investigation and the background is considered statistically significant if the mean particle concentration in workplace air is higher than the *BG* concentrations plus three times the standard deviation ($3\cdot\sigma_{BG}$) of the average *BG* concentration. This means that if the ratio

$$\frac{\text{Particle release}}{3\cdot\sigma_{BG}} > 1 \quad \text{Eq (2)}$$

then, particle release should be considered as significant and in this case the workplace or process concentration is deemed to be significantly increased and must be further assessed for the release of nanoparticles to the workplace air (Tier 3). The suggestion of the factor three is based on the assumed level of significance of elevated exposure concentrations. Important to note that these simplified decision criteria is strictly valid if the relative standard deviations of both background and emission/exposure concentrations reveal the same order of magnitude. If for example the relative standard deviation of the exposure concentration is considerably higher than that of the background concentration, this is an indication for a process where significantly higher short term exposure conditions may be present during the process. In such a case measures that take place in Tier 3 should be performed. In addition to Tier 3 measurements, risk management measures can be employed (e.g. installation of local exhaust ventilation). The effectiveness of new actions should be verified in another Tier 2 measurement.

- *Tier 3: Expert exposure assessment*

Tier 3 (Figure 1.9c) is characterised by the use of extensive measurements that are needed for nanoparticle and health risk evaluation. The aim of this Tier is to obtain as much information as possible on airborne nanoparticles in the breathing air in a workplace in order to determine whether or not exposure can be excluded or if further risk management steps need to be implemented. In Tier 3, online measurement instruments in addition to those used in Tier 2 should be utilised to provide a definitive conclusion regarding the presence of nanoparticles in workplace air.

Typical online instruments included in Tier 3 are the following:

- Electrical mobility analysis for measuring particle number size distributions of submicron nanoparticles.

- Optical or aerodynamic particle sizers or ELPI to measure the particle number size distributions of particles approximately > 500 nm.
- Condensation particle counters or diffusion chargers to measure total particle number concentration.
- Nanoparticle surface area monitors to measure the lung deposited surface area concentration (LDSA), usually alveolar.

As discussed in Tier 2, these online instruments must be supported with personal sampling using filters or grids suitable for particle characterisation (size, shape, agglomeration state, etc.) by SEM-EDX or TEM-EDX, or another chemical analysis technique such ICP-MS or ICP-AES.

If the workplace concentration is significantly increased over the background and higher than reference values (see section regulatory background 1.3), and if the size distribution, morphological and/or chemical analyses clearly show that the increase is a result of nanoparticle release, additional risk management measures (Figure 1.9d) need to be employed for exposure mitigation. The priority is to reduce exposure concentrations and then to increase personal protection. Concentrations may be reduced by changing process methods, altering material usage in the sources, or they may be achieved via structural and/or process changes. The effectiveness of the risk management measures and the potential workers exposure need to be verified by repeating Tier 2 and Tier 3 assessments.

1.2.3.2 Determination of background concentrations

Background particle concentrations, i.e., particles infiltrating from outside or deriving from industrial processes which have potential for nanoparticle release or formation into workplace air become an important variable at lower concentration levels and hence must be accounted for.

Measurements in both Tier 2 and 3 always include the determination of the particle background concentrations in the workplace, either through simultaneous measurements at a representative background location (Demou *et al.*, 2008a; Kaminski *et al.*, 2015; Tsai *et al.*, 2008) or through measurements at the respective workplace prior to or after the activity or the process under investigation (Bello *et al.*, 2008a; Bello *et al.*, 2008b; Fujitani *et al.*, 2008; Kuhlbusch and Fissan, 2006; Methner, 2008; Methner *et al.*, 2007; Yeganeh *et al.*, 2008). The first type of approach is considered a “*far-field background*” and the monitoring location may be found outdoors or at another point in the production building/laboratory, whereas the second type is considered a “*near-field background*” (Brouwer *et al.*, 2009). For the

first type approach, care is required that there is no contribution from the sources of interest, or from other background sources in the far field background sample (Ostraat *et al.*, 2015).

A third approach can be the collection of physical samples of the aerosol for offline analysis to confirm that the peak concentrations observed correspond to an identified nanoparticle source, either by composition (elemental analysis of the primary material) or morphology or both, for example by TEM-EDX and SEM-EDX analysis (Brouwer *et al.*, 2009; Methner *et al.*, 2010).

1.2.4 Control measures to mitigate occupational exposure

In order to reduce occupational exposure several protective measures like structural or process modifications and/or personal protection measures may be applied. Some examples are provided below.

1.2.4.1 Engineering control methods

Protection of workers against nanoparticles increases by implementing well designed, installed and properly used engineering control systems such as:

- Local exhaust ventilation (LEV) and general ventilation, preferably enclosing the sources of nanoparticles (Kaluza *et al.*, 2009).
- Appropriate filtration system for removing nanoparticles from exhaust air, which usually contains multi-stage filters with high efficiency particulate air filter (HEPA) or ultra-low penetration air filters (ULPA) as final filter (Kaluza *et al.*, 2009).

In all cases where engineering controls alone do not sufficiently reduce exposure potential, provision of appropriate personal protective equipment (PPE) for suitably minimizing hazard is required.

1.2.4.2 Personal Protective Equipment

Nanoparticle exposure may often be attributable to the wearing of inadequate PPE. Staff involved in any tasks where potential exposure to nanoparticles exposure exists may use the following PPE (Kaluza *et al.*, 2009):

- Examination gloves: nitrile or rubber examination gloves which cover hands and wrists completely through overlapping sleeve of lab coat.
- Safety glasses or safety goggles (ANSI Z-87 approved), considered the minimum appropriate level of eye protection.

- Lab coats or disposable coveralls that provide complete coverage of skin not otherwise protected by PPE and/or attire.
- Appropriate air-purifying respirators, utilised for all processes where exposure potential is present.

Figure 1.10 shows two examples of well protected researchers performing aerosol experiments during single-walled carbon nanotubes (SWCNT) manufacturing and atmospheric plasma spraying.



Figure 1.10 Well protected researchers assessing occupational exposure to nanoparticles during: a) SWCNT manufacturing, and b) atmospheric plasma spraying applied in ceramic industry.

1.3 Regulatory background

For risk assessment, comparison of measured exposures with accepted risk levels is essential. Although occupational exposure limits (OEL) were established by Council Directive 88/642/EEC as “*the limit of the time-weighted average of the concentration of a chemical agent in the air within the breathing zone of a worker in relation to a specified reference period*” (EC, 1998), no OEL are available regarding nanoparticles yet. Van Broekhuizen *et al.* (2012b) has reported on the usefulness of the proposed OEL in different exposure scenarios. Official OEL are lacking because the relevant exposure scenarios are not well known, measurement metrics are unclear, and epidemiological studies are incomplete (Schulte *et al.*, 2010; van Broekhuizen *et al.*, 2012b).

Currently, there are only recommended OEL for nanomaterials proposed by different international organisations (ECHA, 2015a; IFA, 2009; NIOSH, 2011, 2013; SER, 2012). Table 1.1 summarizes these recommended values. Therefore, the use of these reference values for nanomaterials seems to be an acceptable alternative for precautionary risk management as long as health-based limit values are not regulated. Such reference values represent a warning level for nanoparticles in the

workplace atmosphere that should lead to exposure control measures when this level is exceeded. Furthermore, some companies have established for specific nanomaterials their own OEL values for internal use. For example, for multi-walled carbon nanotubes (MWCNT), Bayer Material Science has set a limit value of 0.05 mg m⁻³ based on inhalation studies, and the company Nanocyl has set a value of 0.0025 mg m⁻³ derived from a lowest observed adverse effect level (LOAEL) of 0.1 mg m⁻³ obtained from an inhalation study during 90 days. The company Swiss National Accident Insurance Fund established in 2011 a limit value for CNT of 0.01 fibres ml⁻¹.

Table 1.1 Recommended occupational exposure limits, proposed by different international organisations.

Nanomaterial	OEL	Reference
Fine TiO ₂ (< 2.5 µm)	2.4 mg m ⁻³	NIOSH
Ultrafine TiO ₂ (10 - 100 nm)	0.3 mg m ⁻³	(2011) ^a
CNTs and nanofibers	0.001 mg m ⁻³	NIOSH (2013) ^a
SiO ₂ fumes (<100 nm)	0.3 mg m ⁻³	ECHA (2015b) ^b
Rigid, biopersistent nanofibers for which effects similar to those of asbestos are not excluded ^c	0.01 fibres cm ⁻³	
Biopersistent granular nanomaterial (1-100nm; density > 6x10 ³ kg m ⁻³) ^d	2 x10 ⁴ cm ⁻³	SER (2012) ^g
Biopersistent granular nanomaterial (1-100nm; density < 6x10 ³ kg m ⁻³) ^e	4 x10 ⁴ cm ⁻³	
Non-biopersistent granular nanomaterials (1-100 nm) ^f	Applicable OEL	

^a Recommended Exposure Limit (REL); 8-h TWA concentrations during a 40-h workweek

^b Derived no-effect level (DNEL)

^c SWCNT or MWCNT or metal oxide fibres for which asbestos-like effects are not excluded

^d Ag, Au, CeO₂, CoO, Fe, Fe_xO_y, La, Pb, Sb₂O₅, SnO₂

^e Al₂O₃, SiO₂, TiN, TiO₂, ZnO, nanoclay carbon black, C₆₀, dendrimers, polystyrene nanofibers for which asbestos-like effects are excluded

^f Fats, NaCl

^g NRV background-corrected 8-h TWA concentrations

The National Institute for Occupational Safety and Health (NIOSH, 2011, 2013) has proposed a recommended exposure limit (REL) of 2.4 mg m⁻³ for fine TiO₂ (defined as < 2.5 µm diameter) and 0.3 mg m⁻³ for TiO₂ nanoparticles (10 - 100 nm) in workplace air on the basis of available toxicity data (IARC, 2010) and has established that the REL for CNT and nanofibers should be 1 µg m⁻³ (NIOSH, 2013).

The guidance of Regulation on registration, evaluation, authorisation and restriction of chemicals guidance (ECHA, 2015b) proposed a derived no-effect level (DNEL - inhalation for workers with long term exposure systemic effects) of 0.3 mg m⁻³ for

respirable SiO₂ fumes (CAS nr. 69012-64-2) which is likely to be in the nano-size range (<100 nm).

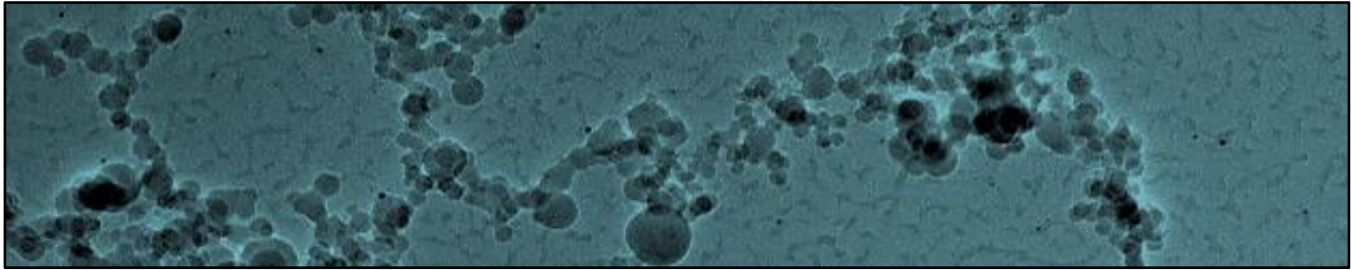
The German Institute for Occupational Safety and Health of the German Social Accident Insurance (IFA, 2009) introduced a particle number-based approach for recommended benchmark limits, arguing that the size and density of the nanoparticles must be employed as classification criteria for derivation of the recommended exposure limits. Based on the IFA-methodology, nano reference values (NRV) were developed by Social and Economic Council of the Netherlands (SER, 2012) regarding worker exposure to ENP. NRV are background-corrected 8-h TWA concentrations. According to SER (2012), for low-density biopersistent granular nanomaterials (density < 6 x 10³ kg m⁻³ such as Al₂O₃, SiO₂, ZnO, etc.) and for high-density biopersistent granular nanomaterials (density > 6 x 10³ kg m⁻³) such as Ag, Au, CeO₂, etc.), the NRV are 4 x 10⁴ cm⁻³ and 2 x 10⁴ cm⁻³, respectively. In general, only the pure metals have a density > 6 x 10³ kg m⁻³ (van Broekhuizen, 2012). For rigid, biopersistent nanofibers that possibly exhibit asbestos-like effects (e.g. SWCNT or MWCNT or metal oxide fibers), SER (2012) took the precautionary stand by using the asbestos OEL as a NRV.

The outcome of the discussions at the international workshop on NRV, which was organised by the Dutch trade unions and employers' organisations and hosted by the Social Economic Council in The Hague in September 2011 (van Broekhuizen *et al.*, 2012b) emphasised the need for a practical tool to assess short term exposure periods as well. For this a short-term NRV_{15-min TWA} was set. This NRV_{15-min TWA} can be derived from the NRV_{8-h TWA}, in analogy with the common risk management approach of the Dutch Labour Inspectorate for assessing short-term exposures to chemical substances:

$$\text{NRV}_{15\text{-min TWA}} = 2 \times \text{NRV}_{8\text{-h TWA}} \quad \text{Eq (3)}$$

NRV was recognised by Dutch authorities as the best available state of the art approach for risk assessment of nanomaterials (van Broekhuizen *et al.*, 2012b). It is clear that the quantitative nanomaterial exposure data is a key factor for the establishment of OEL (van Broekhuizen *et al.*, 2012a). Despite the fact that there have been multiple efforts to define OEL by several international organisations, they have had limited success to date due to the multiple different variants of each type of nanomaterial, all of which may differ in terms of toxicity and their impacts (Savolainen *et al.*, 2013).

Chapter 2. **SCOPE, OBJECTIVES AND STRUCTURE**



2. SCOPE, OBJECTIVES AND STRUCTURE

2.1 Scope and Objectives

The research described in the previous chapter constitutes the state of the art with regard to the characterisation of worker exposure to airborne nanoparticles in industrial settings. However, significant gaps still remain and should be addressed:

- Relevant ENP and PGNP exposure studies are relatively scarce under real-world conditions. As discussed previously, this is associated to the complexity of emissions and factors in industrial workplaces, the need for integrated instrumental approaches and the difficulty of accurately discriminating background aerosol contributions (Brouwer, 2010; Kuhlbusch *et al.*, 2011b; Savolainen *et al.*, 2013).
- Exposure scenarios of PGNP from industrial processes not dealing with ENP as input materials are even scarcer and need to be thoroughly investigated (van Broekhuizen, 2012). The identification and chemical characterisation of PGNP is highly complex due to their (frequently) secondary nature and non-specificity of nanoparticle types and sources.
- The lack of specific online instrumentation for the targeted detection of nanoparticles in real time (Savolainen *et al.*, 2013).

This PhD thesis has been designed to contribute this field of research and aims to reduce existing knowledge gaps by pursuing the following objectives:

1. To assess the performance of novel instrumentation for nanoscale aerosol measurements (portable SMPS NanoScan TSI 3910 and cascade impactors such as nano-BLPI and nano-Moudi).
2. To identify and characterise nanoparticle formation and exposure scenarios in specific industrial settings dealing with ENP. These assessments will be carried out under real-world operating conditions and will be representative of actual worker exposures. Where possible, the effectiveness of mitigation strategies in place will be assessed.
3. To identify and characterise nanoparticle formation and exposure scenarios in specific industrial settings dealing with PGNP. As in the previous objective, the industrial settings under study will be representative of actual worker exposure. Mitigation strategies will be proposed where necessary and assessed when already in place.

2.2 Structure of the thesis

Following this introductory overview, the methodology section describes the monitoring sites in detail, and outlines the measurement strategy and data processing adopted to reach the aforementioned objectives. Results are presented in chapter 4 in form of five research articles published per chronological order in peer-reviewed journals. In chapter 5, a summary discussion of the main findings and how the findings relate to each other is presented, followed by the main conclusions of this thesis and a brief discussion concerning the limitations of the work presented and future research directions. Finally, the founding sources and literature references are listed. At the end of this PhD thesis, an annex that lists the abbreviations, acronyms, and symbols, is included.

The publications included in this PhD thesis are reproduced with the permission of the journals concerned and are briefly described below:

- **Article I:** Fonseca, A. S., Viitanen, A. K., Koivisto, A. J., Kangas, A., Huhtiniemi, M., Hussein, T., Vanhala, E., Viana, M., Querol, X., Hämeri, K. **Characterization of Exposure to Carbon Nanotubes in an Industrial Setting.** *Ann Occup Hyg.* (2015) Jun; 59(5):586-99. doi: 10.1093/annhyg/meu110. Epub 2014 Dec 24. PubMed PMID: 25539647.

In this study, worker exposure to SWCNT during the production of conductive films in a modern up-scaling factory in Helsinki (Finland) was assessed. Particulate matter concentrations (2.5 - 10 μm) and concentrations of CO and CO₂ were monitored by using real-time instruments. Worker exposure levels to SWCNT were qualitatively estimated by analysing particle samples by TEM.

- **Article II:** Fonseca, A. S., Viana, M., Querol, X., Moreno, N., de Francisco, I., Estepa, C., de la Fuente, G. F. **Ultrafine and nanoparticle formation and emission mechanisms during laser processing of ceramic materials.** *Journal of Aerosol Science*, (2015) October; Volume 88, Pages 48-57, ISSN 0021-8502. <http://dx.doi.org/10.1016/j.jaerosci.2015.05.013>

Ultrafine and nanoparticle emissions during processes with potential for unintentional nanoparticle release in the ceramic industry were addressed in this work. Nanoparticle release mechanisms and their impact on exposure in workplace air are characterised in a selected number of release scenarios. For this, real-time and size-resolved particle number, mass, and particle size diameter were determined by using different instrumentation (size range 5 nm - 20 μm) simultaneously at the emission source, in the worker breathing zone, and in outdoor air.

- **Article III:** Fonseca, A. S., Maragkidou, A., Viana, M., Querol, X., Hämeri, K., de Francisco, I., Estepa, C., Borrell, C., Lennikov, V., de la Fuente, G. F. **Process-generated nanoparticles from ceramic tile sintering: Emissions, exposure and environmental release**, *Sci Total Environ* (2016).

<http://dx.doi.org/10.1016/j.scitotenv.2016.01.106>

This work identified the particle formation and release mechanisms, and their impact on personal exposure and the environment during a tile sintering process using a high power CO₂ laser in an industrial up-scaling process, as a follow-up of a previous study in a laboratory-scale plant. In addition, particle transformations in the exhaust system, the potential for particle release to the outdoor environment, and the effectiveness of the filtration system were assessed.

- **Article IV:** Fonseca, A. S., Viana, M., Pérez, N., Alastuey, A., Querol, X., Kaminski, H., Todea, A. M., Monz, C., Asbach, C. **Intercomparison of a portable and two stationary mobility particle sizers for nanoscale aerosol measurements**. (2016) *Aerosol Science & Technology*.

<http://dx.doi.org/10.1080/02786826.2016.1174329>.

The purpose of this study was to compare the performance of the portable NanoScan SMPS TSI 3910 with that of two stationary SMPS instruments and one ultrafine condensation particle counter in a controlled atmosphere and for different particle types (covering a wide range of particle sizes and morphologies) and particle concentrations.

- **Article V:** Fonseca, A. S., Talbot, N., Schwarz, J., Ondráček, J., Ždímal, V., Kozáková, J., Viana, M., karanasiou, A., Querol, X., Alastuey, A., Vu, T. V., Delgado-Saborit, J. M., Harrison, R. M. **Intercomparison of four different cascade impactors for fine and ultrafine particle sampling in two European locations**. *Atmos. Chem. Phys. Discuss.*, 2016, 1-27. doi: 10.5194/acp-2015-1016

The performance of 4 conventional and nano-range cascade impactors (BLPI, nano-BLPI, nano-Moudi and PCIS) was assessed, by means of two intercomparison exercises in 2 European locations (Prague, during winter 2015 and Barcelona during summer 2015) was undertaken. The aim of the campaigns was to test the instruments' performance with regard to the particle mass size distributions under different aerosol compositions resulting from different emission sources, meteorology and seasons.

Chapter 3. **METHODOLOGY**



3. METHODOLOGY

This section describes the instrumentation and strategy adopted during measurements carried out in two types of environments: (i) nanotechnology-related workplaces; and (ii) non-nanotechnology related industrial facilities. A multi-instrument approach, as suggested by Brouwer *et al.* (2012), was used to characterise source-specific worker exposure in order to cover the most relevant metrics and physicochemical characteristics for nanoparticles.

3.1 Monitoring sites and exposure scenarios

The experimental campaigns in this PhD thesis were carried out in three industries: one nanotechnology-related plant located in Helsinki (Finland), and two non-nanotechnology-related plants located in Zaragoza (Spain). These environments provide widely different opportunities to study nanoparticle release, worker exposure and particle formation mechanisms under real-world conditions. Table 3.1 describes each monitoring site and exposure scenarios.

Table 3.1 Description of the monitoring sites and exposure scenarios.

City	Site	Sampling period	Sampling locations	Target activities	Target particles
Helsinki (Finland) ¹	Modern up-scaling factory	Eight consecutive days in May 2013	Between the collection chamber and the worker at face level	<ul style="list-style-type: none"> ▪ Manufacturing of SWCNT films using LEV ▪ Manufacturing one SWCNT film without LEV ▪ Reactor cleaning 	SWCNT
Zaragoza (Spain) ²	Laboratory scale furnace (length = 3 m)	Three consecutive days in October 2013	Emission source (furnace), in the worker breathing zone, and in outdoor air	<ul style="list-style-type: none"> ▪ Laser-based tile sintering process ▪ Laser-based tile ablation process 	PGNP
Zaragoza (Spain) ³	Industrial pilot plant scale furnace (length = 7 m)	Six consecutive days in January 2015	Emission source (furnace), in the worker breathing zone and in three locations along the exhaust tube connecting the emission source to outdoor air	<ul style="list-style-type: none"> ▪ Laser-based tile sintering process 	PGNP

¹ Article I (Fonseca *et al.*, 2015c); ² Article II (Fonseca *et al.*, 2015a); ³ Article III (Fonseca *et al.*, 2016); SWCNT: Single-walled carbon nanotubes; PGNP: Process-generated nanoparticles; LEV: Local exhaust ventilation

3.1.1 SWCNT manufacturing

At the up-scaling factory in Helsinki (Finland) (Article I), SWCNT were produced in a high temperature furnace where carbon monoxide (CO) and iron (Fe) seed particles were introduced. The factory produces annually $\sim 1 \times 10^4$ SWCNT films and employs 20 people. From the reactor where they were synthesised, SWCNT were directed: (i) during collection to the deposition chamber and through a collector filter to the exhaust; and (ii) during filter change to the exhaust. Potential SWCNT emissions

were assumed to potentially occur during: (i) reactor collection chamber opening during normal operation with LEV; (ii) manufacturing SWCNT film without LEV; and (iii) reactor cleaning.

3.1.2 Ceramic tile sintering and ablation

Laser sintering and ablation of ceramic tiles (Article II and III) are innovative high-energy techniques used in the ceramic industry, which have a large potential for global-scale implementation in real-world ceramic industrial facilities. While laser sintering of tiles provides numerous advantages such as speed, temperature and enhanced durability and surface properties of structural materials (de Francisco *et al.*, 2011; Estepa and Fuente, 2006; Gutiérrez Mora *et al.*, 2009; Larrea *et al.*, 2002; Lennikov *et al.*, 2010; Lennikov *et al.*, 2004; Lennikov *et al.*, 2007; Mora *et al.*, 2003) laser ablation is applied to produce engravings on the ceramic tiles by expelling material from a solid surface by irradiating it with a pulsed laser beam (Bäuerle, 1996; Lahoz *et al.*, 2011; Rubahn, 1999). A schematic representation of the physico-chemical processes taking place during tile sintering is shown in Figure 3.1.

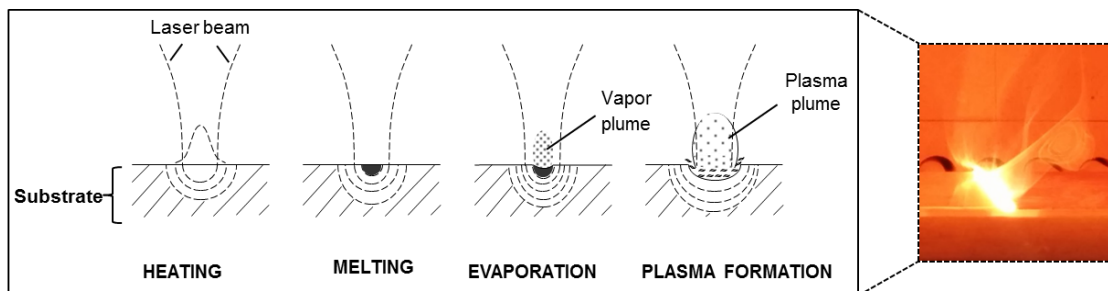


Figure 3.1 Physico-chemical processes occurring during sintering of ceramic tiles. Source: Fonseca *et al.* (2015b); modified from de la Fuente (2013).

Figure 3.2 shows an illustration of laser ablation effects (i.e., presence of a melted layer at the surface of the tile where the laser is irradiating). Because of their high-energy nature, these processes have a significant potential to generate fugitive ultrafine and nanoparticle emissions into the workplace air, influencing the levels of particle concentrations and subsequently worker exposure. Particle emissions and worker exposure were assessed for six different types of frequently used tiles in the industry during laser sintering and for one type of material (raw porcelain) during ablation.

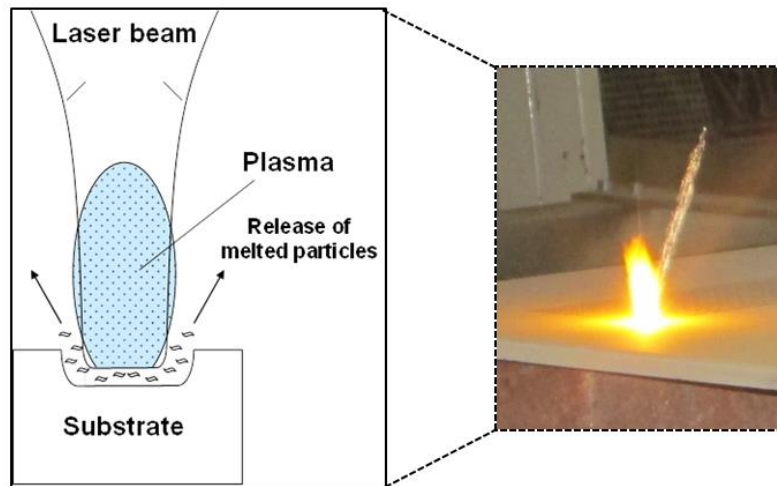


Figure 3.2 Schematic representation of the ablation process. Source: Fonseca et al. (2015b); modified from de la Fuente (2013).

3.2 Measurement instrumentation and techniques

This section presents the instrumentation and techniques applied during each exposure scenario in the framework of this PhD thesis. The following Table 3.2, describes the instrumentation used in each monitoring sites and exposure scenario (Table 3.1) along with the metric which is most frequently used, the size range of particles in which the instrument is expected to provide a reliable performance, and the indirect estimation of other metrics (if available), based on the hypothesis of the relationship between particle number, surface area, and mass.

Table 3.2 Online instrumentation.

Instrument	Metric	Size range	Calculated metric	References	Deployed in exposure scenarios
CPC	<i>N</i>	2.5 nm - >3 μm^{a}	N/A	(Agarwal and Sem, 1980; Hermann <i>et al.</i> , 2007; Wiedensohler <i>et al.</i> , 1997)	Article I and II
Handheld CPC	<i>N</i>	10nm - >1 μm^{b}	N/A	(Matson <i>et al.</i> , 2004; TSI, 2007)	Article I
Stationary SMPS	<i>PSD</i> (based on mobility diameter)	2.5 nm - 1 μm^{c}	<i>M</i> , <i>SA</i> ^d	(Hoppel, 1978; Wang and Flagan, 1990)	Article IV
Portable SMPS (NanoScan SMPS TSI 3910)	<i>PSD</i> (based on mobility diameter)	10-420 nm	<i>M</i> , <i>SA</i> ^d	(Tritscher <i>et al.</i> , 2013)	N/A*
Diffusion charger (DiSCmini)	<i>N</i> , <i>LDSA</i> or <i>D_p</i> or a combination thereof	10 - 700 nm	N/A	(Fierz <i>et al.</i> , 2011; Fierz <i>et al.</i> , 2009)	Article I, II and III
ELPI™	<i>PSD</i> (based on aerodynamic diameter)	6 nm - 10 μm^{c}	<i>M</i> , <i>SA</i> ^e	(Järvinen <i>et al.</i> , 2014; Keskinen <i>et al.</i> , 1992)	Article I
Optical particle sizers (Grimm Model 1.108 and OPS TSI Model 3330)	<i>N</i> , <i>PSD</i> (based on light scattering equivalent diameter)	> 300 nm - 20 μm^{c}	<i>M</i>	(Baron and Willeke, 2001; Burkart <i>et al.</i> , 2010; Grimm and Eatough, 2009; Heim <i>et al.</i> , 2008; Peters <i>et al.</i> , 2006; Yamada <i>et al.</i> , 2015)	Article I, Article II and III
Aerosol photometers (DustTrak™ DRX TSI Model 8533)	<i>PM₁</i> , <i>PM_{2.5}</i> , <i>PM₄</i> and <i>PM₁₀</i>	0.1-15 μm and 0.001 to 150 mg m^{-3}	N/A	(Baron and Willeke, 2001; TSI, 2013a; Wang <i>et al.</i> , 2009)	Article II and III

N/A: Not applicable; *N* = Total particle number concentration; *M* = Total particle mass concentration; *PSD* = Particle number size distribution; *LDSA* = Lung deposited surface area concentration; *D_p* = Mean particle diameter; *SA* = Surface area concentration; *PM₁*, *PM_{2.5}*, *PM₄*, *PM₁₀* = particulate matter < 1, 2.5, 4 and 10 μm , respectively

^aUltrafine butanol condensation particle counter (UCPC, TSI Model 3776)

^b Isopropanol condensation particle counter (CPC, TSI Model 3007)

^c Varying depending on the model

^d Size-selective particle number concentration sampling, enables determination of geometric surface area concentration of spherical particles (Asbach *et al.*, 2009b)

^e Surface area estimation based on the fractal dimensions of the particles (Rogak *et al.*, 1993). By putting ELPI (aerodynamic diameter) and SMPS (mobility diameter) in series the fractal dimensions can be calculated and verified by electron analysis

*Used for an intercomparison study (Article IV)

3.2.1 Nanoparticle monitoring

- Condensation Particle Counter (CPC)

The total particle number concentration was measured from 2.5 nm to 3 μm (Article I) and from 5 nm to over 3 μm (Article II) with two different water-based CPC (N-WCPC TSI Model 3788 shown in Figure 3.3 and, WCPC TSI Model 3785, respectively). In addition, a portable CPC (TSI, Model 3007; Figure 1.8a) was used in Article I to identify local particle sources in the size range between 10 nm and over 1 μm (Tier 1 of the tiered approach for exposure assessment described in previous chapter 1.2.3.1). The aerosol enters the sample inlet and reaches a wetted soaked by either water or butanol, depending on the model. Due to the heater saturator and the

following cooler condenser, the liquid condenses onto the particles causing them to grow or "*amplify*" their size to a value that can be detected easily with a conventional optical system. Particle counters provide time-resolved and size-integrated particle concentration data.

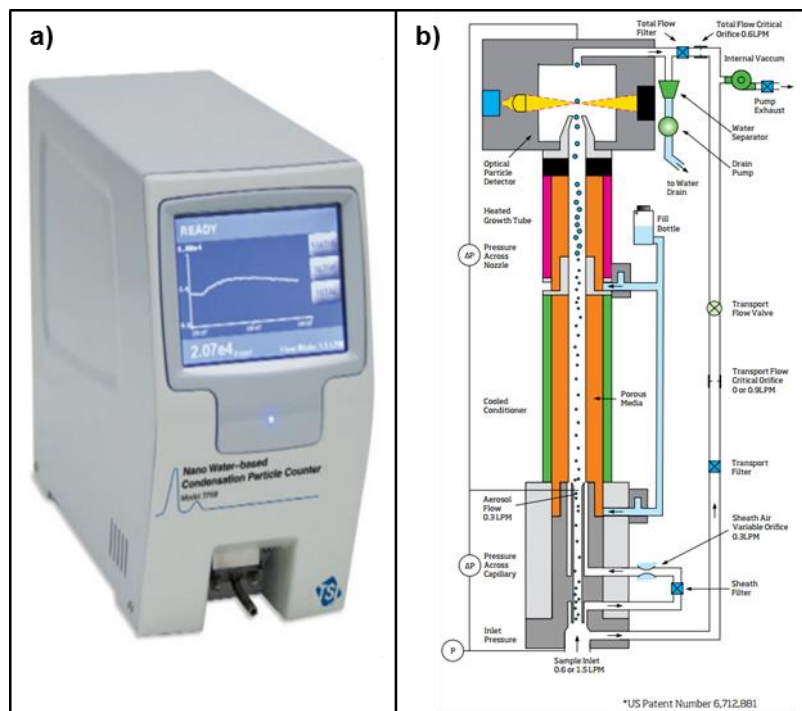


Figure 3.3 Condensation particle counter: a) nano-water based CPC (N-WCPC Model 3788); b) schematic operational principle. Source: TSI (2012a).

- Portable and stationary SMPS

Particle number mobility size distributions were measured with a mobility particle size spectrometer, also known as a scanning mobility particle sizer (SMPS; Wang and Flagan, 1989, 1990). This instrument consists of a differential mobility analyser (DMA) connected to a CPC. Ambient air is pumped through the sampling inlet, reaching a bipolar charger or neutralizer, which is usually a radioactive source such as Kr^{85} . Following neutralisation, aerosols enter the DMA (Chen *et al.*, 1998; Fissan *et al.*, 1996; Knutson and Whitby, 1975; Winklmayr *et al.*, 1991), where they are classified according to their electrical mobility (Wang and Flagan, 1990). The selected monodisperse aerosols exit the DMA and reach the CPC (Agarwal and Sem, 1980), where their number concentration is determined for a specific size range. The main limitation of SMPS systems in workplace applications is their size, weight, and complexity of operation and also the need for radioactive chargers to neutralize the incoming aerosol. In some European countries, the presence of an internal radioactive source restricts its use in occupational exposure studies (Ostraat *et al.*, 2015). Only recently, an X-ray neutralizer became available to replace the radioactive source.

Therefore, a novel portable nanoparticle sizing and counting instrument (NanoScan SMPS TSI 3910; Tritscher *et al.*, 2013) which was recently commercialised, was used in this thesis (Article I, II and III) for real-time mobility particle size distributions within the range from 10 to 420 nm in 13 channels (Figure 3.4). This device incorporates a non-radioactive unipolar diffusion charger (corona jet type) (Medved *et al.*, 2000), a radial differential mobility analyser (rDMA, Zhang *et al.*, 1995; Fissan *et al.*, 1998) and an isopropanol-based CPC. The main advantage of this instrument is its portability (< 9 kg), battery operation without the need to use power supply, small size (LxWxH = 45x23x39 cm), and the use of a nonradioactive unipolar charger which makes it an interesting monitor for real-time workplace measurements without the transport and application restrictions currently affecting traditional SMPS instruments. Another advantage is the use of isopropanol instead of butanol as a working fluid since it is a relatively benign chemical when compared to butanol (TSI, 2015).

Both the stationary SMPS and NanoScan SMPS instruments, as well as the ELPI (described below), provide time and size-resolved particle concentration data.

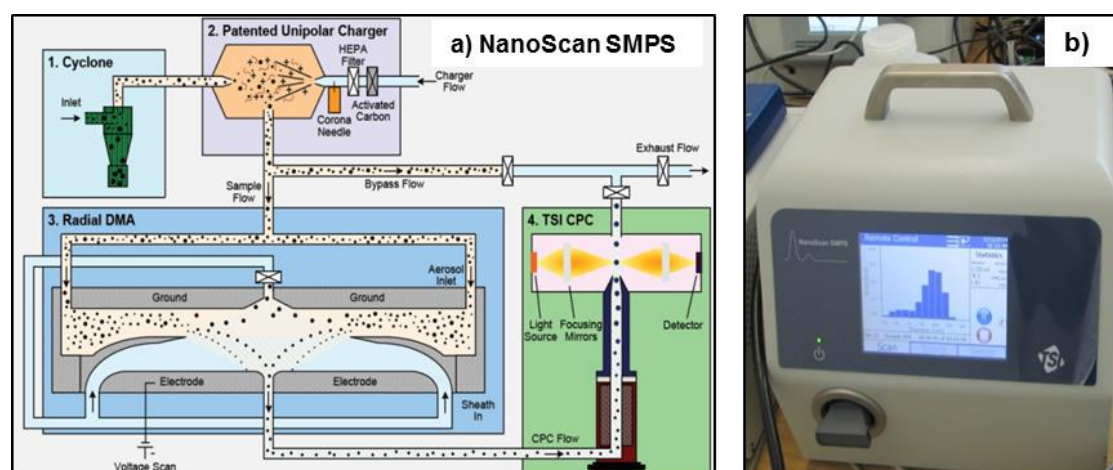


Figure 3.4 Electrical mobility spectrometer for measuring online particle number particle concentration: a) schematic diagram of the functioning of the NanoScan SMPS TSI 3910 (Source: TSI, 2012); b) NanoScan SMPS TSI 3910.

- Diffusion Size Classifier Miniature (DiSCmini)

The miniature diffusion size classifier (DiSCmini Matter Aerosol shown in Figure 3.5a; Fierz *et al.*, 2011) was used in Articles II and III to measure total particle number, mean particle diameter, and the LDSA of particles in the size range of 10-700 nm. This instrument is based on unipolar charging of the particle (corona charger), followed by the removal of excess ions in the ion trap and the particle detection in two electrometer stages (diffusion and filter), allowing for particle sizing and counting. A schematic operation principle of DiSCmini is shown in Figure 3.5b and is detailed

by Fierz *et al.* (2011). It should be noted that DiScmini instrument is calibrated with monodisperse aerosol, and the instrument response for polydisperse aerosols with a lognormal size distribution with a geometric standard deviation $\sigma = 1.9$ is then calculated (Fierz, 2010). As a result, for aerosols that do not match this size distribution, errors may occur both in the number and particle diameter calculation. Furthermore, this instrument was used exclusively with tygon tube ($\frac{1}{4}$ inch inner diameter, approximately 30 cm in length) since the use of different tubing such as conductive black silicone tubing, have resulted in technical failures as corona voltage increases and LDSA concentration decreases (Asbach *et al.*, 2015).

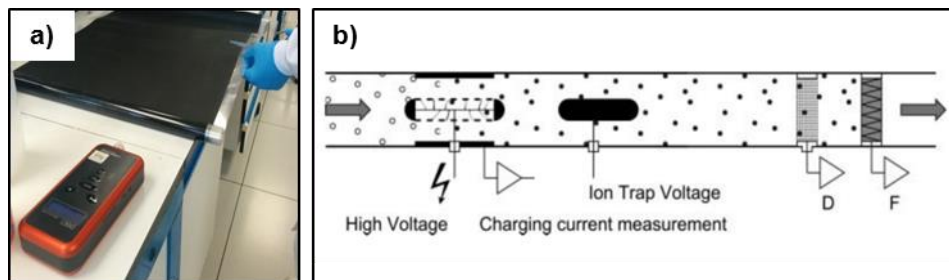


Figure 3.5 Diffusion size classifier miniature: a) Workplace measurements with DiScmini and, b) schematic operational principle where D = diffusion stage and F = filter stage. Source: Fierz *et al.* (2011).

- Electrical low-pressure impactor (ELPI)

Aerosol particles may be also classified according to their inertia by size impaction. The mechanical principle behind size impaction employs the known quantities of Stokes number and slip correction factors to derive particle inertia, therefore ascribing a stopping

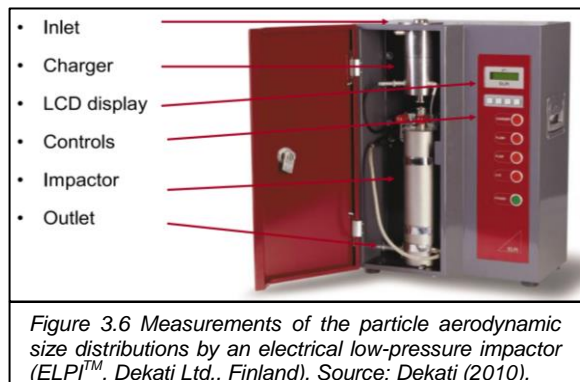


Figure 3.6 Measurements of the particle aerodynamic size distributions by an electrical low-pressure impactor (ELPI™, Dekati Ltd., Finland). Source: Dekati (2010).

distance in accordance to particle size (Hinds, 1999). This metric is called as aerodynamic diameter. In this work, the particle number concentrations and aerodynamic size distributions from 7 nm to 10 μm were measured in Article I by a 13 stages ELPI™ (Dekati Ltd., Finland; Keskinen *et al.*, 1992; Järvinen *et al.*, 2014; Figure 3.6). The operating principle is based on particle charging with a unipolar diffusion charger (corona charger), preceding the particles size classification in the cascade impactor and subsequently, the electrical charge carried by particles are detected in real time with multi-channel electrometers. Particle number units were afterwards converted to mass units by assuming unit density (1 g cm^{-3}) and spherical shape. Even though filter samples were obtained with the ELPI, then were not subsequently analysed in the framework of this PhD thesis.

- Optical particle sizers and aerosol photometers

In optical sizers, such as the optical particle sizers (OPS, TSI Model 3330) single particle scatters light which is collected and measured with a photodetector, where it is converted to a proportional voltage pulse (McMurry, 2000). The scattering light pulse of every single particle is counted and the intensity of its scattering light signal classified to a certain particle size. An example of the measuring principle is schematically shown in Figure 3.7.

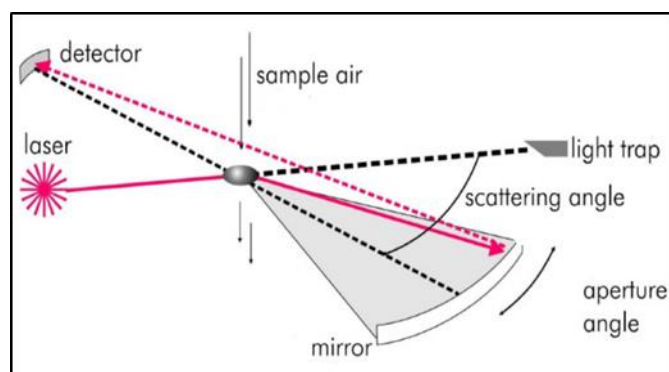


Figure 3.7 Schematic operational principle of a photodetector. Source: Grimm (2007).

The pulse height depends strongly on particle size, shape, and refractive index (Sorensen, 2001). In this PhD thesis, online measurements of the optical particle size distributions from 0.3 to 10 μm (within 16 channels) were performed by an OPS in Articles I and II and by an optical particle counter (OPC; Grimm Model 1.108 shown in Figure 1.7d) from 0.3 to 20 μm (within 15 channels) in articles II and III, which were converted to mass units using particle density-based equation. In addition, determination of the mass fraction concentrations (PM_{10} , $\text{PM}_{2.5}$, PM_1) were monitored continuously by a light-scattering laser photometer (DustTrak™ DRX aerosol monitor TSI, Model 8533; Figure 1.7e) in Article II.

3.2.2 Nanoparticle collection on filter substrates

Size fractionated of particles ($< 0.25 \mu\text{m}$; $0.25\text{-}2.5 \mu\text{m}$ and $>2.5 \mu\text{m}$) were collected in Article II by personal cascade impactor samplers (Sioutas™ PCIS, SKC Inc.; Misra *et al.*, 2002; Figure 3.8a) operating with a flow rate of 9 L min^{-1} at a pressure drop of 11 inches of H_2O (2.7 kPa). The collection substrates were 37 mm quartz fibre filters (Pall) for the $< 0.25 \mu\text{m}$ stage and 25 mm polytetrafluoroethylene filters (PTFE) for the $0.25\text{-}2.5 \mu\text{m}$ and $>2.5 \mu\text{m}$ stages.

Additionally, in Articles II and III, particles were collected on 25 mm polycarbonate filters Orthopore™, with $0.8 \mu\text{m}$ pore size. Samples were collected using 3-piece conductive polypropylene air sampling cassettes (SKC Inc., inlet diameter 1/8 inch;

Figure 3.8b) connected to SKC Leland Legacy pumps operating between 3.5 L min^{-1} and 6 L min^{-1} .

Particle mass concentrations were gravimetrically determined by pre- and post-weighing the filters with a Mettler MT5 electronic microbalance with a $\pm 1 \mu\text{g}$ sensitivity and taking into account the known volume of air sampled. From every batch of ten filters, two were stored to be used as laboratory blanks. All samples were equilibrated for a period of 24-h before weighing in a temperature and relative humidity controlled room. Each sample was weighed three times with an accuracy of mass determination of $\pm 2 \mu\text{g}$. After weighing, the sampled filters were stored in the freezer at $-18 \text{ }^\circ\text{C}$ for subsequent chemical characterisation (details in section 3.2.3).

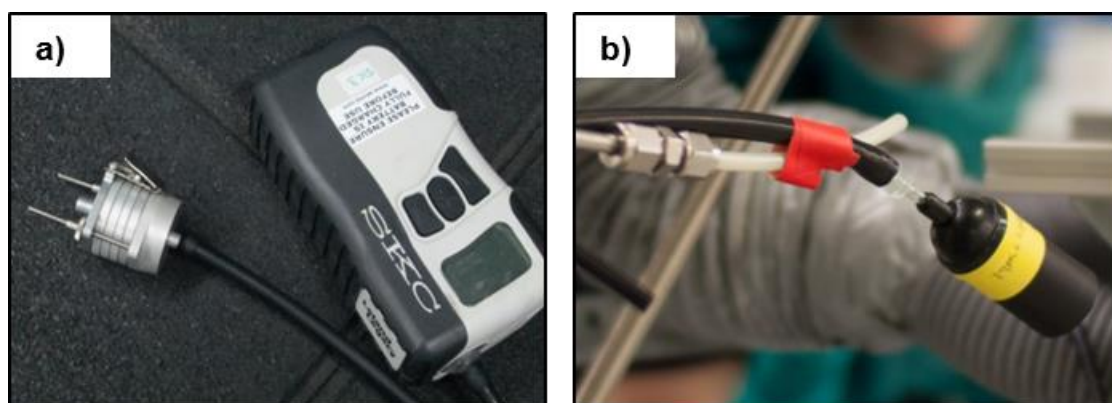


Figure 3.8 Filter collection by: a) personal cascade impactor sampler (Sioutas™ PCIS, SKC Inc.), and b) air sampling cassettes (SKC Inc.).

3.2.3 Chemical characterisation of collected particles

Once the gravimetric determination of the particle mass concentration was performed, an acid digestion of the particles collected on the filters was carried out, following the methodology described by Querol *et al.* (2001). It consists in a complete dissolution of the sample by means of an acid digestion by using nitric acid (HNO_3), hydrofluoric acid (HF) and perchloric acid (HClO_4) for the analysis of major and trace elements by means of ICP-AES (IRIS Advantage TJA Solutions, THERMO) and ICP-MS (X Series II, THERMO), respectively. Bulk concentrations of major elements (Al, Ca, K, Fe, P, Na, S, Mg, Ba, Cu, Mn, Ni, Sr, Pb, Ti, V, Zn) and trace elements (Li, Sc, Ti, V, Cr, Mn, Co, Ni, Cu, Zn, Ga, Ge, As, Se, Rb, Sr, Y, Zr, Nb, Mo, Cd, Sn, Sb, Cs, Ba, La, Ce, Pr, Nd, Gd, Hf, Ta, W, Tl, Pb, Bi, Th, U) were determined in the solution. Laboratory blank filters were analysed following the same procedure. Element concentrations were blank corrected.

The average precision and accuracy for most of the elements fell under the expected analytical errors (in the range of 1-10%), and were checked by repeated analysis of NIST - 1633b (fly ash) reference material.

3.2.4 Electron microscopy

TEM-EDX was used to characterise particle size, morphology and chemical composition of nanoparticles. Samples for TEM were collected directly onto Au or Cu grids. TEM grids were attached (as shown in Figure 3.9a) to the air sampling cassettes described above (SKC Inc., USA, inlet diameter 1/8 inch and filter diameter 25 mm) on mixed cellulose ester (MCE; Article I for SWCNT) or polycarbonate membrane filters with 0.8 μm pore size (Articles II and III during sintering and ablation of ceramic tiles). In addition, during an intercomparison study between a portable NanoScan SMPS and a stationary SMPS (described below), the TEM grids were attached to the electrostatic precipitator shown in Figure 3.9b (NAS; TSI, Model 3089; Li *et al.*, 2010; TSI, 2013b; Dixkens and Fissan, 1999) and charged particles in the range from 2 - 100 nm were sampled.

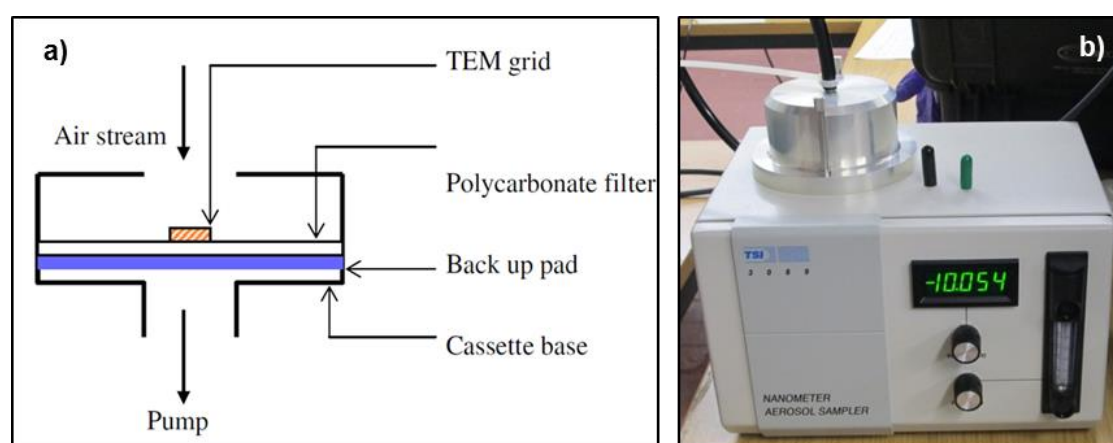


Figure 3.9 TEM grid sampler: a) air sampling cassettes (Tsai *et al.*, 2008) and b) nanometer aerosol sampler (NAS; TSI, Model 3089).

3.2.5 Instrumental and technical limitations

Major limitations of instruments and techniques which have been identified so far include the following:

- **SMPS:** the main limitation of SMPS systems in workplace applications is their size, size, weight, and complexity of operation, and also the need for radioactive chargers to neutralize the incoming aerosol. In some European countries, the presence of an internal radioactive source restricts its use to laboratory applications (Ostraat *et al.*, 2015). Only recently, an X-ray neutralizer became available to replace the radioactive source. In addition, the SMPS has a scanning time of at least 3 minutes, resulting inadequate to monitor dynamic processes. The alternative to SMPS systems is a portable version of SMPS (NanoScan SMPS TSI 3910) which has been tested by Stabile *et al.* (2014) and in the present PhD thesis by Article IV.

- **Diffusion chargers:** direct measurement of the particle number or surface area concentration is not always feasible as in the case of fibres, highly porous nanoparticles, and highly irregular morphologies. It presents accuracy of around $\pm 30\%$ and an increase of measurement error for particles > 400 nm has been registered (Ostraat *et al.*, 2015).
- **Optical particle sizers and aerosol photometers:** their applicable particle size range is outside the nanoscale.
- **ELPI:** this instrument is voluminous and presents similar practical limitations (size and weight) as the SMPS.
- **Cascade impactors:** impactors allow for personal or static sampling with a range of particle size cut points but lacking real-time data output (Berner and Luerzer, 1980; Berner *et al.*, 1979; Hering *et al.*, 1978; Hillamo and Kauppinen, 1991; Preining and Berner, 1979). As with mass-based samplers, it is important to collect sufficient material on each stage to allow for adequate quantification without overloading the upper collection stages. Particle bounce may be an issue, reducing the resolution and accuracy of the size bins. Common approaches to avoid particle overloading include using multiple-orifice collection stages, rotating collection substrates (Marple *et al.*, 2014; Marple *et al.*, 1991), and using coated and/or porous collection substrates.
- **TEM and SEM** analysis can be compromised if there is particle overload on the filter. If the loading is too sparse, an accurate assessment of particle characteristics may not be possible. Both techniques are not quantitative.

3.3 Instrument intercomparisons

In order to ensure the agreement between all the instruments deployed in the different experimental campaigns, instrument intercomparisons are required. A number of factors may affect data compatibility including the size ranges, averaging times, principles of operation, etc. The performance of the instruments employed was assessed with ambient air side by side prior each of the sampling campaigns during a minimum of 12h. With the results of these intercomparisons exercises, the correct operation of all the devices was verified and, if needed, correction factors were obtained to adjust the measurements to each other.

As already mentioned, in order to overcome the current lack of specific instrumentation for characterisation of nanoparticles and related personal exposure (Savolainen *et al.*, 2013) new instruments are being currently developed and

comparisons with other instrumentation is still scarce. This is the case of the novel portable NanoScan SMPS TSI 3910 and several cascade impactors enabling the collection of ultrafine particles (≤ 100 nm).

In order to assess the suitability of the NanoScan SMPS TSI 3910 instrument for occupational exposure studies and determine the reproducibility of data provided and study how it relates to other sampling instruments, an intercomparison study of the performance of this portable SMPS with that of two stationary SMPS instruments (with a long and a nano DMA; SMPS-L and SMPS-N) and one ultrafine butanol condensation particle counter (UCPC) in a controlled atmosphere (Figure 3.10a) and for different particle types (Figure 3.10b, c and d), was undertaken in Article IV. The instruments were simultaneously challenged with intentionally produced particles covering a wide range of particle sizes and morphologies: di-ethyl-hexyl-sebacate (DEHS; spherical), sodium chloride (NaCl; cubic or near spherical shape), and agglomerates as ZnO, spark generated soot and diesel soot particles (Kaminski *et al.*, 2013).

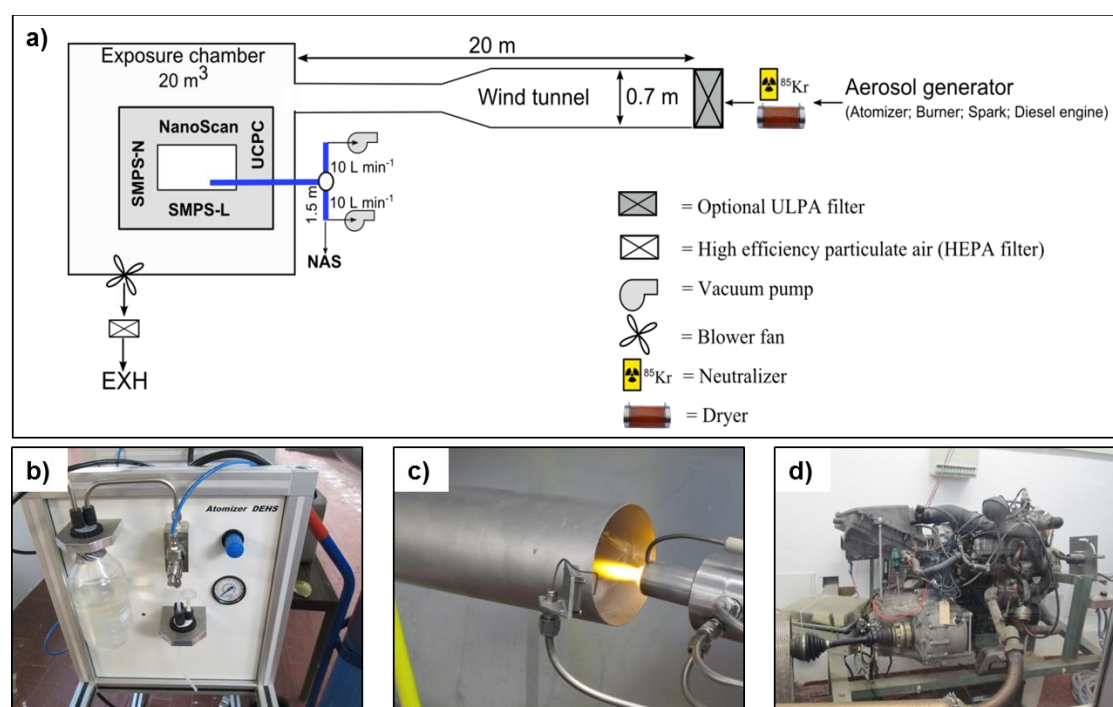


Figure 3.10 Figures illustrating: a) Experimental setup; b) home-made atomizer for DEHS and NaCl particles generation; c) burner generator (FG2, MoTec Konzepte, Bochum Germany) of NaCl and ZnO particles; and d) diesel engine (aspiration type, 2180 cm³, Mercedes Benz 220D, 44 kW at 4200 rotations min⁻¹) for diesel soot particles generation

Finally, to the authors' knowledge there has been no field campaign to-date intercomparing impactor collection efficiency for the nanoparticle size range. Article V in this PhD thesis seeks to address this knowledge gap by assessing the

performance of a number of conventional and nano-range impactors (Figure 3.11), namely BLPI (26 nm - 13.5 μm , 25/0.018/2, Hauke, Austria), nano-BLPI (11 nm - 1.95 μm , 10/0,01, Hauke, Austria), nano-Moudi (10 nm-18 μm , MSP Corp., Shoreview, MN, USA Model 125R; U.S. Patent # 6,431,014B1) and PCIS (< 250 nm - 10 μm , SKC Inc.; Misra *et al.*, 2002), by means of two intercomparison exercises.

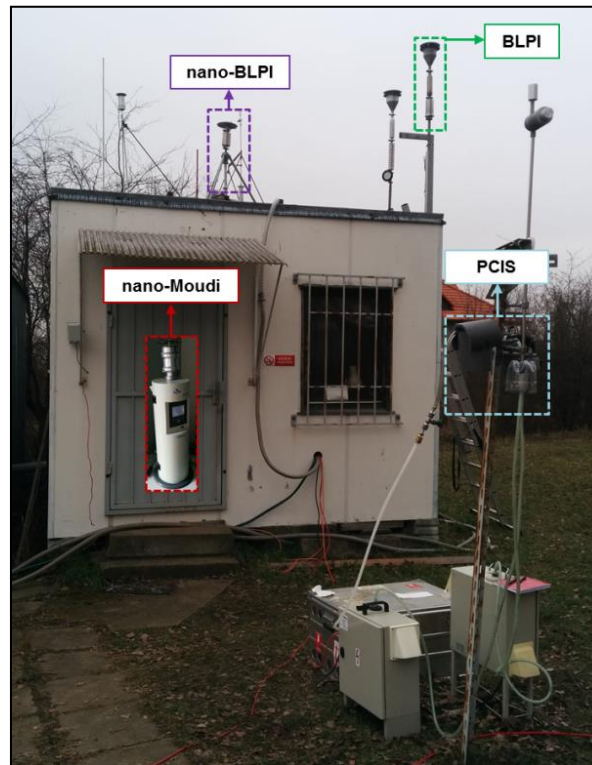


Figure 3.11 Cascade impactors deployed in outdoor during winter in Prague (Czech Republic).

The aim of the campaigns was to test the instruments' performance under different environmental conditions and aerosol loads and types. This study reports on the impactor performances not only with regard to different particle size distributions but also to aerosol composition.

3.4 Measurement strategy

The measurement strategy adopted in the framework of this PhD thesis followed the tiered approach described in previous chapter 1.2.3 and included exposure assessment, exposure control measures and their effectiveness, and compliance with recommended occupational exposure limits.

3.4.1 Personal task-based vs. full shift exposure assessment

Personal task-based (Article I; SWCNT manufacturing without LEV and reactor cleaning activity) as well as full shift-based exposure assessment approaches

(Articles II and III) were applied. Task-based exposure assessment (where samples are collected through the length of a task) allowed for the evaluation of the contribution of specific tasks to overall exposure and thus helps the implementation of control measures on the major source/task (Brouwer *et al.*, 2012; Ramachandran *et al.*, 2011). In addition, simultaneously data was collected over full shifts. Based on these data worker daily exposures (usually 8-h TWA) may be estimated and compared with occupational exposure limits, based on 8-h TWA concentrations.

3.4.2 Multi-instrument approach

Based on the assessment of worker exposures to nanoparticles in different industrial settings, a multi-instrument approach was adopted in which CPC or DiSCmini were used to identify potential sources of emissions (and background sources), an SMPS or ELPI was used to characterise size distributions and how these vary as a function of time or space, combined with collected filters and TEM samples to characterise the chemical and physical form of nanoparticles in the workplace.

3.4.3 Sampling locations

All the sampling inlets were placed close to the emission source, next to worker at the height of the nose and open mouth of the workers “*breathing zone*” (Brouwer *et al.*, 2009), and where possible in outdoor air. Measurements at the emission source allowed for the determination of nanoparticle release and identification of locations most likely to result in worker exposure and possible need for controls. Only data acquired at the breathing zone was considered representative of worker exposure.

3.4.4 Background distinction

Adequate characterisation of exposures cannot be accomplished without successfully distinguishing background nanoparticle contributions. Background distinction in this PhD thesis was achieved by using a time series approach during the non-activity period (measured at the breathing zone without the target process going on) before and after the activity (Brouwer *et al.*, 2009). This approach assumed that the concentration at the working area corresponded to the background and any increase in particle concentrations during the work activity were related to the working process itself. However, it is important to take into consideration that this approach assumes background concentrations to be constant, and possible temporal and spatial changes in the background were not considered.

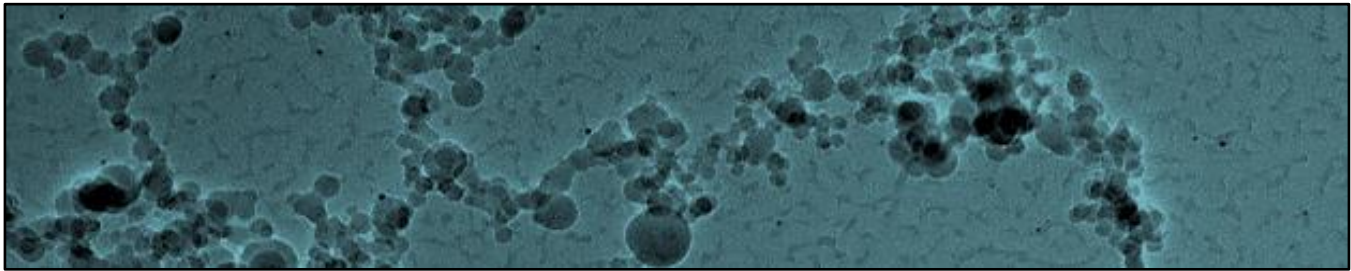
3.4.5 Worker exposure concentrations

Exposure concentrations were calculated by subtracting the background concentrations from the measured particle concentrations at the breathing zone during the work activity, as described in section 1.2.3 by Eq (1). Worker exposure to nanoparticles was considered statistically significant when the previous calculated exposure was higher than three times the standard deviation of the BG concentration ($3 \cdot \sigma_{BG}$; Eq 2). The cumulative worker exposure for an 8-h TWA was estimated as follows:

$$\text{Worker exposure}_{8\text{-h TWA}} = \frac{t}{8h} \frac{1}{n} \sum_{i=1}^n BZ_i \quad \text{Eq (4)}$$

Where, t is the time duration of the activity, BZ_i is the the measured background corrected particle concentration (subtracted the background concentration) and n is the total number of measurements.

Chapter 4. **RESULTS**



4. RESULTS

This section presents the results of this PhD thesis in form of five articles published per chronological order in peer-reviewed journals. In regard to the Article I, the second objective presented in chapter 2 was undertaken by a characterisation of nanoparticle release and exposure in real-world industrial settings, dealing with SWCNT while manufacturing semiconductor thin films. To overcome the third objective dealing with PGNP, both Articles II and III characterised nanoparticle release and exposure in real-world industrial scenarios during conventional processes in the ceramic industry. Lastly, Articles IV and V contributed to overcome the first objective by assessing the performance of novel instruments for nanoscale aerosol measurements (portable NanoScan SMPS TSI 3910, and cascade impactors such as nano-BLPI and nano-Moudi).

4.1 Article I: Characterisation of exposure to carbon nanotubes in an industrial setting

Authors:

Fonseca, A. S.^{1,2}, Viitanen, A. K.³, Koivisto, A. J.^{3,4}, Kangas, A.³, Huhtiniemi, M.³, Hussein, T.^{5,6}, Vanhala, E.³, Viana, M.¹, Querol, X.¹, Hämeri, K.⁵

¹ Institute of Environmental Assessment and Water Research (IDAEA-CSIC), C/ Jordi Girona 18, 08034 Barcelona, Spain.

² University of Barcelona, Faculty of Chemistry, Department of Analytical Chemistry, Martí i Franquès, 1-11, 08028 Barcelona.

³ Finnish Institute of Occupational Health, Nanosafety Research Centre, Topeliuksenkatu 41 a A, FI-00250 Helsinki, Finland.

⁴ National Research Centre for the Working Environment, Lersø Parkallé 105, Copenhagen DK-2100, Denmark.

⁵ University of Helsinki, Department of Physics, P.O. Box 64, FI-00014 Helsinki, Finland.

⁶ University of Jordan, Faculty of Science, Department of Physics, Amman, JO-11942 Jordan.

Published in:

Ann Occup Hyg, 59(5), 586-599, 2015

doi: 10.1093/annhyg/meu110

Accepted date: 24 December 2014 (available online)



Characterization of Exposure to Carbon Nanotubes in an Industrial Setting

Ana Sofia Fonseca^{1,2*}, Anna-Kaisa Viitanen³, Antti J. Koivisto^{3,4},
 Anneli Kangas³, Marika Huhtiniemi³, Tareq Hussein^{5,6}, Esa Vanhala³
 Mar Viana¹, Xavier Querol¹ and Kaarle Hämeri⁵

1. Institute of Environmental Assessment and Water Research (IDAEA-CSIC), C/ Jordi Girona 18, 08034 Barcelona, Spain

2. Faculty of Chemistry, Department of Analytical Chemistry, University of Barcelona, Martí i Franquès, 1–11, 08028 Barcelona, Spain

3. Finnish Institute of Occupational Health, Nanosafety Research Centre, Topeliuksenkatu 41 a A, FI-00250 Helsinki, Finland

4. National Research Centre for the Working Environment, Lersø Parkallé 105, Copenhagen DK-2100, Denmark

5. Department of Physics, University of Helsinki, PO Box 64, FI-00014 Helsinki, Finland

6. Faculty of Science, Department of Physics, University of Jordan, Amman, JO-11942, Jordan

*Author to whom correspondence should be addressed. Tel: +34-934006100; fax: +34-93-2045904; e-mail: ana.godinho@idaea.csic.es

Submitted 24 March 2014; revised 24 September 2014; revised version accepted 26 October 2014.

ABSTRACT

While production and use of carbon nanotubes (CNTs) is increasing, workers exposure to CNTs is expected to increase as well, with inhalation being potentially the main pathway for uptake. However, there have been few studies reporting results about workers' personal exposure to CNTs. In this study, worker exposure to single-walled CNTs (SWCNTs) during the production of conductive films in a modern up-scaling factory was assessed. Particulate matter concentrations (2.5–10 µm) and concentrations of CO and CO₂ were monitored by using real-time instruments. Workers' exposure levels to SWCNTs were qualitatively estimated by analyzing particle samples by transmission electron microscopy (TEM). TEM samples identified high aspect ratio (length/width > 500) SWCNTs in workplace air. SWCNT concentrations estimated from micrographs varied during normal operation, reactor use without local exhaust ventilation (LEV), and cleaning between 1.7×10^{-3} , 5.6 and 6.0×10^{-3} SWCNT cm⁻³, respectively. However, during cleaning it was unclear whether the SWCNTs originated from the cleaning itself or from other reactor openings. We were unable to quantify the SWCNT emissions with online particle instrumentation due to the SWCNT low concentrations compared to background particle concentrations, which were on average $2.6 \pm 1.1 \times 10^3$ cm⁻³. However, CO concentrations were verified as a good indicator of fugitive emissions of SWCNTs. During normal operation, exposure levels were well below proposed limit values (1.0×10^{-2} fibers cm⁻³ and 1 µg m⁻³) when LEV was used. Based on the results in this study, the analysis of TEM grids seems to be the only direct method to detect SWCNTs in workplace air.

KEYWORDS: fibers; industry; nanoparticle; nanotube; occupational exposure limits; SWCNT; workplace exposure

INTRODUCTION

Carbon nanotubes (CNTs) are one of the most prominent commercially produced nanostructures due to their unique mechanical and physicochemical properties which may be adjusted by changing their structure (De Volder *et al.*, 2013; Park *et al.*, 2013; Sun *et al.*, 2013; Yang *et al.*, 2013; Zhang *et al.*, 2013). Currently, CNTs are used in electronics, polymers, composite materials, coatings, and films (De Volder *et al.*, 2013; Zhang *et al.*, 2013). In electronics, CNTs cover applications such as flexible circuits, flexible displays, flexible solar cells, electronic paper, touch screens, implantable medical devices, skin-like pressure sensors, and conformable Radio Frequency Identification tags (De Volder *et al.*, 2013; Park *et al.*, 2013; Sun *et al.*, 2013; Yang *et al.*, 2013). CNTs are used to replace some rare transition metal oxides such as indium tin oxide (Wu *et al.*, 2004). As this market is increasing globally, the potential for worker exposure may also increase. CNTs are promising materials, but they are also considered potentially highly toxic for humans. The inhalation pathway is considered the predominant route of workplace exposure and uptake (Schmoll *et al.*, 2009). Toxicological studies performed by using high concentrations (>typical concentrations found in exposure studies ranging from 0.7 to 53 $\mu\text{g m}^{-3}$; NIOSH, 2013) have shown that certain CNTs induce pulmonary disorders such as fibrosis (Manke *et al.*, 2013, 2014; Donaldson *et al.*, 2013) and unconventional allergic airway inflammation (Rydman *et al.*, 2014). Conversely, Sato *et al.* (2013) showed that oxidized and tangled multiwalled CNTs (MWCNTs) do not evoke adverse health effects but are potentially highly biopersistent. The similarities between single-walled CNTs (SWCNTs) and microtubules has been suggested as the reason why thin nanotubes may be incorporated into cellular structures, which could result in errors of chromosome number (Sargent *et al.*, 2012; Rydman *et al.*, 2013). It has also been suggested that the chromosome-breaking capacity of various fibrous materials is linked to the presence of unencapsulated fiber-associated iron (Kisin *et al.*, 2011; Catalán *et al.*, 2012).

With conflicting literature regarding a potential hazard from exposure to a variety of CNTs, several occupational exposure limits (OEL) have been proposed (Ogura, 2013). The National Institute for Occupational Safety and Health (NIOSH, 2013) has

established that the recommended exposure limit (REL) for CNTs should be 1 $\mu\text{g m}^{-3}$ of respirable elemental carbon (EC) as an 8-h time-weighted average (TWA) concentration (see definition of respirable particles, e.g. by CEN, 1993). In addition, NIOSH recommends an OEL for CNTs of 1 $\mu\text{g m}^{-3}$ during a 40-h workweek, 50 weeks per year, for 45 years. Other investigators and organizations have also been concerned about the CNT effects and have recommended OELs within the range of 1–50 $\mu\text{g m}^{-3}$ (8 h TWA) (Nanocyl, 2009; Aschberger *et al.*, 2010; Pauluhn, 2010). The British Standards Institute (BSI, 2007) and Germany's Institute for Occupational Safety and Health of the German Social Accident Insurance (IFA, 2009) designed the permissible exposure limit (PEL) for 8h TWA for all CNTs as one-tenth of their asbestos fiber exposure limit (0.1 fibers cm^{-3}), resulting in 1.0×10^{-2} fibers cm^{-3} . However, CNTs generally exist in an agglomerated state for which single fibre limit values are difficult to apply.

The majority of CNTs are produced by Chemical Vapor Deposition (CVD) (De Volder *et al.*, 2013). Studies have shown that airborne background concentrations of EC are typically less than 1 $\mu\text{g m}^{-3}$ (Evans *et al.*, 2010; Birch, 2011; Birch *et al.*, 2011; Dahm *et al.*, 2012) and thus an elevated exposure to EC in the workplace may be a reasonable indicator of CNT release for CVD produced CNTs. However, the number of exposure and emission measurements performed at workplaces is low and the occupational CNT exposure data is limited (Hedmer *et al.*, 2013). Both stationary and personal measurements have been performed, but often under specific exposure scenarios and during short sampling periods (Maynard *et al.*, 2004; Bello *et al.*, 2008; Han *et al.*, 2008; Bello *et al.*, 2009; Tsai *et al.*, 2009; Bello *et al.*, 2010; Lee *et al.*, 2010; Methner *et al.*, 2010; Cena and Peters, 2011; Dahm *et al.*, 2012; Huang *et al.*, 2012; Dahm *et al.*, 2013). These observations have emphasized the importance of reliable assessments of workers' exposure to CNTs with inhalation being the primary concern.

In this study, worker exposure to SWCNTs while manufacturing conductive thin films was assessed. Assessment of quantitative SWCNTs concentrations from workplace air were studied by measuring in real-time size-resolved aerosol particle concentrations, gaseous concentrations of carbon monoxide (CO) and carbon dioxide (CO₂), and by analyzing particle

samples collected from workplace air with transmission electron microscopy (TEM). Measured concentration levels were linked with work activity where potential SWCNT emissions occurred. Measurements were performed over eight consecutive days in order to be able to link possible SWCNT emissions to measured particle concentrations and to get a good overview of particle concentration levels inside the factory.

METHODS

Production of SWCNT films

Exposure to CNTs was measured at a modern up-scaling factory producing SWCNT films. SWCNTs were produced in a high temperature furnace where CO and iron (Fe) seed particles were introduced (Fig. 1; see reactor operation principle by Nasibulin *et al.*, 2007).

From the reactor where they were synthesized, SWCNTs were directed (i) during collection to the deposition chamber and through a collector filter to the exhaust and (ii) during filter change to the exhaust (Fig. 1). When the deposition chamber was open for the change of the collector filter SWCNTs and by-product gases, (mainly CO), were potentially released to the workplace air. Local exhaust ventilation

(LEV) was used to prevent emissions to workplace air. The deposition chamber exhaust was under negative pressure (P_V) compared to the room (P_0 ; Fig. 1). The collector filter containing SWCNTs was carried by hand from the deposition chamber to a pressing machine located at work bench (Fig. 2). In the pressing machine, SWCNTs were transferred from the collector filter to a film after which the film was post processed with solutions. Except during gas phase SWCNT synthesis, the potential release of SWCNTs during other process stages by re-suspension can be considered to be low (Nowack *et al.*, 2013). Thus, all SWCNT emissions were assumed to occur during reactor collection chamber opening during normal operation. The dependence of potential SWCNTs emissions during reactor collection chamber opening times with the amount of time that the reactor was closed was not assessed in this study. Since the synthesis of SWCNTs involves CO, it was assumed that CO emission indicates a leak in the process where also SWCNTs may be released into workplace air. The factory produces annually ~10 000 SWCNT films and employs 20 people.

Work environment

The production hall area was 1200 m² and contained two floors with open pathways. The incoming air was ventilated mechanically with filtered outdoor air two to three times per hour. Figure 2 shows a layout of the work area and location of the instruments and active reactors referred as Reactor 1 (R1), Reactor 2 (R2), and Reactor 3 (R3). R1 was the most used reactor and thus was chosen as the main measurement location. It is important to take into account that only R1 was operating with LEV.

Aerosol measurements were conducted over eight consecutive days in May 2013. Three different work events (WE) were registered and monitored: manufacturing of SWCNT films using LEV (113 films were manufactured where SWCNT collection time varied from 1 min to 10 min) (WE1), manufacturing one SWCNT film without LEV using a collection time of 8 min (WE2), and cleaning of one of the reactors (WE3). The reactor hall was an open space where from 5 to 10 workers were working at the same time. One single reactor was operated mainly by one worker and up to three reactors were used simultaneously at the same time during the measurement campaign.

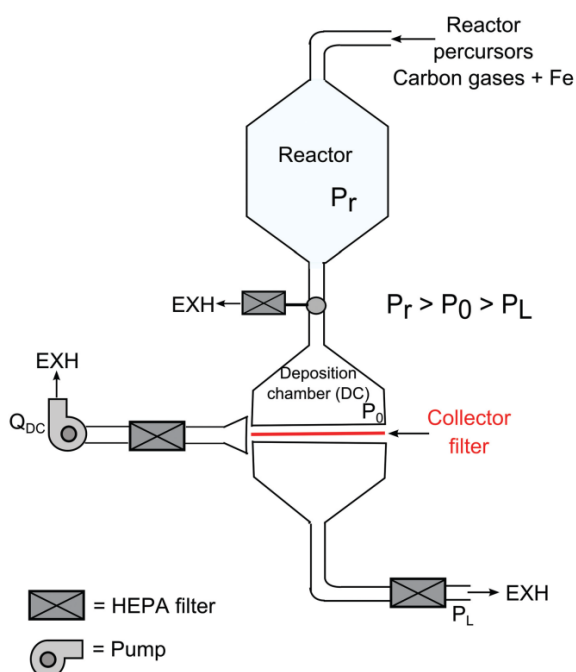


Figure 1 Process flow diagram of SWCNT films production.

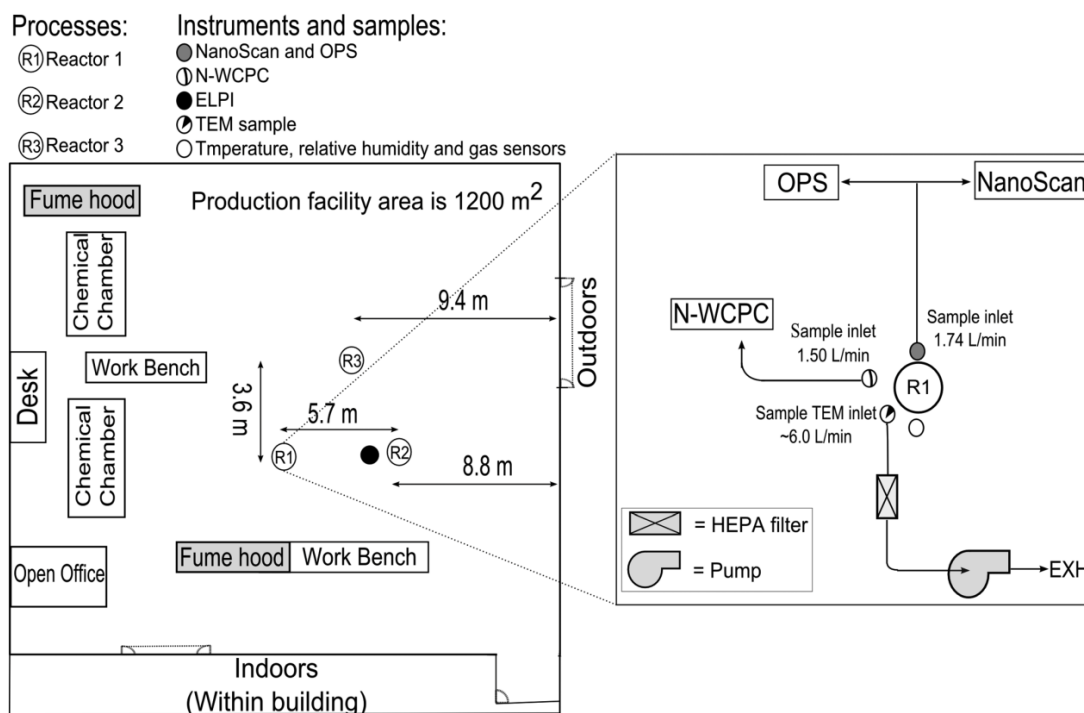


Figure 2 Layout of the work environment showing approximate positions of processes and sampling locations.

Supplied-air face piece respirators and gloves were used by the cleaners during WE3, otherwise the work was performed without personal protective equipment.

Measurement setup

Real-time measurements

Airborne particle concentrations from ~ 2.5 to $10 \mu\text{m}$ were measured by using following instruments:

- Mobility particle size distributions were measured in 13 channels from 10 to 420 nm with an electrical mobility spectrometer (NanoScan, SMPS TSI Inc., Model 3910, Shoreview, MN, USA; sample flow rate 0.7 l min^{-1} ; 105 s scan with 15 s retrace).
- Optical particle size distributions were measured in 16 channels from 0.3 to $10 \mu\text{m}$ with an Optical Particle Sizer (OPS, TSI Inc., Model 3330, Shoreview, MN, USA; sample flow rate 1 l min^{-1} ; 1 s time resolution).
- Total particle number concentration was measured from 2.5 nm to $3 \mu\text{m}$ with a condensation particle counter (N-WCPC, TSI Inc., Model 3788, Shoreview, MN,

USA; sample flow rate 1.5 l min^{-1} ; 0.5 s time resolution) and from 7 nm to over $1 \mu\text{m}$ with a portable condensation particle counter (CPC, TSI Inc., Model 3007, Shoreview, MN, USA; sample flow rate 0.7 l min^{-1}). CPC was used to identify local particle sources.

- Aerodynamic particle size distributions were measured from 7 nm to $10 \mu\text{m}$ in 13 stages with an electrical low-pressure impactor (ELPI, Dekati Ltd., Finland, $Q_s = 9.6 \text{ l min}^{-1}$, Keskinen *et al.*, 1992). Logging time interval was set to 1 s which was averaged to 60 s samples with the ELPIVI 4.0 software for the data analysis using stokes density of 1 g cm^{-3} .

Particle number units were converted to mass units by assuming unit density (1 g cm^{-3}) and spherical shape. Mobility, optical, and aerodynamic diameters were assumed to be equivalent.

The following instruments were used to measure:

- CO_2 volume concentration with Vaisala HM70 indicator using GMP70 CARBOCAP® (Vaisala Oyj, Finland etc.).

- Relative humidity (RH) and temperature (T) with Vaisala HM70 indicator using HMP75 RH&T probe (Vaisala Oyj).
- CO volume concentration with Graywolf IQ-410 (GrayWolf Sensing Solutions LLC, USA).

Transmission electron microscopy samples

Particles for TEM analysis were sampled onto holey carbon film-coated copper grids of 200-mesh size (SPI West Chester, USA) from workplace air (between the collection chamber and worker, ~50 cm from the collection chamber opening) at a height of 1.4 m. TEM-copper grids were attached to air sampling cassettes (SKC Inc., USA, inlet diameter 1/8 inch and filter diameter 25 mm) on mixed cellulose ester (MCE) membrane filters with 0.8 μm pore size. Air flow was driven by a sampling pump at a flow rate of 5–15 l min^{-1} and collection efficiency for SWCNTs was assumed to be 1. Five TEM grids were collected and analyzed without any standard method since the aim was to verify the presence of SWCNTs in workplace air. Particle morphology, chemical composition, and size were analyzed by TEM (Jeol, JEM 1220, Tokyo, Japan equipped with Olympus Veleta CCD TEM camera), coupled with an energy-dispersive X-ray spectroscopy (EDS; Noran System Six, Thermo Fisher Scientific, USA). SWCNT concentrations in air were estimated by counting the number of SWCNTs from scanning grid openings (3–11) and dividing per volume of sampled air. A homogeneous distribution across the grid was assumed. Similar methods for CNT counting have been used in previous studies (Bello *et al.*, 2010; Lee *et al.*, 2010; Dahm *et al.*, 2012).

Particle sampling inlets

Sampling locations are shown in Fig. 2. The OPS and the NanoScan inlet were located between the collection chamber and the worker at face level (~1.5 m). The inlets of the N-WCPC, TEM sampling and gases, RH and T sensors were ~30 cm from the collection chamber at a height of 1.2–1.4 m. The ELPI was located on the balcony, 3 m above the R2. The clocks of all instruments were synchronized prior to the measurement starting time.

Discriminating reactor concentrations from background particles

In this study, background particles were defined as outdoor particles penetrating indoors and particles

emitted by indoor sources that were not SWCNTs (e.g. from a laser printer which was rarely used). The background and collection chamber opening concentrations (peak) were calculated for each reactor separately (see an example in Supplementary Figure S1 available at *Annals of Occupational Hygiene* online). The peak concentration was defined as the average of 2 min, i.e. 1 min before and 1 min after of each collection chamber opening time. Similarly, two background concentrations were calculated with a 1-min gap before and after collection chamber opening times which were averaged to mean background concentration. The background concentration was defined as the average of 4 min, i.e. 2 min before and 2 min after of the corresponding collection chamber opening time.

RESULTS

The production hall T and RH varied from 22.5°C to 25.4°C and 8.2–37.9%, respectively. The work activity took place during weekdays mainly between 08:00 and 17:00 which were classified as working hours (WH). Table 1 provides the geometric mean values of particle number (N) and CO concentration for the entire duration of WH, non-WH including weekend (NWH) and WE. Details of concentrations for each WE and instruments are listed in Supplementary Tables S1 and S2 available at *Annals of Occupational Hygiene* online which show number of minutes sampled (t , min), mean and maximum particle number, CO, and mass concentrations.

Figure 3a shows the time series of particle number and CO concentrations and Fig. 3b shows particle number size distributions. According to the ELPI, mean N_{WH} and N_{NWH} concentrations were on average $3.9 \times 10^3 \text{ cm}^{-3}$ ($6.7 \mu\text{g m}^{-3}$) and mean $2.6 \times 10^3 \text{ cm}^{-3}$ ($4.5 \mu\text{g m}^{-3}$), respectively. According to the NanoScan, N-WCPC, and OPS mean N_{WH} were higher by a factor of 1.5, 4.0, and 1.2 than N_{NWH} , respectively. All instruments showed elevated concentrations during WHs than during non-WHs. A similar trend was seen with CO maximum concentration ($\text{CO}_{\text{WH}} = 6.3 \times 10^5 \mu\text{g m}^{-3}$ vs $\text{CO}_{\text{NWH}} = 1.7 \times 10^3 \mu\text{g m}^{-3}$). CO levels decreased during non-WHs to typical CO concentrations in urban environments (mean maximum 8 h concentration $0.9\text{--}2.6 \times 10^3 \mu\text{g m}^{-3}$; Alm *et al.*, 2001) This suggests that the main significant CO emission source during the industrial process was the process itself that was related to collection chamber openings

Table 1. Mean of particle number and CO concentrations

	N-WCPC, N (cm^{-3})	NanoScan, N (cm^{-3})	ELPI, N (cm^{-3})	OPS, N (cm^{-3})	CO, m ($\mu\text{g m}^{-3}$)
WE1	1.9×10^3	2.0×10^3	3.2×10^3	4.9	8.3×10^2
WE2	2.3×10^3	2.5×10^3	5.7×10^3	11	5.5×10^3
WE3	3.3×10^3	1.9×10^3	2.7×10^3	—	4.9×10^2
WH	5.4×10^3	2.0×10^3 <td 3.9×10^3	16	7.7×10^2	
NWH ^a	1.4×10^3	1.3×10^3	2.6×10^3	13	2.7×10^2

—, Not measured.

^aIncluding weekend.

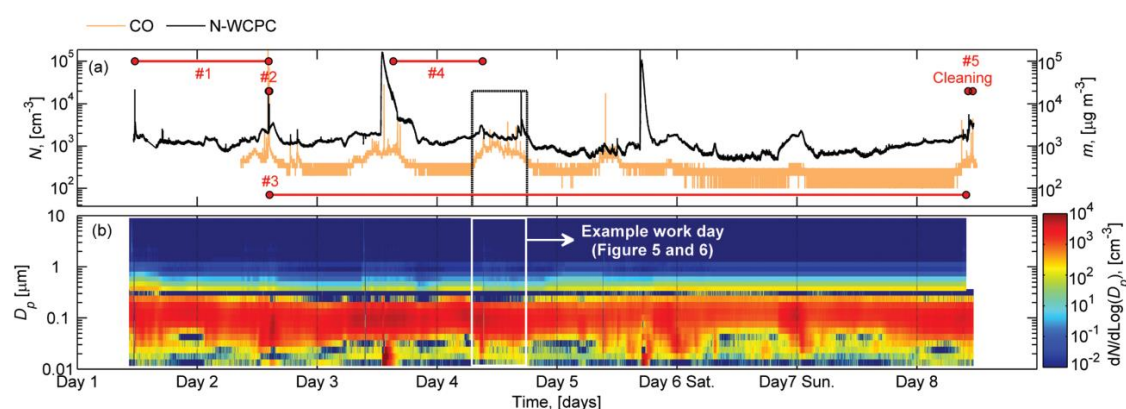


Figure 3 Time series of (a) particle number and CO concentrations and (b) particle number size distributions measured by OPS and NanoScan. #1–#5 in (a) correspond to TEM sampling periods.

which indicate that SWCNTs were also released. CO_2 concentrations remained at similar concentrations increasing only 4% during WHs (430 ppm) compared to non-WH (415 ppm) which was assumed to be mainly caused by human activity. Figure 3b shows that according to the NanoScan, work activities produced mainly particles below 150 nm diameter (>95% in number concentration).

On Day 3 at 12:42 h and Day 5 at 16:40 hr high number concentration peaks were seen (Fig. 3a) consisting of particles mainly smaller than 200 nm in diameter (Fig. 3b). The N-WCPC reached $N_{\text{day3}} = 1 \times 10^5 \text{ cm}^{-3}$ and $N_{\text{day5}} = 4 \times 10^5 \text{ cm}^{-3}$ (on a minute basis), respectively. According to the ELPI, during the Days 3 and 5 events, the calculated particle mass increased from 1 to $50 \mu\text{g m}^{-3}$ and from 1 to $20 \mu\text{g m}^{-3}$, respectively. These peaks did not affect CO concentration levels (Fig. 3a). Furthermore, particles that correspond to the measured size range were not found in the TEM sample #3 (Fig. 4) which suggests that these

incidental particles evaporated in the electron microscope vacuum. Thus, it can be concluded that, in both cases (Days 3 and 5), the maximum number and mass concentrations were dominated by incidental particle release or formation processes and were not SWCNTs or directly related to the production of SWCNTs.

TEM analyses of collected samples evidenced the presence of SWCNTs in workplace air (Fig. 4). Only a rough estimation was provided by TEM image analysis of #2, #4, and #5 (Table 2). Time intervals from the TEM samples are shown in Fig. 3a. Our analysis revealed workplace air concentrations of 1.7×10^{-3} SWCNT fibers cm^{-3} during normal operation and 5.6 SWCNT fibers cm^{-3} during operation without LEV (Table 2). SWCNTs length varied from several micrometers to tens of micrometers. The thickness of SWCNT bundles varied from 10 to 20 nm and a single fiber from 2 to 3 nm. A closer examination of micrographs shows the presence of iron catalyst particles (~ 10 nm in diameter) attached to the nanotubes.

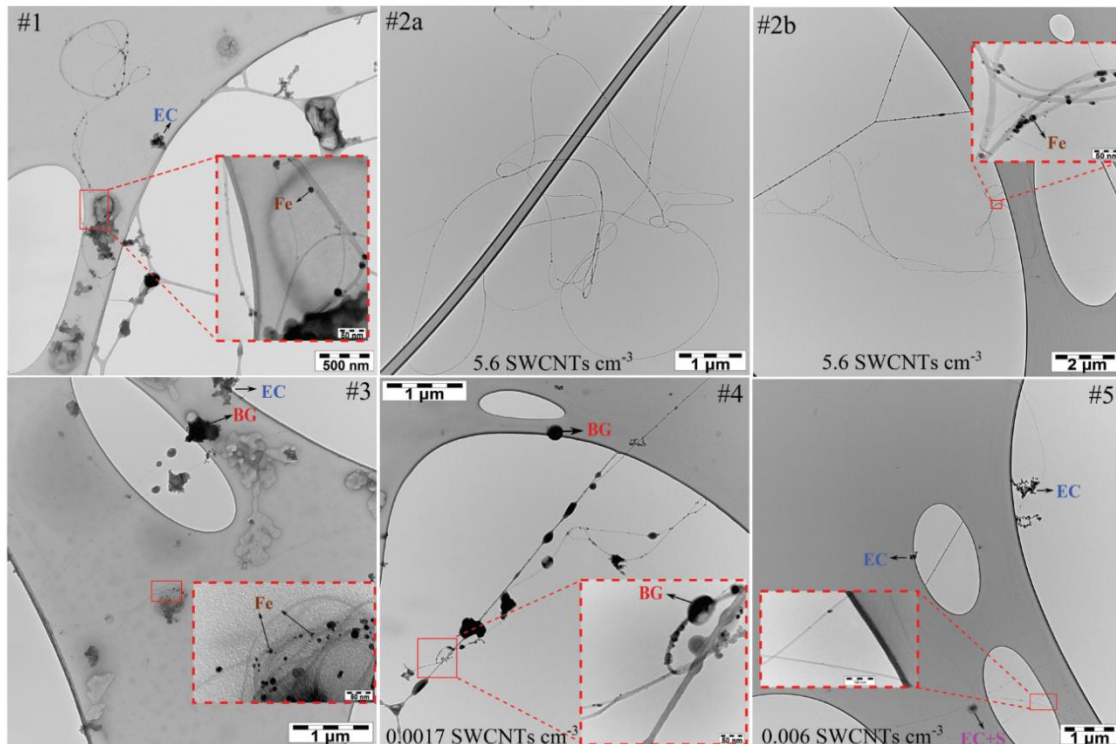


Figure 4 TEM images of SWCNTs collected in workplace air (#1, #3, and #4), during film manufacturing without local ventilation system (#2) and reactor cleaning operations (#5). Dashed rectangles show the magnified area. Corresponding estimated concentrations are shown in each figure (if determined). Identified particles are shown as background particles (BG), elemental carbon (EC), iron (Fe), and sulphur (S).

Table 2. TEM sampling details indicating time sampled (t , min), air volume sampled, the number of collection chamber openings and the corresponding estimated concentration of SWCNTs in workplace air

TEM sample	t (hh:min)	Air volume (m^3)	Collection chamber openings	SWCNT concentrations (SWCNTs cm^{-3})
#1: Workplace air	26:48	9.65	25	Not calculated
#2: Workplace air without LEV	0:08	0.05	1	5.6
#3: Workplace air	139:24	49.6	81	Not calculated
#4: Workplace air	17:52	10.3	5	0.0017 ^a
#5: Reactor cleaning operation	0:44	0.69	3	0.006 ^a

^aLower than PEL of 1.0×10^{-2} fibers cm^{-3} (BSI, 2007; IFA, 2009).

Accurate counting of these nanomaterials with TEM micrographs was not possible for TEM #1 and #3 (see Fig. 4) due to the high aspect ratio of the SWCNTs (length/width > 500) and branching of bundles that could not be distinguished from each fiber. Accurate calculation requires stitching of multiple TEM images

so that it becomes possible to track and count a single fiber bunch (see Fig. 4; #2, #4, and #5). Because stitching should be done for each bunch, the work can be accomplished only with an automatized microscopy system in reasonable time to obtain statistically reasonable results.

Particle concentration analysis during collection chamber openings

The particle number size distributions measured by the ELPI show that average particle number concentrations of R1, R2, and R3 during their opening time (peak) were 3.9×10^3 , 4.6×10^3 and 3.2×10^3 cm^{-3} respectively (see [Supplementary Figure S2](#) available at *Annals of Occupational Hygiene* online). Corresponding background concentrations differ from workplace concentrations by a maximum of 3%. In the case of R3 and for particles $> 1 \mu\text{m}$ in diameter, number concentration increased $\sim 25\%$ while the reactor chamber was opened. However, this increase is not significantly above the instruments signal to noise levels, and thus the concentrations cannot be linked to SWCNT emissions. Similar results were obtained for NanoScan and OPS both in number and mass concentrations. This fact suggests that workers' exposure to SWCNTs during operation could not be distinguished from the background based on the particle measurements in this case.

WE1: example of workday 4 concentrations during normal operation

[Figures 5 and 6](#) show particle number and mass concentrations, respectively, for workday 4 when LEV was used. During this day, ELPI data showed simultaneous elevations, in both N and m up to 1.1×10^4 cm^{-3} and 2.8×10^2 $\mu\text{g m}^{-3}$. The average concentration for the workday was according to the ELPI, NanoScan, and OPS respectively $N_{\text{WE1}} = 3.2 \times 10^3$ cm^{-3} ($m_{\text{WE1}} = 3.4$ $\mu\text{g m}^{-3}$), $N_{\text{WE1}} = 2.0 \times 10^3$ cm^{-3} ($m_{\text{WE1}} = 0.83$ $\mu\text{g m}^{-3}$), and $N_{\text{WE1}} = 4.9$ cm^{-3} ($m_{\text{WE1}} = 0.81$ $\mu\text{g m}^{-3}$).

[Figure 5](#) and [6](#) show that some collection chamber openings coincide with peak number and mass concentrations but there is no evidence that concentration peaks are caused by SWCNT emissions. However, according to the micrograph analysis of TEM #4 there were on average 1.7×10^{-3} SWCNTs cm^{-3} ([Fig. 4](#)). Moreover, maximum CO concentrations during collection chamber opening times were clearly higher (up to 3.8×10^3 $\mu\text{g m}^{-3}$) than the average CO concentrations during WE1 ([Table 1](#); 8.3×10^2 $\mu\text{g m}^{-3}$). These CO concentration peaks suggest that SWCNTs were also released during the collection chamber openings.

It is important to highlight the uncertainties linked to the data provided by online particle instruments mainly due to background concentrations which were relatively high in comparison to the very low concentration of airborne SWCNTs. In addition, the accuracy in response to particles or fibers of irregular shape, high internal surface area, high aspect ratio, and low effective densities may vary ([Bottlinger and Umhauer, 1989](#); [Gebhart, 1991](#); [Szymanski et al., 2009](#)). While most spherical or spherical-like particles can be described either by their geometrical size or fractal geometry, it is not known if such descriptions are applicable to high aspect ratio fibers such as CNTs ([Kulkarni et al., 2009](#)). Thus, whereas monitoring instruments such as particle counters and sizers may respond in a relatively same way to particle concentrations and size classifications for near-spherical particles, this may not be the case for particles with high aspect ratios and irregular shapes. The results of this study seem to suggest that the online instrumentation could be detecting SWCNTs as larger particles, even

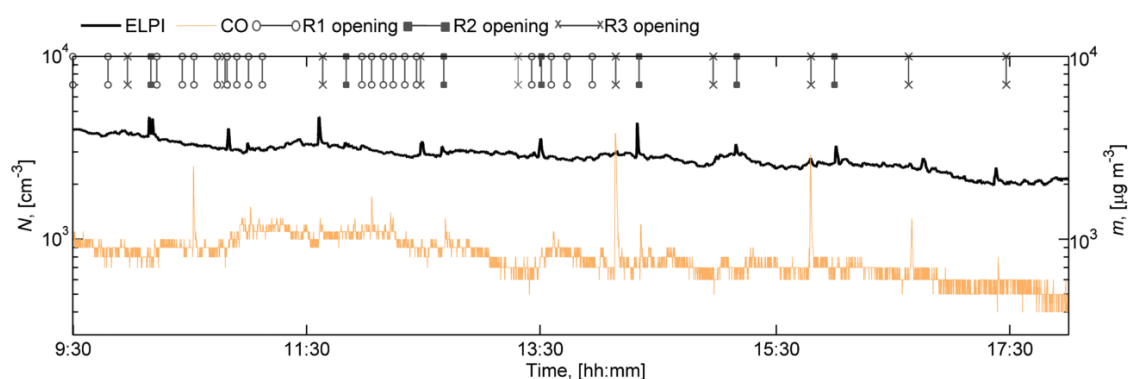


Figure 5 Example of workday 4 particle number and CO concentrations. The vertical lines with circle, square, and cross correspond to R1, R2, and R3 collection chamber opening times, respectively.

though further analyses would be necessary to confirm this hypothesis. Figure 7 shows eight coincidences between the collection chamber opening times and both CO and particle number concentrations measured by the OPS and ELPI for particles with diameter 335 and 318 nm, respectively. However, this was not consistent and did not occur for the remaining 21 collection chamber opening times. Since measured particle diameters did not correspond with the particle diameter for SWCNTs by means of the corresponding TEM images, it could be hypothesized that the fibrous nature of SWCNTs (high aspect ratio > 500 and varying irregular shapes) is causing an overestimation of particle diameter by different online instrumentation as suggested by the eight increases in particles with diameter 318 and 335 nm during collection chamber opening times.

Although there is a large difference in aerodynamic and mobility SWCNT-equivalent diameters due to their surface area, large dynamic shape factors, and low effective densities, the previous supposition can be supported by Moaisal *et al.* (2005). They showed that DMA measurements of SWCNTs suggest an effective electrical mobility diameter higher than the average value observed by TEM imaging and SWCNT perpendicular orientation to the electric field in the DMA. Furthermore, Kulkarni *et al.* (2009) found that the charging-equivalent diameters of SWCNTs are higher than their mobility diameter by a factor of 2.85–4.34. Since physical size of CNTs inferred from microscopy must rely on their property-equivalent diameters, further and more detailed research is currently ongoing to test instrument responses to high aspect ratios nanomaterials. One other possibility

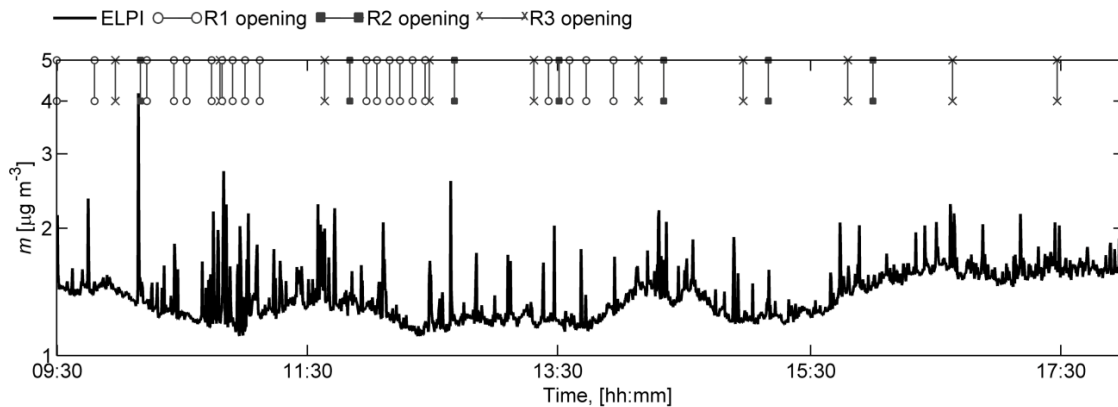


Figure 6 Example of workday 4 particle mass concentrations. The vertical lines with circle, square and cross correspond to R1, R2, and R3 collection chamber opening times, respectively.

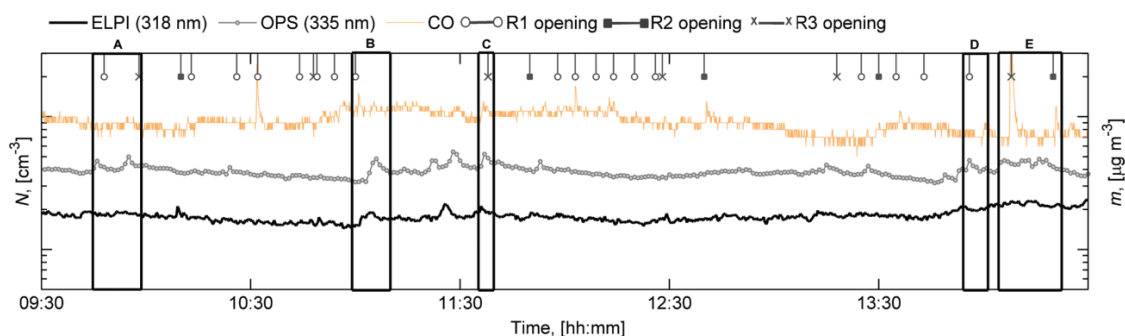


Figure 7 CO and particle number concentrations for ELPI (channel 6, $D_{50} = 318$ nm particle diameter) and OPS (channel 1 $D_{50} = 335$ nm particle diameter) during WE1. The vertical lines with circle, square and cross correspond to R1, R2, and R3 collection chamber opening times, respectively, when the expected SWCNTs emissions may occur. The rectangular areas (A, B, C, D, and E) indicate coincidences between reactor opening times and increased number concentrations for particle sizes 318 and 335 nm.

could be that online instruments detect iron catalyst particles attached to the nanotubes, as larger particles (Nasibulin *et al.*, 2005), although this would be the case on a low percentage of occurrences since it was verified that their diameter was ~ 10 nm (Fig. 4).

WE 2: SWCNT manufacturing without LEV system

In order to test the effectiveness of LEV systems during SWCNT manufacturing the LEV system of R1 was removed during Day 2 from 14:18 to 14:26 (Fig. 3a). Particle peak concentrations of the corresponding collection chamber opening for R1 remained at the same level as the background particle concentrations (differences below 3%), indicating that N and calculated m were not largely different from background concentrations. A different trend was seen for CO, i.e. $1.8 \times 10^4 \mu\text{g m}^{-3}$ as peak concentration and $1.4 \times 10^3 \mu\text{g m}^{-3}$ as background concentration, meaning an order of magnitude increase with respect to background concentrations. Assuming the CO average concentration during one workday operating with LEV ($C_{\text{CO,WE1}} = 8.3 \times 10^2 \mu\text{g m}^{-3}$), the following formula was applied:

$$\frac{(\text{CO without LEV} - \text{CO with LEV})}{\text{CO without LEV}} \times 100 \\ = \% \text{Reduction in CO due to use of LEV}$$

As a result, the CO concentrations associated with use of LEV system were reduced by an average of 95%. However, it should be taken into account that CO diffusion is orders of magnitude higher than SWCNT

diffusion and that CO is only a good indicator if convection dominates the mass transfer of both CO and SWCNTs.

According to TEM analysis, SWCNT concentration was $5.6 \text{ SWCNTs cm}^{-3}$ (Fig. 4; #2) which gives LEV protection factor of 99.6% when compared to TEM sample of workplace with LEV (Fig. 4; #4). These results appear to support the finding that LEV can be effectively used to control emissions of engineered nanomaterials (Methner, 2010). Also CO appears to be a good tracer for SWCNT emissions.

WE 3: reactor cleaning operation

Reactor cleaning was performed with wet wipes and a vacuum cleaner with HEPA filter (Nilfisk Alto Attix 30, Nilfisk-Advance Inc., Morgantown, USA) during Day 8. Figure 8 shows the particle mass concentrations calculated from ELPI during the cleaning operation, between 10:24 hr and 11:08 hr. The total particle number concentration during the cleaning operation was on average $N_{\text{WE3}} = 2.7 \times 10^3 \text{ cm}^{-3}$ and the calculated total mass concentration $m_{\text{WE3}} = 6.1 \mu\text{g m}^{-3}$ (Table 1; Fig. 8). The ELPI measured three sharp concentration peaks increasing in m up to $120 \mu\text{g m}^{-3}$ originating from particles larger than $1 \mu\text{m}$; (Fig. 8b). The estimated SWCNT concentration by TEM images, during the reactor cleaning, was $0.006 \text{ SWCNTs cm}^{-3}$ (Fig. 4; #5). However, it is not clear whether the SWCNTs detected in the TEM samples originate from the cleaning process or reactor R1 openings.

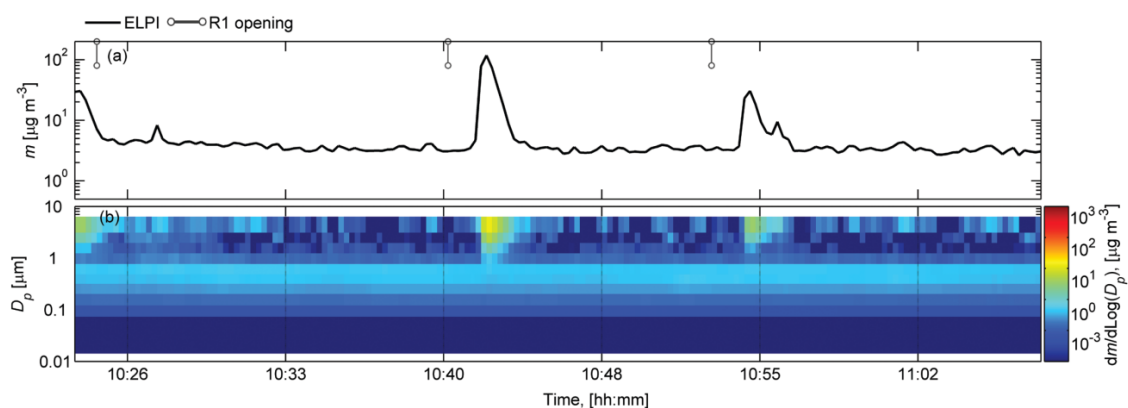


Figure 8 Reactor cleaning operation. (a) Particle mass concentration time series and (b) particle mass size distributions time series measured with ELPI. The vertical line with circle in (a) corresponds to R1 opening times when the expected SWCNTs emissions may occur.

DISCUSSION

The metrics of SWCNT exposure

Overall, WH particle number concentrations were clearly higher than during non-WH mainly due to different worker activities, as well as outdoor sources such as increased traffic emissions during daytime. A similar trend was seen for CO indicating that emissions occurred during the collection chamber openings (see [Supplementary Tables S1 and S2](#) available at *Annals of Occupational Hygiene* online). However, the time series did not reveal any clear correlation between the collection chamber opening times and consistent increases in particle number or mass concentrations when SWCNTs were expected to be released ([Figs 5 and 6](#)). This suggests that the detection of SWCNTs was limited probably due to: (i) the background concentration being relatively higher than the SWCNT concentrations and (ii) instruments response to fibers with irregular shapes and high aspect ratios (length/width > 500; see [Fig. 4](#)).

Of all the instruments, the N-WCPC was the most affected by other particle sources. An example of this can be seen in [Fig. 3a](#), which displays the sampling time-series plot. On Day 3 at 12:42 and Day 5 at 16:40, two number concentration peaks were seen, while the other measurement instruments did not show similar responses. Similar findings were reported by [Dahm et al. \(2013\)](#) and [Evans et al. \(2010\)](#), where the measured number concentration by the N-WCPC was dominated by other nanoparticle sources.

Transmission electron microscopy analysis

Nowadays, TEM based methods appear to be one of the most feasible, reliable, and selective way to assess quantitative worker exposure to CNTs ([Birch et al., 2011](#); [Dahm et al., 2012](#); [Dahm et al., 2013](#)). However, up to date, there is no accepted method for counting especially high aspect ratio CNT structures ([Hedmer et al., 2013](#)).

Despite the inability of the online instruments to accurately detect SWCNT release, the analysis of TEM images was able to confirm their presence in workplace air ([Fig. 4](#)). TEM qualitative analysis revealed workplace air estimations of 1.7×10^{-3} – 5.6 SWCNTs cm^{-3} ([Table 2](#)), depending on the process. The highest SWCNT counts were seen during the worst case scenario where SWCNTs were collected without LEV

(WE2). However, accurate counting of these nanomaterials with TEM micrographs was challenging due to high aspect ratio (length/width > 500) and branching. Accurate count of single fiber bunch required the use of high magnification and the need to stitch multiple TEM images. The counting fibers in TEM #1 and #3 was not possible (see [Fig. 4](#)).

Comparison of SWCNT exposure with exposure limits

According to the workplace TEM sample during the SWCNT manufacturing with LEV (WE1), the estimated concentration of 1.7×10^{-3} SWCNTs cm^{-3} (see [Fig. 4](#); #4) did not exceed the proposed limit value of 1.0×10^{-2} fibers cm^{-3} . In terms of calculated particle mass, assuming SWCNTs bunch with 20 nm of diameter, 10 μm of length, a density of 1 g cm^{-3} , and aspect ratio of ~ 500 , the obtained mass concentration would be $2.14 \times 10^{-5} \mu\text{g m}^{-3}$. Based on these assumptions, SWCNTs manufacturing with LEV would not have exceeded the OEL of $1 \mu\text{g m}^{-3}$ recommended by the NIOSH.

According to the workplace TEM sample during SWCNT manufacturing without LEV (WE2), the estimated concentration of 5.6 SWCNTs cm^{-3} exceeded the personal exposure limit of 1.0×10^{-2} fibers cm^{-3} . Assuming the background as the average mass concentration of NWH ($m_{\text{NWH}} = 4.5 \mu\text{g m}^{-3}$) and subtracting it from the average mass concentration of WE2, which was $25.0 \mu\text{g m}^{-3}$, it suggests that the SWCNTs exposure concentration ($20.5 \mu\text{g m}^{-3}$). This clearly exceeds the OEL of $1 \mu\text{g m}^{-3}$ proposed by NIOSH. This clearly shows that risk control measures are needed. Concerning the reactor cleaning operation (WE3), by subtracting the background mass concentration from average the average mass concentration of WE3, which was $6.1 \mu\text{g m}^{-3}$, it suggests that SWCNTs exposure concentration was 50% higher than OEL of $1 \mu\text{g m}^{-3}$. However, it was well below the established and proposed limit of 1.0×10^{-2} fibers cm^{-3} (see [Fig. 4](#); #5).

CONCLUSIONS

In this study, workers' quantitative exposure levels to SWCNTs while manufacturing conductive thin films in a modern up-scaling factory was assessed. To this end, particulate matter concentrations in the size range of 2.5 nm to 10 μm , and gas phase concentrations (CO,

CO₂) were measured and TEM samples were collected. The following conclusions may be extracted:

1. The analysis of TEM images was able to confirm the presence of SWCNTs in workplace air. The estimated concentrations were 1.7×10^{-3} – 5.6 SWCNTs cm⁻³, depending on the process. There was potential for release of SWCNTs during collection chamber openings, both while using LEV (WE1) and without using LEV (WE2). There was weak evidence that release of the SWCNTs may also happen during cleaning operations performed under pressure with wet wipes (WE3). During WE1 and WE3 exposure levels were well below proposed OEL ($1 \mu\text{g m}^{-3}$ and 1.0×10^{-2} fibers cm⁻³) and during the WE2 it was clearly exceeded (8 min exposure = 5.6 SWCNTs cm⁻³). The collection and analysis of SWCNTs on TEM grids was found to be the only direct method to detect SWCNTs in workplace air. However, defining quantitative exposure levels by counting of SWCNTs with TEM micrographs was challenging due to their high aspect ratio (length/width > 500) and branching. Additional research is required to develop methods for quantitative exposure assessment for this type of CNT structures. For example, in this company CO was used as a tracer gas for potential SWCNT emission;
2. CO concentration was verified as a good indicator of fugitive emissions of SWCNTs, even though correlation between CO concentration and SWCNT concentration was not found due to the low SWCNT concentrations detected in workplace air;
3. Analysis of number and mass concentration time series did not reveal consistent coincidences between increases in particle number or mass and collection chamber opening times when SWCNTs were expected to be released;
4. Despite being unable to directly identify SWCNT emissions, the online instruments used may have detected SWCNTs as larger particles (>300 nm) but further studies are needed to fully understand this behavior;

5. Correct application of LEV to the collection chambers was found to reduce CO and SWCNT emissions by ~95 and 98%, respectively. The operation of the LEV should be systematically verified.

SUPPLEMENTARY DATA

Supplementary data can be found at <http://annhyg.oxfordjournals.org/>.

FUNDING

European Community's Seventh Framework Program HEXACOMM project (FP7-PEOPLE-2012-ITN, project 315760); The Finnish Work Environmental Fund (112132, 112133); National project IMPACT (CGL2011-26574); COST Action (TD1105-14937).

ACKNOWLEDGEMENTS

The authors declare no conflicts of interests. The authors alone are responsible for the content and writing of the article.

REFERENCES

- Alm S, Mukala K, Tiittanen P *et al* (2001). Personal carbon monoxide exposures of preschool children in Helsinki, Finland—comparison to ambient air concentrations. *Atmos Environ*; 35: 6259–66.
- Aschberger K, Johnston HJ, Stone V *et al*. (2010) Review of carbon nanotubes toxicity and exposure—appraisal of human health risk assessment based on open literature. *Crit Rev Toxicol*; 40: 759–90.
- Bello D, Hart J, Ahn K *et al*. (2008). Particle exposure levels during CVD growth and subsequent handling of vertically-aligned carbon nanotube films. *Carbon*; 46: 974–81.
- Bello D, Wardle B, Yamamoto N *et al*. (2009). Exposure to nanoscale particles and fibers during machining of hybrid advanced composites containing carbon nanotubes. *J Nanopart Res*; 11: 231–49.
- Bello D, Wardle B, Zhang J *et al*. (2010) Characterization of exposures to nanoscale particles and fibers during solid core drilling of hybrid carbon nanotube advanced composites. *Int J Occup Environ Health*; 16: 434–50.
- Birch ME. (2011) Exposure and emissions monitoring during carbon nanofiber production—Part II: polycyclic aromatic hydrocarbons. *Ann Occup Hyg*; 55: 1037–47.
- Birch M, Ku B, Evans D *et al*. (2011) Exposure and emissions monitoring during carbon nanofiber production—Part I: elemental carbon and iron-soot aerosols. *Ann Occup Hyg*; 55: 1016–36.
- Bottlinger M, Umhauer H. (1989). Single particle light scattering size analysis: quantification and elimination of the effect

- of particle shape and structure. *Part Part Syst Charact*; 6: 100–9.
- BSI. (2007). British Standard, PD 6699-2:2007. Nanotechnologies - Part 2: Guide to safe handling and disposal of manufactured nanomaterials. BSI Committee NT1/1, Nanotechnologies; ISBN 978 0 580 60832 2; December 2007.
- Catalán J, Järventaus H, Vippola M *et al.* (2012) Induction of chromosomal aberrations by carbon nanotubes and titanium dioxide nanoparticles in human lymphocytes in vitro. *Nanotoxicology*; 6: 825–36.
- CEN. (1993). *European Committee for Standardization, Workplace atmospheres-size fraction definitions for measurement of airborne particles (Report No. BS EN 481:1993)*. London, UK: CEN, British Standards Institute.
- Cena LG, Peters TM. (2011) Characterization and control of airborne particles emitted during production of epoxy/carbon nanotube nanocomposites. *J Occup Environ Hyg*; 8: 86–92.
- Dahm M, Evans D, Schubauer-Berigan M *et al.* (2013) Occupational exposure assessment in carbon nanotube and nanofiber primary and secondary manufacturers: mobile direct-reading sampling. *Ann Occup Hyg*; 57: 328–44.
- Dahm M, Evans D, Schubauer-Berigan M *et al.* (2012) Occupational exposure assessment in carbon nanotube and nanofiber primary and secondary manufacturers. *Ann Occup Hyg*; 56: 542–56.
- De Volder M, Tawfick S, Baughman R *et al.* (2013) Carbon nanotubes: present and future commercial applications. *Science*; 339: 535–39.
- Donaldson K, Poland CA, Murphy FA *et al.* (2013) Pulmonary toxicity of carbon nanotubes and asbestos - similarities and differences. *Adv Drug Deliv Rev*; 65: 2078–86.
- Evans DE, Ku BK, Birch ME *et al.* (2010) Aerosol monitoring during carbon nanofiber production: mobile direct-reading sampling. *Ann Occup Hyg*; 54: 514–31.
- Gebhart J. (1991). Response of single-particle optical counters to particles of irregular shape. *Part Part Syst Charact*; 8: 40–7.
- Han JH, Lee EJ, Lee JH *et al.* (2008) Monitoring multiwalled carbon nanotube exposure in carbon nanotube research facility. *Inhal Toxicol*; 20: 741–49.
- Hedner M, Kåredal M, Gustavsson P *et al.* (2013). The Nordic Expert Group for Criteria Documentation of Health Risks from Chemicals, 148. Carbon nanotubes. *Arbete och Hälsa*; 47.
- Huang G, Park JH, Cena LG *et al.* (2012) Evaluation of Airborne particle emissions from commercial products containing carbon nanotubes. *J Nanopart Res*; 14: 20.
- IFA. (2009). *Criteria for Assessment of the Effectiveness of Protective Measures Institute for Occupational Safety and Health of the German Social Accident Insurance*.
- Keskinen J, Pietarinen K, Lehtimäki M. (1992). Electrical low pressure impactor. *J Aerosol Sci*; 23: 353–60.
- Kisin ER, Murray AR, Sargent L *et al.* (2011) Genotoxicity of carbon nanofibers: are they potentially more or less dangerous than carbon nanotubes or asbestos? *Toxicol Appl Pharmacol*; 252: 1–10.
- Kulkarni P, Deye GJ, Baron PA. (2009). Bipolar diffusion charging characteristics of single-wall carbon nanotube aerosol particles. *J Aerosol Sci*; 40: 164–79.
- Lee JH, Lee SB, Bae GN *et al.* (2010) Exposure assessment of carbon nanotube manufacturing workplaces. *Inhal Toxicol*; 22: 369–81.
- Manke A, Luanpitpong S, Dong C *et al.* (2014) Effect of fiber length on carbon nanotube-induced fibrogenesis. *Int J Mol Sci*; 15: 7444–61.
- Manke A, Wang L, Rojanasakul Y. (2013) Pulmonary toxicity and fibrogenic response of carbon nanotubes. *Toxicol Mech Methods*; 23: 196–206.
- Maynard AD, Baron PA, Foley M *et al.* (2004) Exposure to carbon nanotube material: aerosol release during the handling of unrefined single-walled carbon nanotube material. *J Toxicol Environ Health A*; 67: 87–107.
- Methner MM. (2010) Effectiveness of a custom-fitted flange and local exhaust ventilation (LEV) system in controlling the release of nanoscale metal oxide particulates during reactor cleanout operations. *Int J Occup Environ Health*; 16: 475–87.
- Methner M, Hodson L, Dames A *et al.* (2010) Nanoparticle Emission Assessment Technique (NEAT) for the identification and measurement of potential inhalation exposure to engineered nanomaterials—Part B: Results from 12 field studies. *J Occup Environ Hyg*; 7: 163–76.
- Moisala A, Nasibulin AG, Shandakov SD *et al.* (2005). On-line detection of single-walled carbon nanotube formation during aerosol synthesis methods. *Carbon*; 43: 2066–74.
- Nanocyl. (2009). *Responsible care and nanomaterials case study Nanocyl. Presentation at European Responsible Care Conference, Prague*. Brussels, Belgium: The European Chemical Industry Council (CEFIC).
- Nasibulin AG, Anisimov AS, Pikhitsa PV *et al.* (2007). Investigations of NanoBud formation. *Chem Phys Lett*; 446: 109–14.
- Nasibulin AG, Pikhitsa PV, Jiang H *et al.* (2005). Correlation between catalyst particle and single-walled carbon nanotube diameters. *Carbon*; 43: 2251–57.
- NIOSH. (2013). Occupational exposure to carbon nanotubes and nanofibers, Current Intelligence Bulletin 65. Publication No. 2013–145. Cincinnati: National Institute for Occupational Safety and Health, Department of Health and Human Services. pp. 1–184.
- Nowack B, David RM, Fissan H *et al.* (2013). Potential release scenarios for carbon nanotubes used in composites. *Environ Int*; 59: 1–11.
- Ogura I. (2013). Guide to measuring airborne carbon nanotubes in workplaces: Technology Research Association for Single Wall Carbon Nanotubes (TASC), Research Institute of Science for Safety and Sustainability (RISS), National Institute of Advanced Industrial Science and Technology (AIST).
- Park S, Vosguerichian M, Bao Z. (2013). A review of fabrication and applications of carbon nanotube film-based flexible electronics. *Nanoscale*; 5: 1727–52.

- Pauluhn J. (2010) Multi-walled carbon nanotubes (Baytubes): approach for derivation of occupational exposure limit. *Regul Toxicol Pharmacol*; 57: 78–89.
- Rydman E, Catalán J, Nymark P *et al.* (2013). Evaluation of the health effects of carbon nanotubes. Final report on project number 109137 of the Finnish work environment fund, Finnish Institute of Occupational Health.
- Rydman E, Ilves M, Koivisto A *et al.* (2014). Inhalation of rod-like carbon nanotubes causes unconventional allergic airway inflammation. *Part Fibre Toxicol*; 11: 1–17.
- Sargent LM, Hubbs AF, Young SH *et al.* (2012) Single-walled carbon nanotube-induced mitotic disruption. *Mutat Res*; 745: 28–37.
- Sato Y, Yokoyama A, Nodasaka Y *et al.* (2013) Long-term biopersistence of tangled oxidized carbon nanotubes inside and outside macrophages in rat subcutaneous tissue. *Sci Rep*; 3: 2516.
- Schmoll LH, Elzey S, Grassian VH *et al.* (2009). Nanoparticle aerosol generation methods from bulk powders for inhalation exposure studies. *Nanotoxicology*; 3: 265–75.
- Sun DM, Liu C, Ren WC *et al.* (2013). A review of carbon nanotube- and graphene-based flexible thin-film transistors. [Research Support, Non-U S Gov't]. *Small*; 9: 1188–205.
- Szymanski WW, Nagy A, Czitrovsky A. (2009). Optical particle spectrometry—Problems and prospects. *J Quant Spectrosc Radiat Transf*; 110: 918–29.
- Tsai SJ, Hofmann M, Hallock M *et al.* (2009). Characterization and evaluation of nanoparticle release during the synthesis of single-walled and multiwalled carbon nanotubes by chemical vapor deposition. [Research Support, U S Gov't, Non-P H S]. *Environ Sci Technol*; 43: 6017–23.
- Wu Z, Chen Z, Du X *et al.* (2004). Transparent, conductive carbon nanotube films. *Science*; 305: 1273–76.
- Yang L, Wang S, Zeng Q *et al.* (2013). Carbon nanotube photoelectronic and photovoltaic devices and their applications in infrared detection. [Research Support, Non-U S Gov't]. *Small*; 9: 1225–36.
- Zhang Q, Huang JQ, Qian WZ *et al.* (2013). The road for nanomaterials industry: a review of carbon nanotube production, post-treatment, and bulk applications for composites and energy storage. [Research Support, Non-U S Gov't]. *Small*; 9: 1237–65.

Supplementary material

Characterization of exposure to carbon nanotubes in an industrial setting

A. S. Fonseca^{1,2,*}, A. K. Viitanen³, A. J. Koivisto^{3,4}, A. Kangas³, M. Huhtiniemi³, T. Hussein^{5,6}, E. Vanhala³, M. Viana¹, X. Querol¹, K. Hämeri⁵

¹ Institute of Environmental Assessment and Water Research (IDAEA-CSIC), C/ Jordi Girona 18, 08034 Barcelona, Spain

² University of Barcelona, Faculty of Chemistry, Department of Analytical Chemistry, Martí i Franquès, 1-11, 08028 Barcelona

³ Finnish Institute of Occupational Health, Nanosafety Research Centre, Topeliuksenkatu 41 a A, FI-00250 Helsinki, Finland

⁴ National Research Centre for the Working Environment, Lersø Parkallé 105, Copenhagen DK-2100, Denmark

⁵ University of Helsinki, Department of Physics, P.O. Box 64, FI-00014 Helsinki, Finland

⁶ University of Jordan, Faculty of Science, Department of Physics, Amman, JO-11942 Jordan

*Corresponding author: ana.godinho@idaea.csic.es, telephone: (0034) 656588592

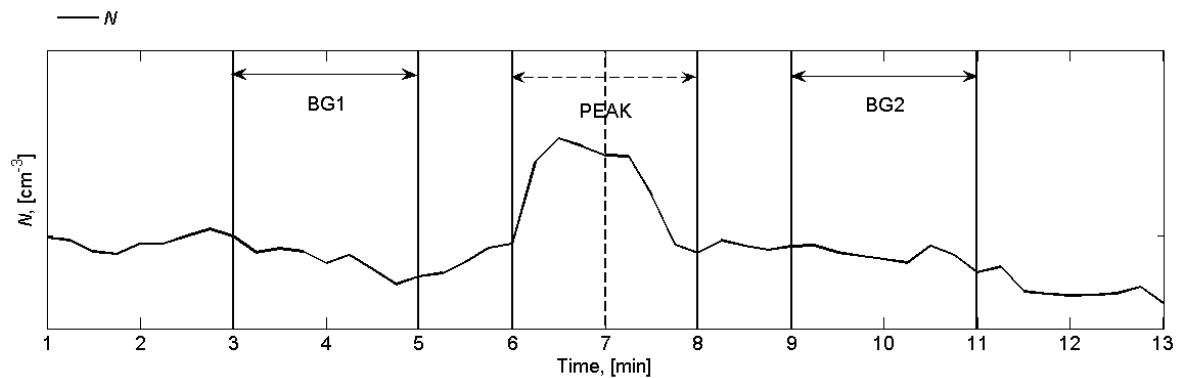


Figure S1. Schematic procedure for calculation of background (BG) and collection chamber opening concentration (peak) for each specific reactor. The vertical dashed line corresponds to the collection chamber opening time. Between the peak and background there is an interval gap of 1 min.

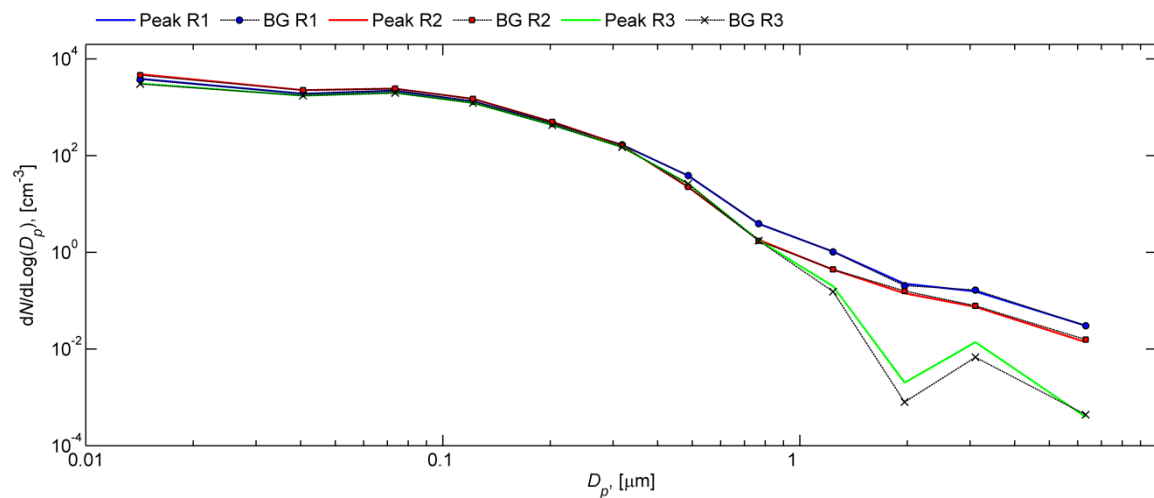


Figure S2. Number particle size distributions measured by ELPI from specific reactor collection chamber openings.

Table S1. Summary results by process and instruments which are further stratified by number of minutes sampled (t , min), geometric mean (N and m), geometric standard deviation (σ) and maximum value of particle number (N max) and CO concentration (CO max).

	N-WCPC			NanoScan			ELPI			OPS			CO			
	t [min]	N [cm^{-3}]	σ [cm^{-3}]	N max [cm^{-3}]	t [min]	N [cm^{-3}]	σ [cm^{-3}]	N max [cm^{-3}]	t [min]	N [cm^{-3}]	σ [cm^{-3}]	N max [cm^{-3}]	t [min]	m [$\mu\text{g m}^{-3}$]	σ [$\mu\text{g m}^{-3}$]	m max [$\mu\text{g m}^{-3}$]
WE																
WE1	540	1.9×10^3	5.0×10^2	2.0×10^4	540	2.0×10^3	4.4×10^2	3.4×10^3	540	4.9	7.8×10^{-1}	7.1	540	8.3×10^2	2.1×10^2	3.8×10^3
WE2	8	2.3×10^3	3.3×10^2	1.0×10^4	8	2.5×10^3	1.3×10^2	2.7×10^3	8	11	1.3×10^{-1}	11	8	5.5×10^3	1.3×10^4	7.3×10^4
WE3	44	3.3×10^3	5.0×10^2	4.3×10^3	44	1.9×10^3	1.2×10^2	2.2×10^3	44	-	-	-	44	4.9×10^2	1.4×10^2	2.1×10^3
WH	2707	5.4×10^3	1.7×10^4	5.7×10^5	2760	2.0×10^3	1.4×10^3	1.3×10^4	2005	3.9×10^3	3.2×10^3	2.7×10^4	2671	7.7×10^2	7.0×10^2	6.3×10^5
NWH*	7380	1.4×10^3	3.4×10^3	9.7×10^4	7380	1.3×10^3	4.8×10^2	2.8×10^3	6480	2.6×10^3	1.1×10^3	9.5×10^3	7380	13	8	28
													6480	2.7×10^2	86.00	1.7×10^3

σ - Standard deviation

* Including weekend

"-" Not measured

Table S2. Summary results of calculated mean of mass concentration (m), geometric standard deviation (σ) and maximum value (m max).

	NanoScan			ELPI			OPS		
	m [$\mu\text{g m}^{-3}$]	σ [$\mu\text{g m}^{-3}$]	m max [$\mu\text{g m}^{-3}$]	m [$\mu\text{g m}^{-3}$]	σ [$\mu\text{g m}^{-3}$]	m max [$\mu\text{g m}^{-3}$]	m [$\mu\text{g m}^{-3}$]	σ [$\mu\text{g m}^{-3}$]	m max [$\mu\text{g m}^{-3}$]
WE									
WE1	8.3×10^{-1}	1.8×10^{-1}	1.3	3.4	22.0	2.8×10^2	8.1×10^{-1}	8.2×10^{-1}	12.0
WE2	1.0	7.1×10^{-2}	1.2	25	3.8	34.0	1.7	6.9×10^{-1}	2.6
WE3	1.2	1.2×10^{-1}	1.4	6.1	12.0	1.2×10^2	-	-	-
WH	1.0	3.2×10^{-1}	4.5	6.7	22.0	3.2×10^2	1.5	5.7	2.2×10^2
NWH*	9.2×10^{-1}	3.1×10^{-1}	2.5	4.5	6.0	34.0	4.2×10^{-1}	2.1×10^{-1}	1.6

σ - Standard deviation

* Including weekend

"-" Not measured

4.2 Article II: Ultrafine and nanoparticle formation and emission mechanisms during laser processing of ceramic materials

Authors:

Fonseca, A. S.^{1,2}, Viana, M.¹, Querol, X.¹, Moreno, N.¹, de Francisco, I.³, Estepa, C.³,
de la Fuente, G.F.³

¹ Institute of Environmental Assessment and Water Research (IDÆA-CSIC), C/ Jordi Girona 18, 08034 Barcelona, Spain.

² Universidad de Barcelona, Facultad de Química, Martí i Franquès 1-11, 08028 Barcelona, Spain.

³ Instituto de Ciencia de Materiales de Aragón (ICMA - Universidad de Zaragoza), María de Luna 3, E-50018 Zaragoza, Spain.

Published in:

J Aerosol Sci, 88, 48-57, 2015
doi:10.1016/j.jaerosci.2015.05.013

Accepted date: 6 June 2015 (available online)



Contents lists available at ScienceDirect

Journal of Aerosol Science

journal homepage: www.elsevier.com/locate/jaerosci

Ultrafine and nanoparticle formation and emission mechanisms during laser processing of ceramic materials



A.S. Fonseca^{a,b,*}, M. Viana^a, X. Querol^a, N. Moreno^a, I. de Francisco^c, C. Estepa^c, G.F. de la Fuente^c

^a Institute of Environmental Assessment and Water Research (IDEA-CSIC), C/Jordi Girona 18, 08034 Barcelona, Spain

^b Universidad de Barcelona, Facultad de Química, Martí i Franquès 1-11, 08028 Barcelona, Spain

^c Instituto de Ciencia de Materiales de Aragón (ICMA – Universidad de Zaragoza), María de Luna 3, E-50018 Zaragoza, Spain

ARTICLE INFO

Article history:

Received 25 February 2015

Received in revised form

25 May 2015

Accepted 27 May 2015

Available online 6 June 2015

Keywords:

Tile sintering

Furnace

New particle formation

LDSA

Particle transport

Indoor air

ABSTRACT

The use of laser technology in the ceramic industry is undergoing an increasing trend, as it improves surface properties. The present work aimed to assess ultrafine and nanoparticle emissions from two different types of laser treatments (tile sintering and ablation) applied to two types of tiles. New particle formation mechanisms were identified, as well as primary nanoparticle emissions, with concentrations reaching up to 6.7×10^6 particles cm^{-3} and a mean diameter of 18 nm. Nanoparticle emission patterns were strongly dependent on temperature and raw tile chemical composition. Nucleation events were detected during the thermal treatment independently of the laser application. TEM images evidenced spherical ultrafine particles, originating from the tile melting processes. When transported across the indoor environment, particles increased in size (up to 38 nm) with concentrations remaining high (2.3×10^6 particles cm^{-3}). Concentrations of metals such as Zn, Pb, Cu, Cr, As and Tl were found in particles < 250 nm.

© 2015 The Authors. Published by Elsevier Ltd. This is an open access article under the CC BY-NC-ND license (<http://creativecommons.org/licenses/by-nc-nd/4.0/>).

1. Introduction

Laser irradiation of ceramic material is a novel technique with numerous advantages regarding the sintering process such as speed, temperature and enhanced durability and surface properties of structural materials (Schmatjko, Endres, Schmidt, & Banz, 1988; Toenshoff & Gedrat, 1991; Jervis, Nastasi, Hubbard, & Hirvonen, 1993; de Francisco et al., 2011; Lahoz, de la Fuente, Pedra, & Carda, 2011). The use of high powered CO₂ lasers for industrial ceramic materials processing was studied in the framework of LIFE projects and is currently being assessed for two different industrial processes: (i) tile sintering in a high-temperature furnace and, (ii) ablation of ceramic materials. A recently developed “in-situ” melting method (tile sintering) makes use of a CO₂ laser scanner combined with simultaneous external heating of the substrate (in a conventional furnace) and uniform movement (Estepa & de la Fuente, 2006; de Francisco et al., 2011). This innovative technology allows to obtain coatings of practically any oxide material on an alumina substrate (Estepa & de la Fuente, 2006; de Francisco et al., 2011). In addition, this novel tool can also make use of CO₂ lasers in pulsed mode (induced laser ablation) to perform engravings on the surface of ceramics (Lahoz et al., 2011).

* Corresponding author at: Institute of Environmental Assessment and Water Research (IDEA-CSIC), C/Jordi Girona 18, 08034 Barcelona, Spain. Tel.: +34 934006100; fax: +34 932045904.

E-mail address: ana.godinho@idaea.csic.es (A.S. Fonseca).

<http://dx.doi.org/10.1016/j.jaerosci.2015.05.013>

0021-8502/© 2015 The Authors. Published by Elsevier Ltd. This is an open access article under the CC BY-NC-ND license (<http://creativecommons.org/licenses/by-nc-nd/4.0/>).

The high-energy nature of these laser processes implies a significant potential for the generation and emission of particles in the ultrafine and nanoparticle size range. However, nanoparticle emissions have so far never been evaluated for these industrial processes, mainly due to the novelty of this technology. The high temperatures applied in the furnace (up to 1195 °C) may cause chemical transformations in the raw tiles and the emission of particulate and/or gaseous pollutants into indoor air, which could be enhanced by the addition of the laser treatment.

Nanoparticle emissions from industrial processes are receiving increasing attention in the literature in recent years (Demou, Peter, & Hellweg, 2008; Pfefferkorn et al., 2010; Curwin & Bertke, 2011; Gandra, Miranda, Vilaça, Velhinho, & Teixeira, 2011; Koivisto et al., 2012; Van Broekhuizen, 2012; Gómez, Irusta, Balas, & Santamaria, 2013; Fonseca et al., 2014; Gomez et al., 2014; Voliotis et al., 2014; Koivisto et al., 2014). These works focus on different types of processes, and reveal that nanoparticle emissions and subsequent exposures may reach up to particle number concentrations of 1×10^6 parts cm^{-3} such as the cases of firing processes where the painting and glazing of ceramics occur (Voliotis et al., 2014), as well as during and welding/soldering (Gómez et al., 2013). However, because of the vast number of industrial processes with potential for nanoparticle emissions, the assessment of nanoparticle emissions under real-world scenarios should be encouraged. The present work addresses the emissions from a highly innovative process with a large potential for global-scale implementation in the ceramic industry, which has so far not been evaluated regarding nanoparticle emissions.

This work aimed to identify and characterize nanoparticle formation and emission mechanisms during tile sintering and laser ablation processes in a pilot plant-scale furnace (3 m long). Special attention was paid to new particle formation processes and their dependence on process variables such as temperature or raw tile chemical composition. Finally, nanoparticle transformations through transport in indoor air are also described.

2. Materials and methods

2.1. Materials and experimental procedure

Nanoparticle monitoring and sampling was conducted over three consecutive days (from 23rd October to 25th October 2013), in a research laboratory at the Instituto de Ciencia de Materiales de Aragón (ICMA) located in Zaragoza, Spain. The experiments were not extended over a longer period of time due to two main reasons: (a) particle emissions detected (see next section) were significantly above background concentrations, and thus the data obtained were considered statistically representative of the processes under study, and (b) the availability of the pilot-plant scale furnace was limited. The laser used included a Rofin-Sinar 350 W SLAB-type CO_2 laser resonator and an optical beam steering system (Estepa & de la Fuente, 2006). Two types of laser-based processes were assessed:

a) Tile sintering

Industrial ceramic tiles were sintered by laser irradiation in a high-temperature furnace. The tile sintering process was performed using a CO_2 laser emitting at a wavelength $\lambda = 10.6 \mu\text{m}$. The tiles were introduced in the furnace at a constant speed (1.5 m h^{-1}) in an orthogonal direction to the laser focus. The samples were gradually externally heated with a resistance furnace in a temperature range from ambient temperature up to 850 °C. Afterwards, the tiles followed the standard thermal cycles used at industrial-scale, with gradually increasing temperatures which reached peak values of about 1195 °C and 1115 °C for porcelain and red clay tiles, respectively.

Six conventional industrial tiles were selected: raw porcelain (#1), porcelain with frit (#2), porcelain with frit and colored decoration (#3), raw red clay (#4), red clay with frit (#5) and red clay with frit and colored decoration (#6). These are six of the most frequently used types of tiles in the industry.

b) Laser ablation

Laser ablation is the process by which material is expelled from a surface by irradiating it with a pulsed laser (Bäuerle, 1996; Rubahn, 1999; Lahoz et al., 2011). Fig. S1 in the supplementary information presents an illustration of these effects. It illustrates the presence of a melted layer at the surface of the porcelain tiles where the laser is irradiating. Particle emissions during laser ablation were only assessed for one type of material (raw porcelain; #7).

2.2. Sampling locations

The laboratory under study had a surface of 29 m^2 . The particle monitors and samplers were placed simultaneously at the emission source, directly above the furnace, at a second location indoors to assess the influence of transport (referred to as the breathing zone), and in outdoor air. Measurements at the emission source were performed between the furnace and the extraction system, and were therefore only influenced by emissions generated in the furnace (no contamination from background air was possible). Fig. S2 of the supplementary information shows the layout of the indoor area under study and sampling locations.

The height of the furnace from the floor is 1.1 m. At the source, instrument inlets were placed inside a 15 cm diameter tube (2.05 m above ground level), which acted as ventilation system for the furnace. In addition, measurements were made in the worker area, located at approximately 2 m from the furnace. Inlets were placed at breathing zone height (~ 1.6 m).

2.3. Real time measurements

Particle measurements in the range 5 nm to 20 μm were performed using different instrumentation, aiming to combine the specific advantages of each of the instruments used with the purpose of overcoming their specific limitations, especially regarding lower particle sizes and maximum particle number concentrations measured:

a) At the emission source:

- An electrical mobility spectrometer (NanoScan, SMPS TSI Model 3910; sample flow rate 0.7 L min⁻¹) to measure the particle mobility size distribution in 13 channels from 10 to 420 nm mobility diameter. Time resolution was 1 min.
- An Optical Particle Sizer (OPS, TSI Model 3330; sample flow rate 1 L min⁻¹) which measures the optical size distribution from 0.3 to 10 μm in 16 channels with 1 min time resolution.
- A water-based condensation particle counter (WCPC, TSI Model 3785; sample flow rate 1 L min⁻¹) measuring total particle number concentration between 5 nm and 3 μm with 1 min time resolution.

In the breathing zone:

- #### b)
- An optical particle counter (OPC; Grimm Model 1.108) to measure particle mass in the range 0.3–20 μm . The sample flow rate and the sampling time interval were 1.2 L min⁻¹ and 1 min, respectively. The particles were classified in 15 channels according to their optical diameter.

In addition, the following instruments were placed simultaneously at the emission source and at the breathing zone:

- Two light-scattering laser photometers (DustTrak™ DRX aerosol monitor TSI Model 8533; sample flow rate 3.0 L min⁻¹) to measure PM₁₀, PM_{2.5}, PM₁ with 1 min time resolution. The PM values in the breathing zone were corrected with respect to reference gravimetric values, using a high-volume reference sampler. This was not possible, however, for the instrument at the emission source, and therefore only uncorrected values are reported.
- Two miniature diffusion size classifiers DiscMini Matter Aerosol (Fierz, Houle, Steigmeier, & Burtscher, 2011) to measure total particle number, mean particle diameter and alveolar lung deposited surface area (LDSA) concentration. The sample flow rate and the sampling time interval were 1 L min⁻¹ and 1 min, respectively. The instrument detects particles with a mode diameter between 10 and 300 nm.

Because certain of these instruments monitored similar parameters (e.g. WCPC and NanoScan monitoring particle number concentrations although in different size ranges), in the results and discussion section only one of the datasets will be discussed for each parameter. In the case of total particle number (N), the results presented will be those obtained with the WCPC, unless otherwise specified, because of the highest concentration range measurable with this instrument (up to 10⁷ parts cm⁻³, as opposed to 10⁶ parts cm⁻³ with NanoScan or DiscMini). The same applies for mean particle diameter, which will be discussed using the DiscMini data, because it is the only instrument for which particle diameter data were available simultaneously in the emission source and breathing zone. In the original setup, the use of different instruments measuring similar parameters aimed to maximize the number of valid data points obtained, given that the risk of exceeding the measurement capabilities of the instruments was high (due to the high nanoparticle emissions expected). Intercomparisons carried out during data processing (not shown) evidenced a high degree of comparability ($\pm 15\%$ of relative difference) between the different instruments for those with matching particle size ranges.

2.4. Sample collection

Particles emitted at the source were collected on 25 mm polycarbonate filters (one sample per ceramic material, plus one sample each night) with 0.8 μm pore size. Samples were collected using cassettes (SKC Inc., inlet diameter 1/8 in.) connected to SKC Leland Legacy pumps operating at 0.21 m³ h⁻¹ (3.5 L min⁻¹). The sampling periods ranged from 20 min to 102 min, which correspond to air volumes sampled between 0.07 m³ and 0.36 m³, respectively.

In addition, one accumulated sample was collected over the entire sampling period (26 h) by means of Personal Cascade Impactor Sampler (Sioutas™ PCIS, SKC Inc.) (Misra et al., 2002). Two PCIS were placed simultaneously indoor and outdoor connected to pumps operating at 9 L min⁻¹. The collection substrates were 37 mm quartz fiber filters for the < 0.25 μm (Pall) stage and 25 mm teflon-PTFE filters for the 0.25–2.5 μm and 2.5–10 μm stages (Pall).

Mass concentrations were gravimetrically determined by pre- and post-weighting the filters on a microbalance.

Particle morphology, chemical composition, and size were analyzed by transmission electron microscopy (TEM, Jeol, JEM 1220, Tokyo, Japan), coupled with an energy-dispersive X-ray (EDX) spectroscopy. Particles for TEM were collected onto Quantifoil® gold (Au) grids with 1 μm diameter holes – 4 μm separation of 200-mesh at the emission source. TEM grids were attached to air sample cassettes (SKC Inc., USA, inlet diameter 1/8 in. and filter diameter 25 mm) on polycarbonate membrane filters. Air flow was driven by pumps operating at 3.5 L min⁻¹ and collection efficiency for particles was assumed to be 100%. TEM sampling durations and sampled air volume were the same as for the polycarbonate filter samples described above.

2.5. Sample treatment and analysis

All the filters and samples of each raw ceramic material were acid digested by using nitric acid (HNO₃), hydrofluoric acid (HF) and perchloric acid (HClO₄) following the method proposed by Querol et al. (2001) for the analysis of major and trace elements by means of ICP-AES (IRIS Advantage TJA Solutions, THERMO) and ICP-MS (X Series II, THERMO). Laboratory blank filters were analyzed following the same methodology. Element concentrations were blank corrected.

In order to identify the mineralogical phases, a portion of each raw studied ceramic material was analyzed by X-ray powder diffraction (XRD).

3. Results and discussion

3.1. Chemical and mineral composition of the raw tiles

The chemical composition of the raw porcelain and red clay tiles is reported in Table S1 of the supplementary information. The composition of red clay and porcelain tiles was clearly distinct. Porcelain was characterized by higher concentrations of SiO₂, Al₂O₃, Na₂O and P₂O₅ with the largest difference being observed for Na₂O (93% higher than in red clay tiles). The relative concentrations of the remaining metal oxides were always higher for red clay tiles. The relative concentrations of trace elements were also higher in red clay tiles, which are enriched in all the elements analyzed, except for Y and Nb.

Fig. S3 of the supplementary information shows the diffraction pattern determined by XRD analysis for each type of tile. Common crystalline constituents found in both types of tiles were quartz, SiO₂ (00-046-1045); kaolinite, Al₂Si₂O₅(OH)₄ (00-014-0164); illite, (K,H₃O)(Al₂Si₃AlO₁₀(OH)₂) (00-026-0911) and, anhydrite, CaSO₄ (00-037-1496). Conversely, mineral phases such as albite, NaAlSi₃O₈ (00-019-1184) were only found in porcelain tiles, whereas calcite, CaCO₃ (00-005-0586), dolomite, CaMg(CO₃)₂ (00-036-0426), hematite, Fe₂O₃ (00-033-0664) and microcline, KAlSi₃O₈ (00-019-0932) were only found in red clay tiles.

The composition of frit and pigments used for decoration may not be provided due to confidentiality reasons. Pigments are essentially composed of oxides of Al, Cu, Cr, Co, Mn, Fe, Pb, and Sn (Taylor, Bull, & Ceramics, 1986; Casasola, Rincón, & Romero, 2012; Celades, 2013). Furthermore, ZrSiO₄, ZrO₂, ZnO, TiO₂ and SnO₂ are frequently used as opacifying agents to produce opaque frits (Jacobs, 1954; Romero, Rincón, & Acosta, 2003; Lahoz et al., 2011; Casasola et al., 2012).

3.2. Nanoparticle emissions

The time series of particle number concentrations, measured at the emission source (the furnace for sintering processes, and outside the furnace for ablation process) are shown in Fig. 1. Table 1 summarizes the mean and maximum concentrations obtained in terms of number and mass concentrations, as well as the mean particle diameter for the emissions from each of the materials sintered (from #1 to #6), the material ablated (#7) and for background air (non-activity period).

Over the two-hour periods during which each of the tiles underwent the thermal treatment, major nanoparticles emissions were registered. On average, mean and maximum *N* minute concentrations were 1 and 2 orders of magnitude (respectively) higher than background levels, and by applying the methodology described by Asbach et al. (2012) and based on the ratio between workplace air concentrations and 3 times the standard deviation of the background concentration, it may be concluded that nanoparticle emissions during thermal treatment were statistically representative. Mean particle diameters were lower (8–18 nm) than in background air (38 nm). The fact that measurements were carried out in a pilot-plant scale furnace suggest that the emission processes detected are likely to take place also at industrial scale.

The highest nanoparticle emissions were registered during red clay tile sintering and, in particular for material #5, reaching a maximum of 6.7×10^6 parts cm⁻³ (particle mean diameter=18 nm). Maximum nanoparticle emissions during sintering of a similarly coated material (#2) were lower by a factor of 2, thus suggesting that majority of the nanoparticles emissions originate from the base of the tiles, as opposed to the coating materials. On average, nanoparticle emissions were

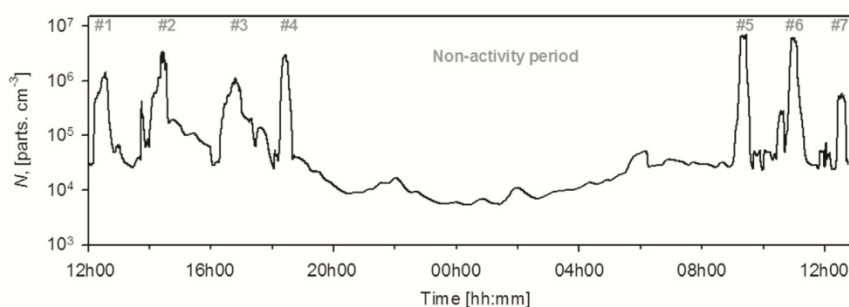


Fig. 1. Time series of particle number concentration measured at emission source.

Table 1

Average and maximum (in parenthesis) particle number concentrations, particle diameter and mass concentrations measured during tile sintering, ablation and background. Mean values corresponding to each sintering and ablation process, approximately 1.5 h and 20 min in duration, respectively. Maximum values are 1 min means.

Material	N [parts cm^{-3}]	D_p [nm]	PM_1 [$\mu\text{g m}^{-3}$]	$\text{PM}_{2.5}$ [$\mu\text{g m}^{-3}$]	PM_{10} [$\mu\text{g m}^{-3}$]
#1: Raw porcelain	2.7×10^5 (1.4×10^6)	8 (16)	5.4 (25.0)	6.5 (26.0)	10.2 (40)
#2: Porcelain with frit coated	5.7×10^5 (3.3×10^6)	11 (24)	6.0 (41.0)	7.0 (48.0)	12.4 (115.0)
#3: Porcelain with frit and decoration coated	3.6×10^5 (1.1×10^6)	11 (22)	22.6 (52.0)	23.5 (53.0)	28.5 (58.0)
#4: Raw red clay	4.2×10^5 (3.1×10^6)	16 (31)	10.2 (43.0)	11.3 (50.0)	16.9 (115.0)
#5: Red clay with frit coated	9.7×10^5 (6.7×10^6)	18 (30)	24.1 (125.0)	25.8 (128.0)	30.4 (131.0)
#6: red clay with frit and decoration coated	9.5×10^5 (6.1×10^6)	15 (25)	19.5 (64.0)	21.5 (66.0)	26.1 (69.0)
#7: Ablation	3.8×10^5 (5.8×10^5)	80 (130)	610 (1110)	650 (1200)	670 (1300)
Background ^a	1.6×10^4 (9.8×10^4)	38 (60)	2.8 (24.0)	3.4 (27.0)	4.7 (57.0)

^a Corresponding to non-activity period.

higher for red clay sintering (7.8×10^5 parts cm^{-3}) when compared to porcelain (4.0×10^5 parts cm^{-3}). This is an especially relevant finding for the tile industry, given that red clay materials are usually preferred because of their lower cost with respect to porcelain. However, due to esthetic reasons, the demand for porcelain tiles is currently increasing in the global ceramic market. Regarding mean particle diameter, emissions from red clay sintering were on average coarser (16 nm) than from porcelain tiles (10 nm), even if both particle diameters are extremely small especially in comparison to background air.

A relatively similar pattern was observed for particle mass. The highest total PM emissions were generated during sintering of frit coated red clay tiles (#5; $32.8 \mu\text{g m}^{-3}$), although followed closely by frit and decoration coated porcelain (#3; $30.5 \mu\text{g m}^{-3}$). The lowest emissions in terms of mass originated from porcelain sintering where a reduce influence on the formation of larger particles were found, especially for coated porcelain.

Fig. 1 and Table 1 also show the results from the ablation (#7). Results show that ablation emissions were highest in terms of mass for all size ranges and materials and lowest in terms of particle number concentration (3.8×10^5 parts cm^{-3}) (with exception of material #1, and #3). Furthermore, the particle size was highest showing a mean diameter of 80 nm. These observations were expected during ablation because it is a mechanical process (as opposed to a thermal process). The TEM samples show a large number of spherical morphology particles below $1 \mu\text{m}$ in indoor air (Fig. 2), especially during the ablation process (d) where aggregates of particles in the nano-size range are observed. This is expected to occur due to the fact that laser engraving induces phase transitions, causing break down of the original material (Lahoz et al., 2011). During ablation, particles are produced with a more spherical shape whereas during sintering (Fig. 2a–c) they are finer and may be interpreted as portions of melted material involved in melting processes at a high temperature under the laser beam. Chemical analysis by EDX showed that the nanoparticles are mostly constituted by elements such as Zn, Cu and Fe due to the extensive use of these substances as opacity and pigmentation agents in ceramic tiles (Casasola et al., 2012; Celades, 2013).

3.3. Particle size distributions

The particle number distributions corresponding to porcelain and red clay sintering are shown in Fig. 3a and b, respectively. Additionally, results from raw porcelain ablation are presented in Fig. 3a. The mean particle diameters produced from sintering were below mostly 35 nm (for > 80% of the particles). Conversely, the ablation process produced mainly particles between 65 and 200 nm (for > 90% of the particles) in number.

The size distributions present different trends during sintering and ablation. During sintering, trimodal shaped distributions were measured, with mode values at 10–20 nm, 20–85 nm and 85–420 nm. This was observed for red clay and porcelain tiles. Conversely, laser ablation of porcelain tiles produced a bimodal curve, with mode values 10–50 nm and 50–420 nm, with a clear prevalence of coarser particles (> 100 nm) as expected.

Particle size distribution seemed to depend on the type of material. In particular, for particles ranging between 10 and 85 nm, mean particle number concentrations from porcelain tiles were higher (4.1×10^5 parts cm^{-3}) than from red clays (3.0×10^5 parts cm^{-3}). However, the number concentration for particles below 11.5 nm during sintering of material #6 were higher than for material #3, respectively. Concerning particles between 85 and 420 nm in diameter, particle number concentrations were higher for red clays (3.7×10^4 parts cm^{-3}) than for porcelain tiles (1.9×10^4 parts cm^{-3}).

3.4. Particle formation and emission mechanisms

Fig. 4 shows an example of time series of particle number concentrations and size for the particles emitted during the entire thermal cycle for porcelain and red clay tiles with frit coating (materials #2 and #5). Table 2 summarizes, for all of the materials, the mean and geometric standard deviation (σ) of particle number concentrations (N) and particle diameter (D_p).

Two different emission behaviors, strongly linked to temperature, were registered. In the first 30 min, when porcelain and red clay tiles were externally heated in the furnace in a temperature range between 850–1195 °C and 850–1115 °C for porcelain and red clay tiles respectively, a thermally-induced emission pattern was observed starting from 1.3×10^5 parts for

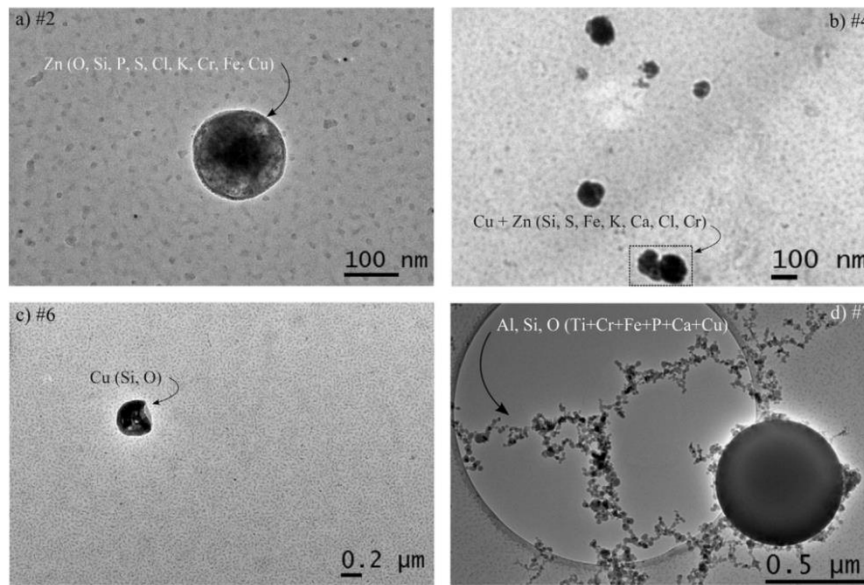


Fig. 2. TEM images of nanoparticles collected in indoor air during: (a) sintering of porcelain with frit coated; (b) sintering of raw red clay; (c) sintering of red clay with frit and decoration coated; (d) ablation of raw porcelain. Corresponding identified particles by EDX are shown in each figure.

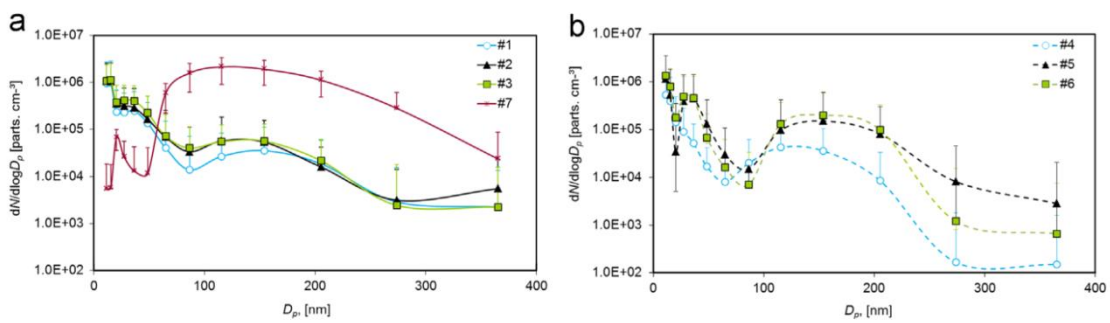


Fig. 3. Size distributions of particles including standard error bars during porcelain and red clay sintering and porcelain ablation. Error bars represent \pm standard deviation (σ).

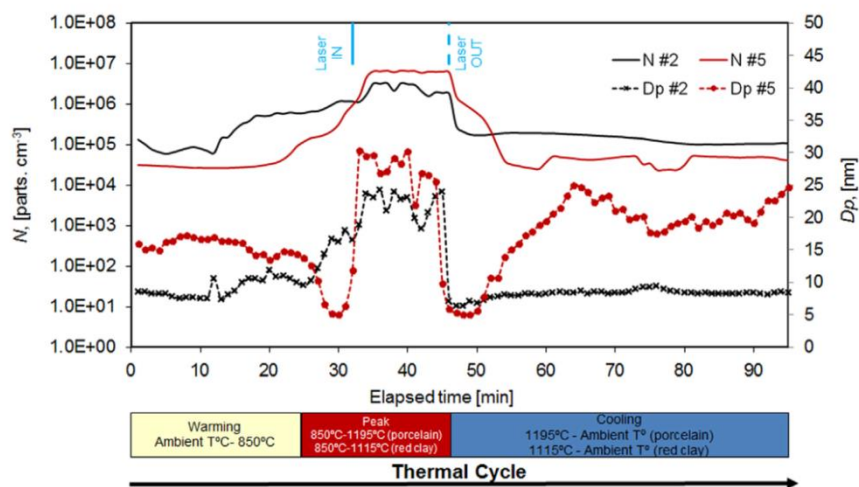


Fig. 4. Time series of particle number concentrations (solid lines) and mean particle size (dashed lines with bullets) during sintering of porcelain and red clay with frit coated.

Table 2

Geometric mean and standard deviation (in parenthesis) of particle number concentrations and particle diameter, only during the period of laser incidence.

Material	N [parts cm^{-3}]	D_p [nm]
#1: Raw porcelain	7.4×10^5 (5.0×10^5)	8 (2)
#2: Porcelain with frit coated	2.5×10^6 (7.0×10^5)	21 (5)
#3: Porcelain with frit and decoration coated	8.5×10^5 (1.6×10^5)	15 (4)
#4: Raw red clay	2.3×10^6 (7.0×10^5)	24 (5)
#5: Red clay with frit coated	5.6×10^6 (1.8×10^6)	24 (8)
#6: red clay with frit and decoration coated	5.0×10^6 (1.4×10^6)	15 (4)

Table 3

Average and maximum (in parenthesis) particle number concentrations, mean particle diameter and mean LDSA measured at breathing zone during tile sintering and background concentrations.

Material	N [parts cm^{-3}]	D_p [nm]	PM_{10} [$\mu\text{g m}^{-3}$]	$\text{PM}_{2.5}$ [$\mu\text{g m}^{-3}$]	PM_{10} [$\mu\text{g m}^{-3}$]	LDSA [$\mu\text{m}^2 \text{cm}^{-3}$]
#1: Raw porcelain	3.0×10^5 (1.2×10^6)	18 (26)	6.1 (8.9)	7.3(12.0)	13.2 (19.9)	277 (1547)
#2: Porcelain with frit coated	5.6×10^5 (1.4×10^6)	13 (28)	5.9 (7.8)	7.0(10.4)	12.5 (21.4)	371 (1686)
#3: Porcelain with frit and decoration coated	8.0×10^5 (2.3×10^6)	16 (29)	8.2 (12.8)	10.7(18.3)	17.0 (26.2)	687 (2271)
#4: Raw red clay	7.5×10^4 (4.7×10^5)	27 (36)	6.5 (8.0)	8.0(10.5)	13.8 (16.7)	69 (223)
#5: Red clay with frit coated	1.1×10^5 (3.1×10^5)	26 (38)	7.3 (9.1)	9.3(12.4)	15.7 (19.4)	115 (229)
#6: red clay with frit and decoration coated	2.7×10^5 (1.2×10^6)	19 (35)	7.7 (13.8)	10.0(20.2)	16.3 (28.5)	213 (551)
Background ^a	2.6×10^4 (1.7×10^5)	36 (58)	5.6 (12.9)	6.4(18.9)	11.4 (30.9)	35 (118)

^a Corresponding to non-activity period min means.

porcelain cm^{-3} and 3.1×10^4 parts cm^{-3} for red clay tiles frit coated. For material #2, the increase in mean particle size also followed the increase of the temperature in the furnace increasing from 9 nm probably due to condensation of pre-existing nanoparticles after emission. The evolution of the particle size of material #5 exhibited a different pattern: for the first 20 min, particle number concentrations and size remained stable and during the following 10 min, particle number concentration started to increase and a decrease in particle size was detected reaching lowest values of 5 nm. This suggests the occurrence of new particle formation processes by nucleation (nanoparticles < 30 nm in diameter being formed; Kumar, Fennell, & Britter, 2008), which would result in higher particle number concentrations with a lower particle size. This was probably due to the S-bearing species in the raw material such as anhydrite (CaSO_4), which decomposes at high temperatures (Chinchón, Querol, Fernández-Turiel, & López-Soler, 1991), into CaO and SO_2 . In the furnace, SO_2 probably causes nucleation events induced by H_2SO_4 as exhaust gases cool down (Kulmala et al., 2004). These events were not detected so clearly with porcelain materials, probably due to their much lower SO_4^{2-} content (0.03%).

Upon introduction of the laser beam (within the peak temperature zone, Fig. 4), the particle number concentrations increased reaching maximum values of 3.3×10^6 parts cm^{-3} (porcelain) and 6.7×10^6 parts cm^{-3} (red clay) with mean diameters of 24 nm and 30 nm, respectively. The increase in both particle size and concentration probably resulted from additional emissions of primary nanoparticles of melted products from the surface materials due to the laser treatment with slightly coarser particle diameters (> 24 nm as opposed to < 20 nm during the thermal treatment). The presence of submicron spherical nanoparticles (most < 100 nm) resulting from melting was confirmed by TEM images (Fig. 2).

Upon completion of the laser treatment (minute 46, Fig. 4), nucleation events were once again detected as a decrease in mean particle size to 5–6 nm. On minute 50 (cooling zone), particle number concentrations for porcelain tiles dropped back to the registered levels in the beginning of the sintering process (1×10^5 parts cm^{-3}). Concerning the red clay tiles, the decrease in particle number concentration to background levels (3×10^4 parts cm^{-3}) occurred slightly later, on minute 55. Finally, whereas a constant of particle number concentration was detected, significant particle growth was observed for red clay tiles during the cooling stage, probably due to condensation of gaseous species and/or the agglomeration of existing finer nanoparticles from nucleation. This particle growth was not observed for porcelain probably due to the less intense particle nucleation rates observed for these materials.

Similar patterns were obtained for all the materials analysed, although with the highest nanoparticle emissions during laser treatment being registered for material #5, followed by material #6, reaching an average of 5.6×10^6 parts cm^{-3} and 5.0×10^6 parts cm^{-3} , respectively. Nanoparticle emissions during laser treatment on similarly coated porcelain materials, such as #2 and #3, were lower than coated red clay tiles by a factor of 2.2 and 5.9, respectively. Although for porcelain and red clay the size of the emitted particles exhibited diameters finer than 24 nm, the particles emitted by porcelain sintering under laser treatment were finer than for red clay. Conversely, particle number concentrations emitted were higher from red clay than from porcelain. These results have direct implications for the ceramic industry, given the current increasing

global demand for porcelain tiles and the similarly decreasing demand for red clay tiles. This would imply increasing exposures to nanoparticles of lower diameters (< 20 nm) in ceramic industrial plants.

3.5. Transport of emissions across indoor air

Table 3 shows the results obtained at the secondary indoor location (the worker breathing zone) during tile sintering. The patterns observed in the breathing zone were somewhat different to those from the emission source.

Particle concentrations decreased from the furnace to the breathing zone for four of the six materials studied. The exceptions were material #1 and material #3. These decreases were interpreted as resulting from dilution of emission with workplace air, and also from coagulation and agglomeration of the particles emitted at the furnace. On average, mean and maximum N minute concentrations in the breathing zone were one order of magnitude higher than background levels for all the materials. Mean particle diameters in the breathing zone were 13–27 nm, larger than in the furnace but smaller than background air (36 nm). This increase in particle diameter with regard to the furnace area is consistent with particle ageing and coagulation particle processes described above.

In contrast to the emissions monitored at the emission source, the highest nanoparticle concentrations in the breathing zone were registered during material #3 with a maximum of 2.3×10^6 parts cm^{-3} (particle mean diameter = 16 nm). On average, nanoparticle concentrations were lower for red clay sintering (1.5×10^5 parts cm^{-3}) when compared to porcelain (5.5×10^5 parts cm^{-3}). Similarly to the mean particle diameter measured at the furnace, particles from red clay sintering were on average coarser (24 nm) than from porcelain tiles (16 nm). Once they reached the breathing zone, particles from porcelain and red clays were 1.6 and 1.5 times coarser than the same particles at the emission source, respectively.

In terms of mass, a relatively similar pattern to the one described for the furnace area, was registered. Increases in particle mass were detected after transport to the breathing zone.

The alveolar LDSA of the nanoparticles emitted during tile sintering and measured in the breathing zone was significantly larger than in background air. Background air LDSA concentrations were $35 \mu\text{m}^2 \text{cm}^{-3}$ and they increased by a factor of 2–20 in the breathing zone. LDSA concentrations were higher during porcelain sintering than during red clay sintering. In terms of average values, sintering of frit coated porcelain tile exhibited the highest mean value ($6.9 \times 10^2 \mu\text{m}^2 \text{cm}^{-3}$). Finally, alveolar LDSA concentrations during tile ablation exceeded the levels recorded during sintering, reaching an average value of $6.3 \times 10^3 \mu\text{m}^2 \text{cm}^{-3}$ (data not shown). Monitored levels of LDSA in both processes were significantly higher than the outdoor levels registered in major European cities such as Dusseldorf, Germany (30 – $45 \mu\text{m}^2 \text{cm}^{-3}$) (Kuhlbusch et al., 2004), Lisbon, Portugal (35 – $89 \mu\text{m}^2 \text{cm}^{-3}$) (Albuquerque, Gomes, & Bordado, 2012; Gomes, Bordado, & Albuquerque, 2012) and Barcelona, Spain ($37 \pm 26 \mu\text{m}^2 \text{cm}^{-3}$) (Reche et al., 2015).

3.6. Particle chemical characterization

The chemical composition of particles collected in indoor and outdoor air for 26 h is summarized in Tables S2 (major species) and S3 (trace elements) of the supplementary information.

Indoor mass concentrations of $\text{PM}_{<0.25}$, $\text{PM}_{0.25-2.5}$, and $\text{PM}_{2.5-10}$ were $43.1 \mu\text{g m}^{-3}$, $5.3 \mu\text{g m}^{-3}$ and $4.8 \mu\text{g m}^{-3}$ respectively. $\text{PM}_{<0.25}$ mass concentrations were higher than in other size fractions for most of the elements analysed in indoor air, evidencing the influence of sintering emissions in the lowest particle size range. The main indoor components of $\text{PM}_{<0.25}$ were SiO_2 ($2.0 \mu\text{g m}^{-3}$), K_2O ($3.7 \mu\text{g m}^{-3}$), SO_4^{2-} ($4.6 \mu\text{g m}^{-3}$), Zn ($0.8 \mu\text{g m}^{-3}$), Cr ($0.6 \mu\text{g m}^{-3}$), Pb ($0.1 \mu\text{g m}^{-3}$) and As ($0.05 \mu\text{g m}^{-3}$). Indoor $\text{PM}_{2.5-10}$, was enriched in Zr (12.2 ng m^{-3}) and Sr (4.3 ng m^{-3}), when compared with outdoor concentrations ($\text{Zr} < \text{detection limit}$ and $\text{Sr} = 1.2 \text{ ng m}^{-3}$ of Sr), probably linked to frit and pigments used in the ceramic tiles (Querol et al., 2007; Minguillon et al., 2009; Sánchez de la Campa et al., 2010). This statement is in agreement with the chemical composition of the PM collected during each sintering and ablation process, which is displayed in Table S4 of the supplementary information.

Indoor/outdoor concentration ratios (I/O) (Fig. S4 in the supplementary information) were especially high for typical tracers of components in $\text{PM}_{<0.25}$ used in the mix of frits and pigments in tile decoration such as Cr, Mn, Ni, Cu, Ce and Pb (Minguillon et al., 2009; Sánchez de la Campa et al., 2010). Concerning $\text{PM}_{0.25-2.5}$, the main species with I/O ratios > 1 were P_2O_5 and ZnO . Zn is very often used in frit and enamel formulas (Casasola et al., 2012; Celades, 2013). Finally, the coarse particles ($\text{PM}_{2.5-10}$) showed a larger occurrence of $\text{I/O} > 1$ for Ba. $\text{I/O} < 1$ indicate the predominance of outdoor sources or particle losses and evaporation processes indoors. This was the case for certain crustal elements of outdoor origin such as Al, Ti and Fe, indicating that their origin is mainly linked to traffic re-suspension of road dust (Querol et al., 2007). As expected, secondary inorganic aerosols such as SO_4^{2-} also showed ratios < 1 in the accumulation mode (Seinfeld & Pandis, 2012; Viana et al., 2014). The chemical profile of particles emitted from red clay sintering was characterized by high concentrations of mainly K, Rb, Tl and probably Zn and SO_4^{2-} , Cu and Sn (Table S4). Inversely, emissions of CaO were found to be 1.2–3.2 times higher from porcelain tiles sintering than from red clay tile sintering.

4. Conclusions

Nanoparticle formation, emission mechanisms, and impact on exposure were assessed for different ceramic materials during tile sintering and laser ablation processes in a pilot plant scale furnace. Six conventional and the most frequently used types of tiles in the ceramic industry were assessed.

The main findings from this study may be summarized as follows:

- Nanoparticle emissions were detected in high concentrations (mean minute concentration up to 9.7×10^5 parts cm^{-3} over 1.5 h), with mean diameter of 18 nm.
- Two different emission behaviors were detected: (i) Thermally induced emission, and (ii) nanoparticle formation through nucleation. These behaviors were, independent of the laser treatment, and they were strongly linked to tile composition.
- It is concluded that temperature plays a major role in particle emission in this kind of industrial process.
- New particle formation processes by nucleation occurred mostly during red clay tile sintering and probably due to S-bearing species in the raw material (e.g., CaSO_4).
- Ablation emissions were highest in terms of mass for all size ranges and highest in terms of particle size (mean diameter of 80 nm).
- When emissions were transported across the indoor area, particle number, mass and LDSA concentration decreased but remained at extremely high levels (up to $N=2.3 \times 10^6$ parts cm^{-3} ; $\text{LDSA}=2.3 \times 10^3 \mu\text{m}^2 \text{cm}^{-3}$) with small particle sizes (13–27 nm). Mean particle diameters in the breathing zone were larger than in the furnace (8–18 nm) but smaller than in background air (36 nm).
- The highest concentrations of metals (mainly Zn, Pb, Cu, Cr, As and Tl) were found in the ultrafine fraction $< 0.25 \mu\text{m}$.

It is recommended that preventive and protective actions (e.g., exhaust fume extraction) should be undertaken in ceramic industries using laser irradiation during tile sintering, but also during conventional thermal treatment.

Further research is underway in order to confirm the findings from this study and to provide a better understanding of nanoparticle formation mechanisms and of potential exposures in workplace air, in a larger number of representative samples and under pilot plant conditions.

Role of funding source

The funding sources had no involvement in study design, in the collection, analysis and interpretation of data, in the writing of the text, nor in the decision to submit the article for publication.

Acknowledgments

This study was supported by the European Community's Seventh Framework Program (FP7-PEOPLE-2012-ITN) under Grant no. 315760 (HEXACOMM Project) and by the National Project IMPACT (CGL2011-26574). Additional funding was provided by LIFE projects AIRUSE (LIFE11 ENV/ES/584), CERAMGLASS (LIFE11 ENV/ES/560) and LASERFIRING (LIFE09 ENV/ES/435). The authors also gratefully acknowledge the technical staff in Materials Science Institute of Aragón (ICMA), especially to Carlos Borrel and the colleagues Jesús Parga, Noemí Pérez and Andres Alastuey from ID/EA-CSIC for their support and collaboration.

Appendix A. Supplementary information

Supplementary data associated with this article can be found in the online version at <http://dx.doi.org/10.1016/j.jaerosci.2015.05.013>.

References

- Albuquerque, P.C., Gomes, J.F., & Bordado, J.C. (2012). Assessment of exposure to airborne ultrafine particles in the urban environment of Lisbon, Portugal. *Journal of the Air & Waste Management Association*, 62(4), 373–380.
- Asbach, C., Kuhlbusch, T., Kaminski, H., Stahlmecke, B., Plitzko, S., Götz, U., et al. (2012). NanoGEM standard operation procedures for assessing exposure to nanomaterials, following a tiered approach.
- Bäuerle, D. (1996). *Laser processing and chemistry*. Springer-Verlag: Berlin.
- Casasola, R., Rincón, J.M., & Romero, M. (2012). Glass–ceramic glazes for ceramic tiles: A review. *Journal of Materials Science*, 47(2), 553–582, <http://dx.doi.org/10.1007/s10853-011-5981-y>.
- Celades, I. (2013). *Caracterización física, química, mineralógica y morfológica del material particulado emitido por focos canalizados de la industria de baldosas y fritas cerámicas [Ph.D.]*. Universitat Jaume I de Castellón: Castellón.
- Chinchón, J.S., Querol, X., Fernández-Turiel, J.L., & López-Soler, A. (1991). Environmental impact of mineral transformations undergone during coal combustion. *Environmental Geology and Water Sciences*, 18(1), 11–15, <http://dx.doi.org/10.1007/bf01704573>.
- Curwin, B., & Bertke, S. (2011). Exposure characterization of metal oxide nanoparticles in the workplace. *Journal of Occupational and Environmental Hygiene*, 8(10), 580–587.
- de Francisco, I., Lennikov, V.V., Bea, J.A., Vegas, A., Carda, J.B., & de la Fuente, G.F. (2011). In-situ laser synthesis of rare earth aluminate coatings in the system Ln–Al–O (Ln=Y, Gd). *Solid State Sciences*, 13(9), 1813–1819, <http://dx.doi.org/10.1016/j.solidstatesciences.2011.07.013>.
- Demou, E., Peter, P., & Hellweg, S. (2008). Exposure to manufactured nanostructured particles in an industrial pilot plant. *Annals of Occupational Hygiene*, 52(8), 695–706.
- Estepa, C., & de la Fuente, G. F. (2006). P 200600560.

- Fierz, M., Houle, C., Steigmeier, P., & Burtcher, H. (2011). Design, calibration, and field performance of a miniature diffusion size classifier. *Aerosol Science and Technology*, 45(1), 1–10. <http://dx.doi.org/10.1080/02786826.2010.516283>.
- Fonseca, A.S., Viitanen, A.-K., Koivisto, A.J., Kangas, A., Huhtiniemi, M., & Hussein, T., et al. (2014). Characterization of exposure to carbon nanotubes in an industrial setting. *Annals of Occupational Hygiene* <http://dx.doi.org/10.1093/annhyg/meu110>.
- Gandra, J., Miranda, R., Vilaça, P., Velhinho, A., & Teixeira, J.P. (2011). Functionally graded materials produced by friction stir processing. *Journal of Materials Processing Technology*, 211(11), 1659–1668. <http://dx.doi.org/10.1016/j.jmatprotec.2011.04.016>.
- Gomes, J., Bordado, J., & Albuquerque, P. (2012). On the assessment of exposure to airborne ultrafine particles in urban environments. *Journal of Toxicology and Environmental Health*, 75(22–23), 1316–1329.
- Gómez, V., Irusta, S., Balas, F., & Santamaria, J. (2013). Intense generation of respirable metal nanoparticles from a low-power soldering unit. *Journal of Hazardous Materials*, 256–257(0), 84–89. <http://dx.doi.org/10.1016/j.jhazmat.2013.03.067>.
- Gomez, V., Levin, M., Saber, A.T., Irusta, S., Dal Maso, M., & Hanoi, R., et al. (2014). Comparison of dust release from epoxy and paint nanocomposites and conventional products during sanding and sawing. [Research Support, Non-U S Gov't]. *Annals of Occupational Hygiene*, 58(8), 983–994.
- Jacobs, C.W.F. (1954). Opacifying crystalline phases present in zirconium-type glazes. *Journal of the American Ceramic Society*, 37(5), 216–220. <http://dx.doi.org/10.1111/j.1151-2916.1954.tb14026.x>.
- Jervis, T.R., Nastasi, M., Hubbard, K.M., & Hirvonen, J.P. (1993). Excimer laser surface processing of ceramics: process and properties. *Journal of the American Ceramic Society*, 76(2), 350–355. <http://dx.doi.org/10.1111/j.1151-2916.1993.tb03791.x>.
- Koivisto, A.J., Lyranen, J., Auvinen, A., Vanhala, E., Hameri, K., & Tuomi, T., et al. (2012). Industrial worker exposure to airborne particles during the packing of pigment and nanoscale titanium dioxide. *Inhalation Toxicology*, 24(12), 839–849.
- Koivisto, A.J., Palomaki, J.E., Viitanen, A.K., Siivola, K.M., Koponen, I.K., & Yu, M., et al. (2014). Range-finding risk assessment of inhalation exposure to nanodiamonds in a laboratory environment. [Research support, Non-U S Gov't]. *International Journal of Environmental Research and Public Health*, 11(5), 5382–5402.
- Kuhlbusch, T.A.J., Quass, U., Koch, M., Fissan, H., Bruckmann, P., & Pfeffer, U. (2004). PM10 source apportionment at three urban background sites in the western Ruhr-area, Germany. *Journal of Aerosol Science*, 35(Supplement 1(0)), 79–90. <http://dx.doi.org/10.1016/j.jaerosci.2004.06.027>.
- Kulmala, M., Vehkamäki, H., Petäjä, T., Dal Maso, M., Lauri, A., & Kerminen, V.M., et al. (2004). Formation and growth rates of ultrafine atmospheric particles: A review of observations. *Journal of Aerosol Science*, 35(2), 143–176. <http://dx.doi.org/10.1016/j.jaerosci.2003.10.003>.
- Kumar, P., Fennell, P., & Britter, R. (2008). Effect of wind direction and speed on the dispersion of nucleation and accumulation mode particles in an urban street canyon. *Science of the Total Environment*, 402(1), 82–94. <http://dx.doi.org/10.1016/j.scitotenv.2008.04.032>.
- Lahoz, R., de la Fuente, G.F., Pedra, J.M., & Carda, J.B. (2011). Laser engraving of ceramic tiles. *International Journal of Applied Ceramic Technology*, 8(5), 1208–1217. <http://dx.doi.org/10.1111/j.1744-7402.2010.02566.x>.
- Minguillon, M.C., Monfort, E., Querol, X., Alastuey, A., Celades, I., & Miro, J.V. (2009). Effect of ceramic industrial particulate emission control on key components of ambient PM10. [Research support, Non-U S Gov't]. *Journal of Environmental Management*, 90(8), 2558–2567.
- Misra, C., Singh, M., Shen, S., Sioutas, C., Hall, P.M., & Sioutas, C., et al. (2002). Development and evaluation of a personal cascade impactor sampler (PCIS). *Journal of Aerosol Science*, 33, 1027–1047.
- Pfefferkorn, F.E., Bello, D., Haddad, G., Park, J.-Y., Powell, M., & McCarthy, J., et al. (2010). Characterization of exposures to airborne nanoscale particles during friction stir welding of aluminum. *Annals of Occupational Hygiene*, 54(5), 486–503. <http://dx.doi.org/10.1093/annhyg/meq037>.
- Querol, X., Alastuey, A., Rodríguez, S., Plana, F., Ruiz, C.R., & Cots, N., et al. (2001). PM10 and PM2.5 source apportionment in the Barcelona Metropolitan Area, Catalonia, Spain. *Atmospheric Environment*, 35, 6407–6419.
- Querol, X., Viana, M., Alastuey, A., Amato, F., Moreno, T., & Castillo, S., et al. (2007). Source origin of trace elements in PM from regional background, urban and industrial sites of Spain. *Atmospheric Environment*, 41(34), 7219–7231. <http://dx.doi.org/10.1016/j.atmosenv.2007.05.022>.
- Reche, C., Viana, M., Brines, M., Pérez, N., Beddows, D., Alastuey, A., & Querol, X. (2015). Determinants of aerosol lung-deposited surface area variation in an urban environment. *Science of The Total Environment*, 517, 38–47.
- Romero, M., Rincón, J.M., & Acosta, A. (2003). Crystallisation of a zirconium-based glaze for ceramic tile coatings. *J Eur Ceram Soc*, 23(10), 1629–1635. [http://dx.doi.org/10.1016/S0955-2219\(02\)00415-6](http://dx.doi.org/10.1016/S0955-2219(02)00415-6).
- Rubahn, H.-G. (1999). *Laser applications in surface science and technology*. John Wiley & Sons: New York.
- Sánchez de la Campa, A.M., de la Rosa, J.D., González-Castanedo, Y., Fernández-Camacho, R., Alastuey, A., & Querol, X., et al. (2010). High concentrations of heavy metals in PM from ceramic factories of Southern Spain. *Atmospheric Research*, 96(4), 633–644. <http://dx.doi.org/10.1016/j.atmosres.2010.02.011>.
- Schmatjko, K. J., Endres, G., Schmidt, U., & Banz, P. H. (1988). Precision machining of ceramic materials by excimer laser irradiation.
- Seinfeld, J.H., & Pandis, S.N. (2012). *Atmospheric chemistry and physics: From air pollution to climate change*. John Wiley & Sons.
- Taylor, J.R., Bull, A.C., & Ceramics, I.O. (1986). *Ceramics glaze technology*. Institute of Ceramics by Pergamon Press.
- Toenshoff, H. K., & Gedrat, O. (1991). Absorption behavior of ceramic materials irradiated with excimer lasers.
- Van Broekhuizen, P. (2012). Nano matters: building blocks for a precautionary approach [Ph.D. thesis]. Available at: www.ivam.uva.nl/?nanomatters.
- Viana, M., Rivas, I., Querol, X., Alastuey, A., Sunyer, J., & Álvarez-Pedrerol, M., et al. (2014). Indoor/outdoor relationships and mass closure of quasi-ultrafine, accumulation and coarse particles in Barcelona schools. *Atmospheric Chemistry and Physics*, 14(9), 4459–4472. <http://dx.doi.org/10.5194/acp-14-4459-2014>.
- Voliotis, A., Bezantakos, S., Giamarelou, M., Valenti, M., Kumar, P., & Biskos, G. (2014). Nanoparticle emissions from traditional pottery manufacturing. [Research support, Non-U S Gov't]. *Environmental Science: Processes & Impacts*, 16(6), 1489–1494.

Supplementary information

Ultrafine and nanoparticle formation and emission mechanisms during laser processing of ceramic materials

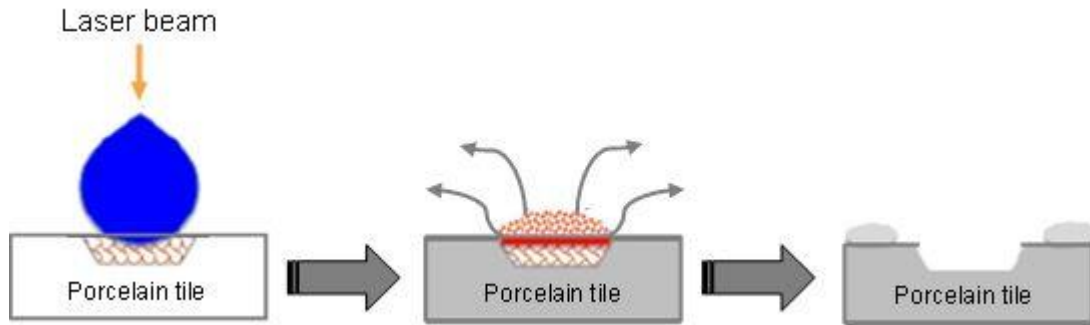


Figure S1. Schematic representation of the ablation process (adapted from (Lahoz *et al.*, 2011)).

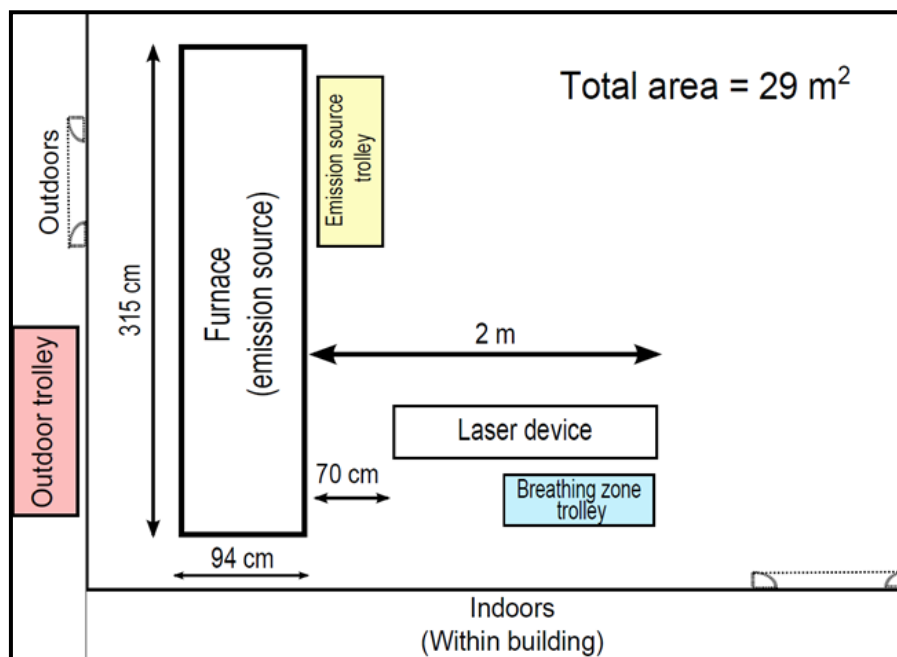


Figure S2. Layout of the indoor environment under study.

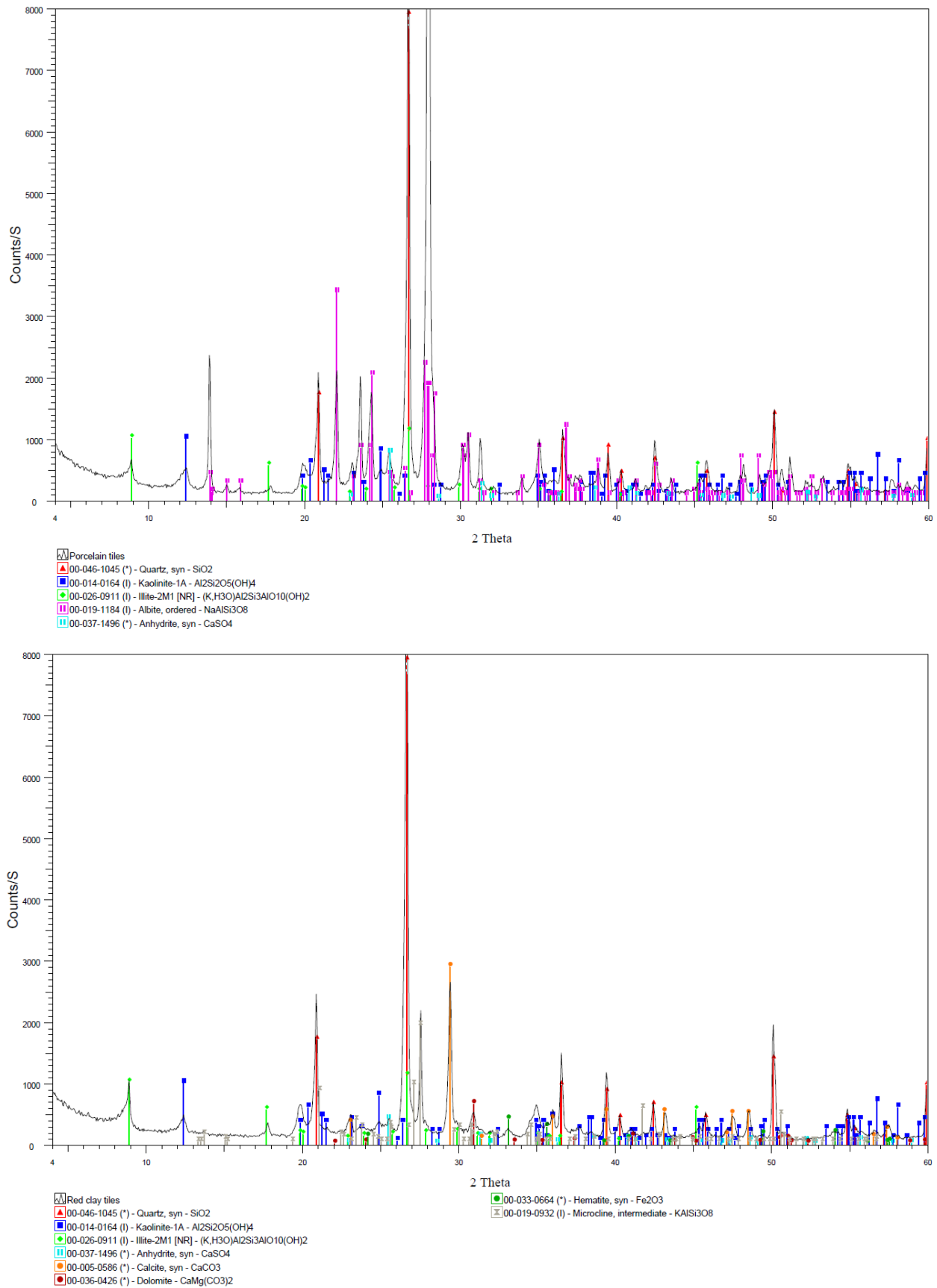


Figure S3. XRD patterns obtained from original raw porcelain (top) and red clay tiles (bottom).

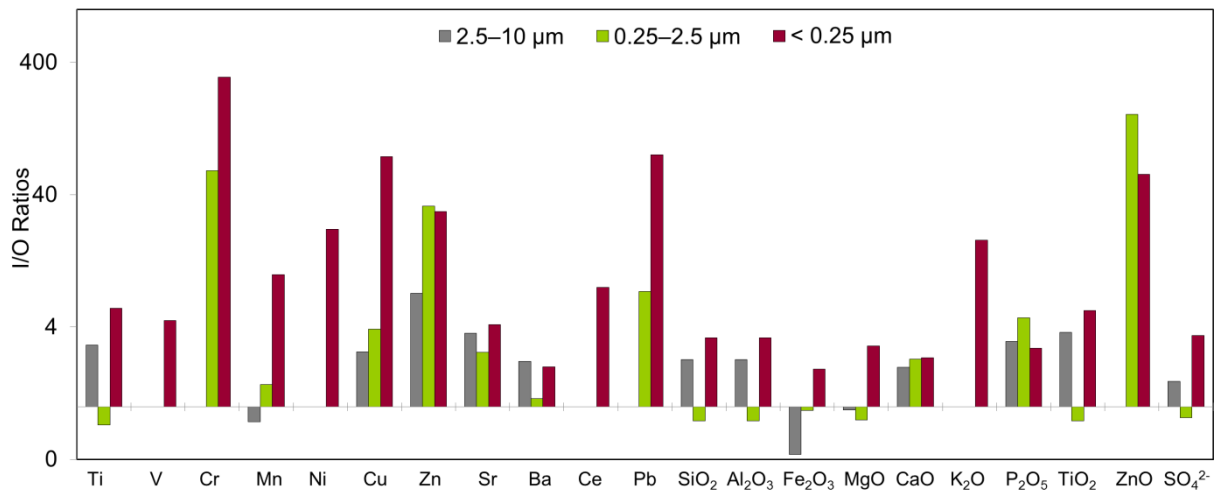


Figure S4. I/O ratios of major and trace elements for size-fractionated particles (excluding ablation process).

Table S1. Relative chemical composition of the raw tiles.

	Porcelain	Red Clay
Major elements ($w_b, g\ kg^{-1}$)		
SiO ₂	487.6	412.1
Al ₂ O ₃	162.5	137.4
Fe ₂ O ₃	4.8	45.3
MgO	2.8	18.0
CaO	6.0	101.2
Na ₂ O	54.3	4.0
K ₂ O	9.2	36.4
P ₂ O ₅	1.5	1.2
TiO ₂	5.5	6.9
ZnO	<0.1	0.5
SO ₄ ²⁻	0.3	0.9
Trace elements ($w_b, mg\ kg^{-1}$)		
Li	17.9	44.4
Sc	6.2	8.2
Ti	3263.2	3425.2
V	50.5	62.3
Cr	42.3	52.6
Mn	20.5	250.5
Co	1.1	10.4
Ni	5.2	12.0
Cu	18.5	16.1
Zn	24.8	305.6
Ga	21.7	15.4
As	5.3	13.0
Rb	55.6	135.3
Sr	142.5	184.7
Y	25.2	23.5
Zr	114.0	346.4
Nb	40.0	29.9
Sn	3.3	6.5
Cs	7.2	11.7
Ba	268.1	423.3
La	29.3	36.5
Ce	58.8	83.3
Pb	25.6	48.8
Th	11.8	12.7

Table S2. Concentration of major elements (in $\mu\text{g m}^{-3}$).

	OUTDOOR			INDOOR		
	2.5–10 μm	0.25–2.5 μm	< 0.25 μm	2.5–10 μm	0.25–2.5 μm	< 0.25 μm
SiO ₂	0.56	0.36	0.59	1.28	0.28	1.96
Al ₂ O ₃	0.19	0.12	0.20	0.43	0.09	0.65
Fe ₂ O ₃	0.16	0.07	0.11	0.07	0.07	0.20
MgO	0.07	0.05	0.03	0.06	0.04	0.08
CaO	0.27	0.09	0.29	0.54	0.20	0.68
Na ₂ O	-	-	-	-	-	0.05
K ₂ O	-	-	0.20	-	-	3.66
P ₂ O ₅	0.01	0.01	0.11	0.04	0.06	0.30
TiO ₂	-	0.01	0.01	0.01	-	0.03
ZnO	-	-	0.02	0.03	0.32	1.03
SO ₄ ²⁻	0.11	0.74	1.32	0.16	0.61	4.55

Table S3. Concentration of trace elements (in ng m^{-3}).

	OUTDOOR			INDOOR		
	2.5–10 μm	0.25–2.5 μm	< 0.25 μm	2.5–10 μm	0.25–2.5 μm	< 0.25 μm
Li	-	-	-	-	-	11.77
Ti	3.00	3.41	2.74	8.78	2.49	15.18
V	-	0.40	1.77	-	-	7.95
Cr	-	0.56	1.83	14.73	34.40	566.99
Mn	1.31	1.36	1.92	1.01	1.99	19.13
Ni	-	-	0.69	2.91	3.31	15.03
Cu	1.26	1.27	0.63	3.28	4.89	48.87
Zn	3.92	7.39	26.01	28.17	242.63	774.39
As	-	-	-	-	1.82	54.67
Se	-	-	-	-	-	25.85
Rb	-	-	-	-	-	18.30
Sr	1.20	0.50	0.66	4.33	1.30	2.74
Zr	-	-	-	12.24	3.35	-
Mo	-	-	6.05	-	-	-
Cd	-	-	-	-	-	1.91
Sn	-	-	-	-	0.32	1.99
Sb	-	-	-	-	-	1.86
Cs	-	-	-	-	-	4.41
Ba	3.13	0.99	1.99	6.89	1.13	3.96
Ce	-	-	0.05	-	-	0.41
W	-	-	-	2.32	2.11	24.78
Tl	-	-	-	-	-	39.33
Pb	-	0.60	1.22	2.96	4.44	96.95
Bi	-	-	-	-	-	3.32
U	-	-	-	-	-	2.86

Table S4. Concentration of major components and trace elements in PM collected (in $\mu\text{g m}^{-3}$).

	NWH*	#1	#2	#3	#4	#5	#6	#7
<i>Major components</i>								
SiO₂	2.95	7.45	12.49	11.51	13.1	5.07	8.82	541.94
Al₂O₃	0.98	2.48	4.16	3.84	4.37	1.69	2.94	180.65
Fe₂O₃	0.18	0.95	0.16	0.56	0.38	0.44	1.98	9.32
MgO	0.24	0.7	1.2	0.66	0.48	0.53	1.23	5.16
CaO	1.38	8.48	13.76	11.92	6.88	4.29	8.44	24.98
Na₂O	-	-	-	-	-	-	-	-
K₂O	-	-	-	-	4.64	22.35	13.14	9.67
P₂O₅	0.11	0.94	1.18	1.8	0.71	1.32	1.24	4.65
TiO₂	0.02	0.17	0.04	0.09	0.11	0.11	0.1	8.24
ZnO	0.12	0.62	0.26	1.86	0.51	10.49	1.7	1.11
SO₄²⁻	1.45	7.28	3.86	13.05	9.81	6.41	10.65	12.15
<i>Trace elements</i>								
Ti	0.02	0.09	0.01	0.03	0.04	0.04	0.03	4.54
V	-	-	-	-	-	-	-	0.04
Cr	0.28	1.68	0.1	2.92	1.1	1.14	1.73	0.45
Mn	0.01	0.05	-	0.14	0.03	0.04	0.05	-
Cu	0.02	0.12	0.02	0.2	0.91	0.15	0.19	0.22
Zn	0.08	0.45	0.22	1.48	0.4	7.81	1.25	0.93
As	-	0.03	-	0.1	-	0.32	0.14	-
Rb	-	-	-	-	0.07	0.12	0.08	-
Sr	0.01	0.02	0.04	0.04	0.02	0.01	0.03	0.18
Zr	0.02	-	-	-	-	-	-	-
Sn	-	-	-	-	0.02	-	-	-
Ba	0.01	0.02	-	0.09	0.03	0.01	0.43	0.21
W	0.01	0.06	-	0.16	0.05	0.05	0.06	-
Tl	-	-	-	-	0.25	0.21	0.23	-
Pb	-	-	-	0.19	0.06	0.04	0.01	0.22

*Non-Working-Hours: average data from 2 nights

4.3 Article III: Process-generated nanoparticles from ceramic tile sintering: emissions, exposure and environmental release

Authors:

Fonseca, A. S.^{1,2}, Maragkidou, A.³, Viana, M.¹, Querol, X.¹, Hämeri, K.³, de Francisco, I.⁴, Estepa, C.⁴, Borrell, C.⁴, Lennikov, V.⁴, de la Fuente, G. F.⁴

¹ Institute of Environmental Assessment and Water Research (IDÆA-CSIC), C/ Jordi Girona 18, 08034 Barcelona, Spain.

² Universidad de Barcelona, Facultad de Química, Martí i Franquès 1-11, 08028 Barcelona, Spain.

³ University of Helsinki, Department of Physics, Division of Atmospheric Sciences, P.O. Box 48 (Erik Palmenin aukio 1, Dynamicum) FI-00014 Finland

⁴ Instituto de Ciencia de Materiales de Aragón (ICMA - Universidad de Zaragoza), María de Luna 3, E-50018 Zaragoza, Spain.

Published in:

Sci Total Environ, 2016
doi:10.1016/j.scitotenv.2016.01.106

Accepted date: 2 February 2016 (available online)

ARTICLE IN PRESS

STOTEN-19119; No of Pages 11

Science of the Total Environment xxx (2016) xxx–xxx



Contents lists available at ScienceDirect

Science of the Total Environment

journal homepage: www.elsevier.com/locate/scitotenv

Process-generated nanoparticles from ceramic tile sintering: Emissions, exposure and environmental release

A.S. Fonseca^{a,b,*}, A. Maragkidou^c, M. Viana^a, X. Querol^a, K. Hämeri^c, I. de Francisco^d, C. Estepa^d, C. Borrell^d, V. Lennikov^d, G.F. de la Fuente^d

^a Institute of Environmental Assessment and Water Research (IDAEA-CSIC), C/ Jordi Girona 18, 08034 Barcelona, Spain

^b Universidad de Barcelona, Facultad de Química, Martí i Franquès 1-11, 08028 Barcelona, Spain

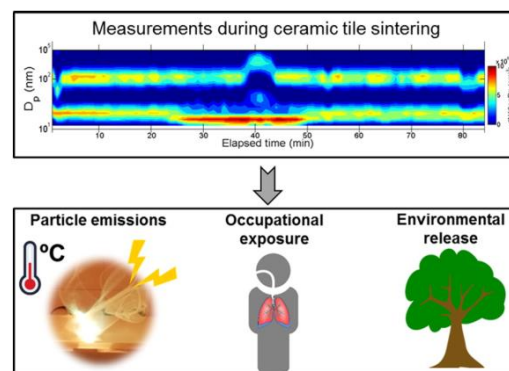
^c University of Helsinki, Department of Physics, Division of Atmospheric Sciences, P.O. Box 48, (Erik Palmenin aukio 1, Dynamicum), FI-00014, Finland

^d Instituto de Ciencia de Materiales de Aragón (ICMA - Universidad de Zaragoza), María de Luna 3, E-50018 Zaragoza, Spain

HIGHLIGHTS

- Particle emissions and impact on worker exposure and the environment were assessed
- Nucleation processes were detected during thermal treatment
- Nanoparticles were emitted into workplace on a statistically significant level
- Workers exposure concentrations would exceed the recommended exposure limits
- A potential risk of nanoparticle release to the outdoor air was identified

GRAPHICAL ABSTRACT



ARTICLE INFO

Article history:

Received 3 December 2015

Received in revised form 15 January 2016

Accepted 18 January 2016

Available online xxxx

Keywords:

Occupational exposure
Industrial laser furnace
New particle formation
Particle transport
Indoor air
Ultrafine particles

ABSTRACT

The ceramic industry is an industrial sector in need of significant process changes, which may benefit from innovative technologies such as laser sintering of ceramic tiles. Such innovations result in a considerable research gap within exposure assessment studies for process-generated ultrafine and nanoparticles. This study addresses this issue aiming to characterise particle formation, release mechanisms and their impact on personal exposure during a tile sintering activity in an industrial-scale pilot plant, as a follow-up of a previous study in a laboratory-scale plant. In addition, possible particle transformations in the exhaust system, the potential for particle release to the outdoor environment, and the effectiveness of the filtration system were also assessed. For this purpose, a tiered measurement strategy was conducted.

The main findings evidence that nanoparticle emission patterns were strongly linked to temperature and tile chemical composition, and mainly independent of the laser treatment. Also, new particle formation (from gaseous precursors) events were detected, with nanoparticles < 30 nm in diameter being formed during the thermal treatment. In addition, ultrafine and nano-sized airborne particles were generated and emitted into workplace air during sintering process on a statistically significant level. These results evidence the risk of occupational exposure to ultrafine and nanoparticles during tile sintering activity since workers would be exposed to

* Corresponding author at: C/ Jordi Girona 18, 08034 Barcelona, Spain.

E-mail address: ana.godinho@idaea.csic.es (A.S. Fonseca).

<http://dx.doi.org/10.1016/j.scitotenv.2016.01.106>

0048-9697/© 2016 The Authors. Published by Elsevier B.V. This is an open access article under the CC BY-NC-ND license (<http://creativecommons.org/licenses/by-nc-nd/4.0/>).

Please cite this article as: Fonseca, A.S., et al., Process-generated nanoparticles from ceramic tile sintering: Emissions, exposure and environmental release, *Sci Total Environ* (2016), <http://dx.doi.org/10.1016/j.scitotenv.2016.01.106>

concentrations above the nano reference value (NRV; $4 \times 10^4 \text{ cm}^{-3}$), with 8-hour time weighted average concentrations in the range of $1.4 \times 10^5 \text{ cm}^{-3}$ and $5.3 \times 10^5 \text{ cm}^{-3}$.

A potential risk for nanoparticle and ultrafine particle release to the environment was also identified, despite the fact that the efficiency of the filtration system was successfully tested and evidenced a >87% efficiency in particle number concentrations removal.

© 2016 The Authors. Published by Elsevier B.V. This is an open access article under the CC BY-NC-ND license (<http://creativecommons.org/licenses/by-nc-nd/4.0/>).

1. Introduction

According to the Ceramic Industry Roadmap to 2050 (Cerame-Unie, 2012) by the European ceramic industry association, the European ceramic industry employs over 200 000 people in the EU-27, around 80% of them in small and medium-sized enterprises (SMEs). Ceramic manufacturing from the EU-27 Member States accounts for 23% of global production of ceramics. Ceramic manufacturing is, thus, considered a robust industrial activity at the global scale. It is also a growing industrial sector, which has benefited from advances made available through nanotechnology and through innovative industrial processes. However, processes applied in ceramic industries where heating or combustion are involved or where electrical and high energy equipments are used, such as the case of firing of the ceramics in kilns (Voliotis et al., 2014), laser tile sintering (Fonseca et al., 2015), or fracturing and abrasion activities (Fonseca et al., 2015), have evidenced that large ultrafine particle concentrations may be released to the workplace environment (up to 10^5 cm^{-3}) and that these particles may have potentially harmful mean diameters (<100 nm, ultrafine and <50 nm nanoparticles). The materials and the technology used may thus be significant sources of process-generated ultrafine and nanoparticles which may impact worker exposure.

The inhalation pathway is considered the predominant route of workplace exposure and uptake (Schmoll et al., 2009; Hansen, 2009). As particles reach smaller diameters they can travel deeper into the lungs (Oberdorster, 2001; Hoet et al., 2004; Heal et al., 2012; Weichenthal, 2012). The health outcomes of exposure to ceramic dusts are chronic obstructive pulmonary disease, reduced lung and respiratory symptoms such as risks of wheezing and breathlessness, dry cough and chronic bronchitis (Trethowan et al., 1995; Jaakkola et al., 2011; Kargar et al., 2013). Therefore, there is a need to characterise ultrafine and nanoparticle release mechanisms in these workplace settings similarly to what is done in industries dealing with engineered nanoparticles, in order to decrease workers exposure (Hameri et al., 2009; Van Broekhuizen, 2012; SER, 2012). However, exposure assessment studies for process-generated ultrafine and nanoparticles, especially as a result of innovations in the manufacturing processes, have received little attention in the scientific literature. Laser sintering of ceramic tiles is an innovative technique with a large potential for global-scale implementation in real-world ceramic industrial facilities. Laser sintering of tiles has numerous advantages such as speed, temperature and enhanced durability and surface properties of structural materials (de Francisco et al., 2011; Lahoz et al., 2011).

In this framework, this study addresses this knowledge gap by characterising particle release mechanisms and their impact on personal exposure during a tile sintering process using a high power CO₂ laser. As a follow-up to a previous study (Fonseca et al., 2015), the present work aims to identify and characterise nanoparticle formation and release mechanisms, as well as their impact on exposure, during the next step of the industrial up-scaling process in a 7 m-long industrial furnace (as opposed to a 3 m-long laboratory scale one) and in a facility emulating industrial-scale manufacture (as opposed to laboratory conditions). In addition, these industrial pilot-plant conditions allowed for the study of possible particle transformations in the exhaust system, the potential for particle release to the outdoor environment, and the effectiveness of mitigation strategies (such as the filtration system) already in place in the pilot plant.

2. Materials and methods

2.1. Measurement strategy

Aerosol measurements were conducted over six consecutive days in January 2015 in an industrial pilot plant scale furnace (length = 7 m) during a laser-based tile sintering process at the Instituto de Ciencia de Materiales de Aragón (ICMA) located in Zaragoza, Spain. It makes use of a 2000 W RoFin DC 025 SLAB CO₂ laser, equipped with the galvanic scan mirrors head emitting at a wavelength $\lambda = 10.6 \mu\text{m}$ and an optical beam steering system (Estepa and de la Fuente, 2006; de Francisco et al., 2011). While the furnace applies heat to the tiles in the conventional sense, the laser is applied to the surface in order to reach higher temperatures which provide enhanced surface properties (Larrea et al., 2002; Mora et al., 2003; Lennikov et al., 2004, 2007, 2010; Estepa and de la Fuente, 2006; Gutiérrez Mora et al., 2009; de Francisco et al., 2011; Fonseca et al., 2015).

The main differences between the laboratory-scale furnace and industrial-scale furnaces should be highlighted here regarding the used fuel, gas flow and furnace length:

- i. *Fuel*: industrial furnaces are powered by gas, as opposed to electricity in the case of the laboratory-scale furnaces.
- ii. *Gas flow*: because of the different fuel used, the gas flow inside the industrial-scale furnaces is much higher than in laboratory-scale furnaces, and therefore, particle release to workplace air is expected to be lower.
- iii. *Length*: industrial-scale facilities are frequently larger in length size and thus, lower particle concentrations at the breathing zone are expected, mainly due to the largest distances between the emission source and the breathing zone.

Based on these differences it seems acceptable to conclude that it is not possible to directly extrapolate the results regarding particle emissions obtained in the laboratory-scale furnace to the industrial-scale ones. In this work, the emissions from the furnace running were not included as they are considered negligible. The industrial furnaces usually are operated with gas, but in case of the present work an electrical furnace was used and therefore no emissions from the fuel are generated. Hence, the particle emissions are generated by the ceramic tile processing.

For the experimental procedure 6 of the most frequently used types of tiles in the ceramic industry were selected: red clay raw (#1), red clay raw with frit (#2), red clay raw with frit and decoration (#3), raw porcelain (#4), raw porcelain with frit (#5) and raw porcelain with frit and decoration (#6). The tile samples were 20 × 30 cm in size. Three replicas for each material were analysed. The tiles were introduced in the furnace at a constant velocity (8 m h^{-1}) in an orthogonal direction to the laser focus, and were gradually externally heated from ambient temperature up to 1000 °C and 950 °C for porcelain and red clay tiles, respectively. Upon reaching the peak temperatures, the laser beam was introduced and directed through an optical beam steering system, which transformed the circular cross-section beam into a line measuring 1 mm in thickness.

The methodology employed in this study followed the tiered measurement strategy described by various authors (Methner et al., 2010; VCI et al., 2011; Ramachandran et al., 2011; Asbach et al., 2012; Brouwer

Please cite this article as: Fonseca, A.S., et al., Process-generated nanoparticles from ceramic tile sintering: Emissions, exposure and environmental release, *Sci Total Environ* (2016), <http://dx.doi.org/10.1016/j.scitotenv.2016.01.106>

et al., 2012) and follow the new harmonized tiered approach published by The Organisation for Economic Co-operation and Development (OECD, 2015). The measurement methods employed in this study aimed to study particles in the range 5 nm–20 µm and can be classified as online (size resolved/integrated and time resolved) and offline (size and time integrated) as follows:

- An electrical mobility spectrometer (NanoScan, SMPS TSI Model 3910; sample flow rate 0.7 L min⁻¹) to measure the particle mobility size distribution in 13 channels from 10 to 420 nm mobility diameter with a time resolution of 1 min.
- Miniature diffusion size classifiers DiscMini Matter Aerosol to measure total particle number, mean particle diameter, alveolar lung deposited surface area (LDSA) concentration as well as particles with a mode diameter between 10 and 700 nm. The sample flow rate and the sampling time interval were 1 L min⁻¹ and 1 min, respectively.
- An optical particle counter (OPC, Grimm Model 1.108) to measure particle mass in the range 0.3 to 20 µm. The sample flow rate and the sampling time interval were 1.2 L min⁻¹ and 1 min, respectively. The particles were classified in 15 channels according to their optical diameter.
- Particles collected on 25 mm polycarbonate filters with 0.8 µm pore size (one sample per ceramic material) for chemical analysis. Samples were gathered using cassettes (SKC Inc., inlet diameter 1/8 in.) connected to SKC Leland Legacy pumps operating at 6 L min⁻¹.
- Particle collection for chemical and morphological analysis by TEM (Jeol, JEM 1220, Tokyo, Japan), coupled with an energy-dispersive X-ray (EDX) spectroscopy were collected onto Quantifoil® Au grids with 1 µm diameter holes–4 µm separation of 200-mesh. TEM-grids were attached to air sample cassettes (SKC Inc., USA, inlet diameter 1/8 in. and filter diameter 25 mm). Air flow was driven by pumps operating at 6 L min⁻¹ and collection efficiency for particles was assumed to be 100%.

All the filters were acid digested by using nitric acid (HNO₃), hydrofluoric acid (HF) and perchloric acid (HClO₄) following the method proposed by Querol et al. (2001) for the analysis of major and trace elements by ICP-AES (IRIS Advantage TJA Solutions, THERMO) and ICP-MS (X Series II, THERMO). Laboratory blank filters were analysed following the same methodology. Element concentrations were blank corrected.

The particle monitors and samplers were placed simultaneously at the emission source (furnace), in the worker breathing zone (BZ). In addition, three locations along the exhaust tube connecting the emission source to outdoor air were also assessed: (i) immediately above the laser chamber, (ii) before the high-efficiency particulate air (HEPA) filter and (iii) after the HEPA filtering system, immediately before the exhaust to outdoors (at 50 cm from outdoor air).

The worker area, where the workers operated the furnace control, was located approximately 1.5 m from the furnace. The sampling tube inlets were placed at the height of the breathing zone of the workers (Brouwer et al., 2009). The work environment showing the instrumentation and sampling locations are shown in Fig. 1.

Background particle concentrations (particles infiltrated from outdoors or other work-related activity occurred in parallel to tile sintering process) may be considered significant at lower concentration in the workplace and hence crucial to take into account in exposure assessment studies (Kaminski et al., 2015). In this particular study, the background was identified by using a time series approach during the non-activity period (measured at the breathing zone without the process of tile sintering in operation) before activity (Brouwer et al., 2009). This approach assumed that the concentration at the working area corresponds to the background and any increase in particle concentrations during the work activity is related to the working process itself (Kaminski et al., 2015). However, it is important to take into consideration that this approach assumes background concentrations to be

constant and possible temporal and spatial changes in the background are not considered. The use of a combined approach of time series and spatial analysis such as described by Kaminski et al. (2015) would allow the background distinction over a full shift period and hence, the estimation of the so called “theoretical background”. However, besides the measurement location at the work area, a second measurement location would be necessary to calculate the background particle concentration in the work area during the work activities. Because tile sintering was the only activity in the plant during this work it was considered not essential to account for the possible temporal and spatial changes in the background.

2.2. Data quality

The use of different instruments monitoring similar parameters at different sampling locations aimed to maximize the number of valid data points obtained, given that the risk of exceeding the measurement ranges of the instruments was high (due to the high nanoparticle emissions expected, Fonseca et al., 2015). This was the case of DiscMini and the NanoScan instruments placed in parallel at the emission source, to monitor particle number concentrations (*N*) although in different size ranges. For this reason, in the results and discussion section only one of the datasets will be discussed for each parameter. In the case of total *N* and for the mean particle diameter (*D_p*), the results presented will be those obtained with the DiscMini data, because it is the only instrument for which particle diameter data were available simultaneously in the emission source and breathing zone. However, concerning the representative particle number size distributions of the released emissions, the NanoScan data will be used.

The particle mass concentration (PM₁₀, PM_{2.5} and PM₁) values monitored with the Grimm monitor were previously calibrated with a collocated EU-reference high-volume sampler with a PM_{2.5} cutoff inlet. PM_{2.5} and PM₁₀ were the only parameters for which an equivalent to an EU reference instrument was available, given that the rest of the parameters are unregulated (Viana et al., 2015). In the case of *N*, one of the DiscMini units was taken as internal reference for the correction of the others employed. The performance of these instruments was assessed with ambient air side by side prior the sampling campaign in terms of mean *D_p* and total *N*. Figs. S1 and S2 in Supplementary data show the regression analysis for the total *N* and mean *D_p* measured with NanoScan and DiscMini 2–DiscMini 4 compared with DiscMini 1 (reference) based on 1-min resolution data for 12 h intercomparison. The black line in each of these figures indicates the linear fit to the data points. The corresponding equations and correlation coefficients *R*² are also given in each graph. The intercomparisons evidenced a high degree of comparability in terms of total *N* concentration between the different instruments with correlation coefficients *R*² > 0.96. Different levels of agreement with DiscMini 1 (Reference) were registered with a slope on the order of 0.74–1.77, hence deviating at a maximum of 77%. Furthermore, the regression analysis obtained for NanoScan shows a higher *y*-intercept than the DiscMini 2–DiscMini 4 regressions mainly due to the lower particle size range measured (10–420 nm). The comparability for mean particle diameter was also reasonable with deviations <67% and with correlation coefficients *R*² in the range of 0.89–0.99.

2.3. Data processing

Workplace air particle concentrations deriving from process-generated particle emissions were calculated by using the similar approach described by Asbach et al. (2012) and Kaminski et al. (2015):

$$\text{Process-generated particle release} = WA - BG \quad (1)$$

where *WA* is the measured particle concentrations at the breathing zone during the work activity and *BG* is the background registered concentrations.

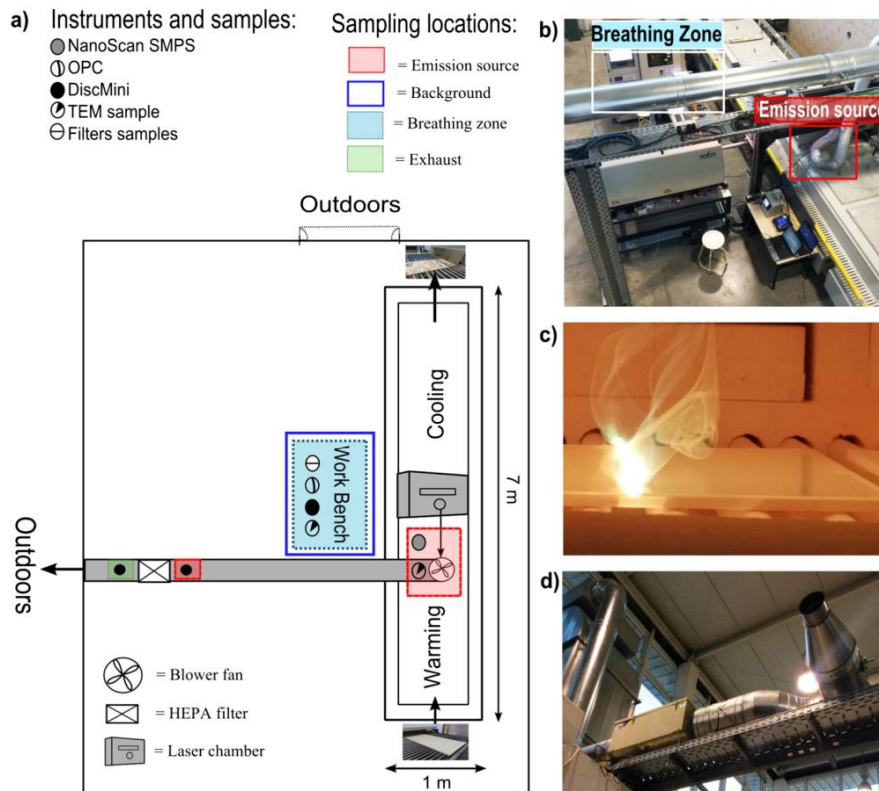


Fig. 1. Layout of the work environment. a) Approximate positions of processes and sampling locations; b) emission source and breathing zone; c) laser incidence on the tile surface, and d) HEPA filtering system.

According to Asbach et al. (2012), the process-generated particle release is statistically significant if the mean particle concentration in workplace air is higher than the BG concentrations plus three times the standard deviation ($3 \cdot \sigma_{BG}$) of the BG concentration. This means that if the ratio

$$\frac{\text{Process-generated particle release}}{3 \cdot \sigma_{BG}} > 1 \quad (2)$$

then particle release should be considered as significant.

The cumulative workers exposure for an 8-hour time weighted average (8 h TWA) was estimated as follows:

$$\text{Worker exposure}_{8\text{h TWA}} = \frac{t}{8\text{h}} \frac{1}{n} \sum_{i=1}^n WA_i \quad (3)$$

where, t is the time duration of the activity, WA_i is the measured background corrected particle concentration (subtracted the background concentration) and n is the total number of measurements.

In this study, an equivalent workers exposure of 7 h working shift during sintering activity with one specific ceramic material and 1 h working shift during non-activity period, was considered.

3. Results and discussion

3.1. Particle concentrations at the source

Fig. 2 summarises the median, mean, minimum, maximum and percentiles (P10, P25, P75 and P90) obtained at emission source in terms of number concentrations (range 10–700 nm), as well as the mean particle diameter emitted by each of the materials sintered (from #1 to #6) and

for background air. Measurements were taken with 1 min time resolution, approximately 1.5 h in duration. Results are presented as average values for the number of replicas of each experiment carried out (data shown in supporting information, Figs. S3, S4 and S5).

As evidenced by Fig. 2, over the 1.5 h periods during which each of the tiles underwent the thermal treatment, major ultrafine and nanoparticle emissions reaching up to $1.0 \times 10^7 \text{ cm}^{-3}$ were registered at the emission source with mean diameters of 14 nm and 12 nm for red clay and porcelain tiles, respectively (Fig. 2). It can be observed that coarser particles (maximum diameters ranging between 28 and 30 nm) were detected during sintering of coated tile materials, independently of the base of the tile. On average, mean N minute concentrations were 2 orders of magnitude higher than background levels and the mean particle diameters were finer (10–16 nm) than in background air (58 nm). On average, mean nanoparticle emissions were moderately higher during porcelain sintering ($2.3 \times 10^6 \text{ cm}^{-3}$) than from red clay sintering ($2.2 \times 10^6 \text{ cm}^{-3}$). This finding is similar to the results from laboratory scale furnace (3 m long) (by measuring in the same range of 10–700 nm) where it was observed that red clay sintering emitted lower N ($2.9 \times 10^6 \text{ cm}^{-3}$) than porcelain sintering ($5.0 \times 10^6 \text{ cm}^{-3}$). Aside from this, it may be concluded that lower N were measured with the industrial-scale furnace when compared to the laboratory-scale one. Nonetheless, the conclusion is then that the larger furnace emits lower N than the laboratory scale furnace (Table 1).

Particle emissions from porcelain and red clay sintering showed similar mean diameters ($12 \pm 3 \text{ nm}$ and $14 \pm 5 \text{ nm}$, respectively), which were markedly finer than those from background air particles ($58 \pm 8 \text{ nm}$), influenced by vehicular traffic emissions (with a high percentage of diesel) in the surroundings of the pilot plant. These results are in agreement with those from the laboratory-scale furnace (Fonseca

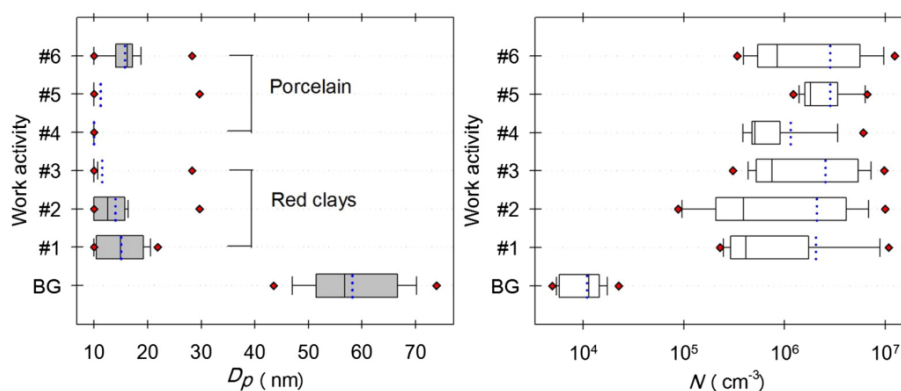


Fig. 2. Horizontal box plots for the tile sintering activity obtained at the emission source and background air with regard to mean particle diameter (D_p ; DiscMini, range 10–700 nm) and particle number concentration (N ; DiscMini, range 10–700 nm). The boundary of the box closest to zero indicates the 25th percentile, a line within the box marks the median, and the boundary of the box farthest from zero indicates the 75th percentile. Whiskers (error bars) above and below the box indicate the 90th and 10th percentiles. In addition, the mean is shown as dotted line and the outlying points as minimum and maximum (in red). Mean D_p was consistently < detection limit during the entire experiment of material #4 (raw porcelain). (For interpretation of the references to colour in this figure legend, the reader is referred to the web version of this article.)

et al., 2015), even if mean particle diameters were slightly different for the different materials then (16 ± 6 nm for red clay tiles and 10 ± 3 nm for porcelain, versus 34 ± 5 nm for background air). These results suggest that the size of the furnace does not have a major impact on the mean diameter of the particles emitted and, which is relatively dependent on the raw materials and coatings used.

As regards N , Table 1 shows that similar results were obtained across all the red clay tiles evaluated, independently of the presence or absence of coating materials ($2.0 \times 10^6 \text{ cm}^{-3}$ for raw red clay, $2.1 \times 10^6 \text{ cm}^{-3}$ for red clay with coating and $2.5 \times 10^6 \text{ cm}^{-3}$ for red clay with coating and decoration). Conversely, with porcelain tiles, higher N were monitored with coated materials ($2.8 \times 10^6 \text{ cm}^{-3}$, Table 1) than with the raw tiles ($1.1 \times 10^6 \text{ cm}^{-3}$). These results were consistent across the different replicas tested. In both cases (red clay and porcelain), the highest mean N concentrations were recorded when sintering coated materials (with frit and/or decorated). These results suggest that nanoparticles may originate from the coating materials, as opposed to the base of tiles (with the exception of the raw red clay tiles).

3.2. Emission patterns

In order to understand the particle emission processes, the time series of N and D_p at the emission source are shown in Figs. 3, 5 and 6 (raw materials and one example of a coated material). The figures show the particle emission patterns as a function of the main parameters of the sintering process (temperature and incidence of the laser beam). The materials shown (raw red clay, raw porcelain, and porcelain coated with frit and decoration) were selected given that they are the most representative of the main emission patterns observed during tile sintering.

Fig. 3 shows the characteristic emission pattern observed for all coated materials, based on the example of porcelain with frit and decoration coating (material #6). Results show that when the tiles were externally heated in the furnace in a temperature range between 450 and 900 °C, constant N and relatively stable particle diameters (for 2 particle diameters, $15 < D_p < 37$ nm and $87 < D_p < 116$ nm) were monitored at the emission source and also impacting exposure in the breathing zone. Upon reaching the peak temperature in the furnace (900–1000 °C), a thermally-induced emission pattern was observed and a decrease in particle size for the smallest particles was detected (reaching minimum values of 10 nm or lower for all the coated materials). The particles with $87 < D_p < 116$ nm were not affected by this increase in temperature. It should be noted that the lower limit of detection of the particle sizing instruments (DiscMini and NanoScan) is 10 nm. As previously discussed by Fonseca et al. (2015), these results suggest the occurrence of new particle formation processes by nucleation (nanoparticles <30 nm in diameter being formed; Kulmala et al., 2004; Kumar et al., 2008) inside the furnace, which would result in higher N with a lower particle size. Nucleation processes from gaseous precursors were probably induced by the cooling down of exhaust gases containing SO_2 emitted from the thermal decomposition of S-bearing minerals present in the tile's raw material (e.g., anhydrite, CaSO_4 , Fig. 4c and e), which decomposes at high temperatures (Chinchón et al., 1991). Upon introduction of the laser beam (still within the peak temperature stage), Fig. 3 shows a decrease in N and an increase in D_p (37 nm for the smallest particles as opposed to 10 nm during the thermal treatment), probably as a result of coagulation/condensation processes. This increase in size also affected the $87 < D_p < 116$ nm particles (increasing to 365 nm). Results seem to

Table 1

Mean and standard deviation ($\pm \sigma$) of particle number concentrations (N) and mean particle diameter measured during tile sintering (D_p ; range 10–700 nm) at the emission source and in background air of the pilot plants (industrial-scale; laboratory-scale, Fonseca et al., 2015). Mean values (from #1 to #6) correspond to the average of the replicas analysed for each specific tile material, approximately 1.5 h in duration, each one. Mean D_p was consistently < detection limit during the entire experiment of material #4 (raw porcelain).

Material	Industrial-scale furnace (7 m)		Laboratory-scale furnace (3 m)*		
	N (cm^{-3})	D_p (nm)	N (cm^{-3})	D_p (nm)	
Red clay tiles	#1	$2.0 \times 10^6 \pm 3.1 \times 10^6$	15.1 ± 4.1	$2.8 \times 10^6 \pm 4.1 \times 10^6$	15.9 ± 7.0
	#2	$2.1 \times 10^6 \pm 2.8 \times 10^6$	14.0 ± 4.8	$2.6 \times 10^6 \pm 5.2 \times 10^6$	17.9 ± 6.2
	#3	$2.5 \times 10^6 \pm 2.9 \times 10^6$	11.4 ± 4.7	$3.4 \times 10^6 \pm 6.1 \times 10^6$	14.5 ± 4.3
Porcelain tiles	#4	$1.1 \times 10^6 \pm 1.4 \times 10^6$	10.0 ± 0	$3.8 \times 10^6 \pm 5.1 \times 10^6$	8.0 ± 2.4
	#5	$2.8 \times 10^6 \pm 1.8 \times 10^6$	11.3 ± 4.7	$6.0 \times 10^6 \pm 3.6 \times 10^6$	10.9 ± 5.0
	#6	$2.8 \times 10^6 \pm 3.6 \times 10^6$	15.8 ± 3.9	$5.1 \times 10^6 \pm 4.0 \times 10^6$	10.5 ± 3.0
BG	$1.1 \times 10^4 \pm 4.7 \times 10^3$	58.2 ± 8.4	$1.3 \times 10^4 \pm 8.6 \times 10^3$	33.9 ± 5.5	

* Fonseca et al. (2015).

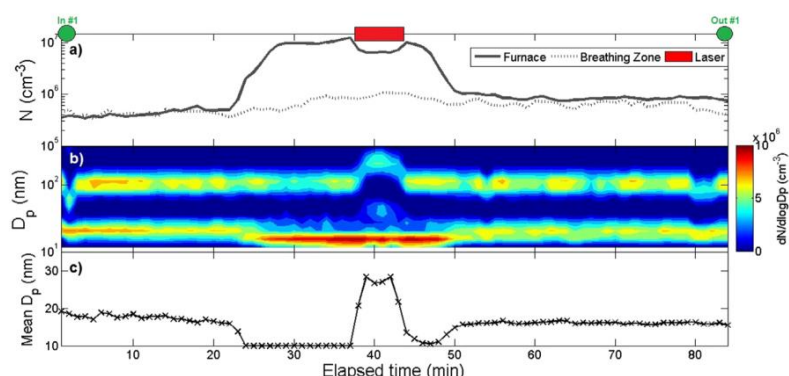


Fig. 3. Porcelain with frit and decoration coating (material #6). (a) Time series of (a) particle number concentrations (N) measured simultaneously at the emission source and the breathing zone (range 10–700 nm), and (b) particle size distributions (range of 10–420 nm), and (c) mean particle diameter (D_p) at the emission source (range 10–700 nm). The laser period is shown as red rectangle and the entrance and exit of material are shown as green circles. Results for one of the replicas analysed of the same material, representative of all the replicas. (For interpretation of the references to colour in this figure legend, the reader is referred to the web version of this article.)

suggest that the incidence of the laser inhibited further particle formation mechanisms, possibly due to the sealing of the tile's surface with the laser, and conversely favoured particle growth. Upon completion of the laser treatment, nucleation events were once again detected as a decrease in mean particle size down to 10 nm and an increase in N . During the cooling stage (temperatures decreasing to 800 °C), N dropped back to the initial concentrations and a significant particle growth was observed, probably due to condensation of gaseous species on pre-existing particles and/or the coagulation processes. As stated above, this pattern was observed for all coated materials (whether using red clay or porcelain as substrate; (Figs. S3, S4 and S5 in Supplementary data).

Fig. 4 shows examples of ultrafine and nanoparticle morphology and composition detected at the emission source during sintering activity. The TEM/EDX analyses of the samples show a large number of spherical ultrafine particles ranging from 10 nm–1000 nm in size diameter which may be interpreted as portions of melted material involved in the tile melting processes. In addition, a large amount of agglomerated particles were collected by TEM (Fig. 4a, d and f), thus confirming the occurrence of particle condensation and/or agglomeration of existing finer nanoparticles (10–30 nm in size diameter) from nucleation process.

Different emission patterns were registered when monitoring raw materials, which were in addition different for the two materials evaluated. Fig. 5 shows the case of raw red clay. The emission pattern observed during raw red clay sintering showed certain similarities with

that described for coated materials (Fig. 3), showing lower N and larger diameters ($15 < D_p < 37$) during the lowest temperature stages and new particle formation processes by nucleation before and after the laser treatment coinciding with the highest temperatures inside the furnace (particle diameters < 20 nm). The main difference with regard to the coated materials was found during the laser treatment, when particle diameters did not increase as much as in Fig. 3 (mean diameter during the laser treatment = 81 nm with coated materials vs. 43 nm with raw red clay). In addition, almost no emissions of larger-sized particles (around 100 nm) were detected from raw red clay sintering (Fig. 5), which points to the coating materials (and not the tile substrate) as their most probable source.

Finally, the emission pattern of raw porcelain sintering was also assessed (Fig. 6). A different pattern was observed on this occasion, which was replicated in all the analyses of raw porcelain carried out. As shown in Fig. 6, particle emissions followed similar trends as in the case of raw red clay, with only one dominant particle size (20 nm, as opposed to two particle sizes obtained with coated materials). However, upon incidence of the laser beam an increase in N was detected, while particle diameter showed a slight decrease (up to 10 nm). This result would suggest that, in contrast to all other materials, during sintering of raw porcelain nucleation events took place during the laser treatment.

To summarise, nucleation process (nanoparticles < 30 nm in diameter being formed) were detected for both materials (red clay and

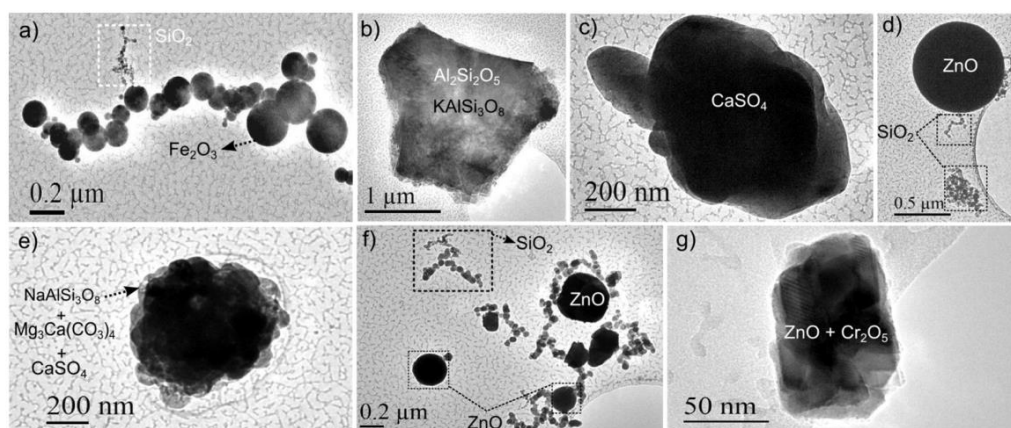


Fig. 4. TEM images of nanoparticles collected at the emission source during different sintering activities: a) red clay raw; b) red clay frit coated; c) and d) red clay frit and decoration coated; e) raw porcelain; f) porcelain frit coated and g) porcelain frit and decoration coated. Corresponding identified particles by TEM/EDX are shown in each figure.

Please cite this article as: Fonseca, A.S., et al., Process-generated nanoparticles from ceramic tile sintering: Emissions, exposure and environmental release, *Sci Total Environ* (2016), <http://dx.doi.org/10.1016/j.scitotenv.2016.01.106>

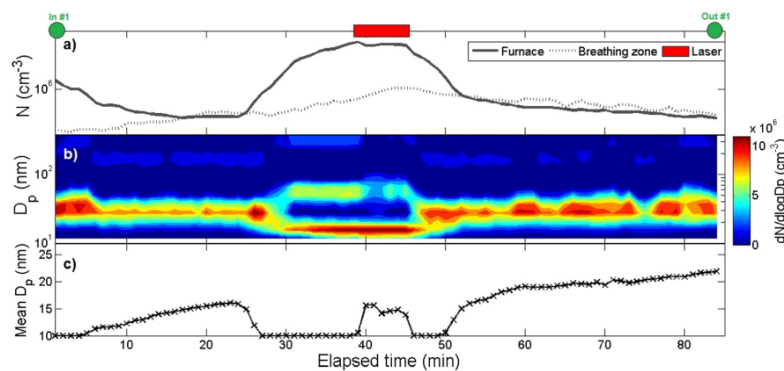


Fig. 5. Raw red clay (material #1). Time series of (a) particle number concentrations (N) measured simultaneously at the emission source and the breathing zone (range 10–700 nm), and (b) particle size distributions (range of 10–420 nm), and (c) mean particle diameter (D_p) at the emission source (range 10–700 nm). The laser period is shown as red rectangle and the entrance and exit of material are shown as green circles. (For interpretation of the references to colour in this figure legend, the reader is referred to the web version of this article.)

porcelain) during the thermal treatment, independently of the laser treatment. This result goes beyond the results from the previous study (under laboratory conditions) where such events were only observed during red clay sintering. Except for the raw porcelain, the influence of the laser treatment results in the emission of larger particles than when compared to the same temperature (950–1000 °C) without the laser. This suggests that the incidence of the laser inhibits new particle formation processes by nucleation which can be observed immediately before the laser treatment.

3.3. Exposure to particles in the breathing zone

The particles emitted inside the furnace were released to workplace air and transported toward the worker area, resulting in potentially health-hazardous exposures for the workers. The mean N and D_p measured in the breathing zone for each of the materials analysed, as well as in background air, are presented in Fig. 7. A comparison with the results from the laboratory-scale furnace (3 m long, Fonseca et al., 2015) is also included.

As shown in Fig. 7, mean N in the breathing zone were in all cases at least 1 order of magnitude higher than background levels, thus confirming the increase in worker exposure to ultrafine and nanoparticles resulting from the sintering process. Regarding particle transport across the workplace, N in the breathing zone were much lower than in the emission source for all the materials, as expected (Figs. 2 and 7) due to dilution of the emissions in combination with particle agglomeration and coagulation. However, in all cases and similarly to previous

laboratory-scale study, N were significantly above background concentrations since mean N in workplace air were always higher than the background concentrations plus three times the standard deviation of the background concentration ($>3.9 \times 10^4 \text{ cm}^{-3}$ and $2.5 \times 10^4 \text{ cm}^{-3}$ for particles in the range of 10–700 nm, at 3 m and 7 m furnace, respectively). As a result, the increase in worker exposure was considered statistically significant.

When comparing the results from the industrial-scale and the laboratory-scale pilot plants (Fonseca et al., 2015), results show that breathing zone N concentrations were lower for most materials in the laboratory-scale plant, with the exception of materials #1 and #2. The highest exposure concentrations were recorded during porcelain sintering ($3.6 \times 10^5 \text{ cm}^{-3}$), and more specifically for the porcelain with frit and decoration tiles (#6), reaching mean N of $6.2 \times 10^5 \text{ cm}^{-3}$. The decrease in exposure concentrations when compared to the laboratory-scale conditions (Fig. 7) was probably related to the higher gas flow inside the industrial-scale furnace than in laboratory-scale one and also to the size of the facility (mainly, the distance between the emission source and the breathing zone). Particle diameters were lower in the industrial-scale plant due to their lower emission diameters.

Worker exposure during the sintering processes was also calculated in terms of particle mass (PM) (Fig. 8). As in the case of N , PM concentrations in the breathing zone were consistently higher than in background air. The maximum mean concentrations registered were $6.0 \mu\text{g m}^{-3}$, $18 \mu\text{g m}^{-3}$ and $70 \mu\text{g m}^{-3}$ for PM_1 , $PM_{2.5}$ and PM_{10} , respectively, for raw porcelain (material #4). The ratio (Eq. (2); Process-generated particle release/ $3 \cdot \sigma_{BG}$) results in 1.1, 2.7 and 7.8, respectively and thus

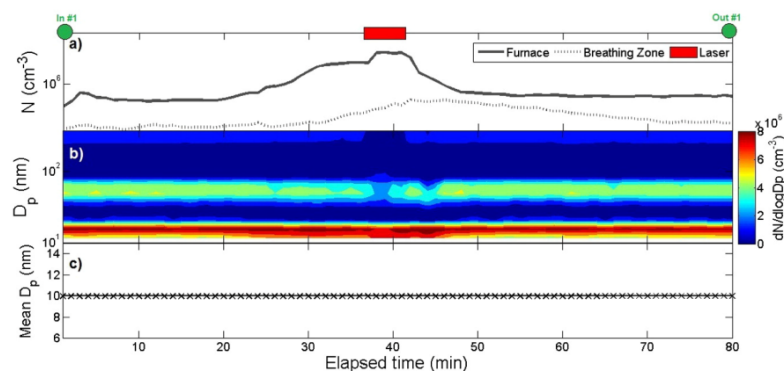


Fig. 6. Raw porcelain (material #4). Time series of (a) particle number concentrations (N) measured simultaneously at the emission source and the breathing zone (range 10–700 nm), and (b) particle size distributions (range of 10–420 nm), and (c) mean particle diameter (D_p) at the emission source (range 10–700 nm). The laser period is shown as red rectangle and the entrance and exit of material are shown as green circles. Mean D_p (c) was consistently $<$ detection limit during the entire experiment. (For interpretation of the references to colour in this figure legend, the reader is referred to the web version of this article.)

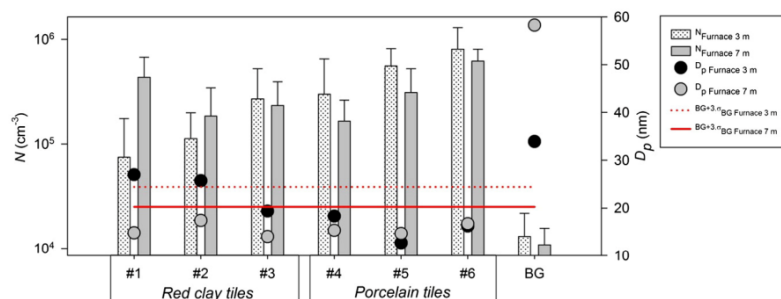


Fig. 7. Particle number concentrations (N) and mean particle diameter (D_p ; range 10–700 nm) measured in the breathing zone for each of the materials analysed, as well as for background air. Mean values correspond to each sintering process, approximately 1.5 h. The left and right y-axis refer to the mean N and mean D_p , respectively. Error bars above the box indicate the standard deviation (σ). The solid and dashed red horizontal lines indicate the significance level of particle release during sintering activity in the workplace air in the pilot-plant (7 m) and laboratory-scale furnaces (3 m), respectively ($BG + 3 \cdot \sigma_{BG}$; Asbach et al., 2012). (For interpretation of the references to colour in this figure legend, the reader is referred to the web version of this article.)

should be considered a statistically significant increase in exposure concentrations, for this material (Asbach et al., 2012). For the rest of the materials, exposure was significantly high only for PM_{10} and for materials #1, #2, #5 and #6 (Fig. 8). This was likely caused by re-suspension of coarse particles which is commonly observed during activities in indoor environments (by walking, etc.). TEM/EDX analyses confirmed the presence of coarse particles (agglomerates, coarse size) in workplace air (Fig. 4a, d and f).

The results concerning the PM concentrations presented here are considerably higher than those found in laboratory scale. Fonseca et al. (2015) measured an average PM_{10} exposure during the same sintering activities varying from 12 to $17 \mu\text{g m}^{-3}$ whereas the results of PM_{10} presented here, showed levels of $7\text{--}70 \mu\text{g m}^{-3}$, although not very high for a working place.

3.4. Particle characterisation

The conducted TEM/EDX analyses of the samples show that quartz (SiO_2) appears to be the main inorganic component released in both types of tiles. Other crystalline constituents found in both types of tiles were albite ($\text{NaAlSi}_3\text{O}_8$), metakaolinite ($\text{Al}_2\text{Si}_2\text{O}_5$), and huntite ($\text{Mg}_3\text{Ca}(\text{CO}_3)_4$). Conversely, mineral phases such as microcline (KAlSi_3O_8) and hematite, (Fe_2O_3) were only found in red clay tiles whereas augite ($\text{CaMg}(\text{Fe, Al, Ti}) (\text{Si, Al})_2\text{O}_6$) only in porcelain tiles. In addition, metal oxide nanoparticles of Zn, Cr, Al and Fe were also found, resulting from their use as opaque frits or pigments (Jacobs, 1954; Romero et al., 2003; Minguillon et al., 2009; de la Sánchez Campa et al., 2010; Lahoz et al., 2011; Casasola et al., 2012; Celades, 2013).

The chemical analysis of particles collected on 25 mm polycarbonate filters revealed also that a considerable amount of SO_4^{2-} (14–24% of

total particle mass) was consistently found in workplace air (Fig. S6 in Supplementary data). Other relevant components found in both raw tiles were CaCO_3 and SiO_2 (6% of particle mass concentration, each). Commonly used in frit and decoration coated tiles, a relevant percentage of ZnO was found for both porcelain and red clay tiles (4% and 7% for red clay frit and decoration coated (material #3) and porcelain frit coated, respectively).

3.5. Comparison of worker exposure concentrations with the nano reference values

Although occupational exposure limits (OELs) were established by Council Directive 88/642/EEC as “the limit of the time-weighted average of the concentration of a chemical agent in the air within the breathing zone of a worker in relation to a specified reference period” (EC, 1998), no OELs are available regarding nanoparticles or nanomaterials yet. Despite this, nano reference values (NRVs) have been set by Social and Economic Council of The Netherlands (SER, 2012) regarding worker exposure to engineered nanoparticles (ENPs). NRVs are background-corrected 8-hour TWA concentrations. However, high-energy processes such as the pone under study may generate nanoparticle emissions to workplace air, which by nature are comparable to ENPs in terms of hazardous properties (Van Broekhuizen, 2012). According the SER (2012), for low-density biopersistent granular nanomaterials (density $< 6000 \text{ kg m}^{-3}$ such as Al_2O_3 , SiO_2 , ZnO, etc.) and for high-density biopersistent granular nanomaterials (density $> 6 \times 10^3 \text{ kg m}^{-3}$) such as Ag, Au, CeO_2 , etc.), the NRVs are $4 \times 10^4 \text{ cm}^{-3}$ and $2 \times 10^4 \text{ cm}^{-3}$, respectively. In the present study, ultrafine and nanoparticles generated from sintering processes (generally metal oxides) were considered as substances with a

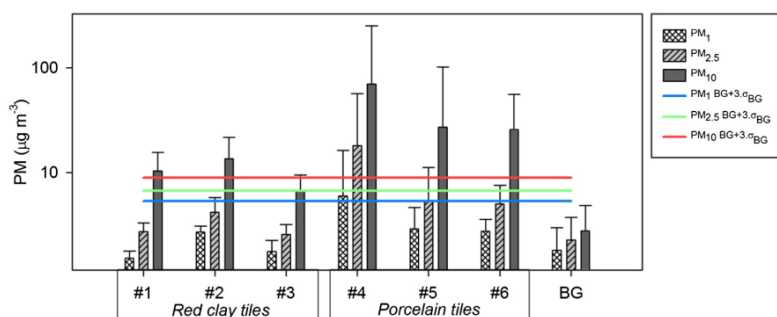


Fig. 8. Particle mass concentrations (PM) measured in the breathing zone for each of the materials analysed, as well as for background air. Mean values correspond to each sintering process, approximately 1.5 h. Error bars above the box indicate the standard deviation (σ). The solid blue, green and red horizontal line indicate the significance level of PM_1 , $PM_{2.5}$ and PM_{10} concentrations during sintering in workplace air, respectively ($BG + 3 \cdot \sigma_{BG}$; Asbach et al., 2012). (For interpretation of the references to colour in this figure legend, the reader is referred to the web version of this article.)

Table 2

Background corrected 8 h-TWA particle number (N) and mass (PM) exposure concentrations obtained for each activity, and comparison with the SER nano-reference value (NRV) and the ACGIH threshold limit value (TLV).

Sintering activity	$N_{8\text{ h-TWA}}$ (cm^{-3})	$\text{NRV}_{8\text{ h-TWA}}$ (cm^{-3}) (SER, 2012)	$N_{8\text{ h-TWA}}/\text{NRV}_{8\text{ h-TWA}}$	$\text{PM}_{1\text{ 8 h-TWA}}$ ($\mu\text{g m}^{-3}$)	$\text{PM}_{2.5\text{ 8 h-TWA}}$ ($\mu\text{g m}^{-3}$)	$\text{PM}_{10\text{ 8 h-TWA}}$ ($\mu\text{g m}^{-3}$)	$\text{TLV}_{8\text{ h-TWA}}$ ($\mu\text{g m}^{-3}$) ACGIH (2013)	$\text{PM}_{10\text{ 8 h-TWA}}/\text{TLV}_{8\text{ h-TWA}}$
#1	3.7×10^5	4.0×10^4	9	<0.1	1.0	7.7	3.0×10^3	3×10^{-3}
#2	1.5×10^5		4	1.0	2.3	10.5		4×10^{-3}
#3	2.0×10^5		5	0.2	0.9	4.5		2×10^{-3}
#4	1.4×10^5		3	3.9	14.4	60.0		2×10^{-2}
#5	2.6×10^5		7	1.2	3.3	22.6		8×10^{-3}
#6	5.3×10^5		13	1.0	3.1	21.5		7×10^{-3}

density $< 6 \times 10^3 \text{ kg m}^{-3}$. In general, only the pure metals have a density $> 6 \times 10^3 \text{ kg m}^{-3}$ (Van Broekhuizen, 2012).

In terms of PM, the only limits available are those established by the American Conference of Governmental Industrial Hygienists (ACGIH, 2013) and the Occupational Safety and Health Administration (OSHA, 2006). These institutions set a permissible exposure limit (PEL; 8 h TWA) of 5 mg m^{-3} for the respirable fraction (PM_{10}) (OSHA, 2006) and of 3 mg m^{-3} (threshold limit value TLV, 8-hour TWA concentration) for respirable particles (PM_{10}) ACGIH (2013).

Table 2 represents the background-corrected 8 h-TWA worker exposure to N and PM concentrations (by Eq. (3)) during the sintering activities under study.

Considering that the workers were exposed to nanoparticle concentrations during a 7-hour working shift of sintering of each material and 1 h working during non-activity period, 8-hour TWA exposure N concentrations were in the range of $1.4 \times 10^5 \text{ cm}^{-3}$ and $5.3 \times 10^5 \text{ cm}^{-3}$. This outcome exceeded the NRV established by the SER (2012) with a ratio ($N_{8\text{ h-TWA}}/\text{NRV}_{8\text{ h-TWA}}$) ranging from 3 to 13 (Table 2). In terms of mass, the 3 mg m^{-3} TLV for the total respirable fraction would not have been exceeded during any sintering condition given that the PM_{10} for 8 h TWA would be in the range of 5–60 $\mu\text{g m}^{-3}$.

3.6. Environmental release and filter efficiency

To mitigate the potential risk for ultrafine and nanoparticle release to the environment (ambient air), a filtration system (with a HEPA filter) was placed at the end of the exhaust duct and before exhaust gases were released to outdoor air. The aim of this system was to remove particles originating from the tile sintering processes from the exhaust gas. However, at the time of the study, the facility managers had no specific data on the performance of the filtration system. Therefore, in order to test the effectiveness of the filtration system during tile sintering activity, particle number concentrations and size distribution were monitored before and after the HEPA filter (Table 3). The following formula was applied for the calculation of the filtration system efficiency:

Efficiency of filtration system to reduce N (%)

$$= \frac{N_{\text{before HEPA}} - N_{\text{after HEPA}}}{N_{\text{before HEPA}}} \times 100 \quad (4)$$

Table 3

Mean particle number concentration (N) measured before and after the HEPA filter, and calculated HEPA filtration efficiency for each sintering process.

Material	$N_{\text{mean before HEPA}}$ (cm^{-3})	$N_{\text{mean after HEPA}}$ (cm^{-3})	Efficiency* (%)
#1	2.0×10^5	1.0×10^5	95%
#2	2.1×10^5	7.4×10^4	96%
#3	2.5×10^5	8.5×10^4	97%
#4	1.1×10^5	5.9×10^4	95%
#5	2.8×10^5	1.6×10^5	94%
#6	2.8×10^5	1.1×10^5	96%

* Calculated by Eq. (4).

Results show that the mean and maximum N concentrations measured after the filtration system were lower than before the system by one or two orders of magnitude, implying a calculated system efficiency of 94–97% (Table 3). However, because of the high N emitted (in the order of 10^6 cm^{-3}), particle emissions to outdoor air in the order of mean 1.5-hour concentrations of 10^5 cm^{-3} were still detected (Table 3). The largest impacts on outdoor air were registered during porcelain sintering ($1.1 \times 10^5 \text{ cm}^{-3}$), and in particular for the porcelain with frit (material #5; $1.6 \times 10^5 \text{ cm}^{-3}$) (Table 3). Because of rapid dilution processes it is not expected that this particle release would generate major environmental or health impacts in outdoor air.

Finally, filter efficiency seemed to be dependent on particle size. Fig. 9 shows the time series of the efficiency of the HEPA filtration system with regard to the mean particle diameters measured before and after the filtration system, for material #3 (red clay with frit and decoration). Similar results were obtained for the rest of the materials. Results evidence a clear inverse relationship between filtration efficiency and initial particle diameter (before the HEPA filter), with efficiency decreasing to $< 94\%$ during the laser treatment periods when particle diameter increased (see Figs. 5 and 7). Conversely, during the thermal treatments (before and after laser incidence) particle size before the filtration system was close to the instrument's detection limit (10 nm) and higher efficiency values were registered ($> 97\%$).

As a result, the efficiency of the filtration system was successfully tested, evidencing a $> 87\%$ efficiency of N removal (on a 1-minute basis), mostly for nanoparticles $< 15 \text{ nm}$ (Fig. 9). The lowest filter efficiency was detected for larger particles released during the laser treatment ($\sim 30 \text{ nm}$).

4. Conclusions

This study aimed to characterise particle formation and release mechanisms, and their impact on personal exposure and the environment during a tile sintering process using a high power CO_2 laser in an industrial up-scaling process. In addition, possible particle transformations during transport through the exhaust system and the effectiveness of the filtration system were also assessed.

Based on the experiments carried out, it was possible to conclude that new particle formation mechanisms from gaseous precursors occurred for both types of ceramic materials (red clay and porcelain) during the thermal treatment, independently of the laser treatment. The incidence of the laser seemed to inhibit new particle formation processes, possibly due to the sealing of the tile surface by the laser.

Ultrafine and nano-sized airborne particles were generated and emitted into workplace air during sintering process on a statistically significant level ($> BG + 3 \cdot \sigma_{BG}$). When comparing exposure levels to the exposure limits available in current regulations, according to SER (2012), exposure concentrations to ultrafine and nanoparticles generated in this workplace would exceed the nano-reference value (NRV) of $4 \times 10^4 \text{ cm}^{-3}$, since their 8 h TWA was in the range of $1.4 \times 10^5 \text{ cm}^{-3}$ and $5.3 \times 10^5 \text{ cm}^{-3}$ (worst case scenario considering an equivalent workers exposure of 7 h working shift during sintering activity and 1 h working shift during non-activity period). In terms of mass, current regulations set a 3 mg m^{-3} TLV (8 h TWA; ACGIH, 2013) for the total

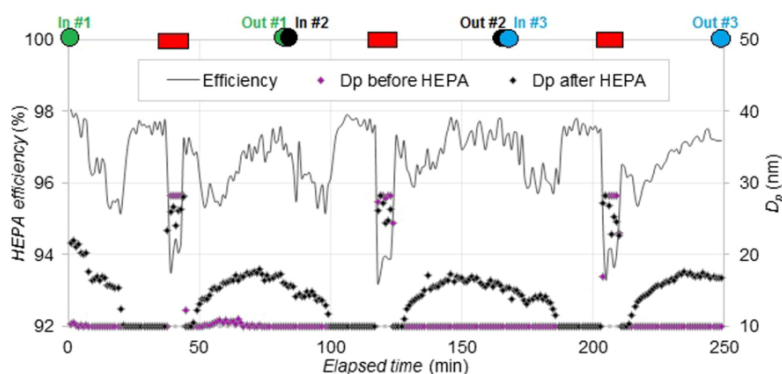


Fig. 9. Example of the efficiency of the HEPA filtration system (in %) as a function of particle diameter (range 10–700 nm) measured before and after the filtration system for each tile sintering process, for material #3 (red clay with frit and decoration). The laser period is shown as red rectangle and the entrance and exit of replicas #1, #2 and #3 are shown as green, black and blue circles, respectively. D_p : mean particle diameter (range 10–700 nm). (For interpretation of the references to colour in this figure legend, the reader is referred to the web version of this article.)

respirable fraction which would not have been exceeded during any sintering condition given that the PM_{10} for 8 h TWA would be in the range of $4.5\text{--}60\ \mu\text{g m}^{-3}$.

A potential risk of ultrafine and nanoparticle release to the outdoor air was identified, despite the mitigation measures in place (a HEPA filtration system). The efficiency of the filtration system was successfully tested, evidencing a $>87\%$ efficiency of N removal (on a 1-minute basis), mostly for nanoparticles $<15\ \text{nm}$ whereas it was slightly less efficient for larger particles released during the laser treatment ($\sim 30\ \text{nm}$).

Overall, the results from this study evidence the risk of occupational exposure to ultrafine and nanoparticles during high-energy laser processes in the ceramic facility under study. Although the results regarding exposures may not be extrapolated directly to real-world ceramic industrial facilities, this study may be taken as reference from a methodological perspective and with regard to the particle formation mechanisms described. In addition, our results could be representative of potential exposures in case of leaks in the process in industrial settings, when major nanoparticle releases would be expected. Hence, the development of mitigation strategies and systematic approaches toward better identifying the processes and/or materials are recommended to enable risk assessments and to reduce worker exposure.

Acknowledgements

This work was supported by the European Commission FP7 (FP7-PEOPLE-2012-ITN) Marie Curie ITN project no. 315760 (HEXACOMM) and by the Spanish MINECO (PCIN-2015-173-C02-01) under the frame of SIINN, the ERA-NET for a Safe Implementation of Innovative Nanoscience and Nanotechnology, through SIINN-ERANET project CERASAFE (id.:16). Additional support was provided by LIFE projects AIRUSE (LIFE11 ENV/ES/584), CERAMGLASS (LIFE11 ENV/ES/560) and LASERFIRING (LIFE09 ENV/ES/435).

Supplementary data

Supplementary data to this article can be found online at <http://dx.doi.org/10.1016/j.scitotenv.2016.01.106>.

References

ACGIH, 2013. Threshold Limit Values for Chemical Substances and Physical Agents and Biological Exposure Indices. American Conference of Governmental Industrial Hygienists.

Asbach, C., Kuhlbusch, T., Kaminski, H., Stahlmecke, B., Plitzko, S., Götz, U., Voetz, M., Kiesling, H.J., Dahmann, D., 2012. NanoGEM standard operation procedures for assessing exposure to nanomaterials, following a tiered approach. http://www.nanogem.de/cms/nanogem/upload/Veroeffentlichungen/nanoGEM_SOPs_Tiered_Approach.pdf.

Brouwer, D., Berges, M., Virji, M.A., Fransman, W., Bello, D., Hodson, L., Gabriel, S., Tielemans, E., 2012. Harmonization of measurement strategies for exposure to manufactured nano-objects; report of a workshop. *Ann. Occup. Hyg.* 56 (1), 1–9.

Brouwer, D., van Duuren-Stuurman, B., Berges, M., Jankowska, E., Bard, D., Mark, D., 2009. From workplace air measurement results toward estimates of exposure? Development of a strategy to assess exposure to manufactured nano-objects. *J. Nanoparticle Res.* 11 (8), 1867–1881. <http://dx.doi.org/10.1007/s11051-009-9772-1>.

Casasola, R., Rincón, J.M., Romero, M., 2012. Glass–ceramic glazes for ceramic tiles: a review. *J. Mater. Sci.* 47 (2), 553–582. <http://dx.doi.org/10.1007/s10853-011-5981-y>.

Celades, I., 2013. Caracterización física, química, mineralógica y morfológica del material particulado emitido por focos canalizados de la industria de baldosas y fritas cerámicas (PhD) Universitat Jaume I de Castellón, Castellón.

Cerame-Unie, 2012. The ceramic industry roadmap: paving the way to 2050. from <http://cerameunie.eu/>.

Chinchón, J.S., Querol, X., Fernández-Turiel, J.L., López-Soler, A., 1991. Environmental impact of mineral transformations undergone during coal combustion. *Environ. Geol. Water Sci.* 18 (1), 11–15. <http://dx.doi.org/10.1007/bf01704573>.

EC, 1998. Council directive 98/24/EC of 7 April 1998 on the protection of the health and safety of workers from the risks related to chemical agents at work (fourteenth individual directive within the meaning of article 16(1) of directive 89/391/EEC). *OJ L 131*, 5.5.1998, p. 11. Retrieved from <http://eur-lex.europa.eu/LexUriServ/LexUriServ.do?uri=OJ:L:1998:131:0011:0023:EN:PDF>.

Estepa, C., de la Fuente, G.F., Patent No. 200600560, 2006.

Fonseca, A.S., Viana, M., Querol, X., Moreno, N., de Francisco, I., Estepa, C., de la Fuente, G.F., 2015. Ultrafine and nanoparticle formation and emission mechanisms during laser processing of ceramic materials. *J. Aerosol Sci.* 88, 48–57. <http://dx.doi.org/10.1016/j.jaerosci.2015.05.013>.

de Francisco, I., Lennikov, V.V., Bea, J.A., Vegas, A., Carda, J.B., de la Fuente, G.F., 2011. In-situ laser synthesis of rare earth aluminate coatings in the system Ln–Al–O (Ln = Y, Gd). *Solid State Sci.* 13 (9), 1813–1819. <http://dx.doi.org/10.1016/j.solidstatesciences.2011.07.013>.

Gutiérrez Mora, F., Domínguez-Rodríguez, A., Lennikov, V.V., de la Fuente, G.F., 2009. Influence of thermal effects produced by laser treatment on the tribological behavior of porcelain ceramic tiles. *Key Eng. Mater.* 423, 41–46.

Hameri, K., Lahde, T., Hussein, T., Koivisto, J., Savolainen, K., 2009. Facing the key workplace challenge: assessing and preventing exposure to nanoparticles at source. *Inhal. Toxicol.* 1, 17–24.

Hansen, S.F., 2009. Regulation and Risk Assessment of Nanomaterials: Technical University of Denmark (DTU).

Heal, M.R., Kumar, P., Harrison, R.M., 2012. Particles, air quality, policy and health (10.1039/C2CS35076A). *Chem. Soc. Rev.* 41 (19), 6606–6630. <http://dx.doi.org/10.1039/c2cs35076a>.

Hoet, P.H., Bruske-Hohlfeld, I., Salata, O.V., 2004. Nanoparticles – known and unknown health risks [Journal article] *J. Nanobiotechnol.* 2 (1), 12.

Jaakkola, M.S., Sripaiboonkij, P., Jaakkola, J.J., 2011. Effects of occupational exposures and smoking on lung function in tile factory workers [Research Support, Non-US Gov't] *Int. Arch. Occup. Environ. Health* 84 (2), 151–158.

Jacobs, C.W.F., 1954. Opacifying crystalline phases present in zirconium-type glazes. *J. Am. Ceram. Soc.* 37 (5), 216–220. <http://dx.doi.org/10.1111/j.1151-2916.1954.tb14026.x>.

Kaminski, H., Beyer, M., Fissan, H., Asbach, C., Kuhlbusch, T.A.J., 2015. Measurements of nanoscale TiO₂ and Al₂O₃ in industrial workplace environments – methodology and results. *Aerosol Air Qual. Res.* 15 (1), 129–141. <http://dx.doi.org/10.4209/aaqr.2014.03.0065>.

Kargar, F., Shahtaheri, S.J., Golbabaei, F., Barkhordari, A., Rahimi-Froushani, A., Khadem, M., 2013. Evaluation of occupational exposure of glazers of a ceramic industry to cobalt blue dye. *Iran. J. Public Health* 42 (8), 868–875.

Kulmala, M., Vehkamäki, H., Petäjä, T., Dal Maso, M., Lauri, A., Kerminen, V.M., Birmili, W., McMurry, P.H., 2004. Formation and growth rates of ultrafine atmospheric particles:

Please cite this article as: Fonseca, A.S., et al., Process-generated nanoparticles from ceramic tile sintering: Emissions, exposure and environmental release, *Sci Total Environ* (2016), <http://dx.doi.org/10.1016/j.scitotenv.2016.01.106>

ARTICLE IN PRESS

A.S. Fonseca et al. / Science of the Total Environment xxx (2016) xxx–xxx

11

- a review of observations. *J. Aerosol Sci.* 35 (2), 143–176. <http://dx.doi.org/10.1016/j.jaerosci.2003.10.003>.
- Kumar, P., Fennell, P., Britter, R., 2008. Effect of wind direction and speed on the dispersion of nucleation and accumulation mode particles in an urban street canyon. *Sci. Total Environ.* 402 (1), 82–94. <http://dx.doi.org/10.1016/j.scitotenv.2008.04.032>.
- Lahoz, R., de la Fuente, G.F., Pedra, J.M., Carda, J.B., 2011. Laser engraving of ceramic tiles. *Int. J. Appl. Ceram. Technol.* 8 (5), 1208–1217. <http://dx.doi.org/10.1111/j.1744-7402.2010.02566.x>.
- Larrea, A., de la Fuente, G.F., Merino, R.I., Orera, V.M., 2002. ZrO₂–Al₂O₃ eutectic plates produced by laser zone melting. *J. Eur. Ceram. Soc.* 22 (2), 191–198. [http://dx.doi.org/10.1016/S0955-2219\(01\)00279-5](http://dx.doi.org/10.1016/S0955-2219(01)00279-5).
- Lennikov, V.V., de Francisco, I., Bea, J.A., Estepa, L.C., de la Fuente, G.F., J.A.García, 2010. Influencia de los efectos térmicos inducidos por el tratamiento con laser CO₂ en la microestructura de baldosas cerámicas. In: Rodríguez y, R. (Ed.), *Actas del XII Congreso Tratermat*, pp. 373–379 (AIN ISBN: 978-84-693-6946-3).
- Lennikov, V.V., Kazin, P.E., Tretyakov, Y.D., de la Fuente, G.F., 2004. Laser zone melting and texture formation in MgO-doped Bi_{2.03}Sr_{1.93}Ca_{1.07}Cu_{2.05}O_{8 + ε}. *Z. Anorg. Allg. Chem.* 630 (13–14), 2337–2342. <http://dx.doi.org/10.1002/zaac.200400311>.
- Lennikov, V.V., Pedra, J.M., Gómez, J.J., de la Fuente, G.F., Carda, J.B., 2007. In situ synthesis of composite MTiO₃–Al₂O₃ coatings via laser zone melting. *Solid State Sci.* 9 (5), 404–409. <http://dx.doi.org/10.1016/j.solidstatesciences.2007.03.013>.
- Methner, M., Hodson, L., Geraci, C., 2010. Nanoparticle Emission Assessment Technique (NEAT) for the identification and measurement of potential inhalation exposure to engineered nanomaterials—part A. *J. Occup. Environ. Hyg.* 7 (3), 127–132. <http://dx.doi.org/10.1080/15459620903476355>.
- Minguillon, M.C., Monfort, E., Querol, X., Alastuey, A., Celades, I., Miro, J.V., 2009. Effect of ceramic industrial particulate emission control on key components of ambient PM₁₀ [Research Support, Non-US Gov't]. *J. Environ. Manag.* 90 (8), 2558–2567.
- Mora, M., Diez, J.C., Lopez-Gascon, C.I., Martínez, E., de la Fuente, G.F., 2003. Laser textured Bi-2212 in planar geometries. *IEEE Trans. Appl. Supercond.* 13 (2), 3188–3191. <http://dx.doi.org/10.1109/tasc.2003.812192>.
- Oberdorster, G., 2001. Pulmonary effects of inhaled ultrafine particles. *Int. Arch. Occup. Environ. Health* 74 (1), 1–8.
- OECD, 2015. Harmonized Tiered Approach to Measure and Assess the Potential Exposure to Airborne Emissions of Engineered Nano-Objects and Their Agglomerates and Aggregates at Workplaces. Series on the Safety of Manufactured Nanomaterials No. 55, ENV/JM/MONO(2015)19. Environment Directorate, Organisation for Economic Co-operation and Development (OECD), Health and Safety Publications, Paris.
- OSHA, 2006. 29 CFR 1910.1000. Z-3 Table.
- Querol, X., Alastuey, A., Rodríguez, S., Plana, F., Ruiz, C.R., Cots, N., Massagué, G., Puig, O., 2001. PM₁₀ and PM_{2.5} source apportionment in the Barcelona Metropolitan Area, Catalonia, Spain. *Atmos. Environ.* 35, 6407–6419.
- Ramachandran, G., Ostraat, M., Evans, D.E., Methner, M.M., O'Shaughnessy, P., D'Arcy, J., Geraci, C.L., Stevenson, E., Maynard, A., Rickabaugh, K., 2011. A strategy for assessing workplace exposures to nanomaterials. *J. Occup. Environ. Hyg.* 8 (11), 673–685.
- Romero, M., Rincón, J.M., Acosta, A., 2003. Crystallisation of a zirconium-based glaze for ceramic tile coatings. *J. Eur. Ceram. Soc.* 23 (10), 1629–1635. [http://dx.doi.org/10.1016/S0955-2219\(02\)00415-6](http://dx.doi.org/10.1016/S0955-2219(02)00415-6).
- de la Sánchez Campa, A.M., de la Rosa, J.D., González-Castanedo, Y., Fernández-Camacho, R., Alastuey, A., Querol, X., Pio, C., 2010. High concentrations of heavy metals in PM from ceramic factories of Southern Spain. *Atmos. Res.* 96 (4), 633–644. <http://dx.doi.org/10.1016/j.atmosres.2010.02.011>.
- Schmoll, L.H., Elzey, S., Grassian, V.H., O'Shaughnessy, P.T., 2009. Nanoparticle aerosol generation methods from bulk powders for inhalation exposure studies. *Nanotoxicology* 3 (4), 265–275. <http://dx.doi.org/10.3109/17435390903121931>.
- SER, 2012. Provisional Nano Reference Values for Engineered Nanomaterials, Advisory Report 12/01. Sociaal Economische Raad, Den Haag.
- Trethowan, W.N., Burge, P.S., Rossiter, C.E., Harrington, J.M., Calvert, I.A., 1995. Study of the respiratory health of employees in seven European plants that manufacture ceramic fibres. *Occup. Environ. Med.* 52 (2), 97–104.
- Van Broekhuizen, P., 2012. Nano Matters: Building Blocks for a Precautionary Approach. (PhD thesis Available at: www.ivam.uva.nl/?nanomatters).
- VCI, BAuA, RCI, B., IFA, IUTA, TUD, 2011. Tiered Approach to an Exposure Measurement and Assessment of Nanoscale Aerosols Released From Engineered Nanomaterials in Workplace Operations.
- Viana, M., Rivas, I., Reche, C., Fonseca, A.S., Pérez, N., Querol, X., Alastuey, A., Álvarez-Pedrerol, M., Sunyer, J., 2015. Field comparison of portable and stationary instruments for outdoor urban air exposure assessments. *Atmos. Environ.* 123 (Part A), 220–228. <http://dx.doi.org/10.1016/j.atmosenv.2015.10.076>.
- Voliotis, A., Bezantakos, S., Giamarelou, M., Valenti, M., Kumar, P., Biskos, G., 2014. Nanoparticle emissions from traditional pottery manufacturing [Research Support, Non-US Gov't]. *Environ. Sci.: Processes Impacts* 16 (6), 1489–1494.
- Weichenenthal, S., 2012. Selected physiological effects of ultrafine particles in acute cardiovascular morbidity [Review]. *Environ. Res.* 115, 26–36.

Please cite this article as: Fonseca, A.S., et al., Process-generated nanoparticles from ceramic tile sintering: Emissions, exposure and environmental release, *Sci Total Environ* (2016), <http://dx.doi.org/10.1016/j.scitotenv.2016.01.106>

Supplementary data

Process-generated nanoparticles from ceramic tile sintering: emissions, exposure and environmental release

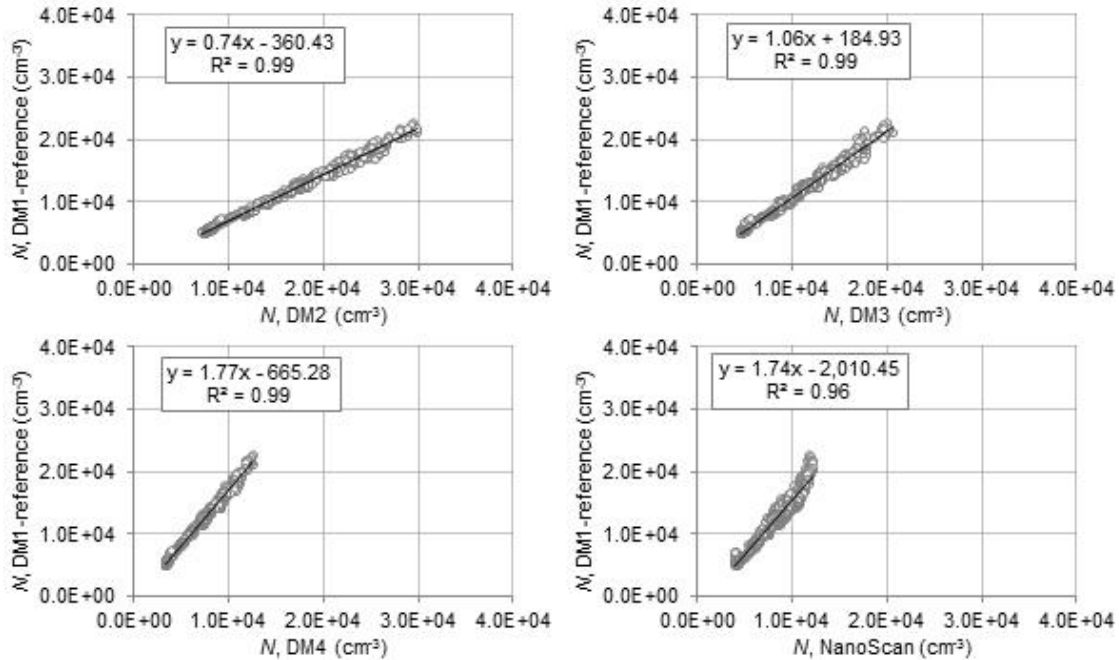


Figure S1. Correlation coefficients and regression equations obtained from the comparison between the reference DiscMini (DM) and the other DM units, and the NanoScan for total particle number (N) monitoring.

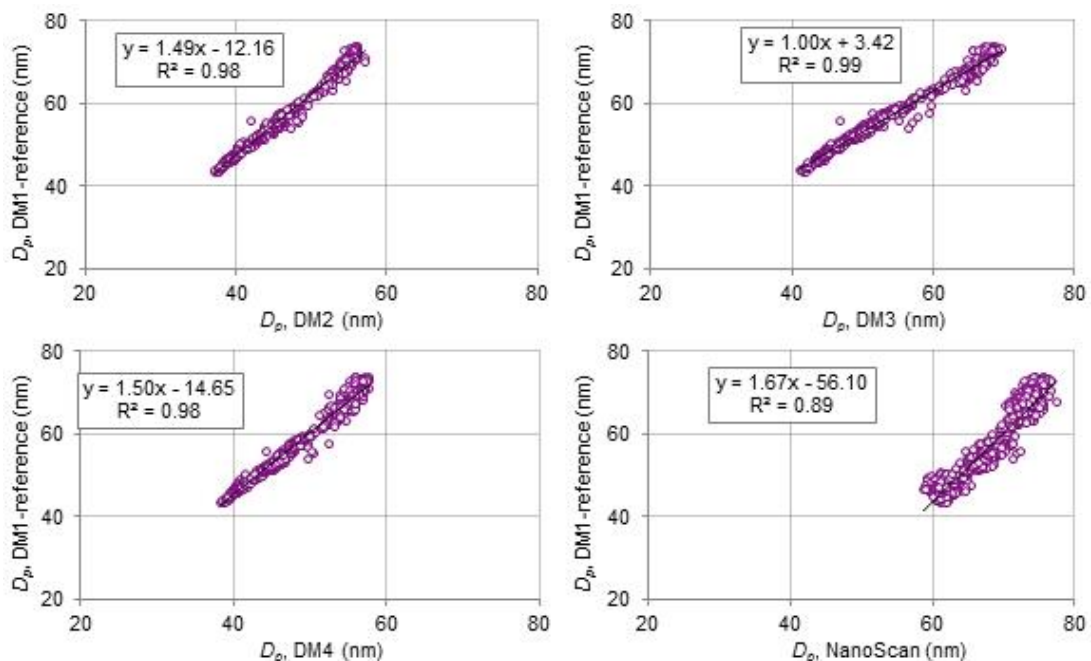


Figure S2. Correlation coefficients and regression equations obtained from the comparison between the reference DiscMini (DM), and the other DM units and the NanoScan for mean particle diameter (D_p) monitoring.

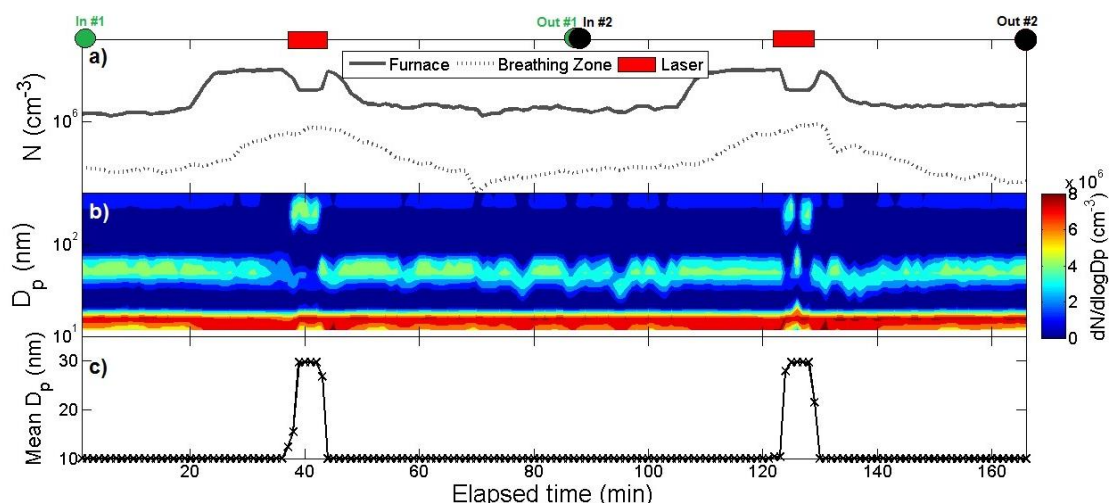


Figure S3. Sintering of porcelain with frit (material #5). Time series of (a) particle number concentrations (N) measured simultaneously at the emission source and in the breathing zone (range 10-700 nm), and (b) particle size distributions (D_p ; range of 10-420 nm), and (c) mean particle diameter at the emission source (range 10-700 nm). The laser period is shown as red circles and the entrance and exit of replicas #1, #2 are shown as green and red crosses, respectively.

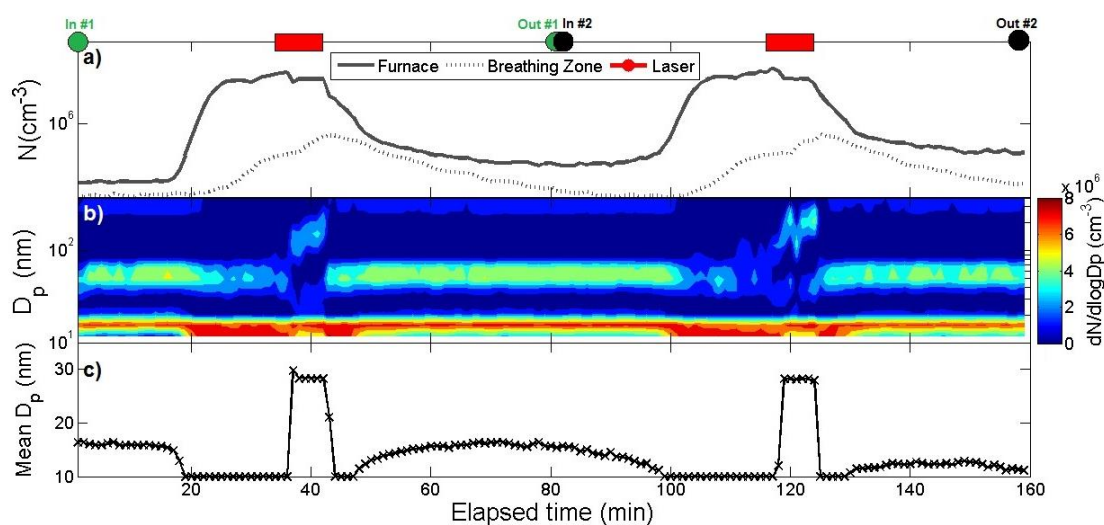


Figure S4. Sintering of red clay with frit (material #2). Time series of (a) particle number concentrations (N) measured simultaneously at the emission source and in the breathing zone (range 10-700 nm), and (b) particle size distributions (D_p ; range of 10-420 nm), and (c) mean particle diameter at the emission source (range 10-700 nm). The laser period is shown as red circles and the entrance and exit of replicas #1, #2 are shown as green and red crosses, respectively.

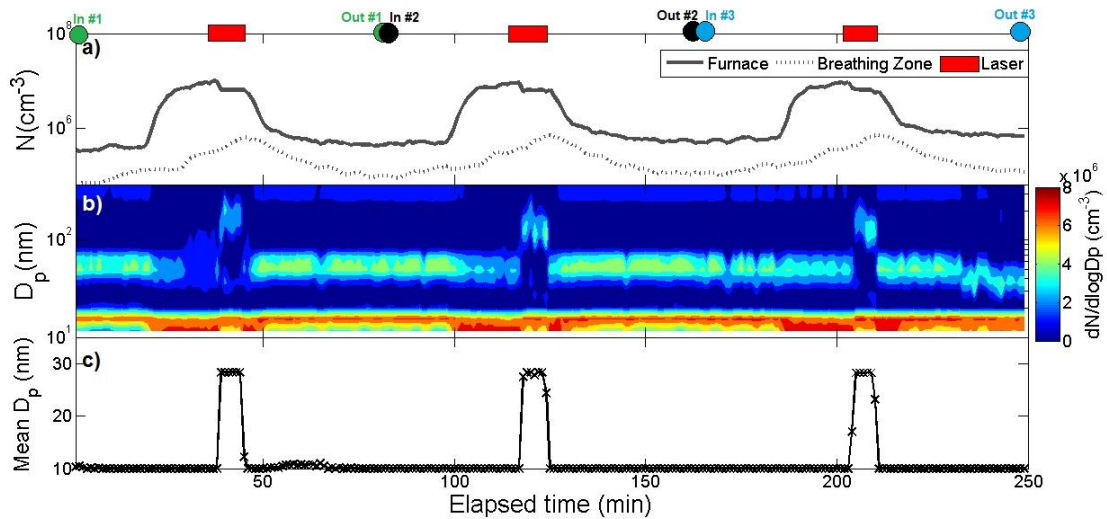


Figure S5. Sintering of red clay with frit and decoration (material #3). Time series of (a) particle number (N) concentrations measured simultaneously at the emission source and in the breathing zone (range 10-700 nm), and (b) particle size distributions (D_p ; range of 10-420 nm), and (c) mean particle diameter at the emission source (range 10-700 nm). The laser period is shown as red circles and the entrance and exit of replicas #1, #2 and #3 are shown as green, red and blue crosses, respectively.

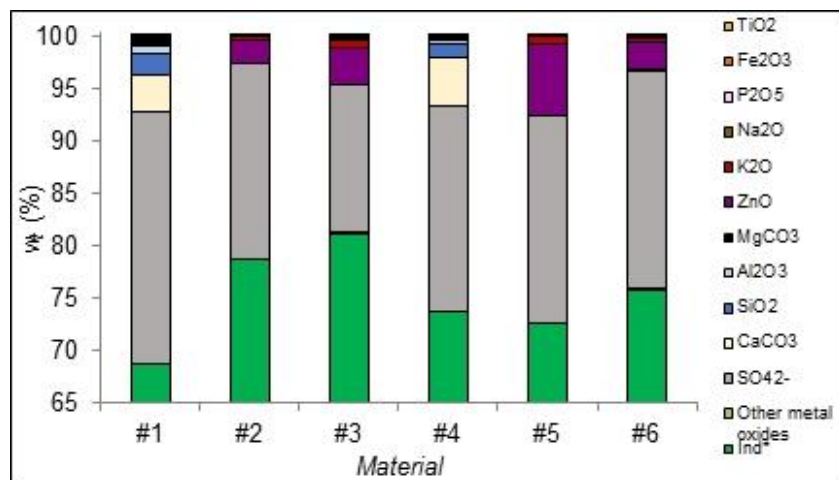


Figure S6. Concentration of major components and trace elements in workplace air particles collected (in %).

4.4 Article IV: Intercomparison of a portable and two stationary mobility particle sizers for nanoscale aerosol measurements

Authors:

Fonseca, A. S.^{1,2}, Viana, M.¹, Pérez, N.¹, Alastuey, A.¹, Querol, X.¹, Kaminski, H.³,
Todea, A. M.³, Monz, C.⁴, Asbach, C.³

¹ Institute of Environmental Assessment and Water Research (IDÆA-CSIC), C/ Jordi Girona 18, 08034 Barcelona, Spain

² Universidad de Barcelona, Facultad de Química, Martí i Franquès 1-11, 08028 Barcelona, Spain

³ Institute of Energy and Environmental Technology (IUTA), 47229 Duisburg, Germany

⁴ Institute for the Research on Hazardous Substances (IGF), 44789 Bochum, Germany

Published in:

Aerosol Sci Technol, 2016
doi: 10.1080/02786826.2016.1174329

Accepted date: 25 March 2016 (in press)

Intercomparison of a portable and two stationary mobility particle sizers for nanoscale aerosol measurements

A. S. Fonseca^{1,2,*}, M. Viana¹, N. Pérez¹, A. Alastuey¹, X. Querol¹, H. Kaminski³, A. M. Todea³, C. Monz⁴, C. Asbach³

¹ Institute of Environmental Assessment and Water Research (IDÆA-CSIC), C/ Jordi Girona 18, 08034 Barcelona, Spain

² Universidad de Barcelona, Facultad de Química, Martí i Franquès 1-11, 08028 Barcelona, Spain

³ Institute of Energy and Environmental Technology (IUTA), 47229 Duisburg, Germany

⁴ Institute for the Research on Hazardous Substances (IGF), 44789 Bochum, Germany

*Corresponding author: ana.godinho@idaea.csic.es, Tel:+34 934006100. Fax: +34 932045904.

Abstract

During occupational exposure studies, the use of conventional scanning mobility particle sizers (SMPS) provides high quality data but may convey transport and application limitations. New instruments aiming to overcome these limitations are being currently developed. The purpose of the present study was to compare the performance of the novel portable NanoScan SMPS TSI 3910 with that of two stationary SMPS instruments and one ultrafine condensation particle counter (UCPC) in a controlled atmosphere and for different particle types and concentrations.

The results show that NanoScan tends to overestimate particle number concentrations with regard to the UCPC, particularly for agglomerated particles (ZnO, spark generated soot and diesel soot particles) with relative differences >20%. The best agreements between the internal reference values and measured number concentrations were obtained when measuring compact and spherical particles (NaCl and DEHS particles). With regard to particle diameter (modal size), results from NanoScan were comparable < [$\pm 20\%$] to those measured by SMPSs for most of the aerosols measured.

The findings of this study show that mobility particle sizers using unipolar and bipolar charging may be affected differently by particle size, morphologies, particle composition and concentration. While the sizing accuracy of the NanoScan SMPS was mostly within $\pm 25\%$, it may miscount total particle number concentration by more than 50% (especially for agglomerated particles), thus making it unsuitable for occupational exposure assessments where high degree of accuracy is required (e.g., in tier 3). However, can be a useful instrument to obtain an estimate of the aerosol size distribution in indoor and workplace air, e.g. in the tier 2.

Keywords: Stationary SMPS, Portable SMPS, CPC, Number concentration, Size distribution, Indoor

1. Introduction

Associations between exposure to ultrafine particles (particles of low solubility with equivalent aerodynamic diameters < 100 nm) and adverse health effects have been identified (Atkinson *et al.*, 2001; Dockery *et al.*, 1993; Donaldson *et al.*, 2006; Kreyling *et al.*, 2002; Maynard and Kuempel, 2005; Oberdorster *et al.*, 2005; Oberdorster *et al.*, 2004). Epidemiological studies have shown that at similar mass concentrations, ultrafine particles can be more harmful than micrometer-size particles due to their ability to penetrate deeper into the lung (Oberdorster *et al.*, 2005; Peters *et al.*, 1997b). Taking into account that nanoscale particles typically contribute negligibly to total mass concentrations, there is evidence that other metrics such as particle number (*PN*) concentration are more sensitive for this type of particles (Kuhlbusch *et al.*, 2011a). In order to assess exposure to potentially health hazardous particles, measurements of particle diameter and mean size are also advisable

Different instruments have been developed to quantify airborne *PN* concentrations such as condensation particle counters - CPC (Agarwal and Sem, 1980; Hermann *et al.*, 2007; Wiedensohler *et al.*, 1997) for the determination of total *PN* concentration, and mobility particle size spectrometers such as Differential Mobility Particle Sizer (DMPS, Kousaka *et al.*, 1985; ten Brink *et al.*, 1983), Scanning Mobility Particle Sizer (SMPS, Wang and Flagan, 1989, 1990) or Fast Mobility Particle Sizer (FMPS, Tammet *et al.*, 2002) for the measurement of *PN* concentrations as a function of particle size, i.e., particle number size distributions.

The theoretical principle of mobility particle size spectrometers is that particles of a specific charge distribution (Fuchs, 1963) may be classified in a differential mobility analyser (DMA, Knutson and Whitby, 1975; Winklmayr *et al.*, 1991; Fissan *et al.*, 1996; Chen *et al.*, 1998) according to their electrical mobility. To obtain the mobility distribution, the electric field strength inside the classifier is sequentially (Fissan *et al.*, 1983) or continuously (Wang and Flagan, 1990) ramped to give the bandwidth of electrical mobilities. Typically the particles exiting the classifier are counted as *PN* with a CPC (Agarwal and Sem, 1980). However, during occupational exposure studies, the use of conventional SMPS conveys transport and application limitations, due to its need for a radioactive or X-ray neutralizer and its bulky nature. Therefore, a novel portable nanoparticle sizing and counting instrument (NanoScan SMPS TSI 3910, Tritscher *et al.*, 2013) was recently commercialised for real-time nanoparticle measurements within the range from 10 to 420 nm. This device incorporates a non-

radioactive unipolar diffusion charger (corona jet type) (Medved *et al.*, 2000), a radial differential mobility analyser (rDMA, Zhang *et al.*, 1995; Fissan *et al.*, 1998) and an isopropanol-based CPC. The main advantage of this instrument is its portability (< 9 kg), battery operation without the need to use power supply, small size (LxWxH = 45x23x39 cm), and the use of a nonradioactive unipolar charger which makes it a suitable monitor for real-time workplace measurements without the transport and application restrictions currently affecting traditional SMPS instruments. Another advantage is the use of isopropanol instead of butanol as a working fluid since it is a relatively benign chemical when compared to butanol (TSI, 2015). The downside of the NanoScan is its lower sizing resolution (only 13 channels) (Stabile *et al.*, 2014). Several studies have reported that based on unipolar diffusion charging of the FMPS, particles are wrongly sized in the upper working size range (Levin *et al.*, 2015; Price *et al.*, 2014; Zimmerman *et al.*, 2015).

To date, few studies have measured the total *PN* concentrations and particle number size distributions by using the above mentioned methods/instruments in a variety of settings and environments such as ambient air (Asmi *et al.*, 2011; Beddows *et al.*, 2014; Brines *et al.*, 2015; Costabile *et al.*, 2009; Cusack *et al.*, 2013; Gómez-Moreno *et al.*, 2015; Reche *et al.*, 2011; Watson *et al.*, 2011; Wehner *et al.*, 2002), indoor air (Buonanno *et al.*, 2010; Buonanno *et al.*, 2013b; Morawska *et al.*, 2009a; Voliotis *et al.*, 2014; Zhang *et al.*, 2010) and industrial and nanotechnology-related workplaces (Brouwer, 2010; Demou *et al.*, 2008b; Fonseca *et al.*, 2015a; Fonseca *et al.*, 2015c; Koivisto *et al.*, 2012; Koivisto *et al.*, 2014; Kuhlbusch *et al.*, 2011a).

Intercomparisons between stationary mobility particle size spectrometers and CPCs can be found in the literature (Asbach *et al.*, 2009a; Asbach *et al.*, 2012a; Jeong and Evans, 2009; Kaminski *et al.*, 2013; Price *et al.*, 2014; Watson *et al.*, 2011; Wiedensohler *et al.*, 2012). However, intercomparisons between stationary SMPS and the novel portable NanoScan are scarce. Only recently, Tritscher *et al.* (2013) studied the comparability between the NanoScan SMPS, two research-grade SMPS reference systems and an ultrafine butanol CPC. Although a good comparability was found, there is still a need to determine the reproducibility of data provided by the NanoScan and study how it relates to other sampling instruments in order to scrutinize the limits concerning different materials, concentrations, particle shapes and sizes. Stabile *et al.* (2014) compared the NanoScan and an SMPS with a variety of different polydisperse test aerosols. They found that the agreement was best for spherical particles, whereas significant deviations were observed for agglomerates. They furthermore found a better agreement between the NanoScan and the SMPS when no diffusion and multiple charge corrections were applied to the latter. It should, however, be noted that only data from an SMPS with both corrections active can be

considered as the most accurate representation of a particle size distribution, whereas SMPS data obtained without these corrections are known to be flawed, especially in the case of the larger e. g. DEHS particles, where the fraction of multiply charged particles is significantly higher and needs to be corrected using the multiple charge correction (Kaminski *et al.*, 2013). Reineking and Porstendörfer (1986) reported that diffusional losses of particles inside a TSI long DMA are equivalent to losses in a 13 m long tube. As an example, losses of 20 nm particles in a long DMA amount to approximately 66% and of 10 nm particles to approximately 75%. Diffusional losses of particularly small particles can therefore be quite significant and need to be corrected for. Deconvolution of the NanoScan raw data is much more complex than for the SMPS data and therefore the multiple charge and diffusion loss correction are already inherently included in the empirical data evaluation routines. In the present study, only SMPS data that had been corrected for multiple charge effects and diffusion losses were used.

The purpose of the present study was to compare the performance of the portable NanoScan SMPS TSI 3910 with that of two stationary SMPS instruments (with a long and a nano DMA) and one ultrafine butanol condensation particle counter (UCPC) in a controlled atmosphere and for different particle types. The ultimate goal was to assess the suitability of the NanoScan instrument for occupational exposure studies, given their specific needs with regard to accuracy, transport and use limitations, etc. The instruments were simultaneously challenged with intentionally produced particles covering a wide range of particle sizes and morphologies: di-ethyl-hexyl-sebacate (DEHS; spherical), sodium chloride (NaCl; cubic or near spherical shape), and agglomerates as zinc oxide (ZnO), spark generated soot and diesel soot particles (Kaminski *et al.*, 2013).

2. Methodology

Instrumentation

Two common stationary and one NanoScan SMPS were used for measuring particle size distributions. In addition, for measuring total size-integrated number concentrations, an ultrafine CPC was used (Table 1).

The two stationary SMPS used as internal reference for the size distribution in this study were: (i) SMPS (TSI, Model 3936 long), which consists of a long-column DMA (TSI, Model 3081; Liu and Pui, 1974) and a butanol CPC (TSI, Model 3772) with a lower detection limit of 10 nm, hereafter referred to as “SMPS-L” and (ii) SMPS (TSI, Model 3936 nano), which consists of a nano-DMA (TSI, Model 3085; Chen *et al.*, 1998) and an Ultrafine Water-based Condensation Particle Counter with a lower detection limit of 2.5 nm (UWCPC, TSI, Model 3786; Hering *et al.*, 2005), hereafter

referred to as “SMPS-N”. Both SMPS used a ^{85}Kr bipolar neutralizer with an initial activity of 74 MBq (TSI, Model 3077). The neutralizer used in SMPS-N was approximately 5 years old and the one in SMPS-L more than 10 years. In the measuring configurations selected for this study, both SMPS-L and SMPS-N delivered size distributions available in 64 channels per size decade. SMPS-L measured in the size range $9.7 \text{ nm} \leq D_p \leq 421.7 \text{ nm}$ (0.6 L min^{-1} aerosol, 6 L min^{-1} sheath flow rate) or $19.1 \text{ nm} \leq D_p \leq 897.7 \text{ nm}$ (0.2 L min^{-1} aerosol, 2 L min^{-1} sheath flow rate) whereas the SMPS-N in the size range $3.2 \text{ nm} \leq D_p \leq 107.5 \text{ nm}$ (0.6 L min^{-1} aerosol, 6 L min^{-1} sheath flow rate). The aerosol flow rate was frequently checked by using a flow meter (TSI, Model 4045) to ensure it remained $\pm 10\%$ of the instrumental flow rate. The SMPS with long DMA was equipped with an impactor (nozzle diameter 0.0508 cm) which removes all particles $> 553 \text{ nm}$ (aerodynamic diameter) at an aerosol flow rate of 0.6 L min^{-1} and $>1,011 \text{ nm}$ at a flow rate of 0.2 L min^{-1} . The SMPS with nanoDMA was equipped with an impactor with a 0.071 cm nozzle with a cut off size around $1 \mu\text{m}$. The latter impactor was mainly used to protect the instrument from larger particles, because no impactor with a cut-off size matching the upper size limit of the DMA is available. Data were collected and evaluated with the TSI Aerosol Instrument Manager software (AIM, version 9.0.0.0, TSI), which allows correcting for particle diffusion losses inside the instruments based on empirical factors as well as for multiple charge correction (Fissan *et al.*, 1983; Hoppel, 1978). The time resolution of both SMPSs was set to 180 sec (120 s upscan, 30 s retrace and 30 s wait time for SMPS-L and 120 s upscan, 20 s retrace and 40 s wait time for SMPS-N, respectively).

Table 1. Specifications of instruments used in this study.

ID	Manufacturer and Model		Studied metric	Size range [nm]	Time resolution [s]	Aerosol flow rate [L min^{-1}]	Sheath flow rate [L min^{-1}]	Software version	Other settings
SMPS-L	TSI Model long	SMPS, 3936	PNC ^a	9.7-421.7	180	0.6	6	AIM, version 9.0.0.0	Long DMA (TSI, Model 3081) + CPC (TSI, Model 3772)
			+ PSD ^b	19.1-897.7		0.2	2		^{85}Kr bipolar neutralizer (74 MBq, TSI model 3077)
SMPS-N	TSI Model nano	SMPS, 3936	PNC ^a + PSD ^b	3.2-107.5	180	0.6	6	AIM, version 9.0.0.0	Nano DMA (TSI, Model 3085) + UWCPC (TSI, Model 3786) ^{85}Kr bipolar neutralizer (74 MBq, TSI model 3077)
NanoScan	TSI Model 3910	SMPS,	PNC ^a + PSD ^b	10-420	60	0.75	-	NanoScan Manager Version 1.0.0.19	Non-radioactive unipolar diffusion charger (corona jet type)
UCPC	TSI Model 3776	UCPC,	PNC ^a	2.5-3000	1	1.5	-	AIM, version 9.0.0.0	-

PNC^a - PN concentration

PSD^b - Particle size distribution

While SMPSs are generally used to measure stable particle size distributions, the time resolution of the portable electrical mobility spectrometer NanoScan SMPS (TSI, Model 3910; aerosol flow rate $0.75 \text{ L min}^{-1} \pm 20 \%$ flow inlet) allows in principle for measuring more rapidly changing particle mobility size distributions in 13 channels. In this study, while the stationary SMPS delivered size distribution data every 3 min, the time resolution of the NanoScan SMPS was 1 min (45 s up-scan in which the measurement occurs, and a 15 s retrace).

An ultrafine butanol condensation particle counter (UCPC, TSI, Model 3776) was used as internal reference to determine the total number concentration. According to the manufacturer's specifications, the UCPC covers the size range between 2.5 nm - 3 μm and uses a single particle count mode measuring up to $3 \times 10^5 \text{ cm}^{-3}$. The UCPC was operated in high flow mode with a flow rate of 1.5 L min^{-1} in order to minimize particle diffusion losses in the system. Particle losses were not corrected, because the UCPC does not record size distributions, which are required for correction of diffusional losses.

In order to confirm the particle morphology and the elemental chemistry of spark generated soot and diesel particles, samples were collected onto Quantifoil® gold (Au) grids with 1 μm diameter holes - 4 μm separation of 200-mesh with the nanometer aerosol sampler (NAS; TSI, Model 3089; Dixkens and Fissan, 1999) for transmission electron microscopy (TEM) and energy dispersive x-ray spectroscopy (EDS) analysis. Charged particles in the range from 2 - 100 nm were sampled onto collection substrates for 10 min at a flow rate of 2.5 L min^{-1} and a collection voltage of +10 kV.

Particle generation

Four different types of aerosol generators were used to intentionally produce five different types of aerosol: (i) NaCl; (ii) DEHS; (iii) ZnO; (iv) spark generated soot and (v) diesel soot. A total of fifteen experiments were performed, to assess the performance of the instruments under different concentration levels and different particle sizes. Twelve of these experiments corresponded to aerosols with unimodal particle size distribution and the remaining three were multimodal (online Supplemental Information Table S1).

Cubic (NaCl) particles with average sizes of 10 nm and 60 nm were produced by a burner (FG2, MoTec Konzepte, Bochum Germany; Monsé *et al.*, 2014) and a home-made atomizer, respectively. ZnO particles with average particle size of 60 nm were generated by using the same burner generator, while small droplets of DEHS were generated by spraying pure DEHS using the aforementioned atomizer.

Agglomerated carbonaceous aerosol (spark generated soot) were produced using a spark generator (GFG 3000, Palas GmbH, Karlsruhe, Germany) equipped with graphite electrodes. The total spark generator current was always 14.6 mA and the argon flow rate approximately 5 L min^{-1} . The generator allows for a dilution of the freshly produced aerosol with particle-free dilution air to avoid rapid coagulation. A dilution air of 17.5 L min^{-1} during experimental runs for the smallest spark generated soot in diameter (#8 and #9), and 5 L min^{-1} during experimental runs for the largest spark generated soot in diameter (#10 and #11), were added. The highly concentrated aerosol was further diluted in a wind tunnel with filtered air ranging from 200 to $2880 \text{ m}^3 \text{ h}^{-1}$. The use of different dilution rates, allowed to understand the performance of the instruments under two different concentration levels, around 10^4 cm^{-3} and 10^5 cm^{-3} . An average particle size of 48 and 67 nm was obtained for experiments spark generated soot #8 and #9, respectively whereas for spark generated soot #10 and #11, particles of 82 and 105 nm in diameter were obtained. Agglomerated diesel soot particles ($\sim 100 \text{ nm}$), were generated by using a diesel engine (aspiration type, 2180 cm^3 , Mercedes Benz 220D, 44 kW at 4200 rotations min^{-1}) idling at 1400 rotations min^{-1} .

Additionally, bimodal size distributions were produced from diesel soot by letting the same diesel engine idling at 800 rotations min^{-1} and NaCl by using burner and NaCl/DEHS trimodal size distributions by a combination of burner and atomizer. For the ZnO, diesel soot and multimodal particle size distributions, only one concentration level was chosen.

All the measured concentrations were within the range specified by the manufacturers for the instruments included in the study.

Experimental setup

Experiments were conducted at the NanoTest-Center of the Institute for the Research on Hazardous Substances (IGF) in Dortmund, Germany. Details of the Nano Test Center can be found in Asbach *et al.* (2009a), Asbach *et al.* (2012a) and Kaminski *et al.* (2013).

Particles from the atomizer and spark generator were neutralised before being introduced into the wind tunnel by passing through a radioactive source ^{85}Kr (TSI, Model 3012A; 370 MBq initial activity, approximately 3 years old). Particles from the atomizer were additionally dried by a silica gel diffusion dryer. Afterwards, they were injected into the wind tunnel (20 m long with a diameter of 0.7 m), where they were mixed with ultra-low penetration air (ULPA) filtered dilution air. The wind tunnel feeds into a 20 m^3 exposure chamber, which is ventilated by a blower that defines the dilution air flow rate in the wind tunnel. A schematic diagram of experimental setup is shown in Figure S1 of the online Supplemental Information.

The dilution air flow rates in the wind tunnel were adjusted to flow rates between 250 and 3660 m³ h⁻¹ in order to produce the desired particle concentration levels. According to Asbach *et al.* (2012a), the aerosol is homogeneously mixed in the exposure chamber so that all instruments placed inside sample identical aerosol concentrations and particle size distributions.

All devices were placed in the mixing chamber and sampled directly without any tubes attached. They were positioned on a table inside the exposure chamber (Figure S1 of the online Supplemental Information), measuring at approximately the same height with adequate distance between each other. The NAS, which required frequent replacement of TEM grids, was placed outside the exposure chamber and connected to a sampling train, operated at 20 L min⁻¹, which splits the total flow into two flows of 10 L min⁻¹.

Before each experimental run, the mixing chamber was flushed with clean air until the background concentration in the exposure chamber reached a level of typically around 1 × 10³ cm⁻³ or below, and after that the respective aerosol generator was connected to the wind tunnel. Measurements started approximately 20 min after the generator was switched on, when the N concentration in the chamber was constant (± 10%). Each experiment consisted of 30 consecutive minutes of particle measurements under stable PN concentrations.

Data analysis

Regarding the measured size distribution data, since the SMPSs and NanoScan instruments use different size channel widths and midpoints, data fitting of the measured size distributions was necessary. Thus, for a quantitative comparison of the measurement results, each experiment data was averaged for the approximately 30 min period and afterwards fitted to lognormal particle number size distributions (characterised by parameters as total number concentration, mode diameter, and standard deviations). Fitting was conducted using the multi-peak fit option of IGOR version 6.2.0.0. The distributions were fitted within the size limits of SMPSs. The probability value (*p-value*) calculated by the Two Sample t Test (unequal variances) provided insights into the quality of the fitting procedure. If the *p-value* is less than or equal to the significance level (α , most often set at *p-value* ≤ 0.05), the test suggests that the observed data are inconsistent with the null hypothesis (that the means of two datasets are equal), so the null hypothesis must be rejected. This test guarantees that the type I error rate (is the incorrect rejection of a true null hypothesis) is at most α . In this study, a *p-value* ≥ 0.05 was considered acceptable in data fitting.

3. Results and discussion

3.1. Unimodal aerosols

The comparison between the response of the NanoScan SMPS with the internal reference response for size distribution (SMPS-L and SMPS-N) and total PN concentrations (UCPC) to unimodal aerosols is shown in Table 2 and Table 3 for compact spherical and agglomerated particles, respectively. It should be noted that the size range of both SMPS-N and SMPS-L is limited due to the nano-DMA and long-DMA, respectively and therefore only in case of the aerosol size range in experiment #1 NaCl was properly covered by SMPS-N and in case of experiments #4, #5 and #6 DEHS, were only covered by SMPS-L. In the case of spark generated soot #10 #11 and diesel soot #12, only the SMPS-L data was used for intercomparison since the SMPS-N size distribution was incomplete and the multiple charge correction was not usable, because it requires the use of an impactor that removes all particles larger than the largest particle size covered by the DMA with the settings used. Such an impactor is not available.

Table 2. Parameters of the fitted lognormal particle number size distributions (total number concentrations, modal diameter, and standard deviations) measured by the SMPSs (NanoScan, SMPS-L and SMPS-N) and UCPC measuring compact and spherical particles (number 1 to 6 in Table S1 of the supplementary information); all concentrations (PN_{total}) in [cm^{-3}] and all diameters (D_{mode}) in [nm]. Values in bold: considered internal reference value for total N concentration (UCPC) and for particle number size distributions (SMPS-N or SMPS-L).

Experiment	NaCl			DEHS		
	#1	#2	#3	#4	#5	#6
UCPC $PN_{total} \pm \sigma$ [cm^{-3}]	$7.9 \pm 0.3 \times 10^4$	$1.8 \pm 0.3 \times 10^4$	$1.6 \pm 0.7 \times 10^5$	$2.1 \pm 0.03 \times 10^4$	$9.9 \pm 0.2 \times 10^4$	$4.2 \pm 0.3 \times 10^4$
NanoScan SMPS-L SMPS-N $PN_{total} \pm \sigma$ [cm^{-3}]	$2.1 \pm 0.1 \times 10^4$ * $7.8 \pm 0.5 \times 10^4$	$1.8 \pm 0.4 \times 10^4$ $1.6 \pm 0.3 \times 10^4$ $1.7 \pm 0.3 \times 10^4$	$2.1 \pm 0.2 \times 10^5$ $1.7 \pm 0.1 \times 10^5$ $1.9 \pm 0.1 \times 10^5$	$2.3 \pm 0.02 \times 10^4$ $2.1 \pm 0.04 \times 10^4$ *	$1.0 \pm 0.1 \times 10^5$ $1.0 \pm 0.05 \times 10^5$ *	$5.1 \pm 0.6 \times 10^4$ $4.0 \pm 0.3 \times 10^4$ *
NanoScan SMPS-L SMPS-N $D_{mode} \pm \sigma$ [nm]	13.2 ± 0.09 * 10.6 ± 0.04	72.9 ± 2.4 64.3 ± 0.3 73.6 ± 1.3	68.6 ± 2.1 58.7 ± 0.3 64.3 ± 0.6	173.6 ± 2.5 231.2 ± 3.9 *	182.2 ± 2.6 228.2 ± 1.4 *	131.6 ± 1.6 198.8 ± 1.3 *

σ - Standard deviation

* - Non-overlapping size

Table 3. Parameters of the fitted lognormal particle number size distributions (total number concentrations, modal diameter, and standard deviations) measured by the SMPSs (NanoScan, SMPS-L and SMPS-N) and UCPC measuring agglomerated particles (number 7 to 12 in Table S1 of the supplementary information); all concentrations (N_{total}) in [cm^{-3}] and all diameters (D_{mode}) in [nm]. Values in bold: considered internal reference value for total PN concentration (UCPC) and for particle number size distributions (SMPS-N or SMPS-L).

Experiment	ZnO	Spark Generated Soot				Diesel Soot
	#7	#8	#9	#10	#11	#12
UCPC $PN_{total} \pm \sigma$ [cm^{-3}]	1.3±0.03x10⁵	1.5±0.02x10⁴	1.0±0.02x10⁵	1.1±0.02x10⁴	7.9±0.2x10⁴	1.2±0.09x10⁵
NanoScan $PN_{total} \pm \sigma$ [cm^{-3}]	1.8±0.2x10 ⁵	1.8±0.1x10 ⁴	1.4±0.1x10 ⁵	1.6±0.02x10 ⁴	1.3±0.05x10 ⁵	1.9±0.2x10 ⁵
SMPS-L $PN_{total} \pm \sigma$ [cm^{-3}]	1.5±0.09x10 ⁵	1.6±0.1x10 ⁴	1.1±0.04x10 ⁵	1.1±0.02x10 ⁴	7.2±0.3x10 ⁴	1.2±0.1x10 ⁵
SMPS-N $PN_{total} \pm \sigma$ [cm^{-3}]	1.5±0.1x10 ⁵	1.8±0.2x10 ⁴	1.1±0.03x10 ⁵	*	*	*
NanoScan $D_{mode} \pm \sigma$ [nm]	67.4±0.9	49.1±0.7	63.2±0.9	74.6±1.1	91.1±1.7	95.1±1.5
SMPS-L $D_{mode} \pm \sigma$ [nm]	66.2±0.3	47.9±0.3	66.7±0.2	81.9±0.2	105.4±0.2	95.6±0.5
SMPS-N $D_{mode} \pm \sigma$ [nm]	66.9±0.3	48.6±0.3	70.7±0.5	*	*	*

σ - Standard deviation

* - Non-overlapping size

As shown in Tables 2 and 3 the variability across instruments was broad for each specific type of aerosol, even at times between the two SMPS instruments. These data should be interpreted bearing in mind the different size ranges measured by each of the instruments, which may significantly influence the total PN concentrations measured. To support the interpretation of these Tables, Figure 1 shows the differences in total PN concentration between the three instruments and the UCPC while Figure 2 shows the relative differences in modal diameters between NanoScan and the other SMPSs.

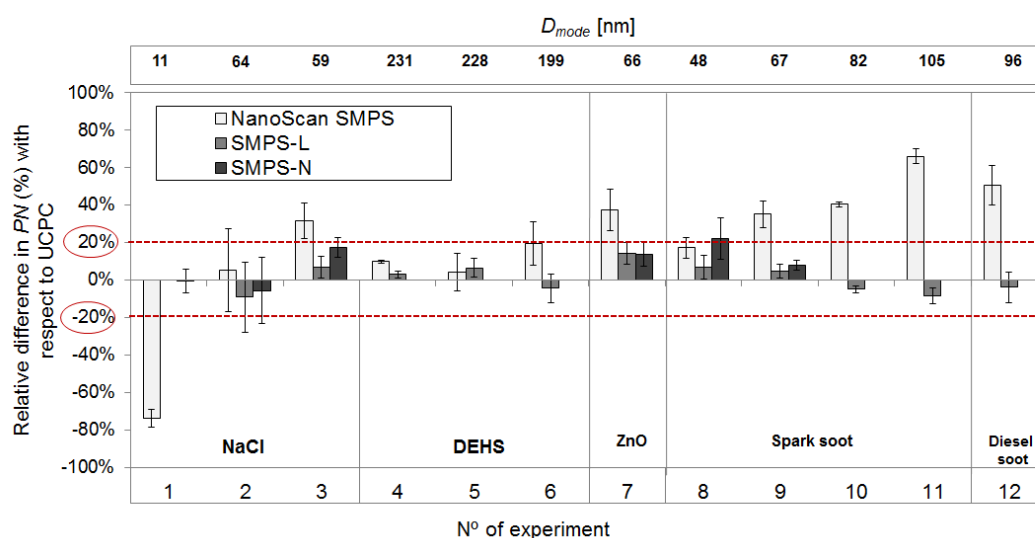


Figure 1. Relative difference in PN concentration between the three SMPSs and UCPC measurement. Error bars indicate the standard deviation ($\pm\sigma$). The dashed

(red) horizontal line indicates the considered arbitrary threshold of $\pm 20\%$ difference between *PN* measured (NanoScan, SMPSs) and *PN* expected (UCPC).

Overall, for aerosols >50 nm NanoScan measured higher *PN* concentrations than the internal reference UCPC, with deviations between 4% and 66% (Figure 1 and Tables 2 and 3). The largest deviations of the total *PN* from the reference instrument UCPC were observed for agglomerated particles although, these type of particles registered the lowest standard deviations ($<\pm 11\%$; error bars shown in Figure 1).

If an arbitrary threshold of 20% difference (representing a worthy performance for a field instrument, and also the sum of the $\pm 10\%$ uncertainty of CPC instruments) between *PN* measured (NanoScan, SMPSs) and *PN* expected (UCPC) is considered, the results obtained with NanoScan were above threshold for 7 of the aerosols (NaCl #1 and #3; ZnO #7; spark generated soot #9, #10 and #11; and diesel soot #12) whereas a good agreement (below threshold) was obtained for 2 of the aerosols for which SMPS-N covered most of the particle size distribution (NaCl #1 and ZnO #7) and for all unimodal aerosols with SMPS-L, excepting NaCl #1 (which is not covered by SMPS-L).

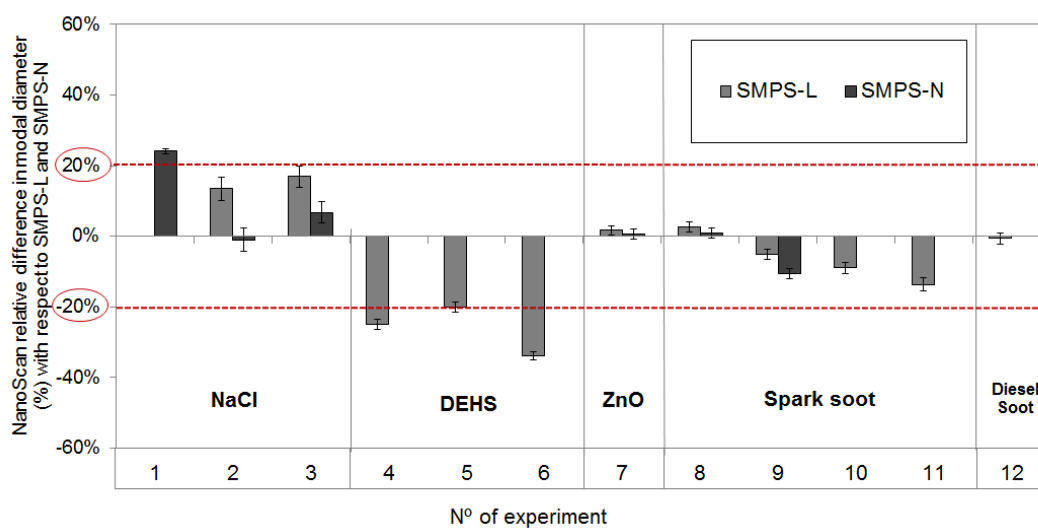


Figure 2. Relative difference in modal diameter between NanoScan and SMPS-L measurement (grey columns) and SMPS-N (black column). Error bars indicate the standard deviation ($\pm\sigma$). The dashed (red) horizontal line indicates the considered arbitrary threshold of $\pm 20\%$ difference between *PN* measured (NanoScan, SMPSs) and *PN* expected (UCPC).

Contrary to the total *PN* concentrations, the particle modal diameter measured by NanoScan and SMPS-L (Figure 2) agreed poorly ($>20\%$ difference) for DEHS particles, but agreed fairly well within $<10\%$ deviation for 66 nm ZnO, 48 and 67 nm spark generated soot at low and high concentrations, 82 nm spark generated soot at low concentrations and 96 nm diesel soot.

Detailed information concerning the performance of each instrument as the measured total *PN* concentration and particle size distribution for each type of aerosol under study is shown and discussed in the following sections.

3.1.1. Compact and spherical particles

In the NaCl experiments, it is important to take into account that the generated aerosol was outside the measurement range of the SMPS-L (19.1 - 897.7 nm) and in lower end of the NanoScan particle size measurement range for 11 nm NaCl #1 and that SMPS-N did not cover the entire range of the generated 60 nm NaCl #2 and #3. When comparing total *PN* between the different instruments and the UCPC (considered here as the internal reference instrument), results showed that, for 11 nm NaCl #1 particles, *PN* concentrations were significantly underestimated (p -value < 0.05) by the NanoScan (74 ± 5%). Total *PN* concentration reported by the SMPS-N agreed with the reference (1 % underestimation; p -value = 0.2). Since the generated 60 nm NaCl #2 and #3 was within the size range of the NanoScan and SMPS-L, the performance of the two instruments in terms of *PN* concentrations improved largely with coarser particles (when compared to 11 nm NaCl #1 particles). At low concentrations (NaCl #2), *PN* concentrations measured by NanoScan and SMPS-L overestimated by 5.1 ± 22 % and underestimated by 9.3 ± 19 % respectively, those measured by the UCPC. At high concentrations (#3), *PN* was overestimated by 32 ± 10 % by NanoScan and by 7 ± 6 % by SMPS-L. Thus, the deviation from the reference value of NanoScan was larger at high concentrations. The size distributions measured for 11 nm NaCl #1 and 60 nm NaCl #3 are illustrated in Figure 3a and 3b, respectively. As for 11 nm NaCl #1, the performance of NanoScan was far from optimal for this type of aerosol since particle size distributions deviated >20% from SMPS-N (Figures 2 and 3a). As a result, care should be taken when using NanoScan data from the lower end of the instrument's particle size range.

Particle size distributions of 60 nm NaCl #2 at low (Figure S2 in the online Supplemental Information) and NaCl #3 at high concentrations (Figure 3b) measured by NanoScan were slightly shifted towards larger particle sizes (73 and 69 nm, respectively) whereas the mode diameters measured by SMPS-L at low and at high NaCl concentrations were 64 and 59 nm, respectively. The standard deviations of mode diameters showed variations in a similarly narrow range between 0.3 and 2.4 (NaCl #2) and between 0.3 and 2.1 nm (NaCl #3). The dilution in the wind tunnel not only affected the concentrations but also influenced particle size (i.e., with an increase of the flow rate inside the wind tunnel, an increase of particle concentration and a decrease in particle diameter are detected due to the shorter residence time

for coagulation). The performance of the NanoScan instrument regarding particle diameters was slightly better for low PN concentrations and larger NaCl particles ($1.8 \pm 0.3 \times 10^4 \text{ cm}^{-3}$; 73 nm; NaCl #2; Figure 2) which was in agreement with the lowest deviations in total PN concentrations observed from NanoScan when compared to the reference value of UCPC. Since the particle mode shifting was more pronounced at higher concentrations of NaCl and lower diameter (69 nm; NaCl #3), the NanoScan overestimation in measuring particle number concentration may possibly be explained by a particle size misclassification in the radial DMA and a corresponding effect on the data deconvolution. However, it should be take into account that these misclassification of particle size is within the uncertainty of 20% of deviations. In addition, this behaviour was not observed for all other spherical aerosol types (e.g., DEHS, see below). Thus, further studies are needed to understand this behaviour.

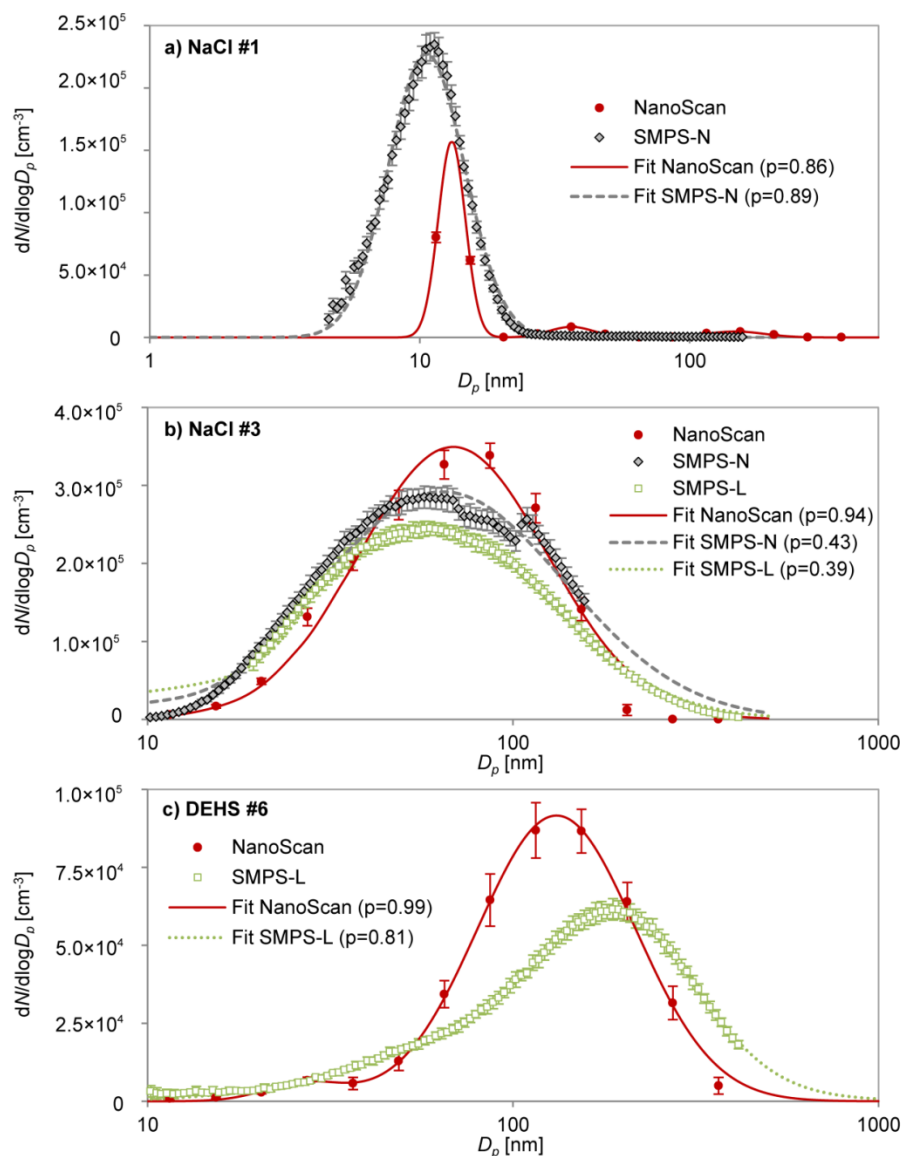


Figure 3. Measurement data and fitted particle number size distribution of generated particles measured in the exposure chamber with SMPS-N, SMPS-L and NanoScan: a) 11 nm NaCl

#1; b) 60 nm NaCl #3 at high concentration and; c) 199 nm DEHS #6. Error bars indicate the standard deviation. $p = p\text{-value}$.

Spherical DEHS particles #4, #5 and #6 were mostly outside the measurement range of the SMPS-N (3.2-107.5 nm). When comparing the measured PN between the SMPS-L, NanoScan and UCPC in experiments ~230 nm DEHS #4 and #5, results showed that PN was overestimated by NanoScan ($10 \pm 1\%$ at low and $4 \pm 10\%$ at high concentrations) and by the SMPS-L ($3 \pm 2\%$ at low and $6 \pm 5\%$ at high concentrations). Regarding the 199 nm DEHS #6 (Table 2), NanoScan measurements agreed with the reference PN concentration within the arbitrary 20% threshold defined above ($19 \pm 12\%$ difference), while the SMPS-L underestimated the reference value with $5 \pm 8\%$ (Table 2 and Figure 1). Especially in the case of NanoScan these values should be considered with care, as the instrument did not cover the entire size range of the test aerosol. A higher overestimation of the reference values might be expected if we consider the results obtained when measuring the 199 nm DEHS #6. However, for both NanoScan and SMPS-L an agreement within 20% is to be expected, which was the case.

For DEHS particles, the particle size distributions measured by NanoScan showed a poor agreement when compared with the ones measured by the SMPS-L (Table 1 and Figure 2). The NanoScan particle size distributions measured for ~230 nm DEHS #4 and #5 (Figure S3 of the online Supplemental Information) and 199 nm DEHS #6 (Figure 3c) were shifted towards smaller particles sizes, measuring mode particle diameters of 174-182 nm and 132 nm (20-25% and 34% lower than reference value of SMPS-L, respectively). The deviations among both instruments were considered not statistically significant ($p\text{-value} > 0.05$) (Table 2 and Figure 2). This difference in NanoScan performance for the DEHS aerosols may be caused by the fact that the Cunningham slip correction factor gets an increasingly weak function of particle diameter with increasing particle size and eventually even passes a minimum (Levin *et al.*, 2015), and hence the electrical mobility of unipolar diffusion charged particles (as acquired in the NanoScan) also becomes less sensitive in measuring the particle diameter (Morawska *et al.*, 2009b) by acquiring a charge level which is nearly proportional to the particle diameter (Asbach *et al.*, 2011; Jung and Kittelson, 2005). It should be noted that a constant and unexpected peak was detected around 22-27 nm with NanoScan in each experimental run with DEHS particles, and it is also suggested by the SMPS-L data. Although these peaks were well below the main peak of the measured size distribution, there is no apparent reason for this occurrence and seems due to a systematic failure e.g. due to an overcompensation in the data deconvolution.

The results from the experiments with compact and spherical particles (DEHS and NaCl aerosols) suggest that the agreement between NanoScan and SMPS concerning sizing and *PN* concentrations is dependent on the combination of total *PN* concentration and particle size, given that the better performances for NanoScan were observed while measuring aerosol NaCl concentrations in the range of 10^4 cm^{-3} (NaCl #2), and excluding those for which particle diameter was at the lower end of the measurement range of the instrument (NaCl#1).

Additionally, the lower accuracy of NanoScan (lower number of channels) and consequently, the particle size misclassification seems to be the reason for the Nanoscan overestimation in measuring particle number concentration. The higher the deviation on the mode particle size, the higher the deviations on the particle counting. From this assessment, the NanoScan underestimated particles larger than 200 nm by up to 34%, thus making it unsuitable for occupational exposure assessments where a high degree of accuracy is required. This instrument may be advisable for tier 2 studies, with an indicative purpose and which require a lower measurement accuracy, but its use should not be encouraged for tier 3 studies.

In addition, it is important to highlight that these results cannot be generalised for all spherical particles. The recent study of Stabile *et al.* (2014) concluded that the spherical atomized dioctyl phthalate (DOP) particles (111 nm by SMPS with diffusion and multiple charge correction) were both correctly counted and sized. Similar results were also published by Tritscher *et al.* (2013), with both polydisperse NaCl and Emery Oil (EO) particles. These discrepancies highlight the need for further research in this field.

3.1.2. Agglomerated particles

While the size distribution agreement between SMPS-L and NanoScan was poor for NaCl particles with sizes around 59-64 nm and DEHS with sizes around 199-231 nm, it agreed well for the tested agglomerated 66 nm ZnO #7 (Figure 4). The size distribution measured by NanoScan showed a narrow range of modal diameter of $67.4 \pm 0.9 \text{ nm}$. However, the total *PN* concentrations measured by NanoScan, SMPS-L and SMPS-N, were $1.8 \pm 0.2 \times 10^5$, $1.5 \pm 0.1 \times 10^5$ and $1.5 \pm 0.1 \times 10^5 \text{ cm}^{-3}$, with deviations from the internal reference UCPC concentration below 20% threshold for both SMPS-L and SMPS-N, and over (37%) for NanoScan (Table 3 and Figure 1). As described above, this significant overestimation ($p\text{-value} < 0.05$) of the *PN* by NanoScan could be related to the ZnO concentrations generated (in the order of 10^5 cm^{-3}), higher than in previous NaCl experiments (in the order of 10^4 cm^{-3}) or, in this case, eventually due to the effect of particle morphology on NanoScan particle unipolar diffusion charger. Previous studies with unipolar diffusion chargers have

recognised that the charging efficiency for agglomerates is different from the ones for spheres (Asbach *et al.*, 2009a; Asbach *et al.*, 2012a; Biskos *et al.*, 2004; Kaminski *et al.*, 2013; Leskinen *et al.*, 2012; Stabile *et al.*, 2014; Zimmerman *et al.*, 2014; Zimmerman *et al.*, 2015). Particle borne pre-existing charges may also affect the charging efficiency (Kaminski *et al.*, 2013; Qi *et al.*, 2009).

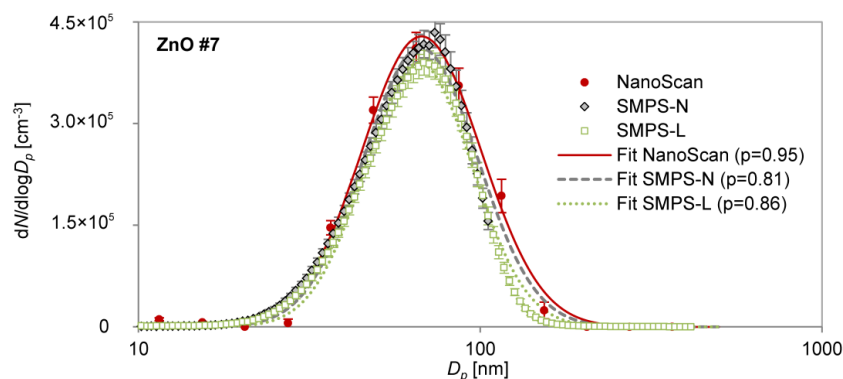


Figure 4. Measurement data and fitted particle number size distribution of generated 66 nm ZnO particles (#7), measured in the exposure chamber with SMPSs and NanoScan. Error bars indicate the standard deviation. $p = p\text{-value}$.

Similarly to ZnO, the spark generated soot particle morphology deviated most from the commonly assumed spherical particle shape. The 48-67 nm spark generated soot particles were produced at low ($1.5 \pm 0.02 \times 10^4 \text{ cm}^{-3}$; spark generated soot #8) and high ($1.0 \pm 0.02 \times 10^5 \text{ cm}^{-3}$; spark generated soot #9) concentrations. In these experiments, SMPS-N did not cover the entire range of the generated aerosol.

When comparing total PN between the SMPSs and the internal reference UCPC, results evidenced that PN concentrations were overestimated by NanoScan above the 20% threshold ($35 \pm 7 \%$ at high concentrations; spark generated soot #9) and below the threshold at low concentrations ($17 \pm 6 \%$; spark generated soot #8), as well as by SMPS-L at low and high concentrations ($7 \pm 6 \%$ for low concentration and $5 \pm 4 \%$ for the high concentration). All these deviations were considered to be statistically significant ($p\text{-value} < 0.05$). The performance of SMPS-L regarding the particle count was better at higher than at lower concentrations, as opposed to NanoScan (in agreement with the results obtained in the previous experiments such as NaCl).

Corresponding TEM images for these generated spark soot particles are shown in Figure 5a whereas the particle size distributions are shown in Figure S6 in the online Supplemental Information. As can be confirmed, the TEM images show a presence of compacted spark generated soot particles of diameter $>50 \text{ nm}$ which agrees fairly well with the delivered diameters by the instruments at high concentrations (63.2 nm spark generated soot #9 by NanoScan and 66.7 nm spark generated soot #9 by SMPS-L).

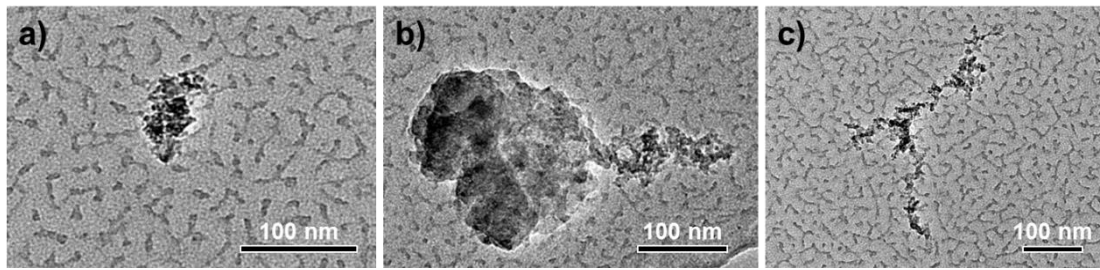


Figure 5. TEM images of collected samples: (a) 67 nm spark soot at high concentration (spark generated soot #9); (b) and (c) 105 nm spark generated soot at high concentration (spark generated soot #11).

Contrary to the total *PN* concentrations measured by NanoScan, the instruments performances regarding particle size distributions were almost identical at high and low concentrations with $3 \pm 1\%$ and $5 \pm 1\%$ difference from the reference, respectively (Figure 2 and Figure S4 in the online Supplemental Information).

Since the NanoScan agreement regarding particle size was better for agglomerated particles (48 - 67 nm spark generated soot #8 and #9 and 66 nm ZnO #7) than for compact particles (59-64 nm NaCl #2 and #3), it can be concluded that the performance of this instrument not only depends on effective particle size but also on particle morphology. Different charging probabilities of the bipolar (SMPSs) and unipolar diffusion charger (NanoScan) under differently shaped particles may be a hypothesis for this dependence. It has been reported that charging is affected by particle morphology (Asbach *et al.*, 2009a; Kaminski *et al.*, 2013; Zimmerman *et al.*, 2014; Zimmerman *et al.*, 2015).

Subsequently, the instruments were exposed to larger spark generated soot particles of 82 nm and 105 nm in diameter using the same settings: low ($1.1 \pm 0.02 \times 10^4 \text{ cm}^{-3}$; spark generated soot #10) and high ($7.9 \pm 0.2 \times 10^4 \text{ cm}^{-3}$; spark generated soot #11) concentrations.

The *PN* concentrations measured by NanoScan significantly overestimated, $40 \pm 1\%$ and $66 \pm 4\%$, those measured by the internal reference UCPC at low and high concentrations, respectively (spark generated soot #10 and #11). As in the case of *PN* concentration with 48-67 nm spark generated soot #8 and #9, the performance of NanoScan decreased from lower to higher concentrations, despite both scenarios being in the order of 10^4 cm^{-3} (Figure 1). Concerning SMPS-L, different behaviours were observed in comparison to those registered for 48-67 nm spark soot, since the *PN* concentrations were underestimated for low (by $5 \pm 2\%$) (spark generated soot #10) and for high concentrations (by $9 \pm 4\%$) (spark generated soot #11).

The corresponding size distributions are shown in Figure S5. Spark generated soot particles sampled on TEM grids are shown in Figures 5b and c. The TEM images show that the spark soot particle sizes were larger than those reported by all of the instruments, evidencing that all of them under-represented the actual spark

generated soot particle size (>100 nm) delivering an electrical mobility diameter much smaller than the geometric extension of the agglomerate spark soot (seen in Figure 5c) and unstructured appearance (seen in Figure 5b). The Figure 5c suggests that the particles were aligned in the electric field and thus, classified as mobility diameter smaller than the particle length itself. However, from Figure 5b it seems that there is two overlapping particles, a less structured and larger particle on the left side (>200 nm) and a more structured particle on the right side of approximately 100 nm as diameter which agrees well with the instrument's response.

As can be seen, the resulting spark generated soot size distributions measured by NanoScan showed smaller modal diameters (75 - 91 nm; Table 3) than the internal reference SMPS-L (82 - 105 nm). In agreement with previous experiments, as in the case of total *PN* concentrations, the shift towards smaller particle sizes according NanoScan was more evident at high particle concentrations. Also, by comparing both spark generated soot particles (48 - 67 nm and 82 - 105 nm), the reported effects were more pronounced by NanoScan when the spark soot agglomerates were larger (Figure 2, Figure 5b and c). Such observations suggest that with an increase of particle size, the electrical mobility of unipolar diffusion charged particles becomes less accurate to the registered particle diameter (Morawska *et al.*, 2009b).

Diesel soot #12 particles were generated at high total *PN* concentrations ($1.2 \pm 0.09 \times 10^5 \text{ cm}^{-3}$ reported by the UCPC). Total *PN* concentrations measured by NanoScan were statistically significantly higher (*p-value*<0.05) than the reference by >20% ($1.9 \pm 0.2 \times 10^5 \text{ cm}^{-3}$), whereas SMPS-L underestimated the reference concentration by $4 \pm 8 \%$ (*p-value*>0.05; not statistically significant) (Figure 1 and Table 3). The diesel soot #12 particle size distribution (Figure 6) measured with NanoScan was found to agree well with the internal reference SMPS-L ($96 \pm 0.5 \text{ nm}$) (Figure 2). The recent study of Stabile *et al.* (2014), observed similar results such as an up to 2-fold overestimation of the actual total particle number concentration obtained through the laboratory SMPS and pointed the effect of particle morphology on the NanoScan particle charging technique should be a possible explanation of the deviations on particle counting. The reason for the better agreement between the reference and measured particle diameters by NanoScan for diesel soot #12 with regard to spark generated soot at high concentrations #11 may be that freshly emitted diesel soot particles are often covered with volatile organic compounds, likely giving the particles a more compact shape than the spark-generated soot particles. The corresponding TEM image (Figure 6) revealed diesel soot particles as fairly compact agglomerates of smaller spherical particles of approximately 100 nm as physical diameter, which is in a good agreement with the modal diameter reported by the SMPS-L and NanoScan.

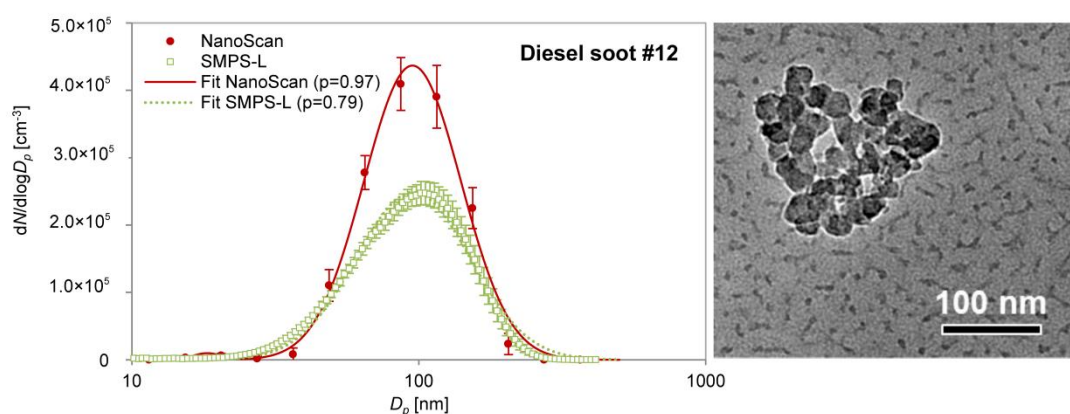


Figure 6. (Left) Measurement data and fitted particle number size distribution of generated 96 nm diesel soot particles at high concentrations, measured in the exposure chamber with SMPS-L and NanoScan. Error bars indicate the standard deviation. p = p -value. (Right) TEM image of collected diesel soot particles.

Based on these findings the NanoScan seems to be a useful instrument to estimate particle size distribution in occupational environments where the target particles are considered as agglomerated. However, total particle number concentrations can be overestimated by up to 66% (see previous sections). For accurate exposure assessment studies (e.g., in the tier 3 of a tiered exposure assessment strategy; Methner *et al.*, 2010; Witschger *et al.*, 2012; Asbach *et al.*, 2014), the stationary SMPS instruments are still the preferred choice to measure simultaneously the total particle number concentration and size distribution.

3.2. Multimodal aerosols

Concerning the multimodal aerosols, the comparison between the NanoScan with the internal reference is shown in Table 4.

Table 4. Parameters of the fitted lognormal particle number size distributions (total number concentrations, modal diameter, and standard deviations) measured by the SMPSs (NanoScan, SMPS-L and SMPS-N) and UCPC measuring multimodal aerosols (number 13 to 15 in Table S1 of the supplementary information); all concentrations (PN_{total}) in $[cm^{-3}]$ and all diameters (D_{mode}) in $[nm]$. Values in bold: considered internal reference value for total PN concentration (UCPC) and for particle number size distributions (SMPS-N or SMPS-L).

N° of experiment	Multimodal aerosols		
	Diesel soot #13	NaCl #14	NaCl/DEHS #15
UCPC $PN_{total} \pm \sigma [cm^{-3}]$	$2.3 \pm 0.07 \times 10^5$	$1.7 \pm 0.04 \times 10^5$	$2.9 \pm 0.4 \times 10^5$
NanoScan SMPS-L SMPS-N $PN_{total} \pm \sigma [cm^{-3}]$	$2.8 \pm 0.1 \times 10^5$ $2.5 \pm 0.1 \times 10^5$ $2.7 \pm 0.2 \times 10^5$	$1.9 \pm 0.2 \times 10^5$ $2.5 \pm 0.07 \times 10^5$ $2.5 \pm 0.1 \times 10^5$	$3.3 \pm 0.9 \times 10^5$ $4.1 \pm 0.7 \times 10^5$ $3.2 \pm 0.5 \times 10^5$
NanoScan SMPS-L SMPS-N $D_{mode} \pm \sigma [nm]$	$30.9 \pm 1.9 / 48.1 \pm 2.2$ $30.7 \pm 0.1 / 136.4 \pm 1.1$ $31.1 \pm 0.1 / 99.4 \pm 2.3$	50.9 ± 0.7 $27.4 \pm 0.2 / 61.0 \pm 0.3$ $27.0 \pm 0.2 / 59.6 \pm 0.3$	66.6 ± 1.1 $26.9 \pm 0.5 / 53.8 \pm 0.4 / 145.4 \pm 2.6$ $23.2 \pm 0.4 / 51.9 \pm 0.3 / 116.5 \pm 5.9$

σ - Standard deviation

Bimodal diesel soot #13 (31+136 nm) and NaCl #14 (27+61 nm) and trimodal NaCl/DEHS #15 (27+54+145 nm), were generated at high total *PN* concentrations ($2.3 \pm 0.07 \times 10^5 \text{ cm}^{-3}$, $1.7 \pm 0.04 \times 10^5 \text{ cm}^{-3}$ and $2.9 \pm 0.4 \times 10^5 \text{ cm}^{-3}$ reported by UCPC, respectively). Total *PN* concentrations measured by NanoScan were below the reference by <20% for all the multimodal aerosols besides considered statistically significant ($p\text{-value} < 0.05$). The SMPS-L and SMPS-N overestimate the reference concentration by 50% and 47%, respectively for the bimodal NaCl aerosol #14 ($p\text{-value} < 0.05$). Although better agreement from NanoScan with regard to total *N* concentrations, the corresponding fitted particle size distributions were found to not agree well with the internal reference SMPS-L and SMPS-N for the bimodal NaCl #14 (Figure S6 in the online Supplemental Information) and the trimodal NaCl/DEHS #15 (Figure S6 in the online Supplemental Information) since an unimodal distribution was obtained in both cases, delivering mode diameters of 51 ± 0.7 and 67 ± 1.1 nm, respectively which correspond to the predominant mode size of the total particle number size distribution. Therefore, the NanoScan does not seem to be able to properly resolve multimodal distributions.

Only in case of bimodal diesel soot #13, the size distribution delivered by NanoScan may be interpreted as bimodal, however its shape and modal diameters are very different from the ones measured with SMPS-L (Figure 7a). Generated diesel soot particles sampled on TEM grids are shown in Figure 7b. The TEM images revealed diesel soot particles as compact agglomerates of spherical primary particles, which fairly agrees with the modal diameters reported by the SMPS-L and the smaller diameter reported by NanoScan (31.1 ± 0.1 nm). Therefore, the NanoScan under-represented the actual diesel soot particle size of 136 nm delivering a mobility diameter much smaller maybe due to its open structure (seen in Figure 7b).

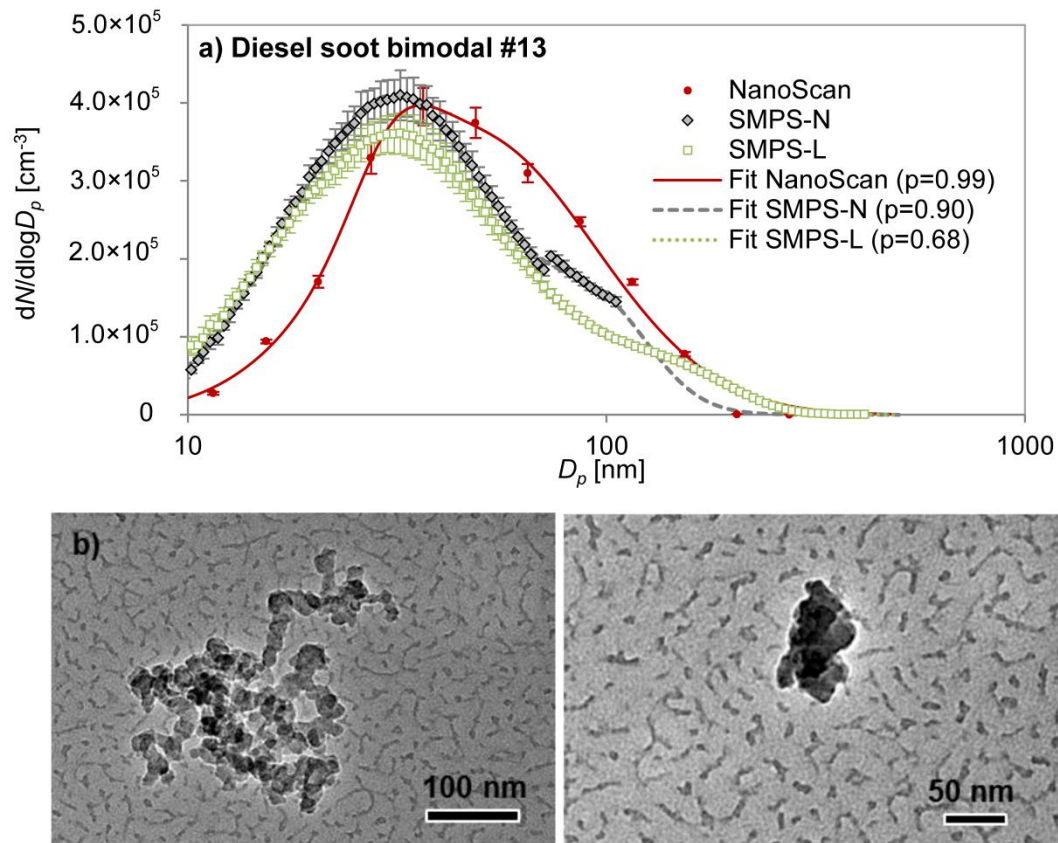


Figure 7. a) Measurement data and fitted particle number size distribution of generated bimodal diesel soot, measured in the exposure chamber with SMPSs and NanoScan. Error bars indicate the standard deviation. p = p -value. b) TEM images of collected 136 nm (left) and 31 nm (right) diesel soot particles.

4. Conclusions

The present study compared the performance of the novel portable NanoScan SMPS TSI 3910 to two reference stationary SMPS instruments (one equipped with a nano-DMA, the other a long-DMA) an ultrafine condensation particle counter (UCPC). The instruments were challenged with five aerosol types with variable morphology and concentrations. The performance of the NanoScan was evaluated with regard to PN concentrations and size distributions and the main findings are summarised as follow:

Total particle number concentration

- NanoScan was able to measure compact and spherical particles (NaCl and DEHS) with a reasonable agreement with an UCPC in terms of PN concentration for particles between 60 nm and 230 nm in diameter, but showed significantly higher deviations for agglomerated particles especially when the spark soot agglomerates were larger and at high concentration (overestimation of 66% compared with the total particle number concentration obtained with the reference UCPC).

- *PN* concentrations measured by NanoScan tended to overestimate those reported by the UCPC, particularly for agglomerated particles such as ZnO, spark generated soot and diesel soot particles (with relative differences >20%), likely because of the differences in the charging efficiency of the NanoScan unipolar charger for compact and agglomerated particles. These observations are consistent with Stabile *et al.* (2014) who conclude that the NanoScan is not able to properly measure diesel-generated particles (fresh aerosol made up of aggregated particles).
- The clear underestimation of 11 nm NaCl particles' *PN* concentration by the NanoScan evidences difficulties to accurately determine *PN* at the lower end of the instrument's particle size measurement range.
- Stationary SMPSs reproduced better agreements with UCPC with regard to *PN* than NanoScan when measuring agglomerated particles such as ZnO, spark soot and diesel soot particles (with relative differences <15% with respect to UCPC).

Particle size distributions

- Results from NanoScan were comparable to those measured by SMPSs (considering an arbitrary 20% threshold) with regard to particle diameter, for most of the aerosols measured, with the exception of 11 nm NaCl and DEHS particles.
- Particle size tended to be underestimated by NanoScan for spherical particles larger than 200 nm (by up to 34%).
- The NanoScan does not seem to be able to properly resolve multimodal distributions.

NanoScan results and their comparability with an SMPS show dependence on particle size, particle morphology, particle composition and particle concentration. Different charge levels acquired by the particles in the unipolar charger might be the reason of this dependence. Although NanoScan instrument is known to provide higher time resolution analysis than the stationary SMPSs, it could be considered slow in certain specific microenvironments but it can be a useful instrument to obtain estimates of the size distribution in workplace air. Due to its portability, it is a valuable tool for simplified exposure assessment, e.g. in the second tier of a tiered exposure assessment strategy (Asbach *et al.*, 2014; Methner *et al.*, 2010; Witschger *et al.*, 2012). However, its accuracy should not be overestimated. While the sizing accuracy was mostly within $\pm 25\%$, measured total concentrations in some cases deviated by more than 50% (especially for agglomerated particles). For accurate measurements, e.g., in tier 3, stationary SMPS instruments are still the preferred choice.

Acknowledgements

This work was supported by grants from the European Community's FP7 (FP7-PEOPLE-2012-ITN) no. 315760 (HEXACOMM project). Additional support was provided by European project nanoIndEx which is supported by the French National Funding Agency for Research (ANR), the German Federal Ministry of Education and Research (BMBF, IUTA grant no.: 03X0127A), the British Technology Strategy Board (TSB) and the Swiss TEMAS AG, under the frame of SIINN, the ERA-NET for a Safe Implementation of Innovative Nanoscience and Nanotechnology.

Supplemental Information

Supplemental information to this article can be found online.

References

- Agarwal, J.K., Sem, G.J. (1980). Continuous flow, single-particle-counting condensation nucleus counter. *Journal of Aerosol Science*, 11(4), 343-357. doi: [http://dx.doi.org/10.1016/0021-8502\(80\)90042-7](http://dx.doi.org/10.1016/0021-8502(80)90042-7)
- Asbach, C., Fissan, H., Kaminski, H., Kuhlbusch, T.A.J., Pui, D.Y.H., Shin, H., Horn, H.G., Hase, T. (2011). A low pressure drop pre-separator for elimination of particles larger 450nm. *Aerosol & Air Quality Research*, 11, 487–496.
- Asbach, C., Kaminski, H., Fissan, H., Monz, C., Dahmann, D., Mülhopt, S., Paur, H., Kiesling, H., Herrmann, F., Voetz, M., Kuhlbusch, T.J. (2009). Comparison of four mobility particle sizers with different time resolution for stationary exposure measurements. *J Nanopart Res*, 11(7), 1593-1609. doi: 10.1007/s11051-009-9679-x
- Asbach, C., Kaminski, H., von Barany, D., Kuhlbusch, T.A., Monz, C., Dziurawitz, N., Pelzer, J., Vossen, K., Berlin, K., Dietrich, S., Gotz, U., Kiesling, H.J., Schierl, R., Dahmann, D. (2012). Comparability of portable nanoparticle exposure monitors. *Ann Occup Hyg*, 56(5), 606-621.
- Asbach, C., Kuhlbusch, T.A.J., Stahlmecke, B., Kaminski, H., Kiesling, H.J., Voetz, M., Dahmann, D., Götz, U., Dziurawitz, N., Plietzko, S. (2014). *Measurement and monitoring strategy for assessing workplace exposure to airborne nanomaterials*: Taylor & Francis.
- Asmi, A., Wiedensohler, A., Laj, P., Fjaeraa, A.M., Sellegri, K., Birmili, W., Weingartner, E., Baltensperger, U., Zdimal, V., Zikova, N., Putaud, J.P., Marinoni, A., Tunved, P., Hansson, H.C., Fiebig, M., Kivekäs, N., Lihavainen, H., Asmi, E., Ulevicius, V., Aalto, P.P., Swietlicki, E., Kristensson, A., Mihalopoulos, N., Kalivitis, N., Kalapov, I., Kiss, G., de Leeuw, G., Henzing, B., Harrison, R.M., Beddows, D., O'Dowd, C., Jennings, S.G., Flentje, H., Weinhold, K., Meinhardt, F., Ries, L., Kulmala, M. (2011). Number size distributions and seasonality of submicron particles in Europe 2008–2009. *Atmos. Chem. Phys.*, 11(11), 5505-5538. doi: 10.5194/acp-11-5505-2011
- Atkinson, R.W., Anderson, H.R., Sunyer, J., Ayres, J., Baccini, M., Vonk, J.M., Boumghar, A., Forastiere, F., Forsberg, B., Touloumi, G., Schwartz, J., Katsouyanni, K. (2001). Acute effects of particulate air pollution on respiratory admissions: results from APHEA 2 project. Air Pollution and Health: a European Approach. [Research Support, Non-U S Gov't]. *Am J Respir Crit Care Med*, 164(10 Pt 1), 1860-1866.
- Beddows, D.C.S., Dall'Osto, M., Harrison, R.M., Kulmala, M., Asmi, A., Wiedensohler, A., Laj, P., Fjaeraa, A.M., Sellegri, K., Birmili, W., Bukowiecki, N., Weingartner, E., Baltensperger, U., Zdimal, V., Zikova, N., Putaud, J.P., Marinoni, A.,

- Tunved, P., Hansson, H.C., Fiebig, M., Kivekäs, N., Swietlicki, E., Lihavainen, H., Asmi, E., Ulevicius, V., Aalto, P.P., Mihalopoulos, N., Kalivitis, N., Kalapov, I., Kiss, G., de Leeuw, G., Henzing, B., O'Dowd, C., Jennings, S.G., Flentje, H., Meinhardt, F., Ries, L., Denier van der Gon, H.A.C., Visschedijk, A.J.H. (2014). Variations in tropospheric submicron particle size distributions across the European continent 2008–2009. *Atmos. Chem. Phys.*, 14(8), 4327-4348. doi: 10.5194/acp-14-4327-2014
- Biskos, G., Mastorakos, E., Collings, N. (2004). Monte-Carlo simulation of unipolar diffusion charging for spherical and non-spherical particles. *Journal of Aerosol Science*, 35(6), 707-730. doi: <http://dx.doi.org/10.1016/j.jaerosci.2003.11.010>
- Brines, M., Dall'Osto, M., Beddows, D.C.S., Harrison, R.M., Gómez-Moreno, F., Núñez, L., Artíñano, B., Costabile, F., Gobbi, G.P., Salimi, F., Morawska, L., Sioutas, C., Querol, X. (2015). Traffic and nucleation events as main sources of ultrafine particles in high-insolation developed world cities. *Atmos. Chem. Phys.*, 15(10), 5929-5945. doi: 10.5194/acp-15-5929-2015
- Brouwer, D. (2010). Exposure to manufactured nanoparticles in different workplaces. *Toxicology*, 269(2-3), 120-127.
- Buonanno, G., Morawska, L., Stabile, L., Viola, A. (2010). Exposure to particle number, surface area and PM concentrations in pizzerias. *Atmospheric Environment*, 44(32), 3963-3969. doi: <http://dx.doi.org/10.1016/j.atmosenv.2010.07.002>
- Buonanno, G., Stabile, L., Morawska, L., Russi, A. (2013). Children exposure assessment to ultrafine particles and black carbon: The role of transport and cooking activities. *Atmospheric Environment*, 79(0), 53-58. doi: <http://dx.doi.org/10.1016/j.atmosenv.2013.06.041>
- Chen, D.R., Pui, D.Y.H., Hummes, D., Fissan, H., Quant, F.R., Sem, G.J. (1998). Design and evaluation of a nanometer aerosol differential mobility analyzer (Nano-DMA). *Journal of Aerosol Science*, 29(5–6), 497-509. doi: [http://dx.doi.org/10.1016/S0021-8502\(97\)10018-0](http://dx.doi.org/10.1016/S0021-8502(97)10018-0)
- Costabile, F., Birmili, W., Klose, S., Tuch, T., Wehner, B., Wiedensohler, A., Franck, U., König, K., Sonntag, A. (2009). Spatio-temporal variability and principal components of the particle number size distribution in an urban atmosphere. *Atmos. Chem. Phys.*, 9(9), 3163-3195. doi: 10.5194/acp-9-3163-2009
- Cusack, M., Pérez, N., Pey, J., Wiedensohler, A., Alastuey, A., Querol, X. (2013). Variability of sub-micrometer particle number size distributions and concentrations in the Western Mediterranean regional background. *Tellus B; Vol 65 (2013)*.
- Demou, E., Peter, P., Hellweg, S. (2008). Exposure to Manufactured Nanostructured Particles in an Industrial Pilot Plant. *Annals of Occupational Hygiene*, 52(8), 695-706. doi: 10.1093/annhyg/men058
- Dixkens, J., Fissan, H. (1999). Development of an Electrostatic Precipitator for Off-Line Particle Analysis. *Aerosol Science and Technology*, 30(5), 438-453. doi: 10.1080/027868299304480
- Dockery, D.W., Pope, C.A., 3rd, Xu, X., Spengler, J.D., Ware, J.H., Fay, M.E., Ferris, B.G., Jr., Speizer, F.E. (1993). An association between air pollution and mortality in six U.S. cities. *N Engl J Med*, 329(24), 1753-1759.
- Donaldson, K., Aitken, R., Tran, L., Stone, V., Duffin, R., Forrest, G., Alexander, A. (2006). Carbon Nanotubes: A Review of Their Properties in Relation to Pulmonary Toxicology and Workplace Safety. *Toxicological Sciences*, 92(1), 5-22. doi: 10.1093/toxsci/kfj130
- Fissan, H., Helsper, C., Thielen, H.J. (1983). Determination of particle size distribution by means of an electrostatic classifier. *J Aerosol Sci*, 14, 354-357.
- Fissan, H., Hummes, D., Stratmann, F., Büscher, P., Neumann, S., Pui, D.Y.H., Chen, D. (1996). Experimental Comparison of Four Differential Mobility Analyzers for Nanometer Aerosol Measurements. *Aerosol Science and Technology*, 24(1), 1-13. doi: 10.1080/02786829608965347

- Fissan, H., Pöcher, A., Neumann, S., Boulaud, D., Pourprix, M. (1998). Analytical and empirical transfer functions of a simplified spectromètre de mobilité électrique circulaire (SMEC) for nano particles. *Journal of Aerosol Science*, 29(3), 289-293. doi: [http://dx.doi.org/10.1016/S0021-8502\(97\)10014-3](http://dx.doi.org/10.1016/S0021-8502(97)10014-3)
- Fonseca, A.S., Viana, M., Querol, X., Moreno, N., de Francisco, I., Estepa, C., de la Fuente, G.F. (2015a). Ultrafine and nanoparticle formation and emission mechanisms during laser processing of ceramic materials. *Journal of Aerosol Science*, 88, 48-57. doi: <http://dx.doi.org/10.1016/j.jaerosci.2015.05.013>
- Fonseca, A.S., Viitanen, A.K., Koivisto, A.J., Kangas, A., Huhtiniemi, M., Hussein, T., Vanhala, E., Viana, M., Querol, X., Hameri, K. (2015b). Characterization of Exposure to Carbon Nanotubes in an Industrial Setting. *Ann Occup Hyg*, 59(5), 586-599.
- Fuchs, N.A. (1963). On the stationary charge distribution on aerosol particles in a bipolar ionic atmosphere. *Geofisica Pura e Applicata*, 56(1), 185-193. doi: 10.1007/bf01993343
- Gómez-Moreno, F.J., Alonso, E., Artíñano, B., Juncal-Bello, V., Iglesias-Samitier, S., Piñeiro Iglesias, M., Mahía, P.L., Pérez, N., Pey, J., Ripoll, A., Alastuey, A., de la Morena, B.A., García, M.I., Rodríguez, S., Sorribas, M., Titos, G., Lyamani, H., Alados-Arboledas, L., Latorre, E., Tritscher, T., Bischof, O.F. (2015). Intercomparisons of Mobility Size Spectrometers and Condensation Particle Counters in the Frame of the Spanish Atmospheric Observational Aerosol Network. *Aerosol Science and Technology*, 49(9), 777-785. doi: 10.1080/02786826.2015.1074656
- Hering, S.V., Stolzenburg, M.R., Quant, F.R., Oberreit, D.R., Keady, P.B. (2005). A Laminar-Flow, Water-Based Condensation Particle Counter (WCPC). *Aerosol Science and Technology*, 39(7), 659-672. doi: 10.1080/02786820500182123
- Hermann, M., Wehner, B., Bischof, O., Han, H.S., Krinke, T., Liu, W., Zerrath, A., Wiedensohler, A. (2007). Particle counting efficiencies of new TSI condensation particle counters. *Journal of Aerosol Science*, 38(6), 674-682. doi: <http://dx.doi.org/10.1016/j.jaerosci.2007.05.001>
- Hoppel, W.A. (1978). Determination of the aerosol size distribution from the mobility distribution of the charged fraction of aerosols. *Journal of Aerosol Science*, 9(1), 41-54. doi: [http://dx.doi.org/10.1016/0021-8502\(78\)90062-9](http://dx.doi.org/10.1016/0021-8502(78)90062-9)
- Jeong, C.-H., Evans, G.J. (2009). Inter-Comparison of a Fast Mobility Particle Sizer and a Scanning Mobility Particle Sizer Incorporating an Ultrafine Water-Based Condensation Particle Counter. *Aerosol Science and Technology*, 43(4), 364-373. doi: 10.1080/02786820802662939
- Jung, H., Kittelson, D.B. (2005). Characterization of Aerosol Surface Instruments in Transition Regime. *Aerosol Science and Technology*, 39(9), 902-911. doi: 10.1080/02786820500295701
- Kaminski, H., Kuhlbusch, T.A.J., Rath, S., Götz, U., Sprenger, M., Wels, D., Polloczek, J., Bachmann, V., Dziurawicz, N., Kiesling, H.-J., Schwiigelshohn, A., Monz, C., Dahmann, D., Asbach, C. (2013). Comparability of mobility particle sizers and diffusion chargers. *Journal of Aerosol Science*, 57(0), 156-178. doi: <http://dx.doi.org/10.1016/j.jaerosci.2012.10.008>
- Knutson, E.O., Whitby, K.T. (1975). Aerosol classification by electric mobility: apparatus, theory, and applications. *Journal of Aerosol Science*, 6(6), 443-451. doi: [http://dx.doi.org/10.1016/0021-8502\(75\)90060-9](http://dx.doi.org/10.1016/0021-8502(75)90060-9)
- Koivisto, A.J., Lyrranen, J., Auvinen, A., Vanhala, E., Hameri, K., Tuomi, T., Jokiniemi, J. (2012). Industrial worker exposure to airborne particles during the packing of pigment and nanoscale titanium dioxide. *Inhal Toxicol*, 24(12), 839-849.
- Koivisto, A.J., Palomaki, J.E., Viitanen, A.K., Siivola, K.M., Koponen, I.K., Yu, M., Kanerva, T.S., Norppa, H., Alenius, H.T., Hussein, T., Savolainen, K.M., Hameri, K.J. (2014). Range-finding risk assessment of inhalation exposure to nanodiamonds in a laboratory environment. [Research Support, Non-U S Gov't]. *Int J Environ Res Public Health*, 11(5), 5382-5402.

- Kousaka, Y., Okuyama, K., Adachi, M. (1985). Determination of Particle Size Distribution of Ultra-Fine Aerosols Using a Differential Mobility Analyzer. *Aerosol Science and Technology*, 4(2), 209-225. doi: 10.1080/02786828508959049
- Kreyling, W.G., Semmler, M., Erbe, F., Mayer, P., Takenaka, S., Schulz, H., Oberdorster, G., Ziesenis, A. (2002). Translocation of ultrafine insoluble iridium particles from lung epithelium to extrapulmonary organs is size dependent but very low. *J Toxicol Environ Health A*, 65(20), 1513-1530.
- Kuhlbusch, T., Asbach, C., Fissan, H., Gohler, D., Stintz, M. (2011). Nanoparticle exposure at nanotechnology workplaces: A review. *Particle and Fibre Toxicology*, 8(1), 22.
- Leskinen, J., Joutsensaari, J., Lyyräinen, J., Koivisto, J., Ruusunen, J., Järvelä, M., Tuomi, T., Hämeri, K., Auvinen, A., Jokiniemi, J. (2012). Comparison of nanoparticle measurement instruments for occupational health applications. *J Nanopart Res*, 14(2), 1-16. doi: 10.1007/s11051-012-0718-7
- Levin, M., Gudmundsson, A., Pagels, J.H., Fierz, M., Møhlhave, K., Löndahl, J., Jensen, K.A., Koponen, I.K. (2015). Limitations in the Use of Unipolar Charging for Electrical Mobility Sizing Instruments: A Study of the Fast Mobility Particle Sizer. *Aerosol Science and Technology*, 49(8), 556-565. doi: 10.1080/02786826.2015.1052039
- Liu, B.Y.H., Pui, D.Y.H. (1974). A submicron aerosol standard and the primary, absolute calibration of the condensation nuclei counter. *Journal of Colloid and Interface Science*, 47(1), 155-171. doi: [http://dx.doi.org/10.1016/0021-9797\(74\)90090-3](http://dx.doi.org/10.1016/0021-9797(74)90090-3)
- Maynard, A., Kuempel, E. (2005). Airborne Nanostructured Particles and Occupational Health. *J Nanopart Res*, 7(6), 587-614. doi: 10.1007/s11051-005-6770-9
- Medved, A., Dorman, F., Kaufman, S.L., Pöcher, A. (2000). A New Corona-based Charger for Aerosol Particles. *J Aerosol Sci*, 31, S616-S661.
- Methner, M., Hodson, L., Geraci, C. (2010). Nanoparticle emission assessment technique (NEAT) for the identification and measurement of potential inhalation exposure to engineered nanomaterials--part A. *J Occup Environ Hyg*, 7(3), 127-132.
- Monsé, C., Monz, C., Dahmann, D., Asbach, C., Stahlmecke, B., Lichtenstein, N., Buchwald, K.-E., Merget, R., Bünger, J., Brüning, T. (2014). Development and Evaluation of a Nanoparticle Generator for Human Inhalation Studies with Airborne Zinc Oxide. *Aerosol Science and Technology*, 48(4), 418-426. doi: 10.1080/02786826.2014.883064
- Morawska, L., He, C., Johnson, G., Guo, H., Uhde, E., Ayoko, G. (2009a). Ultrafine Particles in Indoor Air of a School: Possible Role of Secondary Organic Aerosols. *Environmental Science & Technology*, 43(24), 9103-9109. doi: 10.1021/es902471a
- Morawska, L., Wang, H., Ristovski, Z., Jayaratne, E.R., Johnson, G., Cheung, H.C., Ling, X., He, C. (2009b). JEM spotlight: Environmental monitoring of airborne nanoparticles. [Review]. *J Environ Monit*, 11(10), 1758-1773.
- Oberdörster, G., Oberdorster, E., Oberdorster, J. (2005). Nanotoxicology: an emerging discipline evolving from studies of ultrafine particles. *Environ Health Perspect*, 113(7), 823-839.
- Oberdörster, G., Sharp, Z., Atudorei, V., Elder, A., Gelein, R., Kreyling, W., Cox, C. (2004). Translocation of inhaled ultrafine particles to the brain. *Inhal Toxicol*, 16(6-7), 437-445.
- Peters, A., Wichmann, H.E., Tuch, T., Heinrich, J., Heyder, J. (1997). Respiratory effects are associated with the number of ultrafine particles. *American journal of respiratory and critical care medicine*, 155(4), 1376-1383. doi: 10.1164/ajrccm.155.4.9105082
- Price, H.D., Stahlmecke, B., Arthur, R., Kaminski, H., Lindermann, J., Däuber, E., Asbach, C., Kuhlbusch, T.A.J., Bérubé, K.A., Jones, T.P. (2014). Comparison

- of instruments for particle number size distribution measurements in air quality monitoring. *Journal of Aerosol Science*, 76(0), 48-55. doi: <http://dx.doi.org/10.1016/j.jaerosci.2014.05.001>
- Qi, C., Asbach, C., Shin, W.G., Fissan, H., Pui, D.Y.H. (2009). The Effect of Particle Pre-Existing Charge on Unipolar Charging and Its Implication on Electrical Aerosol Measurements. *Aerosol Science and Technology*, 43(3), 232-240. doi: 10.1080/02786820802587912
- Reche, C., Querol, X., Alastuey, A., Viana, M., Pey, J., Moreno, T., Rodríguez, S., González, Y., Fernández-Camacho, R., de la Rosa, J., Dall'Osto, M., Prévôt, A.S.H., Hueglin, C., Harrison, R.M., Quincey, P. (2011). New considerations for PM, Black Carbon and particle number concentration for air quality monitoring across different European cities. *Atmos. Chem. Phys.*, 11(13), 6207-6227. doi: 10.5194/acp-11-6207-2011
- Reineking A, Porstendörfer J (1986) Measurement of particle loss functions in a differential mobility analyzer (TSI, Model 3071) for different flow rates. *Aerosol Sci Technol* 27:483-486
- Stabile, L., Cauda, E., Marini, S., Buonanno, G. (2014). Metrological Assessment of a Portable Analyzer for Monitoring the Particle Size Distribution of Ultrafine Particles. *Annals of Occupational Hygiene*, 58(7), 860-876. doi: 10.1093/annhyg/meu025
- Tammet, H., Mirme, A., Tamm, E. (2002). Electrical aerosol spectrometer of Tartu University. *Atmospheric Research*, 62(3-4), 315-324. doi: [http://dx.doi.org/10.1016/S0169-8095\(02\)00017-0](http://dx.doi.org/10.1016/S0169-8095(02)00017-0)
- ten Brink, H.M., Plomp, A., Spoelstra, H., van de Vate, J.F. (1983). A high-resolution electrical mobility aerosol spectrometer (MAS). *Journal of Aerosol Science*, 14(5), 589-597. doi: [http://dx.doi.org/10.1016/0021-8502\(83\)90064-2](http://dx.doi.org/10.1016/0021-8502(83)90064-2)
- Tritscher, T., Beeston, M., Zerrath, A.F., Elzey, S., Krinke, T.J., Filimundi, E., Bischof, O.F. (2013). NanoScan SMPS – A Novel, Portable Nanoparticle Sizing and Counting Instrument. *Journal of Physics: Conference Series*, 429(1), 012061.
- TSI. (2015). Choosing the right CPC for your application. APPLICATION NOTE CPC-002 (US). APPLICATION NOTE CPC-002 (US), from http://www.tsi.com/uploadedFiles/Site_Root/Products/Literature/Application_Notes/CPC-002-appnote.pdf
- Voliotis, A., Bezantakos, S., Giamarelou, M., Valenti, M., Kumar, P., Biskos, G. (2014). Nanoparticle emissions from traditional pottery manufacturing. [Research Support, Non-U S Gov't]. *Environ Sci Process Impacts*, 16(6), 1489-1494.
- Wang, S.C., Flagan, R.C. (1989). Scanning electrical mobility spectrometer. *Journal of Aerosol Science*, 20(8), 1485-1488. doi: [http://dx.doi.org/10.1016/0021-8502\(89\)90868-9](http://dx.doi.org/10.1016/0021-8502(89)90868-9)
- Wang, S.C., Flagan, R.C. (1990). Scanning Electrical Mobility Spectrometer. *Aerosol Science and Technology*, 13(2), 230-240. doi: 10.1080/02786829008959441
- Watson, J.G., Chow, J.C., Sodeman, D.A., Lowenthal, D.H., Chang, M.C.O., Park, K., Wang, X. (2011). Comparison of four scanning mobility particle sizers at the Fresno Supersite. *Particuology*, 9(3), 204-209. doi: <http://dx.doi.org/10.1016/j.partic.2011.03.002>
- Wehner, B., Birmili, W., Gnauk, T., Wiedensohler, A. (2002). Particle number size distributions in a street canyon and their transformation into the urban-air background: measurements and a simple model study. *Atmospheric Environment*, 36(13), 2215-2223. doi: [http://dx.doi.org/10.1016/S1352-2310\(02\)00174-7](http://dx.doi.org/10.1016/S1352-2310(02)00174-7)
- Wiedensohler, A., Birmili, W., Nowak, A., Sonntag, A., Weinhold, K., Merkel, M., Wehner, B., Tuch, T., Pfeifer, S., Fiebig, M., Fjåraa, A.M., Asmi, E., Sellegri, K., Depuy, R., Venzac, H., Villani, P., Laj, P., Aalto, P., Ogren, J.A., Swietlicki, E., Williams, P., Roldin, P., Quincey, P., Hüglin, C., Fierz-Schmidhauser, R., Gysel, M., Weingartner, E., Riccobono, F., Santos, S., Gröning, C., Faloon, K., Beddows, D., Harrison, R., Monahan, C., Jennings, S.G., O'Dowd, C.D.,

- Marinoni, A., Horn, H.G., Keck, L., Jiang, J., Scheckman, J., McMurry, P.H., Deng, Z., Zhao, C.S., Moerman, M., Henzing, B., de Leeuw, G., Löschau, G., Bastian, S. (2012). Mobility particle size spectrometers: harmonization of technical standards and data structure to facilitate high quality long-term observations of atmospheric particle number size distributions. *Atmos. Meas. Tech.*, 5(3), 657-685. doi: 10.5194/amt-5-657-2012
- Wiedensohler, A., Orsini, D., Covert, D.S., Coffmann, D., Cantrell, W., Havlicek, M., Brechtel, F.J., Russell, L.M., Weber, R.J., Gras, J., Hudson, J.G., Litchy, M. (1997). Intercomparison Study of the Size-Dependent Counting Efficiency of 26 Condensation Particle Counters. *Aerosol Science and Technology*, 27(2), 224-242. doi: 10.1080/02786829708965469
- Winklmayr, W., Reischl, G.P., Lindner, A.O., Berner, A. (1991). A new electromobility spectrometer for the measurement of aerosol size distributions in the size range from 1 to 1000 nm. *Journal of Aerosol Science*, 22(3), 289-296. doi: [http://dx.doi.org/10.1016/S0021-8502\(05\)80007-2](http://dx.doi.org/10.1016/S0021-8502(05)80007-2)
- Witschger, O., Bihan, O., Reynier, M., Durand, C., Marchetto, A., Zimmermann, E., Charpentier, D. (2012). Préconisation en matière de caractérisation et d'exposition des potentiels d'émission et d'exposition professionnelle aux aérosols lors d'opérations nanomatériaux
- Zhang, Q., Gangupomu, R.H., Ramirez, D., Zhu, Y. (2010). Measurement of ultrafine particles and other air pollutants emitted by cooking activities. [Research Support, U S Gov't, Non-P H S]. *Int J Environ Res Public Health*, 7(4), 1744-1759.
- Zhang, S.-H., Akutsu, Y., Russell, L.M., Flagan, R.C., Seinfeld, J.H. (1995). Radial Differential Mobility Analyzer. *Aerosol Science and Technology*, 23(3), 357-372. doi: 10.1080/02786829508965320
- Zimmerman, N., Godri Pollitt, K.J., Jeong, C.-H., Wang, J.M., Jung, T., Cooper, J.M., Wallace, J.S., Evans, G.J. (2014). Comparison of three nanoparticle sizing instruments: The influence of particle morphology. *Atmospheric Environment*, 86, 140-147. doi: <http://dx.doi.org/10.1016/j.atmosenv.2013.12.023>
- Zimmerman, N., Jeong, C.-H., Wang, J.M., Ramos, M., Wallace, J.S., Evans, G.J. (2015). A source-independent empirical correction procedure for the fast mobility and engine exhaust particle sizers. *Atmospheric Environment*, 100, 178-184. doi: <http://dx.doi.org/10.1016/j.atmosenv.2014.10.054>

Supplemental Information

Intercomparison of a portable and two stationary mobility particle sizers for nanoscale aerosol measurements

A. S. Fonseca^{1,2,*}, M. Viana¹, N. Pérez¹, A. Alastuey¹, X. Querol¹, H. Kaminski³, A. M. Todea³, C. Monz⁴, C. Asbach³

¹ Institute of Environmental Assessment and Water Research (ID/EA-CSIC), C/ Jordi Girona 18, 08034 Barcelona, Spain

² Universidad de Barcelona, Facultad de Química, Martí i Franquès 1-11, 08028 Barcelona, Spain

³ Institute of Energy and Environmental Technology (IUTA), 47229 Duisburg, Germany

⁴ Institute for the Research on Hazardous Substances (IGF), 44789 Bochum, Germany

*Corresponding author: ana.godinho@idaea.csic.es, Tel:+34 934006100. Fax: +34 932045904.

Table S1. Experiments performed in this study.

Nº of experiment	Aerosol	Modal Diameter [nm]	PNconcentration [cm ⁻³]	Type of generator
1	NaCl	11	78 600±3 000	Burner
2	NaCl	64	17 500 ± 3 230	Atomizer
3	NaCl	59	163 000 ± 6 630	Atomizer
4	DEHS	231	20 800 ± 280	Atomizer
5	DEHS	228	98 600 ± 2 440	Atomizer
6	DEHS	199	42 400 ± 3 130	Atomizer
7	ZnO	66	124 900 ± 4 ,730	Burner
8	Spark soot	48	15 000 ± 240	Spark
9	Spark soot	67	101 600 ± 1 800	Spark
10	Spark soot	82	11 100 ± 180	Spark
11	Spark soot	105	78 700 ± 2 350	Spark
12	Diesel soot	96	123 900 ± 8 760	Diesel engine
13	Diesel soot bimodal	31+137	233 000 ± 7 220	Diesel engine
14	NaCl bimodal	27+60	168 400 ± 3 720	Burner
15	NaCl/DEHS trimodal	27+54+146	292 400 ± 40 450	Burner + atomizer

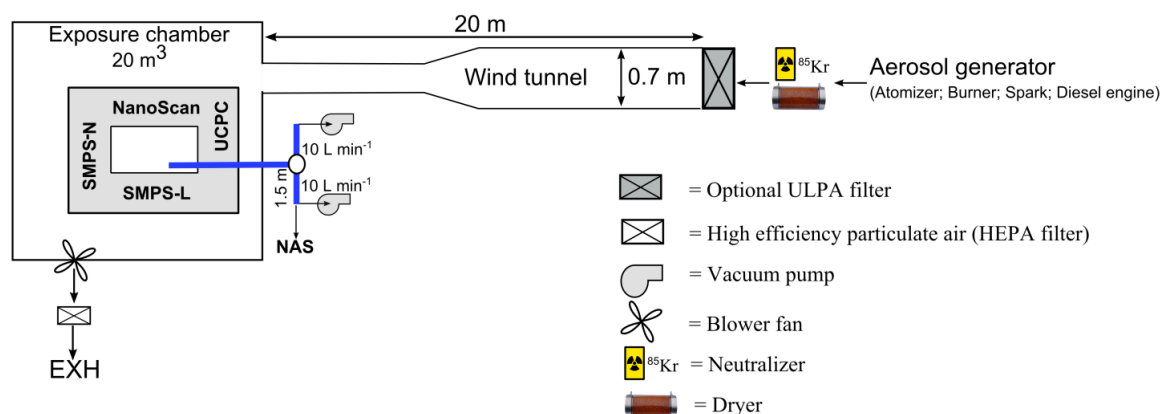


Figure S1. Schematic diagram of experimental setup (not to scale).

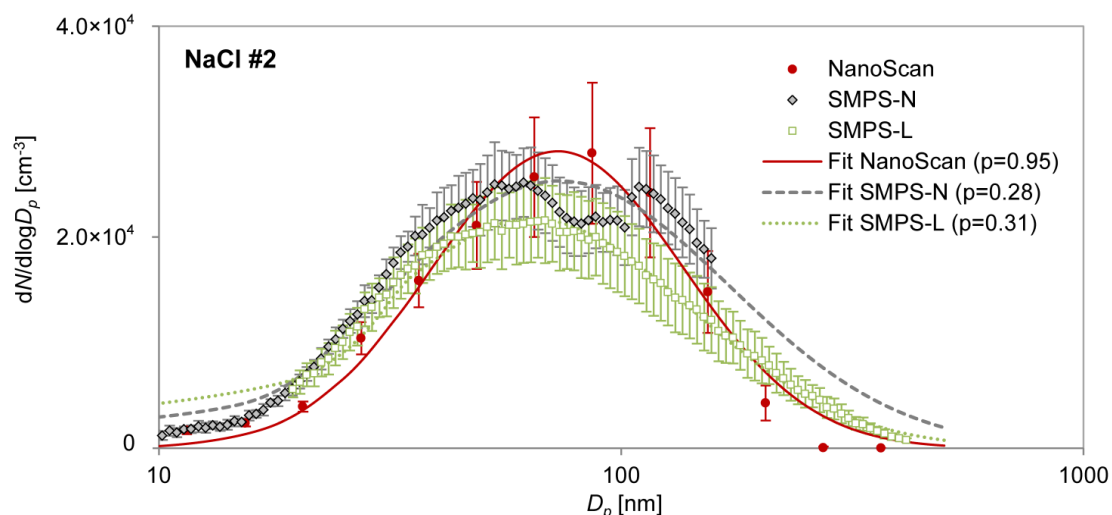


Figure S2. Measurement data and fitted particle number size distribution of generated 60 nm NaCl particles at low (#4) concentrations, measured in the exposure chamber with SMPS-L and NanoScan. Error bars indicate the standard deviation. Error bars indicate the standard deviation. $p = p$ -value.

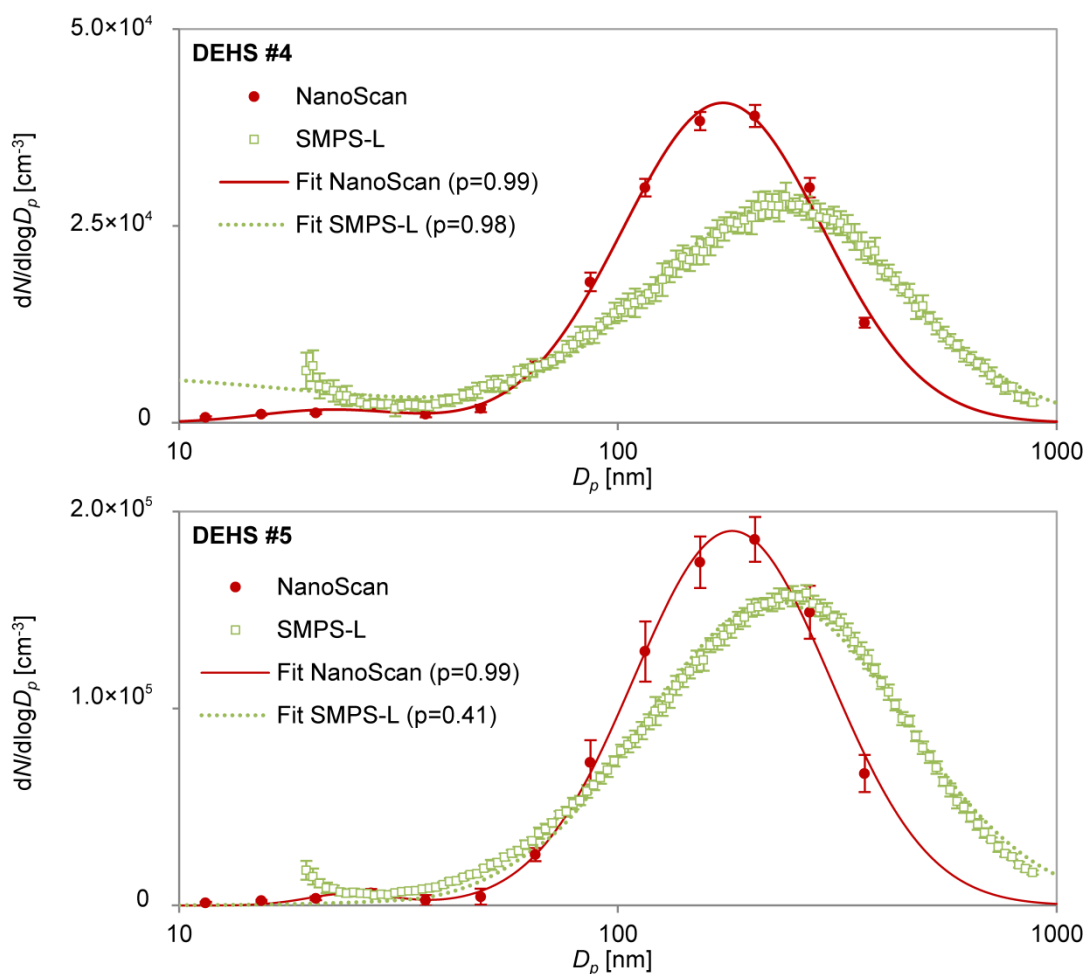


Figure S3. Measurement data and fitted particle number size distribution of generated ~230 nm DEHS particles at low (#4; top) and high (#5; bottom) concentrations, measured in the exposure chamber with SMPS-L and NanoScan. Error bars indicate the standard deviation. Error bars indicate the standard deviation. $p = p$ -value.

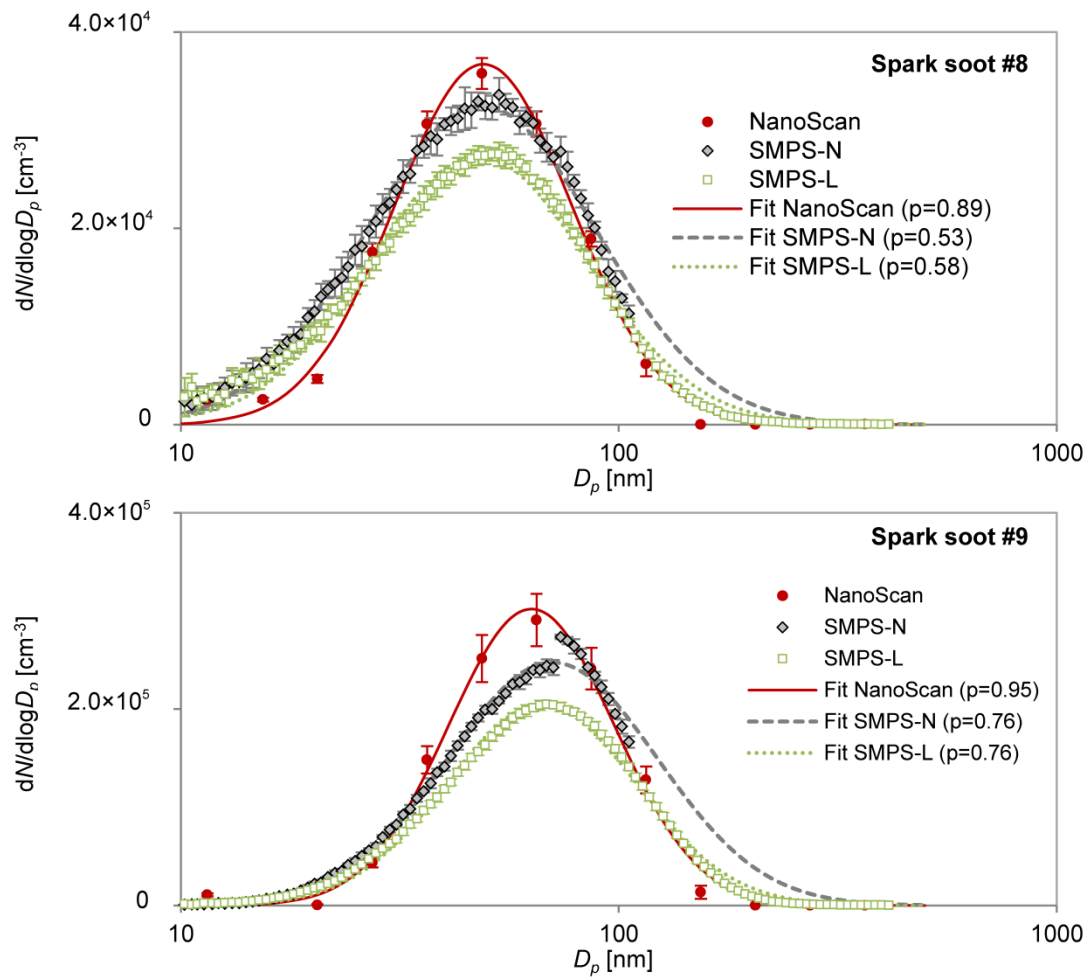


Figure S4. Measurement data and fitted particle number size distribution of generated 48 - 67 nm spark soot particles at low (#8; top) and high (#9; bottom), measured in the exposure chamber with SMPSs and NanoScan. Error bars indicate the standard deviation. p = p -value.

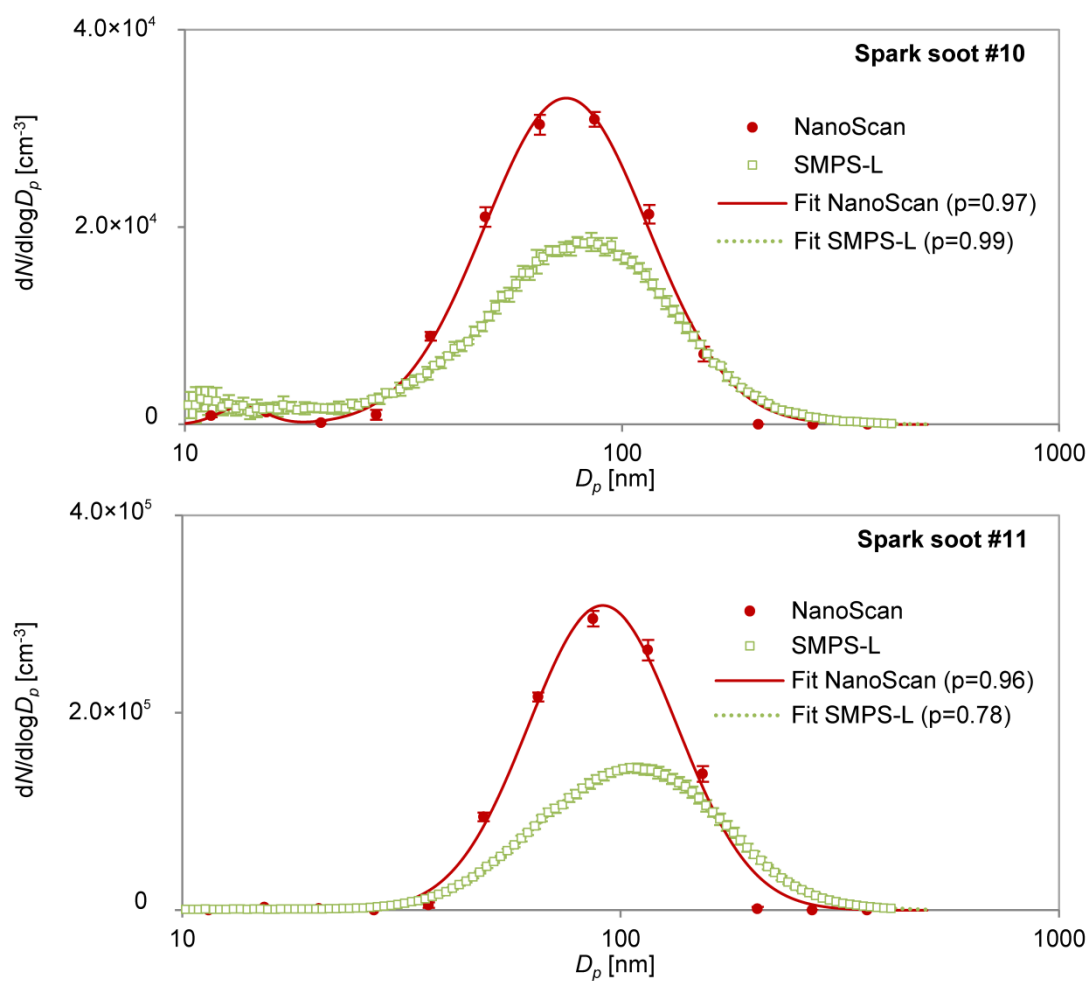


Figure S5. Measurement data and fitted particle number size distribution of generated 82-105 nm spark soot particles at low (10; top) and high (#11; bottom), measured in the exposure chamber with SMPS-L and NanoScan. Error bars indicate the standard deviation. p = p -value.

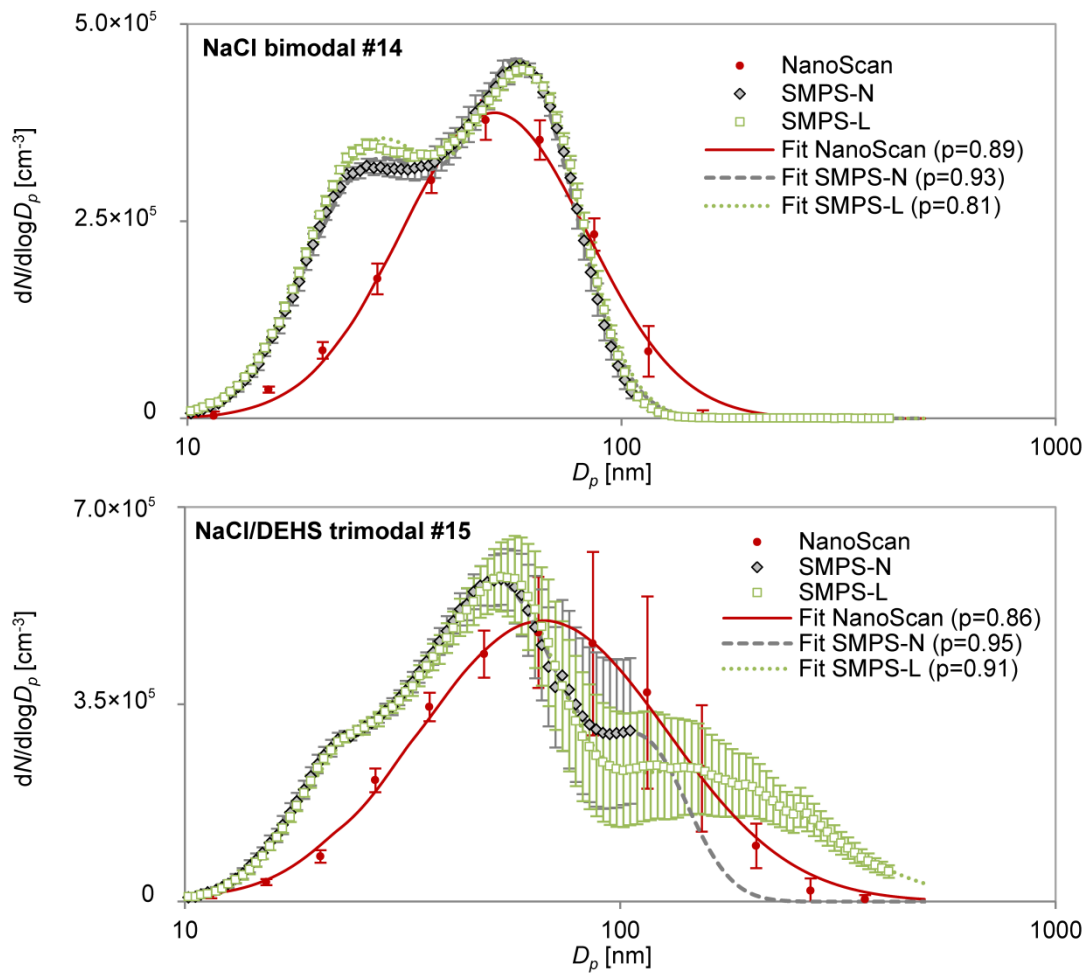


Figure S6. Measurement data and fitted particle number size distribution of generated bimodal NaCl (#14; top) and trimodal NaCl/DEHS (#15; bottom) measured in the exposure chamber with SMPSS and NanoScan. Error bars indicate the standard deviation. p = p -value.

4.5 Article V: Intercomparison of four different cascade impactors for fine and ultrafine particle sampling in indoor and outdoor air

Authors:

Fonseca, A. S.^{1,2}, Talbot, N.^{3,4}, Schwarz, J.³, Ondráček, J.³, Ždímal, V.³, Kozáková, J.^{3,4}, Viana, M.¹, Karanasiou, A.¹, Querol, X.¹, Alastuey, A.¹, Vu, T. V.⁵, Delgado-Saborit, J. M.⁵, Harrison, R. M.^{5,†}

¹ Institute of Environmental Assessment and Water Research (IDÆA-CSIC), Barcelona, 08034, Spain

² Universidad de Barcelona, Facultad de Química, Barcelona, 08028, Spain

³ Institute of Chemical Process Fundamentals of the ASCR, v.v.i. (ICPF), Prague, 165 02, Czech Republic

⁴ Charles University in Prague, Faculty of Science, Institute for Environmental Studies, Prague, 128 43, Czech Republic

⁵ University of Birmingham, Division of Environmental Health & Risk Management, Birmingham, B15 2TT, UK

†Also at: Department of Environmental Sciences / Center of Excellence in Environmental Studies, King Abdulaziz University, PO Box 80203, Jeddah, 21589, Saudi Arabia

Published in:

Atmos Chem Phys Discuss, 1-27, 2016

doi: 10.5194/acp-2015-1016

Accepted date: 19 January 2016 (available online)

Intercomparison of four different cascade impactors for fine and ultrafine particle sampling in indoor and outdoor air

A. S. Fonseca^{1,2,*}, N. Talbot^{3,4}, J. Schwarz³, J. Ondráček³, V. Ždímal³, J. Kozáková^{3,4}, M. Viana¹, A. Karanasiou¹, X. Querol¹, A. Alastuey¹, T. V. Vu⁵, J. M. Delgado-Saborit⁵, R. M. Harrison^{5, †}

¹ Institute of Environmental Assessment and Water Research (IDÆA-CSIC), Barcelona, 08034, Spain

² Universidad de Barcelona, Facultad de Química, Barcelona, 08028, Spain

³ Institute of Chemical Process Fundamentals of the ASCR, v.v.i. (ICPF), Prague, 165 02, Czech Republic

⁴ Charles University in Prague, Faculty of Science, Institute for Environmental Studies, Prague, 128 43, Czech Republic

⁵ University of Birmingham, Division of Environmental Health & Risk Management, Birmingham, B15 2TT, UK

[†] Also at: Department of Environmental Sciences / Center of Excellence in Environmental Studies, King Abdulaziz University, PO Box 80203, Jeddah, 21589, Saudi Arabia

*Correspondence to: A. S. Fonseca (ana.godinho@idaea.csic.es)

Abstract

Due to the need to better characterise the ultrafine particles fraction and related personal exposure, several impactors have been developed to enable the collection of ultrafine particles (<100 nm). However, to the authors' knowledge there have been no field campaigns to-date intercomparing impactor collection of ultrafine particles. The purpose of this study was two-fold: 1) to assess the performance of a number of conventional and nano-range cascade impactors with regard to the particle mass size distribution under different environmental conditions in indoor and outdoor air, and 2) to characterise aerosol size distributions including ultrafine particles using impactors in 2 European locations. The impactors used were: (i) Berner low-pressure impactor (BLPI; 26 nm - 13.5 µm), (ii) nano-Berner low-pressure impactor (nano-BLPI; 11 nm - 1.95 µm) and (iii) Nano-microorifice uniform deposit impactor (nano-Moudi; 10 nm-18 µm), and (iv) Personal cascade impactor Sioutas (PCIS; < 250 nm - 10 µm). Only the BLPI substrates were coated with a thin layer of vacuum grease, therefore particle bounce that may occur during dry collection should only be considered for the other impactors.

Taking the BLPI as an internal reference, the best agreement regarding mass size distributions was obtained with the nano-BLPI, independently of the aerosol load and aerosol chemical composition. The nano-Moudi showed a good agreement for particle sizes >320 nm, whereas for particle diameters <320 nm this instrument recorded larger mass concentrations in outdoor air than the internal reference. This difference could be due to particle bounce, to the dissociation of semi volatiles in the coarser stages and/or to particle shrinkage during transport through the impactor due

to higher temperature inside this impactor. Further research is needed to understand this behaviour. With regard to the PCIS, their size-resolved mass concentrations were comparable with other impactors, but the cut-off at 250 nm did not seem to be consistent with that of the internal reference. Chemical processes linked to aerosol infiltration (e.g., evaporation) were identified in indoor air samples.

Keywords: Mass size distribution; Chemical characterisation; Ultra-fine particles; Cascade Impactors; Nanoparticles; Ultrafine particles

1. Introduction

Used in numerous areas of air quality research, cascade impactors are established, relatively simple, and robust instruments. They collect airborne aerosols and segregate them into a number of aerodynamic sizes for subsequent determination of mass size distribution, chemical and/or physical properties (Hitzenberger *et al.*, 2004; Seinfeld and Pandis, 2006). The mechanical principle behind size impaction employs the known quantities of Stokes number and slip correction factors to derive particle inertia, therefore ascribing a stopping distance in accordance to particle size (Hinds, 1999). Particulates are collected onto substrates, frequently made of quartz, polytetrafluoroethylene (PTFE; best known as Teflon), polyethylene terephthalate (commonly abbreviated PET, otherwise known as Mylar), polycarbonate or aluminium (Howell *et al.*, 1998; Schaap *et al.*, 2004; Tursic *et al.*, 2008). The choice of substrate is dependent on the type of impactor, sampling conditions and analytical techniques intended to be carried out (Fujitani *et al.*, 2006). A variety of cascade impactor designs have appeared since May (1945) first reported on an initial design to sample coarse aerosols ($>2.5 \mu\text{m}$). Since then, sampling size fractions for traditionally designed commercially available cascade impactors allowed for particle collection from coarse to fine fractions ($<2.5 \mu\text{m}$), for example $10 \mu\text{m} - 0.034 \mu\text{m}$ for the Berner low-pressure impactor (BLPI) (Hering *et al.*, 1978; Berner and Luerzer, 1980; Hillamo and Kauppinen, 1991) and size cuts as small as $0.056 \mu\text{m}$ for the micro-orifice uniform deposit impactor (Moudi) (Marple *et al.*, 1991).

However, epidemiological studies have evidenced the need to focus on ultrafine particles (UFP; $D_p < 100 \text{ nm}$), due to their possibly larger impacts on health when compared to coarser particles (Oberdörster, 2000; Oberdörster *et al.*, 2005). Recently, due to the growing need to better characterise the UFP fraction, the second generation of Moudi impactors (Model 122 and Model 125 Nano-Moudi-II™, MSP Corp., Shoreview, MN, USA), both available in the rotating version (122-R and 125-R) and in the non-rotating version (122-NR and 125-NR) and nano-BLPI (not commercially available) were introduced, both adaptations of the original Moudi (Marple *et al.*, 1991) and BLPI impactors (Hering *et al.*, 1978; Berner and Luerzer,

1980; Hillamo and Kauppinen, 1991), modified to enable the collection of UFP down to 11 nm. Also, the need to better understand and characterise personal exposure led to the development of portable, light-weight impactors such as the personal cascade impactor sampler (PCIS; Misra *et al.*, 2002).

Due to the physical principle of particle collection associated with all impactors sampling artefacts can occur, including particle bounce, particle blow off, and particle wall loss (Wall *et al.*, 1988; Schwarz *et al.*, 2012). These artefacts vary according to the impactor type (Hillamo and Kauppinen, 1991; Howell *et al.*, 1998; Štefancová *et al.*, 2011) loads, composition of the aerosol sampled (Huang *et al.*, 2004; Sardar *et al.*, 2005; Fujitani *et al.*, 2006; Crilley *et al.*, 2013), and the type of substrate used (Fujitani *et al.*, 2006; Nie *et al.*, 2010). Also, because long sampling time is required for having enough mass of the finest UFP for chemical analysis may produce sampling artefacts of volatilisation or absorption.

As well as those previously described, the sampling and accurate sizing of UFP/nanoparticles also present challenges. There is a need to produce a fast flowing jet of air onto an impactor plate, creating the inertia allowing for collection of the smallest size fractions producing a high pressure differential at the lowest cut sizes. This pressure drop changes the vapour pressure in the bulk which can then enhance volatilisation (Hering and Cass, 1999). Attempts to address this issue were successfully carried out by decreasing the pressure drop over a reduced number of stages (Marple *et al.*, 1991; Štefancová *et al.*, 2011). Moreover, the low mass of UFP requires a greater collection concentration which then increases the possibility of mass overloading on the larger fractions. The commercially available Nano-Moudi-II™ seeks to reduce jet velocity, pressure drop, particle bounce, re-entrainment and evaporative loss by incorporating micro-orifice nozzles (up to 2000 as small as 50 µm in diameter in the 10 L/min Model 125 and up to 6 000 of 50 µm diameter in the 30 L min⁻¹ Model 122). The rotating Nano-Moudi-II™ versions (Model 122-R and 125-R) have internal embedded stepper motors for the rotation of the sampling stages, thereby spreading the sample over the filter to reduce build-up (Marple *et al.*, 2014). However, as will be described below, this spreading of the sample may lead to new uncertainties and complications.

Cascade impactors have been deployed in a diverse array of measurement campaigns utilising their versatility, characterising size-fractionated chemical composition of urban aerosols (Sardar *et al.*, 2005; Schwarz *et al.*, 2012), particle volatility (Hering and Cass, 1999; Huang *et al.*, 2004), vapour-particle phase partitioning (Delgado-Saborit *et al.*, 2014), influence of relative humidity (Štefancová *et al.*, 2010), indoor - outdoor relationship (Smolík *et al.*, 2008), archive contamination (Mašková *et al.*, 2015), metals in particles collected near a busy road

(Lin *et al.*, 2005; Karanasiou *et al.*, 2007; Ondráček *et al.*, 2011), size-segregated emission particles in a coal-fired power station (Tursic *et al.*, 2008), whilst extensive theoretical investigations and experimental characterisation of cascade impactors tended to focus on the performance of one type of cascade impactor (Biswas and Flagan, 1984; Wang and John, 1988; Štefancová *et al.*, 2011; Jiménez and Ballester, 2011; Marple *et al.*, 2014). Howell *et al.* (1998) carried out an intercomparison of 'traditional' BLPI and Moudi impactors during a field campaign. Field campaigns usually provide a greater variation of conditions than controlled laboratory based conditions, offering a more robust analysis of comparable instrumentation. Another notable intercomparison study was conducted by Pennanen *et al.* (2007) who tested a modified 4-stage Harvard high-volume cascade impactor against a reference 10-stage BLPI in 6 different European locations over different seasons. The authors note the implicit effects on individual impactors of meteorology and aerosol composition. Other studies have run two or more impactors in tandem measuring simultaneously indoors and outdoors (Smolík *et al.*, 2008; Mašková *et al.*, 2015), to cover extended particle size distributions (Geller *et al.*, 2002), or characterise artefacts caused by particle volatility (Huang *et al.*, 2004; Schaap *et al.*, 2004) or changes in size distribution due to different relative humidity (Štefancová *et al.*, 2010).

To the authors' knowledge there has been no field campaign to-date intercomparing impactor collection efficiency of UFP. As a result, this paper seeks to address this by assessing the performance of a number of conventional and nano-range impactors, namely Berner low-pressure impactor (BLPI, 25/0.018/2, Hauke, Austria), nano-Berner low-pressure impactor (nano-BLPI, 10/0,01, Hauke, Austria), nano-microorifice uniform deposit impactor (Nano-Moudi-II™, MSP Corp., Shoreview, MN, USA Model 125R; U.S. Patent # 6,431,014B1) and Personal cascade impactor Sioutas (Sioutas™ PCIS, SKC Inc.; Misra *et al.*, 2002), by means of two intercomparison exercises in indoor and outdoor air. The aim of the campaigns was to test the instruments' performance under different environmental conditions and aerosol loads and types, with an emphasis on the transport of outdoor aerosols into the indoor air. Our work reports on the impactor performances not only with regard to different particle size distributions but also aerosol composition and meteorology.

2. Methodology

2.1. Sampling sites and sampling set-up

2.1.1. Prague

The field intercomparison initially took place in outdoor air (6th-23rd February 2015) and it was subsequently moved indoors (23rd February 2015 - 2nd March 2015) in Prague, Suchdol at the Institute of Chemical Process Fundamentals (ICPF),

Academy of Sciences of the Czech Republic (ASCR) compound (50°7'36.47"N, 14°23'5.51"E, 277 m.a.s.l). Suchdol is a residential area in north-western Prague, about 6 km from the city centre. It is recognised as a suburban background site with residential houses and a university campus interspersed between plenty of green spaces. The traffic flow is moderate along one major 2-lane road (average traffic of 10000-15000 vehicles day⁻¹) with regular bus services. Due to its location on a plateau above the river Vltava there are not many contributory roads alongside (Figure S1 in the supplementary information). Detailed information of the area where the impactors were located were previously provided by Smolík *et al.* (2008) and Hussein *et al.* (2006).

Outdoor sampling consisted of 3 weekend sampling periods (6 - 9th, 13 - 16th and 20th - 23rd February 2015), and 2 week-day samplings, (10 - 12th and 17 - 20st February 2015).

In addition, indoor samples were also collected during 2 week-day samplings (23rd - 25th and 25th - 27th February 2015) and a final 3-day weekend sampling period (27th February 2015 - 2nd March 2015). This resulted in a total of 5 valid outdoor samples (three weekend and two week-day) and two valid indoor samples (one weekend and one week-day). For both outdoor and indoor sampling, the weekend runs started on the preceding Friday between 11:00h-13:00h local time and finished at 9:00h local time on the following Monday. The week-day samplings started between 11h00-14h00 and terminated at 9h00. The sample duration in Prague was defined based on the experience from previous research (Smolík *et al.*, 2008; Štefancová *et al.*, 2011). Based on ambient PM concentrations it was considered that samples should be collected over no more than 72 hours, to avoid substrate overload.

2.1.2. Barcelona

The Barcelona intercomparison was conducted exclusively outdoors at an air quality monitoring station at IDAEA-CSIC located in an urban background site in the southwest of Barcelona (41°23'14" N, 02°06'56"E., 78 m.a.s.l) from 18th May to 3rd July 2015 (Figure S2 in the supplementary information). The sampling site, described in detail by Reche *et al.* (2015), is influenced by vehicular emissions from one of the city's main traffic avenues (Diagonal avenue), located at approximately 200 m from the site and with a mean traffic density of 90 000 vehicles/day⁻¹ (Amato *et al.*, 2015). Even though the site is officially classified as urban background, it is located in a city with very high road traffic and influenced by the emissions of one of the largest arterial roads of the city.

Outdoor sampling in Barcelona consisted of 4-day (during week-days) samples, each of them accounting for 96h (4 consecutive days). A total of 4 samples (4-days each) was collected. The runs started every Monday between 10:00h-12:00h local time and finished on Fridays around 14:00h-16:00h local time. The sample duration in Barcelona was set longer than in Prague since the averages of particle mass collected during a sampling less than 4 days would not be sufficient for further chemical analysis. Indoor intercomparisons were not carried out due to the absence of an appropriate location for indoor air sampling.

2.2. Instrument set-up and experimental specifications

In the present study, the mass size distribution of the aerosol was measured by different types of cascade impactors:

- A Berner low-pressure impactor (BLPI, 25/0.018/2, Hauke, Austria; (Berner et al., 1979; Preining and Berner, 1979) which collects particles onto PET foils (Mylar 13 μm thick) (flow rate 24.8 L min^{-1}). The impactors separated particle mass into 10 size fractions. The cut diameters of the stages were 0.026, 0.056, 0.1, 0.16, 0.25, 0.43, 0.86, 1.73, 3.425, and 6.61 μm (Štefancová et al., 2011). The impactors were equipped with inlets with the cut-point calculated as 14 μm .
- A modified BLPI (denominated as nano-BLPI, 10/0.01, Hauke, Austria) collecting particles on PET foils (Mylar 13 μm thick) (flow rate 17.2 L min^{-1}) from 0.01 μm to 1.95 μm in 8 size stages. The aerodynamic cut diameters of stages 1 to 8 were 0.011, 0.024, 0.039, 0.062, 0.095, 0.24, 0.49, 1.0 μm , and the inlet cut-point was calculated as 1.95 μm . Given that the nano-BLPI is a custom made instrument, the design parameters of each of its impaction stages are shown in Table S1 in the supplementary information.
- A nano-microorifice uniform deposit area impactor (Nano-Moudi-II™, MSP Corp., Shoreview, MN, USA Model 125R; U.S. Patent # 6,431,014B1) equipped with PTFE filters (with diameters of 47 mm, 0.5 μm pore and 0.14 mm thick) was used to collect size-resolved aerosol samples.
- This impactor effectively separated the particulate matter into 13 stages with nominal cut diameters of 0.010, 0.018, 0.03, 0.06, 0.10, 0.18, 0.32, 0.56, 1.0, 1.8, 3.2, 5.6, 10 μm and the inlet cut-point as 18 μm when operated at an inlet flow rate of 10 L min^{-1} .
- Three personal cascade impactor samplers (Sioutas™ PCIS, SKC Inc; Misra et al, 2002) operating with a flow rate of 9 L min^{-1} at a pressure drop of 11 inches of H_2O (2.7 kPa). Particles can be separated in the following aerodynamic particle diameter ranges: <0.25; 0.25 to 0.5; 0.5 to 1.0; 1.0 to 2.5; and >2.5 μm . The collection substrates were 37 mm PTFE filters (Pall) in Prague or quartz fibre filters

(Pall) in Barcelona for the $< 0.25 \mu\text{m}$ filter stage, and 25 mm PTFE filters (Pall) for the 0.25-2.5 μm and $>2.5\mu\text{m}$ impactor stages. Two of the PCIS deployed in Prague separated particle mass in all of the 5 size fractions while another unit collected particles only at 3 of the stages ($< 0.25 \mu\text{m}$; 0.25-2.5 μm and $>2.5 \mu\text{m}$). In order to facilitate interpretation of the data, a lower cut diameter of 30 nm was assumed for the last filter stage of particles $< 0.25 \mu\text{m}$ (quasi-UFP).

All the cascade impactors were loaded with uncoated substrates to avoid possible interferences in future chemical analysis (mainly, determination of organics), so the particle bounce that might occur during dry collection has to be considered excepting for the case of BLPI which foils were coated with a thin layer of vacuum grease (Apiezon L, Apiezon products, M&I Materials Ltd, Manchester, England) to ensure adherence of deposited particles and reduce the artefact of bounce.

For the Prague winter intercomparison, the abovementioned six different impactors were deployed simultaneously in both outdoor and indoor sampling periods. The cascade impactors and their inlets were positioned outside above the roof of ICPF building, 285 m.a.s.l. The nano-Moudi, in order to protect its electrical components, was kept inside an air-conditioned cabin with a temperature continually lower than 20°C and a metal pipe (about 300 cm long) was extended through the roof of the building. With regard to indoor sampling, the impactors were placed inside Laboratory of Aerosol Chemistry and Physics experimental hall on the 2nd floor where office and other experimental activities take place. In both campaigns (indoor and outdoor), the pump exhausts were extended far of the sampling spots in order to avoid sampling artefacts.

For the Barcelona summer intercomparison, the same cascade impactors were deployed (except for the PCIS) at the urban background monitoring site located in IDAEA-CSIC (78 m.a.s.l.; South West part of the city) within the University Campus and they were positioned under a plastic shelter to protect them from rain while allowing free ventilation. All the impactor pumps were placed 5 m distance from the impactors whilst long tubes (10 m) were connected to the exhausts to avoid contamination of the samples.

The error in the sampling flow rate and sampled volume in both campaigns was $< 5\%$. Thus, it is assumed that flow rates did not affect the particle size cut-offs. The uncertainty in the particle mass concentration determination was $< 15\%$ except in some cases for the smallest stages of nano-BLPI and nano-Moudi impactor which reached mass value deviations $> 20\%$ (standard deviation).

The specifications of the campaigns and the impactors deployed in the intercomparison study are summarised in Table 1. The BLPI was used as internal reference for the size distribution in this study as it was calibrated with the method

described by Hillamo and Kauppinen (1991) for the fine stages and by Štefancová *et al.* (2011) for coarse stages.

Table 1. Impactors deployed in Prague and Barcelona and their specifications.

Impactor type	BLPI	nano-BLPI	nano-Moudi	PCIS (5 stages) ^c	PCIS (3 stages) ^d
Number of samplings in Prague	5x outdoor (3x weekend-days + 2x week-days)	5x outdoor (3x weekend-days + 2x week-days)			
	2 x indoor (1xweekend-days + 1x week-days)	2 x indoor (1xweekend-days + 1x week-days)			
Number of samplings in in Barcelona	4 x outdoor (4 x week-days)	4 x outdoor (4 x week-days)	4 x outdoor (4 x week-days)	N/A	N/A
Flow rate (L min ⁻¹) ^a	24.8	17.2	10	9	9
Sampling substrates	PET foils (MYLAR) 13 µm thick	PET foils (MYLAR) 13 µm thick	PTFE 47 mm	37 mm PTFE filters (Pall) < 0.25 µm stage and 25 mm PTFE filters (Pall) for the 0.25-2.5 µm and 2.5-10 µm stages	37 mm quartz-fibre filters (Pall) < 0.25 µm stage and 25 mm PTFE filters (Pall) for the 0.25-2.5 µm and >2.5 µm stages
N° Stages	10	8	13	5	3
Lower cut sizes (µm) ^b	0.026	0.011	0.01	0.03	0.03
	0.056	0.024	0.018	0.25	0.25
	0.10	0.039	0.032	0.50	2.50
	0.16	0.062	0.056	1.00	
	0.25	0.095	0.10	2.50	
	0.43	0.24	0.18		
	0.86	0.49	0.32		
	1.73	1.0	0.56		
	3.42		1.00		
	6.61		1.80		
			3.20		
		5.60			
		10			
Inlet cut-point (µm)	14	1.95	18	10	>2.5

^a Volumetric flow rate at 20°C and ambient pressure

^b All sizes are aerodynamic equivalent diameters

^c Two units deployed; A cyclone was installed ahead which cut PM₁₀

^d One single unit deployed

N/A – Not available

2.3. Sample conservation and gravimetric analysis

Particle mass concentrations on impactor substrates were gravimetrically determined by pre- and post-weighing the Mylar foils and filters (PTFE and quartz fibre) with a Sartorius M5P-000V001 electronic microbalance in Prague and a Mettler MT5 electronic microbalance in Barcelona, both with a ±1 µg sensitivity. Blank samples (1 per sample) were collected per each impactor type in both intercomparison (Prague

and Barcelona) for each of the sampling periods. The deviation of mass values due to varying conditions was corrected with the help of the corresponding blanks.

All samples were equilibrated for a period of 24 hours before weighing in a temperature and relative humidity controlled room (20.0 ± 0.2 °C; 45.4 ± 0.6 % RH). The electrostatic charges of the filters were removed using an U-shaped electrostatic neutralizer (Haug, type PRX U) in Prague and a zerostat anti-static instrument (Z108812-1EA, Sigma-Aldrich Co. LLC.) in Barcelona. Each sample was weighed three times with an accuracy of mass determination of ± 2 μg . After weighing, the sampled foils and filters were stored in the freezer at -18 °C.

2.4. Ion chromatography analysis

Ion chromatography analysis were only carried out for the Prague samples and for the BLPI, nano-BLPI and nano-Moudi impactors with the aim to support the interpretation of the particle mass size distributions data. The PCIS filters were not analysed due to the differences observed for the finest size fraction with the other impactors, as will be discussed below.

The whole nano-Moudi impactor samples were extracted in 7 ml of ultrapure water. In case of the Berner impactors, approximately 1/3 of each foil with samples from each stage was cut out and number of aerosol spots on cut piece was calculated. The ratio between cut and total number of spots at each impactor stage was used to recalculate results to overall ion amount on each stage. All samples were then extracted with 7 ml of ultrapure water, sonicated for 30 min in ultrasonic bath and shaken for 1 hour using a shaker. The extracts were then analysed using a Dionex 5000 system both for cations (Na^+ , NH_4^+ , K^+ , Ca^{2+} and Mg^{2+}) and anions (SO_4^{2-} , NO_3^- , Cl^-) in parallel. An IonPac AS11-HC 2 x 250 mm column was used for anions using hydroxide eluent, IonPac CS18 2 x 250 mm for cations using methane sulfonic acid solution as an eluent. Both anion and cation set-up were equipped with electrochemical suppressors. External calibration was done using NIST traceable calibration solutions.

3. Results

3.1. Meteorological data and mean aerosol concentrations in outdoor air

Table 2 displays the meteorological data (ambient temperature, relative humidity, ambient pressure and wind speed), the mean and standard deviations ($\pm\sigma$) of aerosol concentrations for Prague and Barcelona and season during sampling with BLPI.

Table 2. Meteorological data and mean daily aerosol concentrations in outdoor air in Prague from 6th to 23rd February 2015 and in in Barcelona from 18th May to 3rd July 2015.

Sampling site	Temperature (°C)		Relative humidity (RH, %)		Barometric pressure recalculated to sea level (mbar)	Wind Speed (km h ⁻¹)	Mean PM ₁₄ (µg m ⁻³)
	Min	Max	Min	Max			
Prague (winter)	-3.4±2.6	3.9±3.3	51±15.4	92±2.1	1023±9.4	12.5±6.6	34.6 ± 15.8
Barcelona (summer)	18±3.3	26±3.3	39±9.9	85±7.1	1018±3.1	12±2.6	15.2 ± 2.1

During the winter campaign in outdoor air from 6th to 23rd February 2015 in Prague, the daily maximum average temperature was 3.9±3.3 °C and the minimum average temperature was -3.4±2.6 °C. The relative humidity varied in the range of 51-92% from day to day. As expected, higher temperatures during summer were monitored in Barcelona from 18th May to 3rd July 2015 (minimum of 18±3 °C and maximum of 26±3 °C). However, slightly lower RH (minimum of 39±10 % and maximum of 85±7%), similar pressure (1018±3 mbar) and wind speed (12±3 km h⁻¹) values were recorded. The results imply that aqueous particles may have been collected on an impaction stage different from the stage where they ought to be collected due to the flow-induced relative humidity changes during the day (Fang *et al.*, 1991; Štefancová *et al.*, 2010). Aqueous particles can shrink due to evaporation caused by pressure drop through the impactor and/or grow due to condensation caused by aerodynamic cooling. Also, a distortion of the size distribution due to bounce-off should not be neglected for Barcelona in the nano-BLPI, nano-Moudi and PCIS given that foils were not greased prior to sampling. The same artefact is not expected to occur during winter in Prague (outdoors). This is supported by previous tests from BLPI (authors' unpublished data) showing no difference between two identical impactors when one of them used greased foils and the other one ungreased foils in winter conditions.

In Prague, the mean PM₁₄ mass concentration measured outdoors (with BLPI) was 34.6 ± 15.8 µg m⁻³ whilst in Barcelona (with BLPI) it was 15.2 ± 2.1 µg m⁻³ (Table 2), in a similar order of magnitude as during previous results from 2008 winter campaign in ICPF (Schwarz *et al.* 2012; PM₁₄=34 µg m⁻³) and during a 2014 summer campaign in the monitoring station at IDAEA-CSIC (PM₁₀=19.6 µg m⁻³). The reason of higher averages of particle mass concentrations in winter in Prague than in summer in Barcelona are due to higher emissions (mainly due to coal and biomass burning used for residential heating) and meteorological conditions such as the lower mixing

heights of the boundary layer or even temperature inversions occurring in Prague (Schwarz *et al.*, 2012).

3.2. Average particle mass concentrations per stage for the different impactors

To estimate the cumulative mass concentration for the different size ranges in each of the impactors, the integrated curve of the measured particle mass size distributions was determined by Eq (1):

$$M_i = M_{i-1} + \int_{D_{pi-1}}^{D_{pi}} \frac{dM}{d \log D_p} \times d \log D_p \quad \text{Eq. (1)}$$

Where, M_i is the estimated mass concentration for each impactor stage i , D_{pi-1} and D_{pi} are respectively the lower and upper cut-off diameters of the impactor stage i

The cumulative curves of the particle mass size distributions from Prague (indoor and outdoor) and Barcelona are shown in Figures 1 and 2, respectively.

Results show that the nano-BLPI behaved similarly to the internal reference considered for this work (BLPI), especially for particles larger than 250 nm. Outdoors and indoors, the nano-Moudi was in agreement with the BLPI for particles larger than 320 nm (independent of the aerosol load and type). However, for particles below 320 nm, the particle mass concentration of the nano-Moudi tended to be higher than for the BLPI, especially during winter in Prague. In indoor air, the nano-Moudi cumulative curve of the mass size distributions was closer to the curve obtained for the BLPI impactor.

While in Prague, the nano-Moudi mass size distributions for particles $>1 \mu\text{m}$ were lower than the rest of the impactors, in Barcelona, this trend was not so evident (Figure 1 and 2). This different behaviour could be ascribed to a number of causes: (a) in outdoor air the effect of particle bounce and/or the shrinkage of semi volatile compounds may have caused a shift in particle mass towards the lower sizes of the nano-Moudi, especially in winter in Prague resulting in higher concentrations for particles below 320 nm; and/or (b) indoors, the mechanism of the nano-Moudi of spreading the sample (rotating plates) and also the heat generated from the sensor board of nano-Moudi, with the increase in temperature, both in indoor air and inside the nano-Moudi cabinet, could favour particle dissociation/evaporation from the PTFE filters and thus result in lower mass loads across the lower size ranges, and thus the nano-Moudi curve would appear to be closer to the internal reference BLPI. This effect would not be so prominent in outdoor air, given that the instrument does not reach such temperature increments since it was kept inside an air-conditioned cabin with a temperature continually lower than 20°C while indoors, the temperature was continually higher than 23°C. For one sampling exercise outdoors, in Prague, the instrument's temperature shown on nano-Moudi cabinet's screen increased from

18.8 °C up to 26.6 °C after 4 hours sampling, and then increased up to 31.6 °C at the end of one of the sampling periods (3 days sampling; 72h). The temperature increase (both indoors and outdoors) was significant and able to explain dissociation of ammonium nitrate which increases progressively with increasing temperature (Allen *et al.*, 1989; Stelson and Seinfeld, 1982; Talbot *et al.*, 2016). Ammonium chloride is known to behave similarly (Pio and Harrison, 1987a,b; Allen *et al.*, 1989). Nie *et al.* (2010) also attributed the loss of volatile compounds to the increase of the temperature inside the MOUDI. However, nitrate concentrations were low in indoor air (see sections below), and therefore the volatilisation of this species would have had a low impact on particle mass (leaving only the organic fraction to account for this). Further research is necessary to clarify the different behaviours observed.

The average PM₁₄ mass concentrations and corresponding standard deviation obtained using the internal reference (BLPI) in Prague outdoors were 34.6 ± 15.8 µg m⁻³. In Barcelona, the PM₁₄ mass concentrations and standard deviation in summer were 15.2 ± 2.1 µg m⁻³. Comparison of independent data from Grimm laser spectrometer (corrected with high volume sampler) and the impactors with PM₁ and PM₁₀ size cuts, was carried out for the outdoor campaign in Barcelona (4 samples). A slope of 0.98 and a R² of 0.7 was obtained for the PM₁₄ for BLPI with PM₁₀ from an online laser spectrometer (corrected with regard to reference instrumentation) whereas for PM₁, a slope of 0.7 and a better fit of the data was obtained (R²=0.9). Similarly to BLPI, the nano-BLPI shows a slope of 0.7 and a R² of 1 for the cut point PM₁. The mass differences detected for PM₁ suggest that impactors sampling artefacts such as particle blow off, particle wall losses and/or particle bounce occurred.

Finally, the portable PCIS were only used in Prague during winter given the differences obtained with regard to the BLPI for the quasi-ultrafine size mode (<250 nm; PM_{0.25}). A similar pattern was observed for indoor air, although with a relatively smaller difference. A possible reason for the discrepancies observed regarding the PM_{0.25} fraction could be ascribed to the different pressure drops across the impactor stages. The higher pressure drop in the stationary impactors (e.g., BLPI) may increase the probability of volatilisation of semi-volatile species during prolonged sampling, and could contribute to an underestimation of the PM_{0.25} when compared to the PCIS (Sioutas, 2004).

The differences with regard to the coarse fractions were much smaller when compared to the quasi-UFP fractions. In outdoor air, the PCIS showed consistently higher concentrations for particles larger than 1 µm. Similar results were reported by Sioutas (2004) where an average ratio PCIS to Moudi (Model 110, MSP Corp, Minneapolis, MN) of 2.02 (± 0.59) and 1.21 (± 0.35) was reported for an aerodynamic

size range $< 0.25 \mu\text{m}$ and $2.5\text{-}1 \mu\text{m}$, respectively. However, in indoor air a consistent underestimation was observed for an aerodynamic size range $1\text{-}10 \mu\text{m}$.

In summary, for the aerosols and sampling conditions in this work, the PCIS provided comparable size-resolved mass concentrations for particles $> 1 \mu\text{m}$ while the cut-off at 250 nm did not seem to be consistent with the internal reference BLPI. In order to fully understand these phenomena, a more systematic evaluation might be required. For this reason, data from PCIS will not be discussed in the following sections.

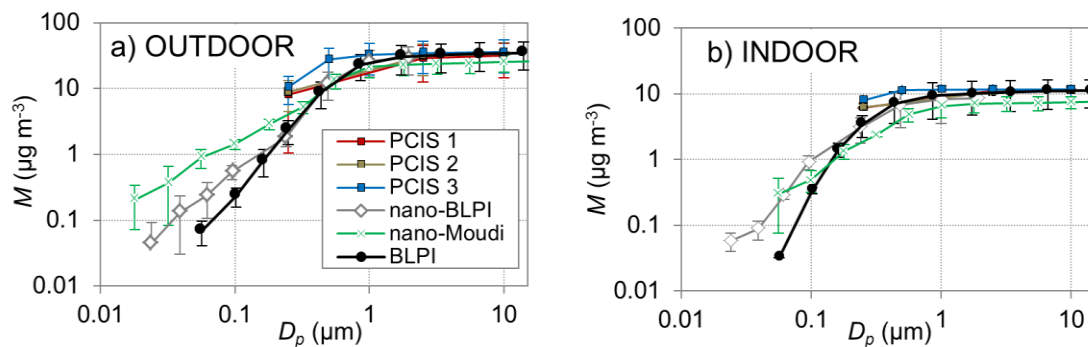


Figure 1. Cumulative mass concentrations measured by the six impactors in Prague: (a) outdoors and (b) indoors. Error bars indicate the standard deviation ($\pm\sigma$).

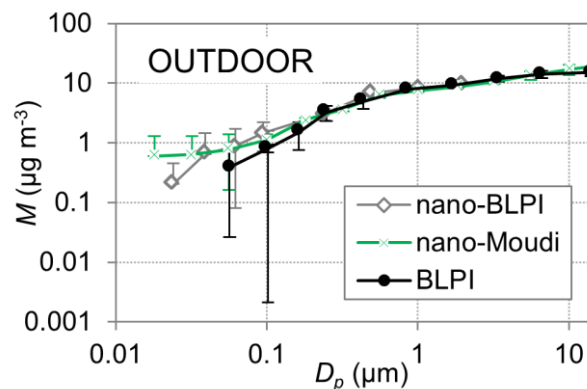


Figure 2. Cumulative mass concentrations measured by the three impactors in Barcelona, outdoors. Error bars indicate the standard deviation ($\pm\sigma$).

3.3. Aerosol mass size distributions

3.3.1. Particle size distribution in outdoor air

The average particle mass size distributions obtained in the outdoor intercomparison study (Prague and Barcelona) can be found in Figure 3.

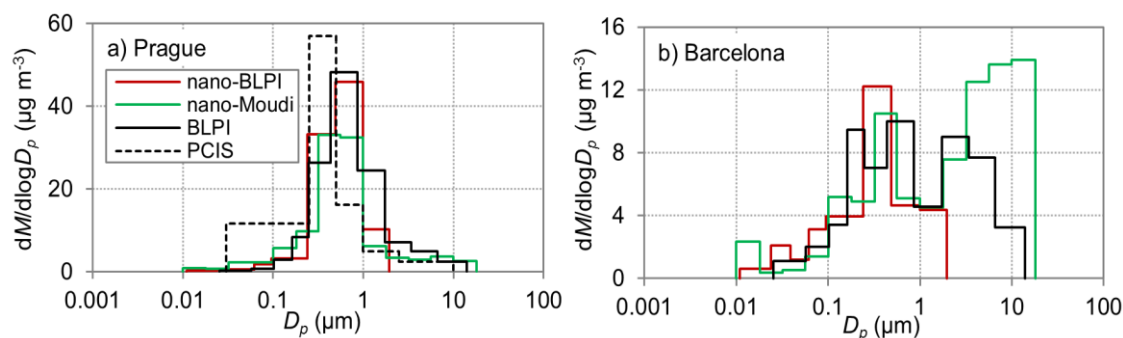


Figure 3. Average mass size distributions obtained outdoors: (a) winter in Prague and (b) summer in Barcelona.

As can be seen, the particle mass size distributions are very different depending on the season and sampling location. During winter in Prague (outdoors), the mass size distributions have a predominantly fine mode, with the coarse mode being almost negligible (by all impactors). The maximum mass concentration obtained in the fine size fraction mode was between 0.4-0.9 μm , whereas in summer in Barcelona, this maximum was shifted towards smaller size fractions between 0.2 and 0.4 μm . In addition to the different aerosol types, this shift to lower sizes might be caused by a lower average relative humidity during sampling in Barcelona that could have caused the particle drying (Tables 2) and therefore, be a reason for particle bounce (Fang *et al.*, 1991; Štefancová *et al.*, 2010). In Prague (outdoors), particle bounce had a negligible effect because high RH was recorded. In the same time only few coarse particles were present and the high share of primary, less oxygenated organics was found (Kubelová *et al.*, 2015; Vodička *et al.*, 2013). Although it is known that RH is lowered at each stage of any cascade impactor this decrease is only moderate for the first stages. For example, the pressure below stage 6 of the BLPI which corresponds to particles as small as 440 nm is only 6% lower than ambient. A similar value is found for nano-BLPI for equivalent stage. The nano-Moudi has even smaller pressure drops at equivalent stages. The drying becomes important for lower stages, however, it is known that kinetic effect limiting drying of particles would be more pronounced at lower temperatures in winter due to lower equilibrium water vapor pressure. In any case, atmospheric particles in the size range below 250 nm are comprised mostly of organics, especially in winter (see e.g Kubelová *et al.*, 2015). These fractions of organics are often of semiliquid nature and this fact efficiently prevents bounce.

While in Prague during winter the coarse mode was mostly insignificant, in Barcelona during summer the mass size distributions were clearly bimodal, with larger coarse mode concentrations (Figure 3). The coarse mode obtained may be due to mineral and marine aerosol contributions in the study area (Querol *et al.*, 2008).

The majority of mass concentrations were found in the accumulation mode (PM_{10}) for both campaigns ($7.9 \pm 0.7 \mu\text{g m}^{-3}$ and $22.9 \pm 9.8 \mu\text{g m}^{-3}$ according the internal reference BLPI in summer Barcelona and winter Prague, respectively). With the increase in mass there was an increase in agreement between the impactors, where the closest agreement was observed (between 200-600 nm) (Figure 3).

Figure 3 reveals that the nano-Moudi recorded higher particle mass concentrations in the ultrafine range (<100 nm) than the reference BLPI during winter in Prague (5 samples in total outdoors). Although differences were smaller, the same is true for the Barcelona summer campaign (4 samples in total, Figure 3). As previously mentioned, to protect the electrical components of the nano-Moudi during winter campaign in Prague outdoors, it was kept inside a climate controlled cabin with a temperature continually lower than 20°C. At these temperatures dissociation of ammonium nitrate can still occur at a slow rate (Smolík *et al.*, 2008). In addition, during the sampling, an increase of temperature inside the nano-Moudi cabinet was detected due to the internal mechanism of spreading the sample (rotating plates) and the electric current in the sensor board which generates heat. It is therefore likely that the internal temperature in the nano-Moudi (always >30 °C) was higher than that of the cabin (<20 °C) and thus led to particle volatilisation (Štefancová *et al.*, 2010). The lower nitrate and chloride concentrations in the accumulation mode on the nano-Moudi filters (see below) would support this interpretation. It is also known that a 5°C difference between the PTFE filter (of the type used in the nano-Moudi) and sampling temperature may accelerate the dissociation of ammonium nitrate on PTFE filters up to 20% (Hering and Cass, 1999). The BLPI and nano-BLPI have no internal warming mechanisms and were located outdoors in Prague and Barcelona, so it is expected that lower volatilisation would occur in these scenarios. However, drying of particles before they are deposited on a substrate may happen also in the BLPI and nano-BLPI due to higher pressure drops (at equivalent sizes) despite lower residence times in comparison with the nano-Moudi. This would increase the driving force for evaporation at those stages, which would encourage particle shrinkage. However the situation is more complicated while a particle is incorporated into a deposit of particles where other processes like diffusion in semiliquid mixture of other organics or Raoult's law play their roles. This process influences the measured concentrations and therefore the impactors comparison.

Furthermore, decomposition of ammonium nitrate and chloride, is probably also enhanced in the nano-Moudi due to the spreading of the sample on the whole filter surface, in comparison with thick individual spots of material obtained with the BLPI and nano-BLPI impactors. All these previous facts (temperature, RH, high surface area) appear to enhance the evaporation of semi-volatiles (and dissociation of

ammonium nitrate) and therefore particle shrinkage during transport through the nano-Moudi explaining the mass size distributions from the nano-Moudi being skewed towards smaller particle fractions during the Barcelona and Prague campaigns (Figure 3). It should be stated that the rotation of the impaction plates and the nozzle plates of the nano-Moudi was specifically designed to achieve a uniform deposit on the collection substrates and therefore, eradicate the particle bounce-off artefact (Marple *et al.*, 2014) that may otherwise occur. Particle bounce-off would only be expected when collecting particles in dry conditions such as in Barcelona (< 50% RH) (Table 2) or indoors. Finally, the overall internal volumes in the low pressure stages seem similar in all of the impactors tested; however, this would need experimental confirmation.

3.3.2. Particle size distribution in indoor air

In Prague, indoor concentrations were lower than outdoors mainly due to a change in weather conditions resulting in cleaner air masses during sampling periods (Figure 3 and Figure 4). Reduced penetration efficiency and faster settling times probably explain the lower indoor coarse mode mass obtained (Figure 4; Hussein *et al.*, 2007). Once again, the nano-BLPI measured similar mass concentrations to the reference BLPI while the nano-Moudi recorded notably lower mass from fine to coarse modes. In addition, the nano-Moudi size distribution showed a slight shift towards larger particle sizes (Figure 4). The difference between the BLPIs and the nano-Moudi could suggest that the latter underestimated mass during this campaign for all particle cut sizes. Initially this would appear to reduce the possibility of volatility losses being responsible for this difference, as ammonium nitrate dissociates readily indoors thereby causing equal losses to all impactors (Lunden *et al.*, 2003). However, because of the way the sample is spread across the substrate in the nano-Moudi, as described above, the ammonium nitrate collected would be more prone to volatilisation than that collected on the other impactors. Therefore it could be considered that the mechanism of the nano-Moudi of spreading the sample (rotating plates), with the increase in temperatures, both indoors and inside the nano-Moudi cabinet, could enhance dissociation/evaporation from the nano-Moudi PTFE substrates. This conclusion can be supported by Figures 5 and 6, which show significantly lower mass concentrations of major species of ammonium nitrate with the nano-Moudi, in comparison with the BLPI.

A number of sources of uncertainty in this interpretation should be taken into account:

- a) Increased uncertainty in the mass determination due to lower mass concentrations and shorter sampling times
- b) No blank correction available for nano-Moudi IC data

- c) No uncertainty calculations for mass determinations available for nano-Moudi, possibly resulting in negative mass concentrations in the lower stages
- d) Only 2 valid samples available for indoor air (for all impactors)

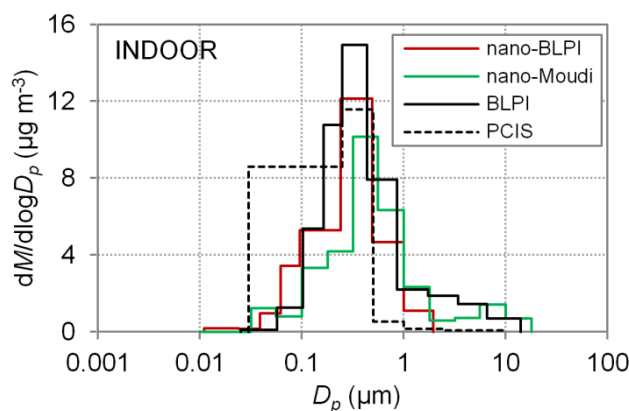


Figure 4. Average mass size distributions in Prague during winter in indoor air.

3.3.3. Size distribution of inorganic ions

Figures 5 and 6 show the particle mass size distributions of major (SO_4^{2-} , NO_3^- and NH_4^+) and minor (Cl^- , Na^+ , K^+ , Mg^{2+} and Ca^{2+}) aerosol constituents for the winter campaign in Prague in outdoor and indoor air, respectively. Corresponding actual mean values for mass concentrations for all of the ions analysed for each of the environments (indoor and outdoor) in Prague, are shown in Table S2 of the supplementary information. The uncertainty of the blanks is also included in the Table S2.

In the winter in Prague, the mass size distributions of components have a predominantly fine mode ($< 1 \mu\text{m}$), with the coarse mode being almost negligible in winter in Prague (by all impactors) but highly significant in Barcelona during summer, such as the case for BLPI.

While the fine mode was dominant for the particle mass concentration and all the predominant aerosol constituents (SO_4^{2-} , NO_3^- and NH_4^+) for both indoor and outdoor air during winter in Prague, the average mass size distributions for minor species (Cl^- , Na^+ , K^+ , Mg^{2+} and Ca^{2+}), were clearly multimodal (Figures 5 and 6). Similar mass size distributions of these species were obtained by the nano-BLPI and the reference BLPI both outdoors and indoors in Prague. However marked differences in the mass size distributions of these species were observed with the nano-Moudi impactor. In outdoor air there is a clear decrease of NO_3^- concentrations measured with the nano-Moudi ($\text{PM}_{10} = 1.7 \mu\text{g m}^{-3}$; Table S2), confirming the interpretations provided in the previous sections. The same is valid for fine chlorides that are missing on some nano-Moudi samples showing ammonium chloride evaporation (NH_4Cl). Nitrates present indoors (due to indoor ammonium nitrate dissociation; Allen *et al.*, 1989;

Stelson and Seinfeld, 1982; Talbot et al., 2016) are influenced by other species different to ammonium salts (e.g. sodium or potassium nitrate) that are not prone to dissociation. For this reason, the difference between nano-Moudi and the other impactors indoors (Figure 6) was much smaller compared to outdoors (Figure 5). The lower sulphate and mass concentration on nano-Moudi indoor samples were caused by other factors (possibly bounce) given that average RH indoors in winter was low (21%). In addition, outdoors in Prague, the mass size distributions obtained by the BLPI showed that Ca^{2+} , Na^+ and Mg^{2+} were dominated by coarse modes and for the case of K^+ , the fine mode is the dominant one (suggesting biomass combustion as a possible emission source). As for Cl^- , the mass size distributions were clearly bimodal. The nano-Moudi outdoors had different size distributions from the BLPI for Cl^- , Na^+ , Ca^{2+} and Mg^{2+} . Only for K^+ the size distribution is similar. Mass size distributions of Cl^- and Na^+ may have been influenced by filter contamination. The Ca^{2+} peak detected at around 100 nm obtained by the nano-BLPI in outdoor air may possibly be ascribed also to filter contamination, although no specific data are available to support this interpretation. Similar peaks at 10 and 50 nm were observed indoors with the nano-Moudi and nano-BLPI which may suggest bounce, contamination or blank variability.

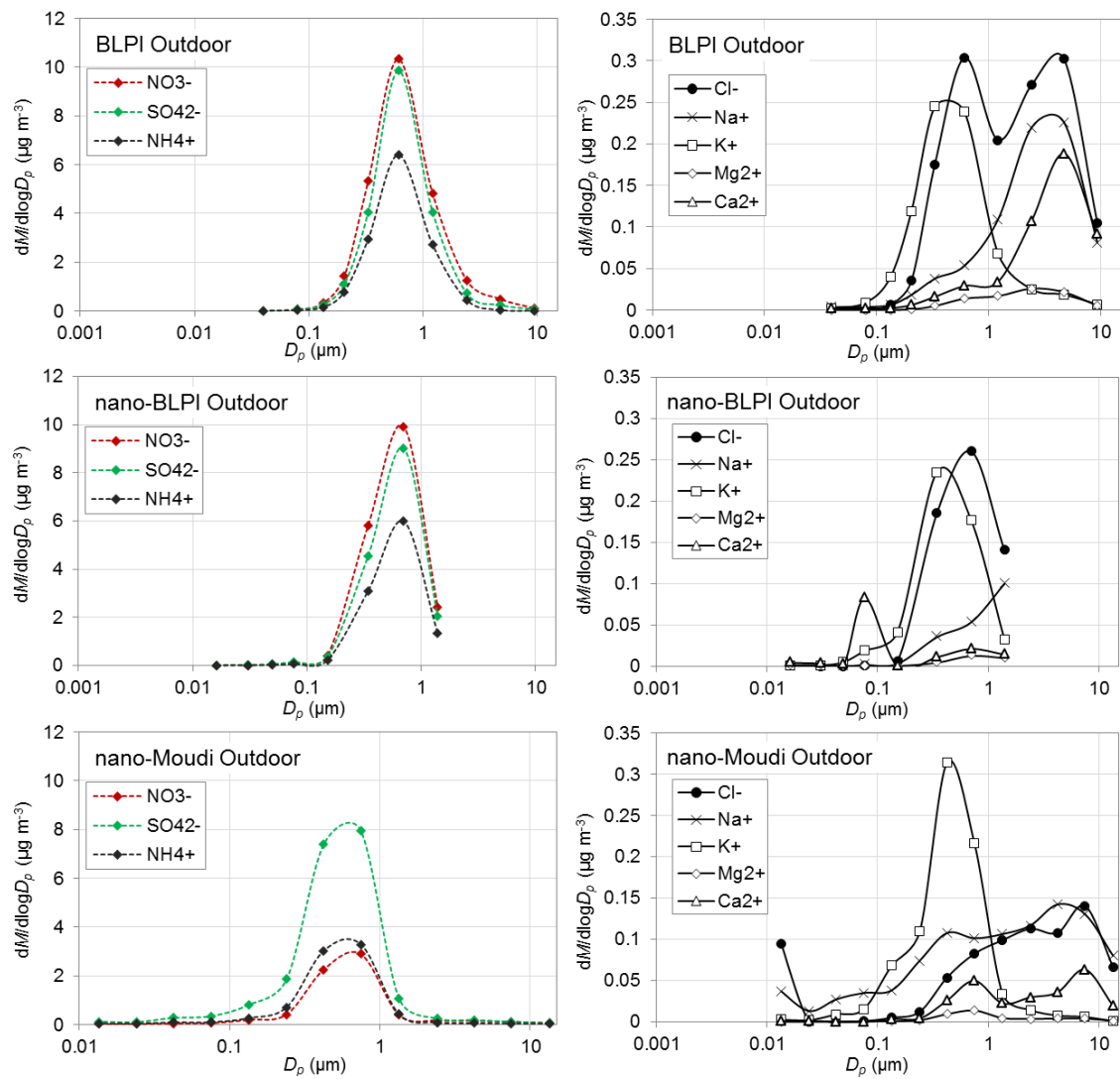


Figure 5. Average mass size distributions for different ionic species (left: SO_4^{2-} , NO_3^- and NH_4^+ and right: Cl^- , Na^+ , K^+ , Mg^{2+} and Ca^{2+}) during winter in outdoor air in Prague.

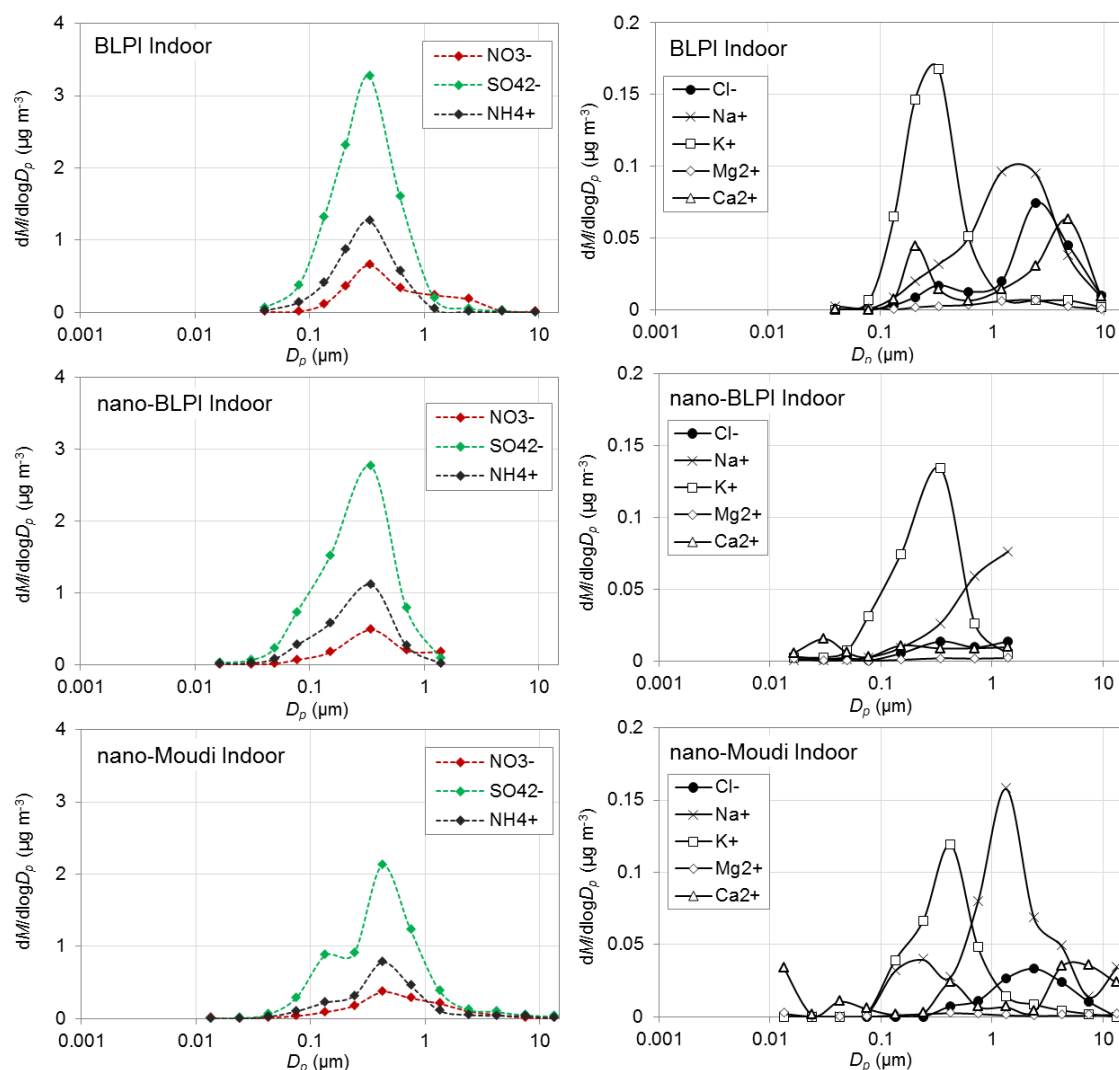


Figure 6. Average mass size distributions for different ionic species (left: SO_4^{2-} , NO_3^- and NH_4^+ and right: Cl^- , Na^+ , K^+ , Mg^{2+} and Ca^{2+}) during winter in indoor air in Prague.

4. Conclusions

This work aimed to assess the performance of four conventional and nano-range impactors, by means of two intercomparison exercises in Prague, during winter 2015 and in Barcelona during summer 2015. The aim of the campaigns was to test the instruments' performance with regard to the particle mass size distributions under different aerosol compositions resulting from different emission sources, meteorology, seasons, and air mass origins. All the cascade impactors were loaded with uncoated substrates excepting for the case of BLPI which foils were coated.

Taking the BLPI as an internal reference, the best agreement regarding mass size distributions was obtained with the nano-BLPI, especially for particles larger than 250 nm. The nano-Moudi showed a good agreement for particle sizes >320 nm, whereas for particle diameters <320 nm this instrument recorded larger mass concentrations than the internal reference. Different particle effects may have caused the differences regarding particle mass concentrations collected in indoor and outdoor air by the

nano-Moudi. Particle volatilisation may have occurred due to the internal rotating mechanisms and the electric current in the sensor board of nano-Moudi which heat the impactor casing up. Decomposition of ammonium nitrate and chloride, as evidenced by the lower nitrate and chloride concentrations in the accumulation mode, is probably also enhanced in the nano-Moudi due to the spreading of the sample on the whole filter surface, in comparison with thick individual spots of material obtained with the BLPI and nano-BLPI impactors. Further research is needed to clarify this issue. With regard to the PCIS, their size-resolved mass concentrations were comparable with other impactors, but the cut-off at 0.25 μm was not consistent with that of the internal reference.

In Barcelona, the sampling took place under dry conditions (< 50% RH) and thus, particle bounce would be expected since some particles (depending on composition) could get dry. Inversely, bounce can be probably neglected for the Prague outdoor intercomparison since the RH was always >50 % indicating the presence of droplet aerosols that tend to adhere to the impaction substrate.

Aerosol mass size distributions were assessed for the Prague and Barcelona campaigns. During winter in Prague (outdoors), the mass size distributions showed a predominantly fine mode, with the coarse mode being almost negligible (by all impactors). However, in Barcelona, the coarse size fractions showed larger mass concentrations, evidencing the higher influence of mineral and marine aerosols.

This study concludes that comparability between the different types of impactors assessed was dependent on particle size. Different performances when challenged with secondary aerosols (due to volatilization) with regard to primary aerosols (potential bounce, also affecting secondary inorganics), were observed. Specifically, the influence of the differences in impactor construction (number of jets, flow, vapour pressure, etc.) on UFP mass concentrations should be further addressed. In addition, further research is necessary with regard to the particle processes (evaporation, bounce, etc.) behind the differences in particle mass observed across size fractions in this study.

The conclusions from this work allow us to extract the following recommendations with regard to ultrafine particle sampling with cascade impactors:

- To avoid particle bounce and increase the accuracy of the size cuts, impactor substrates should be greased especially in areas and seasons with low humidity.
- Detailed assessments of the sampling duration should be carried out to allow sufficient collection of material on each stage for adequate quantification without overloading the upper collection stages. Common approaches to avoid particle

overloading include using multiple-orifice collection stages, and rotating collection substrates (Marple et al., 2014; Marple et al., 1991).

- Attention should be paid to volatilization issues during aerosol transport inside the impactors especially with regard to temperature increases associated with internal rotating mechanisms and the electric current in the sensor board of nano-Moudi.
- Attention should also be paid to sample storage, to avoid evaporation of already deposited particles that may lead to a decrease of mass on a given stage. This evaporation would modify the observed aerosol size distribution, and would affect all impactor types.

Acknowledgements

The research leading to these results received funding from the European Community's Seventh Framework Program (FP7-PEOPLE-2012-ITN) no. 315760 (HEXACOMM project). It was also supported by Charles University in Prague, under the project GA UK no. 274213 and the Spanish MINECO, under the frame of SIINN, the ERA-NET for a Safe Implementation of Innovative Nanoscience and Nanotechnology, in the framework of ERANET-SIINN project CERASAFE (id.:16).

References

- Allen, A.G., Harrison, R.M., Erisman, J.-W. (1989). Field measurements of the dissociation of ammonium nitrate and ammonium chloride aerosols. *Atmospheric Environment* (1967), 23(7), 1591-1599. doi: [http://dx.doi.org/10.1016/0004-6981\(89\)90418-6](http://dx.doi.org/10.1016/0004-6981(89)90418-6)
- Amato, F., Alastuey, A., Karanasiou, A., Lucarelli, F., Nava, S., Calzolari, G., Severi, M., Becagli, S., Gianelle, V.L., Colombi, C., Alves, C., Custódio, D., Nunes, T., Cerqueira, M., Pio, C., Eleftheriadis, K., Diapouli, E., Reche, C., Minguillón, M.C., Manousakas, M., Maggos, T., Vratolis, S., Harrison, R.M., Querol, X. (2015). AIRUSE-LIFE+: a harmonized PM speciation and source apportionment in 5 Southern European cities. *Atmos. Chem. Phys. Discuss.*, 15(17), 23989-24039. doi: 10.5194/acpd-15-23989-2015
- BcnMap. (2015). Barcelona Map, Ajuntament de Barcelona, from http://w20.bcn.cat/Guiamap/Default_en.aspx#x=27601.01&y=83987.71&z=0&w=980&h=574&base=GuiaMartorell
- Berner, A., Luerzer, C. (1980). Mass size distributions of traffic aerosols at Vienna. *The Journal of Physical Chemistry*, 84(16), 2079-2083. doi: 10.1021/j100453a016
- Berner, A., Lürzer, C., Pohl, F., Preining, O., Wagner, P. (1979). The size distribution of the urban aerosol in Vienna. *Science of The Total Environment*, 13(3), 245-261. doi: [http://dx.doi.org/10.1016/0048-9697\(79\)90105-0](http://dx.doi.org/10.1016/0048-9697(79)90105-0)
- Biswas, P., Flagan, R.C. (1984). High-velocity inertial impactors. *Environmental Science & Technology*, 18(8), 611-616. doi: 10.1021/es00126a009
- Crilley, L.R., Ayoko, G.A., Jayaratne, E.R., Salimi, F., Morawska, L. (2013). Aerosol mass spectrometric analysis of the chemical composition of non-refractory PM1 samples from school environments in Brisbane, Australia. *Science of The Total Environment*, 458-460, 81-89. doi: <http://dx.doi.org/10.1016/j.scitotenv.2013.04.007>
- Delgado-Saborit, J.M., Stark, C., Harrison, R.M. (2014). Use of a versatile high efficiency multiparallel denuder for the sampling of PAHs in ambient air: gas

- and particle phase concentrations, particle size distribution and artifact formation. [Research Support, Non-U S Gov't]. *Environ Sci Technol*, 48(1), 499-507.
- Fang, C.P., McMurry, P.H., Marple, V.A., Rubow, K.L. (1991). Effect of Flow-induced Relative Humidity Changes on Size Cuts for Sulfuric Acid Droplets in the Microorifice Uniform Deposit Impactor (MOUDI). *Aerosol Science and Technology*, 14(2), 266-277. doi: 10.1080/02786829108959489
- Fujitani, Y., Hasegawa, S., Fushimi, A., Kondo, Y., Tanabe, K., Kobayashi, S., Kobayashi, T. (2006). Collection characteristics of low-pressure impactors with various impaction substrate materials. *Atmospheric Environment*, 40(18), 3221-3229. doi: <http://dx.doi.org/10.1016/j.atmosenv.2006.02.001>
- Geller, M.D., Kim, S., Misra, C., Sioutas, C., Olson, B.A., Marple, V.A. (2002). A Methodology for Measuring Size-Dependent Chemical Composition of Ultrafine Particles. *Aerosol Science and Technology*, 36(6), 748-762. doi: 10.1080/02786820290038447
- Hering, S., Cass, G. (1999). The Magnitude of Bias in the Measurement of PM_{2.5} Arising from Volatilization of Particulate Nitrate from Teflon Filters. *Journal of the Air & Waste Management Association*, 49(6), 725-733. doi: 10.1080/10473289.1999.10463843
- Hering, S.V., Flagan, R.C., Friedlander, S.K. (1978). Design and evaluation of new low-pressure impactor. I. *Environmental Science & Technology*, 12(6), 667-673. doi: 10.1021/es60142a004
- Hillamo, R.E., Kauppinen, E.I. (1991). On the Performance of the Berner Low Pressure Impactor. *Aerosol Science and Technology*, 14(1), 33-47. doi: 10.1080/02786829108959469
- Hinds, W.C. (1999). *Aerosol technology : properties, behavior, and measurement of airborne particles*. New York: Wiley.
- Hitzenberger, R., Berner, A., Galambos, Z., Maenhaut, W., Cafmeyer, J., Schwarz, J., Müller, K., Spindler, G., Wieprecht, W., Acker, K., Hillamo, R., Mäkelä, T. (2004). Intercomparison of methods to measure the mass concentration of the atmospheric aerosol during INTERCOMP2000-influence of instrumentation and size cuts. *Atmospheric Environment*, 38(38), 6467-6476. doi: <http://dx.doi.org/10.1016/j.atmosenv.2004.08.025>
- Howell, S., Pszenny, A.A.P., Quinn, P., Huebert, B. (1998). A Field Intercomparison of Three Cascade Impactors. *Aerosol Science and Technology*, 29(6), 475-492. doi: 10.1080/02786829808965585
- Huang, Z., Harrison, R.M., Allen, A.G., James, J.D., Tilling, R.M., Yin, J. (2004). Field intercomparison of filter pack and impactor sampling for aerosol nitrate, ammonium, and sulphate at coastal and inland sites. *Atmospheric Research*, 71(3), 215-232. doi: <http://dx.doi.org/10.1016/j.atmosres.2004.05.002>
- Hussein, T., Glytsos, T., Ondráček, J., Dohányosová, P., Ždímal, V., Hämeri, K., Lazaridis, M., Smolík, J., Kulmala, M. (2006). Particle size characterization and emission rates during indoor activities in a house. *Atmospheric Environment*, 40(23), 4285-4307. doi: <http://dx.doi.org/10.1016/j.atmosenv.2006.03.053>
- Hussein, T., Kukkonen, J., Korhonen, H., Pohjola, M., Pirjola, L., Wraith, D., Härkönen, J., Teinilä, K., Koponen, I.K., Karppinen, A., Hillamo, R., Kulmala, M. (2007). Evaluation and modeling of the size fractionated aerosol particle number concentration measurements nearby a major road in Helsinki – Part II: Aerosol measurements within the SAPPHIRE project. *Atmos. Chem. Phys.*, 7(15), 4081-4094. doi: 10.5194/acp-7-4081-2007
- IPR. (2015). Geoportal Praha, Prague geographic data in one place, Prague Institute of Planning and Development (IPR Praha), from <http://www.geoportalpraha.cz/en/maps-online#.VIIWWLerR1s>
- Jiménez, S., Ballester, J. (2011). Use of a Berner Low-Pressure Impactor at Low Inlet Pressures. Application to the Study of Aerosols and Vapors at High

- Temperature. *Aerosol Science and Technology*, 45(7), 861-871. doi: 10.1080/02786826.2011.566900
- Karanasiou, A.A., Sitaras, I.E., Siskos, P.A., Eleftheriadis, K. (2007). Size distribution and sources of trace metals and n-alkanes in the Athens urban aerosol during summer. *Atmospheric Environment*, 41(11), 2368-2381. doi: <http://dx.doi.org/10.1016/j.atmosenv.2006.11.006>
- Kubelová, L., Vodička, P., Schwarz, J., Cusack, M., Makeš, O., Ondráček, J., Ždímal, V. (2015). A study of summer and winter highly time-resolved submicron aerosol composition measured at a suburban site in Prague. *Atmospheric Environment*, 118, 45-57. doi: <http://dx.doi.org/10.1016/j.atmosenv.2015.07.030>
- Lin, C.-C., Chen, S.-J., Huang, K.-L., Hwang, W.-I., Chang-Chien, G.-P., Lin, W.-Y. (2005). Characteristics of Metals in Nano/Ultrafine/Fine/Coarse Particles Collected Beside a Heavily Trafficked Road. *Environmental Science & Technology*, 39(21), 8113-8122. doi: 10.1021/es048182a
- Lunden, M.M., Revzan, K.L., Fischer, M.L., Thatcher, T.L., Littlejohn, D., Hering, S.V., Brown, N.J. (2003). The transformation of outdoor ammonium nitrate aerosols in the indoor environment. *Atmospheric Environment*, 37(39-40), 5633-5644. doi: <http://dx.doi.org/10.1016/j.atmosenv.2003.09.035>
- Marple, V., Olson, B., Romay, F., Hudak, G., Geerts, S.M., Lundgren, D. (2014). Second Generation Micro-Orifice Uniform Deposit Impactor, 120 MOUDI-II: Design, Evaluation, and Application to Long-Term Ambient Sampling. *Aerosol Science and Technology*, 48(4), 427-433. doi: 10.1080/02786826.2014.884274
- Marple, V.A., Rubow, K.L., Behm, S.M. (1991). A Microorifice Uniform Deposit Impactor (MOUDI): Description, Calibration, and Use. *Aerosol Science and Technology*, 14(4), 434-446. doi: 10.1080/02786829108959504
- Mašková, L., Smolík, J., Vodička, P. (2015). Characterisation of particulate matter in different types of archives. *Atmospheric Environment*, 107, 217-224. doi: <http://dx.doi.org/10.1016/j.atmosenv.2015.02.049>
- May, K.R. (1945). The Cascade Impactor. *Journal of Scientific Instruments*, 22(12), 247.
- Misra, C., Singh, M., Shen, S., Sioutas, C., Hall, P.M. (2002). Development and evaluation of a personal cascade impactor sampler (PCIS). *Journal of Aerosol Science*, 33(7), 1027-1047. doi: 10.1016/s0021-8502(02)00055-1
- Nie, W., Wang, T., Gao, X., Pathak, R.K., Wang, X., Gao, R., Zhang, Q., Yang, L., Wang, W. (2010). Comparison among filter-based, impactor-based and continuous techniques for measuring atmospheric fine sulfate and nitrate. *Atmospheric Environment*, 44(35), 4396-4403. doi: <http://dx.doi.org/10.1016/j.atmosenv.2010.07.047>
- Oberdörster, G. (2000). Pulmonary effects of inhaled ultrafine particles. *Int Arch Occup Environ Health*, 74(1), 1-8. doi: 10.1007/s004200000185
- Oberdorster, G., Oberdorster, E., Oberdorster, J. (2005). Nanotoxicology: an emerging discipline evolving from studies of ultrafine particles. *Environ Health Perspect*, 113(7), 823-839.
- Ondráček, J., Schwarz, J., Ždímal, V., Andělová, L., Vodička, P., Bízek, V., Tsai, C.J., Chen, S.C., Smolík, J. (2011). Contribution of the road traffic to air pollution in the Prague city (busy speedway and suburban crossroads). *Atmospheric Environment*, 45(29), 5090-5100. doi: <http://dx.doi.org/10.1016/j.atmosenv.2011.06.036>
- Pennanen, A.S., Sillanpaa, M., Hillamo, R., Quass, U., John, A.C., Branis, M., Hunova, I., Meliefste, K., Janssen, N.A., Koskentalo, T., Castano-Vinyals, G., Bouso, L., Chalbot, M.C., Kavouras, I.G., Salonen, R.O. (2007). Performance of a high-volume cascade impactor in six European urban environments: mass measurement and chemical characterization of size-segregated particulate samples. *Sci Total Environ*, 374(2-3), 297-310.

- Pio, C.A. and Harrison, R.M. (1987a). The equilibrium of ammonium chloride aerosol with gaseous hydrochloric acid and ammonia under tropospheric conditions. *Atmospheric Environment*, 21, 1243-1246.
- Pio, C.A. and Harrison, R.M. (1987b). Vapour Pressure of ammonium chloride aerosol. Effect of temperature and humidity. *Atmospheric Environment*, 21, 2711-2715.
- Preining, O., Berner, A. (1979). Aerosol Measurements in the Submicron Size Range. *EPA report, EPA-600/2-79-105*. Washington, DC: EPA.
- Querol, X., Alastuey, A., Moreno, T., Viana, M.M., Castillo, S., Pey, J., Rodríguez, S., Artiñano, B., Salvador, P., Sánchez, M., Garcia Dos Santos, S., Herce Garraleta, M.D., Fernandez-Patier, R., Moreno-Grau, S., Negral, L., Minguillón, M.C., Monfort, E., Sanz, M.J., Palomo-Marín, R., Pinilla-Gil, E., Cuevas, E., de la Rosa, J., Sánchez de la Campa, A. (2008). Spatial and temporal variations in airborne particulate matter (PM₁₀ and PM_{2.5}) across Spain 1999–2005. *Atmospheric Environment*, 42(17), 3964-3979. doi: <http://dx.doi.org/10.1016/j.atmosenv.2006.10.071>
- Reche, C., Viana, M., Brines, M., Perez, N., Beddows, D., Alastuey, A., Querol, X. (2015). Determinants of aerosol lung-deposited surface area variation in an urban environment. [Research Support, Non-U S Gov't]. *Sci Total Environ*, 517, 38-47.
- Sardar, S.B., Fine, P.M., Mayo, P.R., Sioutas, C. (2005). Size-Fractionated Measurements of Ambient Ultrafine Particle Chemical Composition in Los Angeles Using the NanoMOUDI. *Environmental Science & Technology*, 39(4), 932-944. doi: 10.1021/es049478j
- Schaap, M., Spindler, G., Schulz, M., Acker, K., Maenhaut, W., Berner, A., Wiedprecht, W., Streit, N., Müller, K., Brüggemann, E., Chi, X., Putaud, J.P., Hitznerberger, R., Puxbaum, H., Baltensperger, U., ten Brink, H. (2004). Artefacts in the sampling of nitrate studied in the "INTERCOMP" campaigns of EUROTRAC-AEROSOL. *Atmos. Environ.*, 38(38), 6487-6496. doi: <http://dx.doi.org/10.1016/j.atmosenv.2004.08.026>
- Schwarz, J., Štefancová, L., Maenhaut, W., Smolík, J., Ždímal, V. (2012). Mass and chemically speciated size distribution of Prague aerosol using an aerosol dryer--the influence of air mass origin. *Sci Total Environ*, 437, 348-362. doi: 10.1016/j.scitotenv.2012.07.050
- Seinfeld, J.H., Pandis, S.N. (2006). Atmospheric Chemistry and Physics: From Air Pollution to Climate Change, 2nd edition. *J. Wiley, New York*.
- Sioutas, C. (2004). Development of New Generation Personal Monitors for Fine Particulate Matter (PM) and its Metal Content. *NUATRC Research Report No. 2*.
- Smolík, J., Dohányosová, P., Schwarz, J., Ždímal, V., Lazaridis, M. (2008). Characterization of Indoor and Outdoor Aerosols in a Suburban Area of Prague. *Water Air Soil Pollut: Focus*, 8(1), 35-47. doi: 10.1007/s11267-007-9141-y
- Štefancová, L., Schwarz, J., Maenhaut, W., Chi, X., Smolík, J. (2010). Hygroscopic growth of atmospheric aerosol sampled in Prague 2008 using humidity controlled inlets. *Atmospheric Research*, 98(2–4), 237-248. doi: <http://dx.doi.org/10.1016/j.atmosres.2010.04.009>
- Štefancová, L., Schwarz, J., Mäkelä, T., Hillamo, R., Smolík, J. (2011). Comprehensive Characterization of Original 10-Stage and 7-Stage Modified Berner Type Impactors. *Aerosol Science and Technology*, 45(1), 88-100. doi: 10.1080/02786826.2010.524266
- Stelson, A.W., Seinfeld, J.H. (1982). Relative humidity and temperature dependence of the ammonium nitrate dissociation constant. *Atmospheric Environment* (1967), 16(5), 983-992. doi: [http://dx.doi.org/10.1016/0004-6981\(82\)90184-6](http://dx.doi.org/10.1016/0004-6981(82)90184-6)
- Talbot, N., Kubelova, L., Makes, O., Cusack, M., Ondracek, J., Vodička, P., Schwarz, J., Zdímal, V. (2016). Outdoor and indoor aerosol size, number, mass and compositional dynamics at an urban background site during warm season.

- Atmospheric Environment*, 131, 171-184. doi: <http://dx.doi.org/10.1016/j.atmosenv.2016.01.055>
- Tursic, J., Grgic, I., Berner, A., Skantar, J., Cuhalev, I. (2008). Measurements of size-segregated emission particles by a sampling system based on the cascade impactor. [Research Support, Non-U S Gov't]. *Environ Sci Technol*, 42(3), 878-883.
- Vodička, P., Schwarz, J., Ždímal, V. (2013). Analysis of one year's OC/EC data at a Prague suburban site with 2-h time resolution. *Atmospheric Environment*, 77, 865-872. doi: <http://dx.doi.org/10.1016/j.atmosenv.2013.06.013>
- Wall, S.M., John, W., Ondo, J.L. (1988). Measurement of aerosol size distributions for nitrate and major ionic species. *Atmospheric Environment (1967)*, 22(8), 1649-1656. doi: [http://dx.doi.org/10.1016/0004-6981\(88\)90392-7](http://dx.doi.org/10.1016/0004-6981(88)90392-7)
- Wang, H.-C., John, W. (1988). Characteristics of the Berner Impactor for Sampling Inorganic Ions. *Aerosol Science and Technology*, 8(2), 157-172. doi: 10.1080/02786828808959179

Table S1. Design parameters of the stages from nano-BLPI.

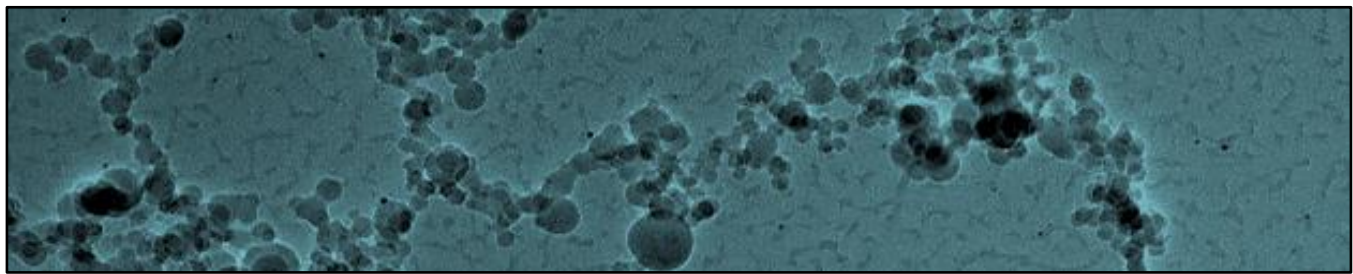
Stage number	Lower cut sizes (μm)	Number of nozzles	Nozzle Diameter (mm)
9	1.95	1	3.60
8	1.00	39	0.70
7	0.49	17	0.60
6	0.24	8	0.54
5	0.095	43	0.27
4	0.062	88	0.25
3	0.039	142	0.25
2	0.024	237	0.25
1	0.011	408	0.25

Table S2. Average mass concentrations for different ionic species during winter in outdoor and indoor air in Prague.

Type of environment	Impactor	Mass ionic species ($\mu\text{g m}^{-3}$)							
		NO_3^-	SO_4^{2-}	NH_4^+	Cl^-	Na^+	K^+	Mg^{2+}	Ca^{2+}
Outdoor	BLPI (PM_{14})	6.72	5.72	3.78	0.40	0.22	0.20	0.03	0.14
	nano-BLPI ($\text{PM}_{1.95}$)	5.78	4.99	3.31	0.18	0.06	0.16	0.01	0.03
	nano-Moudi (PM_{10})	1.71	5.12	2.06	0.19	0.25	0.20	0.01	0.06
Indoor	BLPI (PM_{14})	0.49	2.15	0.78	0.05	0.10	0.10	0.01	0.05
	nano-BLPI ($\text{PM}_{1.95}$)	0.35	1.93	0.73	0.02	0.05	0.09	0.00	0.02
	nano-Moudi (PM_{10})	0.34	1.53	0.53	0.03	0.13	0.08	0.00	0.05
	Blank uncertainty*	1.3×10^{-3}	9.4×10^{-4}	2.0×10^{-4}	3.0×10^{-4}	2.0×10^{-4}	2.0×10^{-4}	1.0×10^{-4}	3.0×10^{-4}

* Recalculated per 1m^3 of air for BLPI for 72 h sampling.

Chapter 5. **DISCUSSION**



5. DISCUSSION

In spite of nanotechnology being a research field with continuous innovation, considerable knowledge gaps remain concerning ENP and N-ENP release and exposure in industrial workplaces. The same is true for novel industrial technologies and processes such as those described in this PhD thesis (e.g., ceramic applications of laser technologies). Two of the main reasons for this are: (i) the relative novelty of “*nanosafety*” as a field of research, and (ii) the fact that adequate analytical techniques and monitoring instrumentation have only recently become available (Asbach *et al.*, 2015).

As presented in chapter 2, the objectives of this PhD thesis were:

1. To evaluate the performance of specific nanoparticle monitoring and sampling instrumentation, under real-world conditions.
2. To characterise nanoparticle release and exposure in real-world industrial settings, dealing with ENP.
3. To characterise nanoparticle release and exposure in real-world industrial settings, dealing with PGNP.

In regard to the first, the ability of online instrumentation to detect nanoparticles and characterise exposure in real-time is currently a major knowledge gap. This PhD thesis contributed to overcome this issue by assessing the performance of two novel instruments (portable NanoScan SMPS TSI 3910, and cascade impactors such as nano-BLPI and nano-Moudi) for nanoscale aerosol measurements.

Concerning the second and third objectives, nanoparticle formation and release mechanisms, and exposure, were characterised during two main types of real-world industrial scenarios: (i) production and application of SWCNT while manufacturing semiconductor thin films, and (ii) during conventional processes in the ceramic industry (not involving nanoparticles as input materials) with potential for unintentional nanoparticle release (ceramic tile sintering and ablation by laser technology processes).

In the framework of the latter two objectives, these exposure assessments were followed by the evaluation of the effectiveness of occupational exposure mitigation strategies already in place in the industrial facilities under study through experiments under real-world operating conditions.

5.1 Performance of nanoparticle monitoring and sampling instrumentation

In order to fulfil the first main objective, two dedicated studies were designed: the evaluation of the performance of the novel portable NanoScan SMPS TSI 3910, and the assessment of cascade impactors (nano-BLPI) for nanoparticle sampling. In addition, the experimental work in this thesis gave the opportunity to identify instrumental limitations that were evident during the course of the experiments. These limitations refer to the online detection of high aspect ratio nanoparticles (e.g., nanofibers), and to the monitoring of high concentration of coarse particles with diffusion chargers (e.g., DiSCmini). Both types of studies are discussed below.

5.1.1 Intercomparison studies

The results from the intercomparison study among the novel portable SMPS (NanoScan SMPS TSI 3910) and the stationary SMPS showed a dependence on particle size, particle morphology, particle composition and particle concentration. Differences in the charging efficiency of the NanoScan unipolar charger when compared to bipolar charger from the stationary SMPS might be the reason of this dependence. Although the NanoScan instrument is known to provide higher time resolution analysis than the stationary SMPS, it could be considered slow in certain specific microenvironments but it can be a useful tool to obtain estimates of the size distribution in workplace air. Due to its portability, it is a valuable tool for simplified exposure assessment, e.g. in the basic exposure assessment described in Tier 2 (section 1.2.3). However, its accuracy should not be overestimated. While the sizing accuracy for unimodal distributions was mostly within $\pm 25\%$ (Figure 5.1a), measured total concentrations in some cases deviated by more than 50% (especially for agglomerated particles such as spark soot; Figure 5.1b). These observations are consistent with Stabile *et al.* (2014) who conclude that the NanoScan is not able to properly measure diesel-generated particles (fresh aerosol made up of aggregated particles).

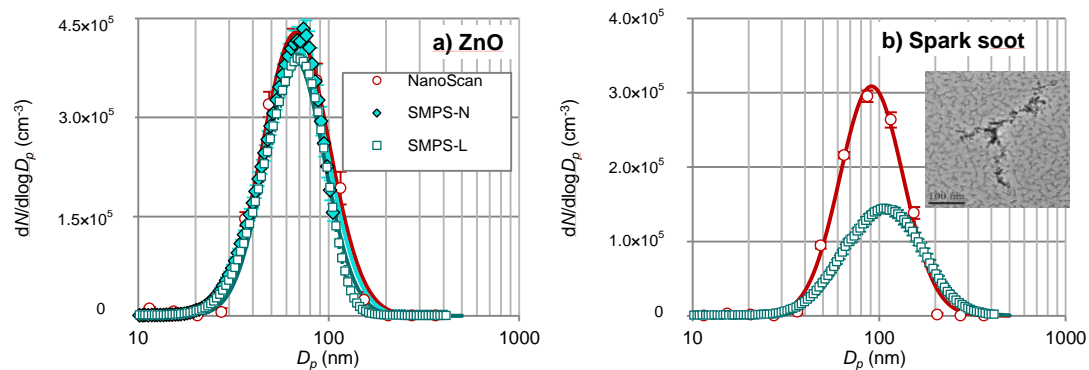


Figure 5.1 Measurement data and fitted particle number size distribution of: a) generated ZnO and b) spark soot particles, measured in the exposure chamber with portable and stationary SMPS. Error bars indicate the standard deviation.

As for multimodal distributions, the NanoScan SMPS did not seem to be able to properly resolve them. For accurate measurements, e.g., in the expert exposure assessment in Tier 3, stationary SMPS instruments are still the preferred choice. It should be noted that only one NanoScan SMPS unit was tested, and that results could be unit-dependent. Therefore, further research is required in this direction.

The performance assessment of four conventional and nano-range impactors have showed different impactor behaviours when challenged with secondary aerosols (due to volatilization) with regard to primary aerosols (potential bounce, also affecting secondary inorganics). Major differences regarding particle mass concentrations collected in indoor and outdoor air were observed for the nano-Moudi impactor probably due to the following particle effects:

- Particle volatilisation due to the internal rotating mechanisms which heats the impactor casing up.
- Decomposition of ammonium nitrate (NH_4NO_3) and chloride (NH_4Cl), also probably enhanced due to the spreading of the sample on the whole filter surface, in comparison with thick individual spots of material obtained with the BLPI and nano-BLPI impactors.

Previous conclusions regarding nano-Moudi can be supported by the example provided in Figure 5.2, which shows significantly lower mass concentrations of major species sulphate (SO_4^{2-}), ammonium (NH_4^+) and nitrate (NO_3^-) with the nano-Moudi, in comparison with the BLPI. The same is valid for fine chlorides that are missing on same nano-Moudi samples showing NH_4Cl evaporation (data not shown).

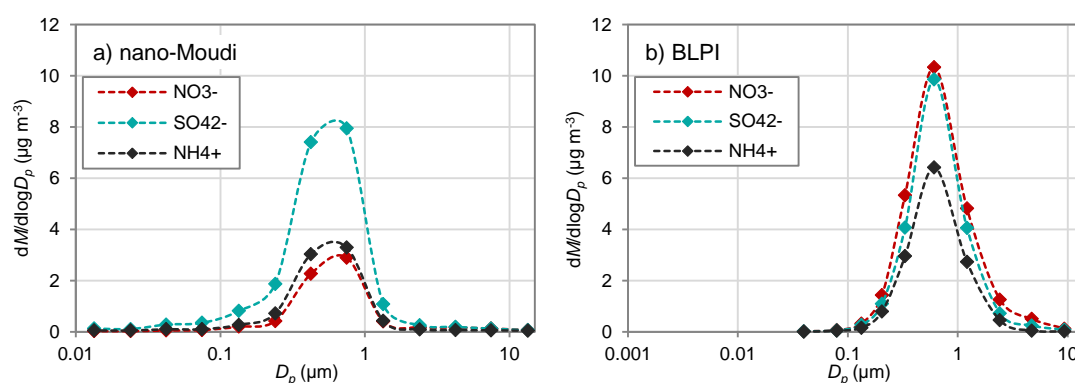


Figure 5.2 Average mass size distributions for different ionic species (SO_4^{2-} , NO_3^- and NH_4^+) in outdoor air in Prague.

With regard to the PCIS, their size-resolved mass concentrations were comparable with other impactors, but the cut-off at $0.25 \mu\text{m}$ was not consistent with that of the internal reference.

In conclusion, the following recommendations may be extracted based on the instrument performance assessments carried out in the framework of this PhD thesis:

- The portable NanoScan SMPS is a valid tool for Tier 2 exposure assessments. For Tier 3, conventional SMPS systems should be the preferred choice.
- Nanoparticle sampling with impactors should follow the following recommendations:
 - To avoid particle bounce and increase the accuracy of the size cuts, impactor substrates should be greased especially in areas and seasons with low humidity.
 - Detailed assessments of the sampling duration should be carried out to allow sufficient collection of material on each stage for adequate quantification without overloading the upper collection stages. Common approaches to avoid particle overloading include using multiple-orifice collection stages, and rotating collection substrates (Marple et al., 2014; Marple et al., 1991).
 - Attention should be paid to volatilization issues during aerosol transport inside the impactors especially with regard to temperature increases associated with internal rotating mechanisms and the electric current in the sensor board of nano-Moudi.
 - Attention should also be paid to sample storage, to avoid evaporation of already deposited particles that may lead to a decrease of mass on a given stage. This evaporation would modify the observed aerosol size distribution, and would affect all impactor types.

- Particle sampling with portable PCIS impactors did not provide comparable results for the ultrafine and nanoparticle fraction (<250 nm) with regard to other impactors.

As a result, and based on the evidences from this work, the multiple metric and instrumentation approach proposed by Brouwer *et al.* (2012) seems to be confirmed as optimal for nanoparticle assessments under real-world settings. Only through the combination of diverse monitoring techniques and parameters does it become possible to obtain a detailed characterisation of nanoparticle exposure routes and scenarios.

5.1.2 Instrumental limitations during field measurements

A number of instrument limitations during field measurements were identified. The first was related to the detection of nanofibers, specifically SWCNT (Article I). Figure 5.3 shows a TEM image of SWCNT collected in the workplace air, evidencing their release during the industrial process. However, no clear correlation between the collection chamber opening times and consistent increases in particle number (by ELPI, CPC, NanoScan SMPS or OPS) or mass concentrations (by ELPI or OPS) were obtained (when SWCNT were expected to be released). This suggests that the detection of SWCNT was limited due to the inaccurate response of monitoring instruments to nanofibers with irregular shapes and high aspect ratios (length/width > 500).

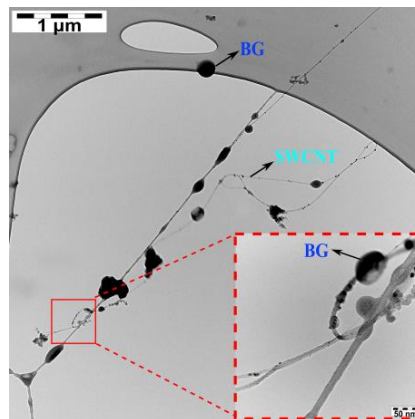


Figure 5.3 TEM images of SWCNT and background particles collected in workplace air during film manufacturing. Dashed rectangles show the magnified area. Identified particles are shown as background particles (BG), and SWCNT.

This work revealed that TEM based methods are the most feasible, reliable, and selective way to assess qualitative worker exposure to nanofibers. However, qualitative assessments with TEM can be compromised due to the high aspect ratio and branching of the fibres.

Another example of a limitation of nanoparticle monitors was identified during an experimental field campaign, while using a diffusion charging particle monitor (DiSCmini). The results from this experiment are not included in the results section (chapter 4) given that they were not published as a research paper. The experimental work was carried out in the milling plant at the Institute for Ceramic Technology (ITC) in Castellón, during October 2014. The objective of the work was to monitor ultrafine and nanoparticle emissions during milling of ceramic tiles using a pendular mill. A number of monitoring instruments were deployed in close proximity to the pendular mill, including particle counters (DiSCmini, 10 - 700 nm; TSI butanol CPC, Model 3775, 4 nm-1.5 μm) and particle sizers (NanoScan SMPS, 10 - 420 nm). The instruments were deployed simultaneously in indoor and outdoor air. Figure 5.4 shows the results from one of the milling experiments.

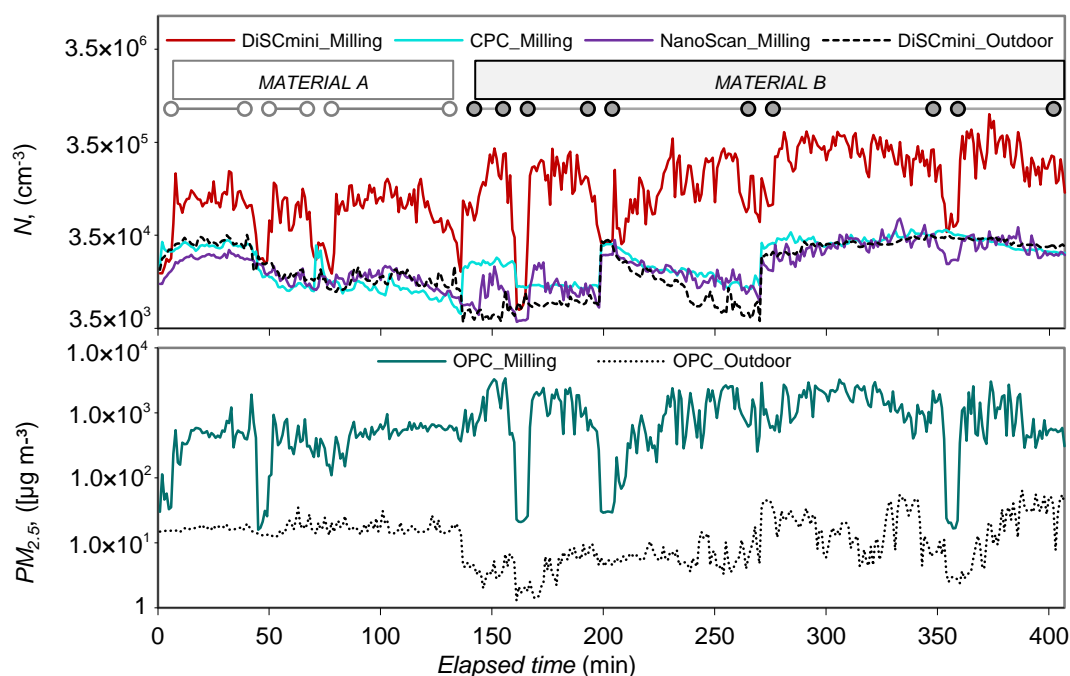


Figure 5.4 Particle number (N_p) and particle mass ($PM_{2.5}$), concentrations measured simultaneously in the industrial site during ceramic milling activities and outdoor air.

As shown in the Figure 5.4, the time series of particle number concentrations monitored by the CPC, NanoScan and the outdoor DiSCmini followed similar patterns, which however were markedly different to the trend shown by the indoor DiSCmini (Figure 5.4, top). Therefore, the time series of the indoor DiSCmini did not seem to be representative of indoor particle number concentrations, and conversely it showed a high degree of similarity with the particle mass concentration time series monitored with the indoor OPC (Figure 5.4, bottom). These results suggested a poor performance of the indoor DiSCmini unit. In order to clarify the reasons behind it, this

instrument was intercompared with the NanoScan SMPS during non-activity hours (night-time) at low coarse $PM_{2.5}$ ($20 - 50 \mu\text{g m}^{-3}$), obtaining highly comparable results with regard to particle number concentration ($R^2=0.97$; slope =1.19; Figure 5.5b).

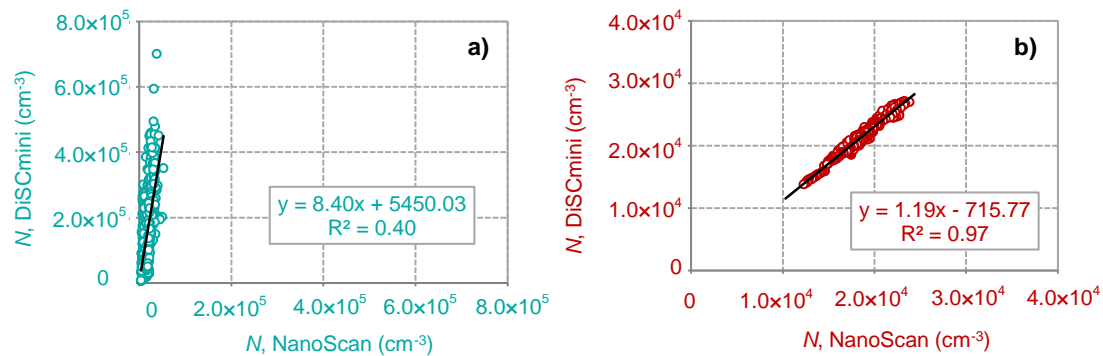


Figure 5.5 Correlation coefficients and regression equations obtained from the comparison between the DiSCmini and the NanoScan SMPS, for total particle number (N) monitoring during: a) milling activity at high coarse particle mass concentration ($500\text{-}1400 \mu\text{g m}^{-3}$ $PM_{2.5}$) and b) real-world conditions at low coarse particle mass concentrations ($20\text{-}50 \mu\text{g m}^{-3}$ $PM_{2.5}$).

The optimal results obtained during this intercomparison exercise evidenced the correct performance of the DiSCmini unit, and suggested that the poor performance observed during the milling process was related to the type and concentration of particles monitored.

Particle mass concentrations during the milling experiment ranged between $500\text{-}1400 \mu\text{g PM}_{2.5} \text{m}^{-3}$). The different DiSCmini response observed when compared to the CPC and NanoScan (Figure 5.4 and Figure 5.5a) may probably be explained by the varying shapes and geometric standard deviation of the size distributions of the aerosol monitored. The DiSCmini is calibrated with monodisperse aerosol, and the instrument response for polydisperse aerosols with a lognormal size distribution with a geometric standard deviation of 1.9 is then calculated (Fierz, 2010). As a result, for aerosols that are far from this size distribution, errors may occur both in the number and diameter calculation. This was probably the underlying cause behind the poor performance of the DiSCmini which was deployed in indoor air. As a result, it may be concluded that the performance of diffusion chargers such as the DiSCmini is not optimal when exposure scenarios are characterized by high concentrations of coarse ($>2.5 \mu\text{m}$) particles, and therefore that their use should be discouraged in these scenarios.

In conclusion, the following issues were identified during this work with regard to instrumental limitations:

- Detection of high aspect ratio particles (e.g., nanofibers) using current online instrumentation is highly complex. Currently we are aware of research on specially designed DMA for the selective separation of nanofibers, but these instruments are still under development (Prof. K-H Ahn, University of Hanyang, South Korea, pers. Com.). TEM-based methods are identified as the most adequate tool to qualitatively assess exposure to nanofibers in indoor air, given that they allow for the qualitative detection of airborne nanofibers. However, quantification of these exposures still remains a challenge, both with TEM and online methods.
- The performance of DiSCmini instruments under real-world conditions with regard to particle number concentrations was within the expected uncertainty (10-30%; Asbach *et al.*, 2012a; Fierz, 2011). However, under scenarios characterized by high coarse particle (>2.5 µm) concentrations (outside of the instrument's measurement range) the results from this monitor become unreliable, with a higher correlation with particle mass than with particle number concentrations. Under these circumstances other types of particle monitors (particle mass concentration monitors or CPC) should be the preferred choice.

5.2 Nanoparticle exposure scenarios

Nanoparticle emission into workplace air and their influence on worker's exposure was assessed in five different workplaces: (i) production and application of SWCNT while manufacturing semiconductor thin films (Article I), (ii) laser-based ceramic tile sintering in a laboratory-scale furnace (Article II), (iii) laser-based ceramic tile sintering in an industrial pilot plant scale furnace (Article III), (iv) ceramic laser ablation at laboratory-scale (Article I), and (v) atmospheric plasma spraying in an industrial-scale pilot plant (Article in preparation). This last workplace, although not directly included in the framework of this PhD thesis as a research publication, was taken into consideration in this section for comparison of particle concentration levels obtained during a high-energy nature processes frequently used in ceramic industries. Atmospheric plasma spraying is used in the ceramic industry to deposit different coatings on a number of surfaces in order to achieve enhanced properties such as wear, corrosion, electrical insulation or heat resistance, while maintaining the structural properties of the underlying material (Fauchais *et al.*, 2013). In total, ten different exposure scenarios (hereafter described as #1 to #10; Table 5.1), were characterized. Three of the exposure scenarios have relation with ENP (specifically SWCNT) and the remaining 7 scenarios with PGNP.

Table 5.1 Description of the exposure scenarios.

Exposure scenario	Description	Target particles
#1 ^a	Best case: Manufacturing of SWCNT films using LEV	
#2 ^a	Worst case: Manufacturing of a SWCNT film without LEV	SWCNT
#3 ^a	Reactor cleaning performed under pressure with wet wipes	
#4 ^b	Laser-based porcelain tile sintering in a laboratory-scale furnace (length = 3 m)	
#5 ^b	Laser-based red clay tile sintering in a laboratory-scale furnace (length = 3 m)	
#6 ^c	Laser-based porcelain tile sintering in an industrial pilot plant scale furnace (length = 7 m)	
#7 ^c	Laser-based red clay tile sintering in an industrial pilot plant scale furnace (length = 7 m)	
#8 ^b	Laser-based ablation of porcelain tiles	PGNP
#9	Atmospheric plasma spraying of a ceramic glass powder (microsuspension Na-Si-Ca-P; Na ₂ O; SiO ₂ ; CaO; P ₂ O ₅) before application of mitigation strategies	
#10	Atmospheric plasma spraying of a ceramic glass powder (microsuspension Na-Si-Ca-P; Na ₂ O; SiO ₂ ; CaO; P ₂ O ₅) after application of mitigation strategies	

^a Article I (Fonseca *et al.*, 2015c); ^b Article II (Fonseca *et al.*, 2015a); ^c Article III (Fonseca *et al.*, 2016); SWCNT: Single-walled carbon nanotubes; PGNP: Process-generated nanoparticles; LEV: Local exhaust ventilation

For the sake of clarity, the results described below regarding exposure scenarios #4 and #6 refer to mean concentrations monitored during sintering of different types of porcelain materials. The same is true for #5 and #7 for red clay tiles.

5.2.1 Exposure to particles in the worker breathing zone

The impact of particle emissions into workplace air on worker exposure were monitored in the workers' breathing zone and compared with an average exposure to background particles defined in section 3.4.4. Table 5.2 summarises the results of each exposure scenario and corresponding background air concentrations including data on number of minutes sampled (t), mean particle number (N_{mean}) and mass (M_{mean}) concentrations, standard deviation ($\pm\sigma$), maximum particle number concentrations recorded (N_{max}), as well as the mean particle diameter (D_p) monitored. Measurements were taken with a 1-min time resolution. The statistical significance level of particle exposure in each exposure scenario ($BG+3\cdot\sigma_{BG}$; Asbach *et al.*, 2012b) is shown in Figure 5.6.

As evidenced by Table 5.2 and Figure 5.6, non-significant nanoparticle exposure levels (in terms of N and M) were found during the exposure scenarios dealing with nanofibers ($SWCNT < BG+3\cdot\sigma_{BG}$).

Table 5.2 Summary results of exposure scenarios. Number of minutes sampled (t), mean (N_{mean} and M_{mean}), PM_{10} , $PM_{2.5}$ and PM_{10} , standard deviation ($\pm\sigma$) and maximum particle number concentration (N_{max}), particle diameter (D_p). BG: mean background concentrations.

Exposure scenario	t (min)	$N_{\text{mean}} \pm \sigma$ (cm^{-3})	N_{max} (cm^{-3})	$D_p \pm \sigma$ (nm)	$M_{\text{mean}} \pm \sigma$ ($\mu\text{g m}^{-3}$)	$PM_{10} \pm \sigma$ ($\mu\text{g m}^{-3}$)	$PM_{2.5} \pm \sigma$ ($\mu\text{g m}^{-3}$)	$PM_{10} \pm \sigma$ ($\mu\text{g m}^{-3}$)
#1 ^a	540	$1.9 \pm 0.5 \times 10^3$	2.0×10^4		3.4 ± 22			
#2 ^a	8	$2.3 \pm 0.3 \times 10^3$	1.0×10^4	<200 nm (>95 %) ^b	25 ± 3.8		N/A	
#3 ^a	44	$3.3 \pm 0.5 \times 10^3$	4.3×10^3		6.1 ± 12			
BG ^a		$1.4 \pm 3.4 \times 10^3$	9.7×10^4		4.5 ± 6			
#4 ^b	90	$5.5 \pm 3.7 \times 10^5$	1.6×10^6	15.7 ± 5.9		6.7 ± 1.0	8.3 ± 1.7	14.2 ± 2.3
#5 ^b	90	$1.5 \pm 1.5 \times 10^5$	6.5×10^5	24.0 ± 6.9	N/A	7.1 ± 1.0	9.1 ± 1.7	15.2 ± 2.1
BG ^b		$1.3 \pm 0.9 \times 10^4$	6.0×10^4	33.9 ± 5.5		5.3 ± 0.1	5.9 ± 0.2	10.8 ± 0.3
#6 ^c	90	$3.6 \pm 1.7 \times 10^5$	8.0×10^5	15.5 ± 2.7		3.9 ± 4.3	9.5 ± 15.7	41.2 ± 95.5
#7 ^c	90	$2.8 \pm 1.9 \times 10^5$	8.0×10^5	15.4 ± 3.3	N/A	2.0 ± 0.4	3.2 ± 0.9	10.2 ± 5.4
BG ^c		$1.1 \pm 0.5 \times 10^4$	2.3×10^4	58.2 ± 8.4		1.8 ± 1.2	2.3 ± 1.5	2.8 ± 2.1
#8 ^d	20	$3.8 \pm 1.9 \times 10^5$	5.8×10^5	79.5 ± 26.6	N/A	608 ± 365	650 ± 391	673 ± 395
BG ^b		$1.3 \pm 0.9 \times 10^4$	6.0×10^4	33.9 ± 5.5		5.3 ± 0.1	5.9 ± 0.2	10.8 ± 0.3
#9 ^e	10	$7.7 \pm 7.6 \times 10^5$	2.7×10^6	67.0 ± 21.0	N/A			
BG ^e		$1.0 \pm 0.04 \times 10^4$	1.1×10^4	58.3 ± 1.3				
#10 ^e	10	$1.7 \pm 1.8 \times 10^5$	7.6×10^5	53.6 ± 12.0	N/A			
BG ^e		$2.5 \pm 0.3 \times 10^4$	2.9×10^4	37.8 ± 1.5				

^a N_{mean} measured by N-WCPC Model 3788 (2.5 nm - 3 μm); D_p measured by NanoScan SMPS (10-420 nm); M_{mean} measured by ELPITM (7 nm - 10 μm)

^b N_{mean} measured by DiSCmini (10 - 700 nm); D_p measured by DiSCmini (10 - 700 nm); PM_{10} , $PM_{2.5}$ and PM_{10} measured by DustTrakTM DRX TSI Model 8533 (0.1 - 15 μm)

^c N_{mean} measured by DiSCmini (10 - 700 nm); D_p measured by DiSCmini (10 - 700 nm); PM_{10} , $PM_{2.5}$ and PM_{10} measured by DustTrakTM DRX TSI Model 8533 (0.1 - 15 μm)

^d N_{mean} measured by WCPC TSI Model 3785 (2.5 nm - 3 μm); D_p measured by DiSCmini (10 - 700 nm); PM_{10} , $PM_{2.5}$ and PM_{10} measured by Grimm Model 1.108 (0.3 - 20 μm)

^e N_{mean} measured by butanol CPC TSI Model 3775 (4 nm - 1.5 μm); D_p measured by measured by NanoScan SMPS (10-420 nm)

As described previously, the online instruments did not seem able to accurately detect SWCNT release during collection chamber openings (both while using and without using LEV; exposure scenario #1 and #2) or during cleaning operations performed under pressure with wet wipes (exposure scenario #3), where SWCNT were potentially released. This suggests that the detection of SWCNT was limited probably due to the instruments' response to nanofibers, and therefore that the exposure concentrations reported above are probably underestimated. The results of this study suggest that the online instrumentation could be detecting SWCNT as larger particles (> 300 nm), even though further analyses would be necessary to confirm this hypothesis. Although the counting of SWCNT with TEM micrographs was challenging due to high aspect ratio and branching, the analysis of TEM images were able to confirm the presence of SWCNT in workplace air. SWCNT length varied from several micrometers to tens of micrometers. The thickness of SWCNT bundles varied from 10 to 20 nm and a single fibre from 2 to 3 nm. The estimated concentrations

varied between 1.7×10^{-3} - $5.6 \text{ SWCNT cm}^{-3}$, depending on the process. The highest SWCNT counts were seen during the worst case scenario where SWCNT were collected without LEV (exposure scenario #2; 8 min of exposure = $5.6 \text{ SWCNT cm}^{-3}$). This study concluded that the collection and analysis of SWCNT on TEM grids was the only direct method to detect SWCNT release in workplace air. Therefore, the development of new methods to accurately characterise the exposure of this type of fibres are required. For example, in this particular study, CO was used as a tracer gas to detect fugitive emissions of SWCNT, even though correlation between CO concentrations and SWCNT concentrations was not found due to the low SWCNT concentrations detected in workplace air.

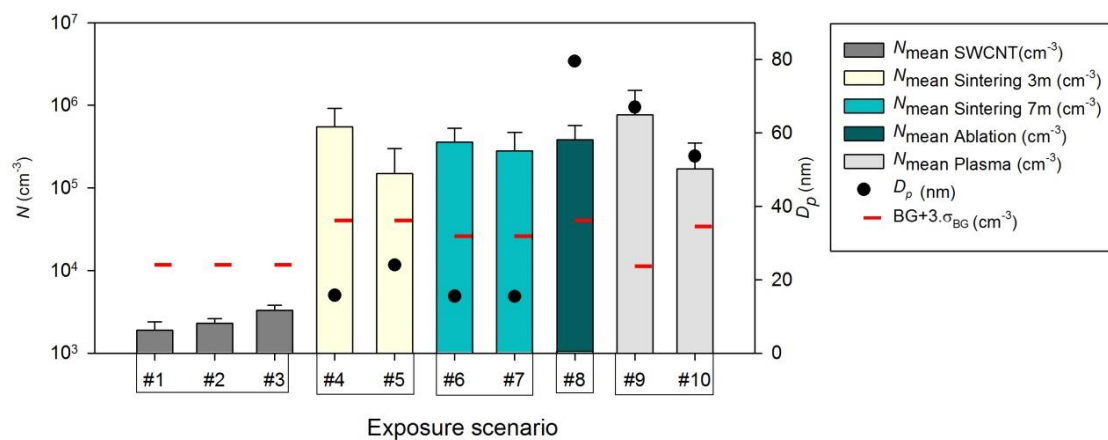


Figure 5.6 Particle number concentrations (N_{mean}) and mean particle diameter (D_p) measured in the breathing zone for each of the exposure scenarios analysed, as well as the significance level of particle exposure during each activity ($BG+3\sigma_{BG}$; Asbach et al., 2012b). The left and right y-axis refer to the N_{mean} and mean D_p , respectively. Error bars above the box indicate the standard deviation (σ).

Major nanoparticle exposures ($> 1.0 \times 10^5 \text{ cm}^{-3}$) were registered in the worker breathing zone during high-energy laser processes such as tile sintering and ablation (exposure scenarios from # 4 to #8) and especially during atmospheric plasma spraying (exposure scenarios #9 and #10) reaching a maximum of $2.7 \times 10^6 \text{ cm}^{-3}$. The unexpectedly high exposure concentrations monitored during atmospheric plasma spraying gave rise to the implementation of a risk prevention protocol aiming to reduce worker exposure to such particle number concentrations. The effectiveness of the risk prevention protocol was evaluated in scenario #10 (plasma spraying after the implementation of mitigation measures), which included: (i) forced ventilation in the breathing zone (by increasing > 12 air changes per hour); (ii) enhanced the sealing of the exhaust fume extraction system; and (iii) implemented new chamber-opening protocol. Nanoparticle concentrations monitored after the implementation of the mitigation measures (exposure scenario #10) proved their effectiveness, with a

decrease in particle concentrations by 78% (from 7.7×10^5 up to $1.7 \times 10^5 \text{ cm}^{-3}$). However, these levels are still considered high when compared to the NRV and thus, improvements in these strategies should be proposed and tested specifically for this environment, tailored to its needs.

When looking at the ceramic tile sintering scenarios (#4 to #7), both in the industrial- and laboratory-scale pilot plants (Articles II and III), results show that breathing zone N_{mean} were lowest for red clay materials. This has relevant exposure implications, given that even though red clay materials are the most frequently used in the industry due to their lower cost, the use of porcelain materials (with higher exposure concentrations) is increasing largely due to aesthetic reasons. The decrease in exposure concentrations at industrial pilot plant scale when compared to the laboratory-scale conditions (exposure scenario #4 vs. #6; Table 5.2 and Figure 5.6) was probably related to the higher gas flow inside the industrial-scale furnace and also to the size of the facility (mainly, the distance between the emission source and the breathing zone, which favoured nanoparticle dispersion and agglomeration). As shown in Table 5.2 and Figure 5.6, exposure to PGNP during tile sintering was statistically significant and reached exposure concentrations which were highly relevant in terms of particle number concentration (N_{mean} up to $5.5 \times 10^5 \text{ cm}^{-3}$). It is important to highlight that nanoparticle formation and release during sintering was consistent over time and detected systematically during all the experiments carried out.

With regard to particle diameter, the smallest mean diameters detected during all of the exposure scenarios were those monitored during laser sintering activities ($D_p < 24 \text{ nm}$), which were in addition markedly finer than those from background air particles ($D_p > 33.9 \pm 5.5 \text{ nm}$), influenced by vehicular traffic emissions (with a high percentage of diesel) in the surroundings of the laboratory or pilot plant scale furnaces. The result of higher N_{mean} with a lower particle size detected in these type of industrial activities suggest the occurrence of new particle formation processes by nucleation (nanoparticles $\leq 30 \text{ nm}$ in diameter being formed; Kulmala *et al.*, 2004; Kumar *et al.*, 2008). Nucleation processes from gaseous precursors were probably induced by the cooling down of exhaust gases containing SO_2 emitted from the thermal decomposition of S-bearing minerals present in the ceramic tiles (e.g., anhydrite, CaSO_4 , Figure 5.7b), which decomposes at high temperatures (Chinchón *et al.*, 1991). Results suggest that nucleation events occurred for both types of ceramic materials (red clay and porcelain) and in both furnaces (industrial and laboratory scale) during the thermal treatment, and that this process was independent of the laser treatment. Actually, the incidence of the laser seemed to

inhibit new particle formation processes, possibly due to the sealing of the tile surface by the laser. Detailed explanations of emission patterns observed for each material are described in the results chapter (Article II and III). TEM-EDX analyses of the samples show a large number of spherical ultrafine particles ranging from 10 nm - 1 μm in diameter which may be interpreted as portions of melted material involved in the tile melting processes. Particle condensation and/or agglomeration of existing finer nanoparticles (10 - 30 nm in size diameter) from nucleation process were also identified by the large amount of agglomerated particles observed by TEM (Figures 5.7c and d).

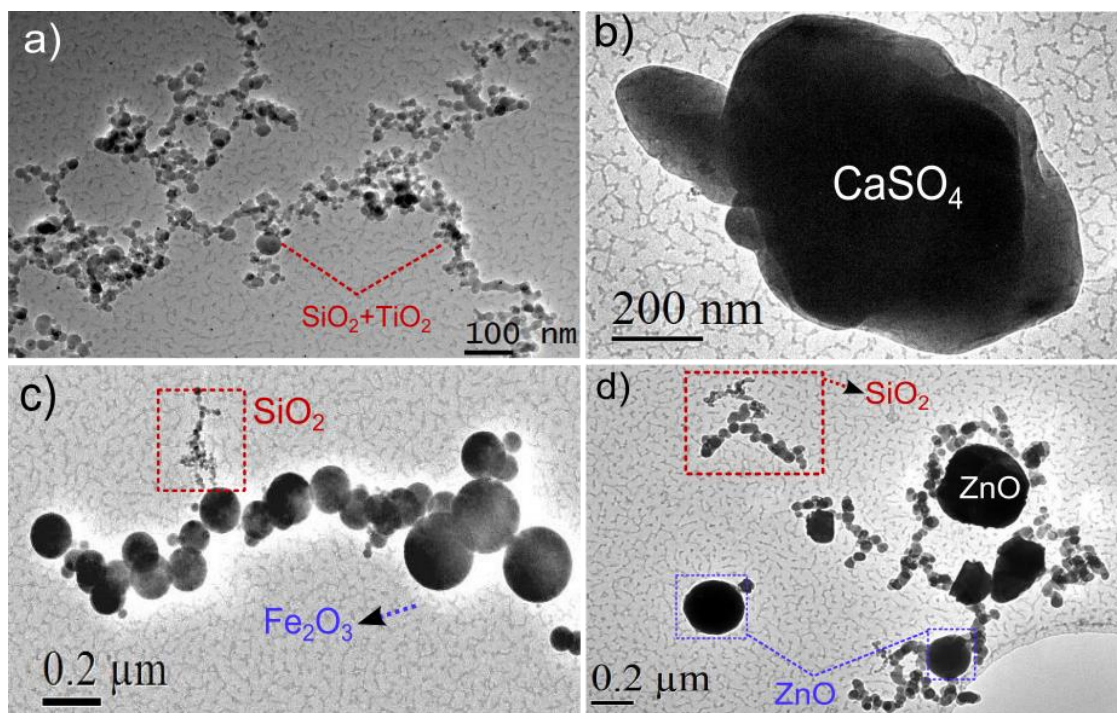


Figure 5.7. TEM images of nanoparticles collected in indoor air during high-energy processes: a) ablation of raw porcelain; b); c); and d) tile sintering of red clay. Corresponding identified particles by TEM-EDX are shown in each image.

Finally, worker exposure was assessed using particle mass concentration as a more effective metric during tile ablation, due to the coarser diameter of the particles emitted (Table 5.2). As in the case of N , PM concentrations in the breathing zone were consistently higher than in background air. Maximum mean concentrations registered were $608 \mu\text{g m}^{-3}$; $650 \mu\text{g m}^{-3}$ and $673 \mu\text{g m}^{-3}$ for PM_1 , $PM_{2.5}$ and PM_{10} , respectively, for porcelain ablation (exposure scenario #8). Coarser particle diameters were expected to occur due to the fact that laser engraving induces phase transitions, causing catastrophic break down of the original material (Lahoz *et al.*, 2011). Overall, particles in the nanoparticle size range ($D_p = 79.5 \pm 26.6 \text{ nm}$) were released into workplace air but TEM-EDX analyses confirmed the prevalence of

coarse particles (agglomerates, coarse size) in workplace air during laser tile ablation (Figure 5.7a) which were markedly larger than those from background air particles ($D_p = 33.9 \pm 5.5$ nm).

Overall, nano-sized particles ($D_p \leq 100$ nm) were generated and emitted into workplace air on a statistically significant level ($> BG+3.\sigma_{BG}$) during all of the processes evaluated (with the exception of SWCNT manufacturing; exposure scenarios #1 to #3). These results imply that the exposures monitored may result in potential health-hazards for the workers, based on the nanoGEM standard operation procedures for assessing exposure to nanomaterials (Asbach *et al.*, 2012b). On average, N_{mean} concentrations during these non-intentional nanoparticle release processes were 1 order of magnitude higher than background concentrations, in terms of particle number concentration.

5.2.2 Comparison of worker exposure concentrations with exposure limits

For the comparison between the exposure concentrations monitored and exposure limits available in current regulations, nanoparticles generated from tile sintering (#4 to #7), ablation (#8), and atmospheric plasma spraying processes (#9 and #10) (generally metal oxides) were considered as substances with a density $< 6 \times 10^3$ kg m⁻³ (low-density biopersistent granular nanomaterials) which is assigned a NRV of 4×10^4 cm⁻³ (SER, 2012). As for SWCNT released from exposure scenarios #1 to #3, these were considered as rigid, biopersistent nanofibers for which effects similar to those of asbestos are not excluded and consequently they were compared with the NRV of 1.0×10^{-2} fibers cm⁻³ (SER, 2012) and the REL of $1 \mu\text{g m}^{-3}$ established by NIOSH (2013) for CNT and nanofibers. All the NRV and the REL are 8-h TWA concentrations.

In terms of mass concentration, the only limits available are those established by ACGIH (2013) and the OSHA (2006). These institutions set a PEL for 8-h TWA of 5 mg m^{-3} (OSHA, 2006) and of 3 mg m^{-3} (TLV, 8-h TWA concentration) for respirable particles (PM₁₀; ACGIH, 2013).

Table 5.3 represents the background-corrected 8-h TWA worker exposure to N and M concentrations (by Eq 4) during each exposure scenario underlying in this PhD thesis.

Table 5.3 Background corrected particle number (N) and mass (M) exposure concentrations obtained for each activity, and comparison with occupational exposure limits.

Exposure scenario	N (cm^{-3})	OEL (cm^{-3})	M_{mean} ($\mu\text{g m}^{-3}$)	PM_1 ($\mu\text{g m}^{-3}$) ^f	$PM_{2.5}$ ($\mu\text{g m}^{-3}$) ^f	PM_{10} ($\mu\text{g m}^{-3}$) ^f	OEL ($\mu\text{g m}^{-3}$)
#1	1.7×10^{-3} ^a		2.14×10^{-5} ^c				
#2	5.6×10^{-3} ^a	1.0×10^{-2} ^b	20.5 ^d		N/A		1.0 ^e
#3	6.0×10^{-3} ^a		1.6 ^d				
#4	4.7×10^5 ^g		N/A	1.9 ^g	2.8 ^g	4.3 ^g	
#5	1.2×10^5 ^g	4.0×10^4 ^b		2.2 ^g	3.5 ^g	5.2 ^g	3.0×10^3 ^h
#6	3.1×10^5 ^g		N/A	2.1 ^g	6.6 ^g	34.0 ^g	
#7	2.4×10^5 ^g		N/A	0.4 ^g	1.1 ^g	6.8 ^g	
#8	3.7×10^{5i}	8.0×10^{4j}	N/A	6.0×10^{2i}	6.4×10^{2i}	6.6×10^{2i}	3.0×10^{3h}
#9	7.6×10^{5i}	8.0×10^{4j}	N/A	N/A	N/A	N/A	
#10	1.5×10^{5i}		N/A	N/A	N/A	N/A	

^a Estimated by TEM counting

^b NRV; SER (2012)

^c Calculated by N assuming SWCNT bunch with 20 nm of D_p , 10 μm of length (aspect ratio = 500) and a density of 1 g cm^{-3}

^d Background corrected M_{mean} measured by ELPITM

^e REL; NIOSH (2013)

^f Measured by Grimm Model 1.108

^g 8-h TWA concentrations calculated by Eq (4) considering an equivalent workers exposure of 7h working shift during sintering activity and 1h working shift during non-activity period

^h TLV; ACGIH, (2013)

ⁱ Background corrected concentrations for the corresponding time of activity

^j NRV_{15-min} TWA defined in Eq (3)

According to the exposure scenarios involving ENP, the estimated concentration of $5.6 \text{ SWCNTs cm}^{-3}$ exceeded the personal exposure limit of $1.0 \times 10^{-2} \text{ fibres cm}^{-3}$ only during SWCNT manufacturing in the worst case scenario (without LEV, #2). An exceedance of the REL of $1 \mu\text{g m}^{-3}$ proposed by NIOSH (2013) was also detected during this exposure scenario as well as during the reactor cleaning operation (#3). It should be noted that, whereas scenario #2 represents a case of malfunctioning mitigation tools (e.g., the LEV) and it is not expected to occur on a regular basis in the workplace, scenario #3 (reactor cleaning operation) is a standard procedure which is carried out on a regular basis in the workplace under study.

In the case of tile sintering, considering that the workers were exposed to nanoparticle concentrations during a 7h working shift (plus 1h with no activity in the furnace), the calculated $N_{8-h \text{ TWA}}$ exposure concentrations were in the range of $1.2 \times 10^5 \text{ cm}^{-3}$ and $4.7 \times 10^5 \text{ cm}^{-3}$. This outcome exceeded broadly the NRV established by the SER (2012) (Table 5.3). In terms of mass, the 3 mg m^{-3} TLV for the total respirable fraction would not have been exceeded during any exposure scenario given that the PM_{10} for 8-h TWA would be in the range of $5\text{--}34 \mu\text{g m}^{-3}$, if #8 scenario is excluded ($660 \mu\text{g m}^{-3}$).

Finally, similarly to the sintering activities described above, the ablation process (#8) and atmospheric plasma spraying (#9 and #10) generated particle emissions which resulted in exposure concentrations exceeding the short-term $NRV_{15\text{min-TWA}}$ as defined by Eq (3) (assuming a $NRV_{8\text{-h TWA}}$ of $4 \times 10^4 \text{ cm}^{-3}$). Also similarly to sintering activities, exposure concentrations lower than the 3 mg m^{-3} TLV set by ACGIH (2013) were obtained during tile ablation.

5.3 Mitigation strategies

A potential risk of worker exposure to nanoparticles was identified in all of the industrial settings evaluated (dealing with ENP and with PGNP), despite the mitigation measures in place (mainly, LEV systems).

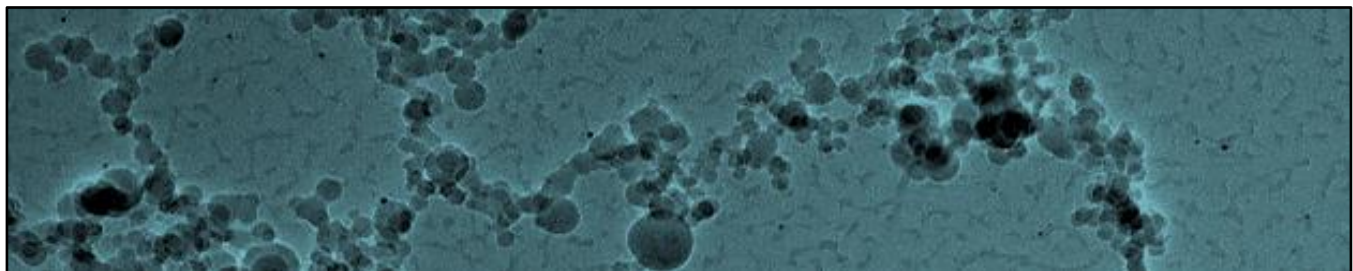
When dealing with ENP, applying adequate mitigation strategies is complex given the frequently low emission concentrations registered in workplaces, as shown in Article I. Discrimination of ENP from background aerosols presents currently major limitations, as discussed in previous sections. In addition, online instrumentation is still unable to deal adequately with high aspect ratio particles (e.g., fibres, Article I). Therefore, assessing the efficiency of strategies to mitigate ENP release, which focus mainly on local exhaust ventilation systems, is complex under real-world scenarios such as the ones evaluated in this PhD thesis. The assessment carried out in exposure scenario #2 showed that an improper performance of the mitigation measure in place (LEV system) can result in exceedances of occupational exposure limit values. Hence, the operation of the LEV in industries dealing with fibres should be systematically verified. Correct application of LEV to the collection chambers was found to reduce CO and SWCNT emissions by approximately 95 % and 98 %, respectively.

When dealing with PGNP from high-energy processes, on the other hand, the interference of background aerosols becomes less relevant due to the frequently high concentrations recorded. Therefore, mitigation strategies appear to be easier to be implemented in industries dealing with high-energy processes (e.g., exposure scenarios #4 - #10). As an example, in the case of atmospheric plasma spraying (exposure scenarios #9 and #10), specific mitigation strategies not already in place were proposed and implemented in the framework of this PhD thesis based on increased ventilation in breathing zone, enhanced the sealing of the exhaust fume extraction system and implementation of a new chamber-opening protocol which resulted in a marked decrease (78%) in exposure concentrations in the worker breathing zone. However, the identification and chemical characterisation of PGNP is highly complex due to their (frequently) secondary nature and non-specificity of

nanoparticle types and sources. Sampling of PGNP for subsequent quantitative chemical analysis is hindered by their low mass in comparison to background aerosols, and as a result, only qualitative characterization is possible by microscopy tools (e.g., TEM or SEM). This implies the inability to carry out toxicological assessments for this kind of particles, which constitutes a major knowledge gap, and which are relatively available for ENP. Hence, the development of mitigation strategies and systematic approaches towards better identifying the processes and sources of PGNP are recommended to enable risk assessments and to reduce worker exposure.

Additionally, the effectiveness of already existing mitigation strategies was also tested in the tile sintering facility (exposure scenarios #6 and #7). In this case, a HEPA filtration system was in place in the tile sintering facility when the nanoparticle exposure measurement campaigns took place, but its effectiveness with regard to nanoparticle collection had not been previously assessed. As discussed in Article III, the efficiency of the filtration system was successfully tested, evidencing a >87 % efficiency of *N* removal (on a 1-min basis) mostly for nanoparticles < 15 nm whereas it was slightly less efficient for larger particles released during the laser treatment (~30 nm).

Chapter 6. **CONCLUSIONS**



6. CONCLUSIONS

This PhD thesis addressed the detection and exposure assessment of nanoparticles emitted in workplaces during ENP (SWCNT) manufacturing and application processes, as well as during unintentional nanoparticle release scenarios (emission of PGNP) which do not involve ENP as input materials (tile ablation and sintering with laser technologies, and atmospheric plasma spraying in the ceramic industry). In addition, possible particle transformations, the potential for particle release to the outdoor environment, and the effectiveness of control measures were assessed. Following the structure of the discussion chapter, the main conclusions that were extracted from this work can be divided in three sections:

(i) Performance of nanoparticle monitoring instrumentation

- **NanoScan SMPS TSI 3910:** the assessment of the novel portable SMPS regarding its application in workplace exposure studies revealed that the results from this instrument are dependent on particle size, morphology, composition and concentration. Different charge levels acquired by the particles in the unipolar charger might be the reason of this dependence. Although the NanoScan is known to provide higher time resolution analysis than the stationary SMPSs, it could be considered slow in certain specific microenvironments but it can be a useful instrument to obtain estimates of the size distribution in workplace air. Due to its portability, it is a valid tool for simplified exposure assessment, such as in Tier 2. However, its accuracy should not be overestimated. While the sizing accuracy was mostly within $\pm 25\%$, measured total concentrations in some cases deviated by more than 50% (especially for agglomerated particles). For Tier 3 exposure assessments, conventional and stationary SMPS instruments are still the preferred choice.
- **Cascade impactors for nanoparticle sampling:** the performance of cascade impactors for sampling of nano-scale aerosols was assessed. Physical and chemical processes such as particle volatilisation and particle bounce were identified as playing a major role in the collection efficiency and in the aerosol size distribution by the impactors evaluated. Results were mostly comparable between the two BLPI impactors tested. Particle sampling with portable PCIS impactors did not provide comparable results for the ultrafine and nanoparticle fraction (<250 nm) with regard to other impactors. As for the nano-Moudi impactor, results evidenced differences regarding particle mass concentrations which may have occurred due to the internal rotating mechanisms and the

electric current in the sensor board of nano-Moudi, which heat the impactor casing up and induce aerosol volatilization. Specific recommendations were extracted, including greasing of the impactor collection substrates.

- **Online instrumentation for monitoring of nanofiber concentrations:** detection of high aspect ratio particles (e.g., SWCNT) using current online instrumentation appears to be highly complex. Research is currently underway on especially designed DMA for the selective separation of nanofibers (Prof. K-H Ahn, University of Hanyang, South Korea, pers. com.), but these instruments are still under development. TEM-based methods were identified as the most adequate tool to qualitatively assess exposure to nanofibers in indoor air, given that they allowed for the qualitative detection of airborne nanofibers. However, quantification of these exposures still remains a challenge, both with TEM and online methods.
- **DiSCmini:** the performance of DiSCmini instruments under real-world conditions with regard to particle number concentrations was within the expected uncertainty (10 - 30%). However, under scenarios characterized by high coarse particle (>2.5 μm) concentrations (outside of the instrument's measurement range) the results from this monitor become unreliable, with a higher correlation with particle mass than with particle number concentrations. Under these circumstances, other types of particle monitors (particle mass concentration monitors or CPC) should be the preferred choice.
- **Exposure monitoring strategy:** the multi-metric and multi-instrument approach suggested by Brower et al. (2012) seems to be confirmed as the best available strategy for occupational exposure assessments.

(ii) Nanoparticle exposure scenarios

- In the study where workers' quantitative exposure to SWCNT while manufacturing conductive thin films was assessed, it was found that the conventional production and application of SWCNT showed only very limited nanoparticle emissions into the workplace air, with exposure concentrations below the occupational exposure limits available. However, a failure of the LEV in reactor process may give rise to high airborne nanoparticle concentrations near the worker breathing zone (exceeding the $\text{NRV}_{8\text{-h TWA}}$ concentrations and the REL). During reactor cleaning activities, the REL of $1 \mu\text{g m}^{-3}$ was exceeded (NIOSH, 2013).

- The measurements performed in ceramic industries showed that ENP are not the only source of workplace exposure to nanoparticles. Also important can be the exposure to PGNP. High-thermal processes applied frequently in ceramic industries such as tile sintering, ablation and atmospheric plasma spraying, may give rise to nanoparticle exposure concentrations which are significantly higher than those registered in industries which use ENP as input materials. Nanoparticle exposure concentrations in workplace air during these high-thermal processes were, in addition, statistically significant ($>BG+3\sigma_{BG}$). Thus, the contributions of PGNP to the total nanoparticle workers exposure should not be ignored in risk assessments.
- Because the toxicity of PGNP is not necessarily different from the assumed toxicity of ENP, the comparison of particle exposure concentrations with the available NRV is advisable. Since workers were exposed to concentrations above the NRV ($4 \times 10^4 \text{ cm}^{-3}$), during the high-thermal processes under study, there was a clear evidence of the risk of occupational exposure to nanoparticles. In terms of mass, current regulations set a 3 mg m^{-3} TLV (8-h TWA; ACGIH, 2013) for the total respirable fraction which would not have been exceeded during any process condition. However, the results obtained in terms of particle mass concentration during ablation of ceramic tiles should be highlighted due to the considerably higher concentrations monitored with regard to other exposure scenarios.
- Nanoparticle emission patterns from tile sintering processes were strongly linked to temperature and tile chemical composition, and mainly independent of the laser treatment. New particle formation mechanisms from gaseous precursors occurred for both types of ceramic materials (red clay and porcelain) with nanoparticles $<30 \text{ nm}$ in diameter being formed during the thermal treatment. The incidence of the laser seemed to inhibit new particle formation processes, possibly due to the sealing of the tile surface by the laser.

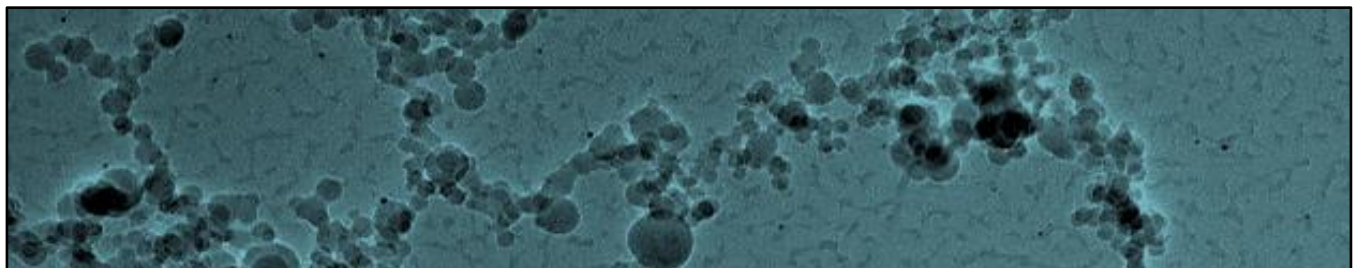
(iii) Mitigation strategies

- The correct application of LEV to the collection chambers in the SWCNT manufacturing facility was found to reduce CO and SWCNT emissions by approximately 95% and 98%, respectively. The operation of the LEV should be systematically verified.
- A specific exposure mitigation protocol was devised and implemented in the plasma spraying facility. It included increased air exchange, delayed door

openings and sealing of the exhaust extraction system. These measures resulted in a quantitative reduction of exposure concentrations in the breathing zone of 78% of particle number concentrations.

- A potential risk for nanoparticle release to the outdoor air was identified, despite the mitigation measures in place (a HEPA filtration system) in the tile sintering facility. The efficiency of the filtration system was successfully tested, evidencing a >87 % efficiency in particle number concentrations removal. However, this efficiency was dependent on particle size. It is recommended that the efficiency of mitigation strategies should be tested for the specific particle sizes under evaluation.

Chapter 7. **LIMITATIONS AND FUTURE RESEARCH NEEDS**



7. LIMITATIONS AND FUTURE RESEARCH NEEDS

From the results of this PhD thesis, the following research needs and potential future lines of research have been identified:

- Industries which have benefited from advances made available through nanotechnology and through innovative industrial processes not only should be safe themselves but should also guarantee human health and environmental protection while still remaining competitive. Therefore, measurements at workplaces under real-world conditions dealing with ENP or PGNP are needed for risk assessment in order to characterise exposure scenarios and exposure pathways of nanoparticle uptake. The large variability encountered in these scenarios also highlights the need for further studies on exposure scenarios.
- In this respect, sampling and characterisation of PGNP in workplace environments is one of the major remaining challenges. Nanoparticles display a wide range of toxicities, with many being perfectly safe and others being harmful to human health or the environment. Although the toxicity of specific ENP is relatively better known, this is unknown for PGNP. To tackle the issues associated with the complex composition of the PGNP (due to their frequently secondary nature and non-specificity of nanoparticle types and sources), validated sampling strategies and assessments on the basis of particle physical/chemical properties should be developed and applied for process-generated nanoparticles. This would enable in addition their toxicological assessment.
- Existing monitoring and sampling instrumentation is faced with a number of major limitations, with regard to real-world exposure assessments. Thus, the development of new and more robust and easy to use, portable real-time instruments is necessary to improve exposure and risk assessment studies. Specific aspects which require improvement are:
 - Particle size: considering that ENPs may present mean diameters as low as 1 nm, instrumentation with a lower cut-off of 10 - 20 nm seems insufficient. Decreasing the lower size detection limit of real-time instruments should be a priority in this field of research.
 - Discrimination of particles by type (e.g. ENP vs. background vs. PGNP): this is a key challenge with regard to quantification of personal exposures, especially in view of health impact assessments. ENPs could be especially targeted with dedicated instrumentation able to carry out this discrimination in

real-time, by focusing on physical or chemical properties of the particle such as density, hygroscopicity, etc.

- Detection of non-spherical particles: as shown in this PhD thesis, the challenge of monitoring high aspect ratio nanoparticles (e.g., SWCNT) still remains. Work should be carried out to improve the performance of particle monitors to enable them to deal with complex non-spherical structures.
- International agreement on particle metric for better description of exposure and better links with the biological response (i.e., toxicity) is needed for occupational exposure studies. At present, the best approach still seems to be based on the combination of multiple parameters and metrics.
- Similarly, dedicated regulation should be developed for the metrics identified as best representing worker exposure (e.g., particle number concentration, chemical composition, etc.). A revision of the existing limit values, based on particle mass concentrations for 8-h TWA (5 mg m^{-3} by OSHA, 2006 and 3 mg m^{-3} by ACGIH, 2013), would be advisable given the current development of certain industrial processes which tend to generate higher particle emissions in terms of particle number concentration (as opposed to mass). A review and decrease of the current limit value in terms of mass would also be advisable.
- Future research on exposure scenarios dealing with ENP and PGNP will hopefully contribute to epidemiological studies which are so far lacking inputs from the nanoparticle monitoring scientific community. The outcome of epidemiological studies will be highly relevant to establish and evaluate threshold limit values such as OEL values in occupational settings for workers.
- Exposure and risk assessment tools (risk/control banding tools) should be tested and validated for nano-sized particles, in order to identify potential hot spots for risk and to enable straightforward interpretation of the exposure scenarios. This type of tool is already in use for micro-scaled particles.
- Modelling tools to describe the dispersion and transformation of nanoparticles in the workplace should be validated with experimental measurements to a) assess locations of maximal exposures, and b) to develop and plan safe working environments.
- Life-cycle considerations should be integrated into risk assessments, i.e., assessment of potential environmental impacts of nanoparticles focusing on specific environmental compartments such as water or soil where originally airborne nanoparticles might accumulate.

- Taking into account the high level exposure concentrations encountered in ceramic industries, the development and promotion of good practices during innovative processes in the ceramic industry are needed in view of worker protection. It would also be interesting to extend this kind of approach to other types of innovative technologies such as laser-based metal-cutting, welding or micro-abrasion of metallic surfaces (e.g., ships) during maintenance operations.

FUNDING SOURCES

I gratefully acknowledge the funding sources that made my research possible. My PhD was undertaken in the framework of the HEXACOMM project (*Human EXposure to Aerosol Contaminants in Modern Microenvironments*) under grant agreement no. 315760 which is funded by the European Community's Seventh Framework Program "FP-7 People" and is part of the Marie-Curie Action: "Initial Training Networks" (FP7-PEOPLE-2012-ITN).

Additional support was provided by the Finnish Work Environmental Fund (112132, 112133); the National project IMPACT (CGL2011-26574); the Spanish MINECO (PCIN-2015-173-C02-01) under the frame of SIINN, the ERA-NET for a Safe Implementation of Innovative Nanoscience and Nanotechnology, through project CERASAFE (id.:16); LIFE projects AIRUSE (LIFE11 ENV/ES/584), CERAMGLASS (LIFE11 ENV/ES/560) and LASERFIRING (LIFE09 ENV/ES/435); and the European project nanoIndEx which is supported by the French National Funding Agency for Research (ANR), the German Federal Ministry of Education and Research (BMBF, IUTA grant no. 03X0127A), the British Technology Strategy Board (TSB) and the Swiss TEMAS AG, under the frame of SIINN, the ERA-NET for a Safe Implementation of Innovative Nanoscience and Nanotechnology.

A four-months stay in the University of Helsinki was supported the European Cooperation in Science and Technology (COST-STSM-TD1105-14937).

The Institute for Ceramic Technology (ITC) in Castellón is gratefully acknowledged for its support of the experimental campaigns dealing with atmospheric plasma spraying.

REFERENCES

- Abbott, L.C., Maynard, A.D. (2010). Exposure assessment approaches for engineered nanomaterials. *Risk Anal*, 30(11), 1634-1644.
- ACGIH. (2013). Threshold Limit Values for Chemical Substances and Physical Agents and Biological Exposure Indices. American Conference of Governmental Industrial Hygienists.
- Adlakha-Hutcheon, G., Khaydarov, R., Korenstein, R., Varma, R., Vaseashta, A., Stamm, H., Abdel-Mottaleb, M. (2009). Nanomaterials, Nanotechnology. In I. Linkov & J. Steevens (Eds.), *Nanomaterials: Risks and Benefits* (pp. 195-207). Dordrecht: Springer Netherlands.
- Agarwal, J.K., Sem, G.J. (1980). Continuous flow, single-particle-counting condensation nucleus counter. *Journal of Aerosol Science*, 11(4), 343-357. doi: [http://dx.doi.org/10.1016/0021-8502\(80\)90042-7](http://dx.doi.org/10.1016/0021-8502(80)90042-7)
- Aitken, R.J., Chaudhry, M.Q., Boxall, A.B., Hull, M. (2006). Manufacture and use of nanomaterials: current status in the UK and global trends. [Research Support, Non-U S Gov't Review]. *Occup Med*, 56(5), 300-306.
- Aitken, R.J., Creely, K.S., Tran, C.L. (2004). Nanoparticles: an occupational hygiene review. HSE Research Report 274. United Kingdom: Health & Safety Executive.
- Allen, A.G., Harrison, R.M., Erisman, J.-W. (1989). Field measurements of the dissociation of ammonium nitrate and ammonium chloride aerosols. *Atmospheric Environment* (1967), 23(7), 1591-1599. doi: [http://dx.doi.org/10.1016/0004-6981\(89\)90418-6](http://dx.doi.org/10.1016/0004-6981(89)90418-6)
- Almeida, S.M., Canha, N., Silva, A., Freitas, M.d.C., Pegas, P., Alves, C., Evtugina, M., Pio, C.A. (2011). Children exposure to atmospheric particles in indoor of Lisbon primary schools. *Atmospheric Environment*, 45(40), 7594-7599. doi: <http://dx.doi.org/10.1016/j.atmosenv.2010.11.052>
- Alzona, J., Cohen, B.L., Rudolph, H., Jow, H.N., Frohlinger, J.O. (1979). Indoor-outdoor relationships for airborne particulate matter of outdoor origin. *Atmospheric Environment* (1967), 13(1), 55-60. doi: [http://dx.doi.org/10.1016/0004-6981\(79\)90244-0](http://dx.doi.org/10.1016/0004-6981(79)90244-0)
- Asbach, C., Fissan, H., Kaminski, H., Kuhlbusch, T.A.J., Pui, D.Y.H., Shin, H., Horn, H.G., Hase, T. (2011). A low pressure drop pre-separator for elimination of particles larger 450nm. *Aerosol & Air Quality Research*, 11, 487-496.
- Asbach, C., Kaminski, H., Beckmann, S., Monz, C., Dahmann, D., Fierz, M., Clavaguera, S., Faure, B., Dziurawicz, N., Meyer-Plath, A., Simonow, B., Iavicoli, I., Fontana, L., Fonseca, A.S., Viana, M., Todea, A.M. (2015). *Field Applicability of Personal Monitors for Assessing Worker Exposure to Airborne Nanomaterials*. Paper presented at the European Aerosol Conference 2015, Italy, Milan (2015).
- Asbach, C., Kaminski, H., Fissan, H., Monz, C., Dahmann, D., Mülhopt, S., Paur, H., Kiesling, H., Herrmann, F., Voetz, M., Kuhlbusch, T.J. (2009a). Comparison of four mobility particle sizers with different time resolution for stationary exposure measurements. *J Nanopart Res*, 11(7), 1593-1609. doi: 10.1007/s11051-009-9679-x
- Asbach, C., Kaminski, H., Fissan, H., Monz, C., Dahmann, D., Mülhopt, S., Paur, H.R., Kiesling, H.J., Herrmann, F., Voetz, M., Kuhlbusch, T.A.J. (2009b). Comparison of four mobility particle sizers with different time resolution for stationary exposure measurements. [journal article]. *J Nanopart Res*, 11(7), 1593-1609. doi: 10.1007/s11051-009-9679-x

- Asbach, C., Kaminski, H., von Barany, D., Kuhlbusch, T.A., Monz, C., Dziurawicz, N., Pelzer, J., Vossen, K., Berlin, K., Dietrich, S., Gotz, U., Kiesling, H.J., Schierl, R., Dahmann, D. (2012a). Comparability of portable nanoparticle exposure monitors. [Comparative Study
Research Support, Non-U S Gov't]. *Ann Occup Hyg*, 56(5), 606-621.
- Asbach, C., Kuhlbusch, T., Kaminski, H., Stahlmecke, B., Plitzko, S., Götz, U., Voetz, M., Kiesling, H.J., Dahmann, D. (2012b). NanoGEM Standard Operation Procedures for assessing exposure to nanomaterials, following a tiered approach.
- Asbach, C., Kuhlbusch, T.A.J., Stahlmecke, B., Kaminski, H., Kiesling, H.J., Voetz, M., Dahmann, D., Götz, U., Dziurawicz, N., Plitzko, S. (2014). *Measurement and monitoring strategy for assessing workplace exposure to airborne nanomaterials*: Taylor & Francis.
- Asmi, A., Wiedensohler, A., Laj, P., Fjaeraa, A.M., Sellegri, K., Birmili, W., Weingartner, E., Baltensperger, U., Zdimal, V., Zikova, N., Putaud, J.P., Marinoni, A., Tunved, P., Hansson, H.C., Fiebig, M., Kivekäs, N., Lihavainen, H., Asmi, E., Ulevicius, V., Aalto, P.P., Swietlicki, E., Kristensson, A., Mihalopoulos, N., Kalivitis, N., Kalapov, I., Kiss, G., de Leeuw, G., Henzing, B., Harrison, R.M., Beddows, D., O'Dowd, C., Jennings, S.G., Flentje, H., Weinhold, K., Meinhardt, F., Ries, L., Kulmala, M. (2011). Number size distributions and seasonality of submicron particles in Europe 2008–2009. *Atmos. Chem. Phys.*, 11(11), 5505-5538. doi: 10.5194/acp-11-5505-2011
- Atkinson, R.W., Anderson, H.R., Sunyer, J., Ayres, J., Baccini, M., Vonk, J.M., Boumghar, A., Forastiere, F., Forsberg, B., Touloumi, G., Schwartz, J., Katsouyanni, K. (2001). Acute effects of particulate air pollution on respiratory admissions: results from APHEA 2 project. Air Pollution and Health: a European Approach. [Research Support, Non-U S Gov't]. *Am J Respir Crit Care Med*, 164(10 Pt 1), 1860-1866.
- Atkinson, R.W., Mills, I.C., Walton, H.A., Anderson, H.R. (2015). Fine particle components and health—a systematic review and meta-analysis of epidemiological time series studies of daily mortality and hospital admissions. [Original Article]. *J Expos Sci Environ Epidemiol*, 25(2), 208-214. doi: 10.1038/jes.2014.63
- Azarmi, F., Kumar, P., Mulheron, M. (2014). The exposure to coarse, fine and ultrafine particle emissions from concrete mixing, drilling and cutting activities. *Journal of Hazardous Materials*, 279, 268-279. doi: <http://dx.doi.org/10.1016/j.jhazmat.2014.07.003>
- Balas, F., Arruebo, M., Urrutia, J., Santamaria, J. (2010). Reported nanosafety practices in research laboratories worldwide. [10.1038/nano.2010.1]. *Nat Nano*, 5(2), 93-96. doi: http://www.nature.com/nano/journal/v5/n2/suppinfo/nano.2010.1_S1.html
- Barcikowski, S., Bärsch, N., Ostendorf, A. (2007). Generation of Nano-Particles During Laser Ablation – Risk Assessment of Non-beam Hazards During Laser Cleaning. In J. Nimmrichter, W. Kautek & M. Schreiner (Eds.), *Lasers in the Conservation of Artworks* (Vol. 116, pp. 631-640): Springer Berlin Heidelberg.
- Baron, P.A., Willeke, K. (2001). *Aerosol measurement: principles, techniques, and applications*: Wiley.
- Bäuerle, D. (1996). *Laser Processing and Chemistry*: Springer-Verlag, Berlin.
- Beddows, D.C.S., Dall'Osto, M., Harrison, R.M., Kulmala, M., Asmi, A., Wiedensohler, A., Laj, P., Fjaeraa, A.M., Sellegri, K., Birmili, W., Bukowiecki, N., Weingartner, E., Baltensperger, U., Zdimal, V., Zikova, N., Putaud, J.P., Marinoni, A., Tunved, P., Hansson, H.C., Fiebig, M., Kivekäs, N., Swietlicki, E., Lihavainen, H., Asmi, E., Ulevicius, V., Aalto, P.P., Mihalopoulos, N., Kalivitis, N., Kalapov, I., Kiss, G., de Leeuw, G., Henzing, B., O'Dowd, C., Jennings, S.G., Flentje, H., Meinhardt, F., Ries, L., Denier van der Gon, H.A.C., Visschedijk, A.J.H. (2014). Variations in tropospheric submicron particle size distributions across

- the European continent 2008–2009. *Atmos. Chem. Phys.*, 14(8), 4327-4348. doi: 10.5194/acp-14-4327-2014
- Bello, D., Hart, A.J., Ahn, K., Hallock, M., Yamamoto, N., Garcia, E.J., Ellenbecker, M.J., Wardle, B.L. (2008a). Particle exposure levels during CVD growth and subsequent handling of vertically-aligned carbon nanotube films. *Carbon*, 46(6), 974-977. doi: <http://dx.doi.org/10.1016/j.carbon.2008.03.003>
- Bello, D., Wardle, B.L., Yamamoto, N., Guzman deVilloria, R., Garcia, E.J., Hart, A.J., Ahn, K., Ellenbecker, M.J., Hallock, M. (2008b). Exposure to nanoscale particles and fibers during machining of hybrid advanced composites containing carbon nanotubes. [journal article]. *J Nanopart Res*, 11(1), 231-249. doi: 10.1007/s11051-008-9499-4
- Bello, D., Wardle, B.L., Zhang, J., Yamamoto, N., Santeufemio, C., Hallock, M., Virji, M.A. (2010). Characterization of exposures to nanoscale particles and fibers during solid core drilling of hybrid carbon nanotube advanced composites. [Research Support, Non-U S Gov't
- Research Support, U S Gov't, Non-P H S]. *Int J Occup Environ Health*, 16(4), 434-450.
- Bémer, D., Régnier, R., Subra, I., Sutter, B., Lecler, M.T., Morele, Y. (2010). Ultrafine Particles Emitted by Flame and Electric Arc Guns for Thermal Spraying of Metals. *Annals of Occupational Hygiene*, 54(6), 607-614. doi: 10.1093/annhyg/meq052
- Bennett, D.H., Koutrakis, P. (2006). Determining the infiltration of outdoor particles in the indoor environment using a dynamic model. *Journal of Aerosol Science*, 37(6), 766-785. doi: <http://dx.doi.org/10.1016/j.jaerosci.2005.05.020>
- Berner, A., Luerzer, C. (1980). Mass size distributions of traffic aerosols at Vienna. *The Journal of Physical Chemistry*, 84(16), 2079-2083. doi: 10.1021/j100453a016
- Berner, A., Lürzer, C., Pohl, F., Preining, O., Wagner, P. (1979). The size distribution of the urban aerosol in Vienna. *Science of The Total Environment*, 13(3), 245-261. doi: [http://dx.doi.org/10.1016/0048-9697\(79\)90105-0](http://dx.doi.org/10.1016/0048-9697(79)90105-0)
- Bhangar, S., Mullen, N.A., Hering, S.V., Kreisberg, N.M., Nazaroff, W.W. (2011). Ultrafine particle concentrations and exposures in seven residences in northern California. [Research Support, U S Gov't, Non-P H S]. *Indoor Air*, 21(2), 132-144.
- Biskos, G., Mastorakos, E., Collings, N. (2004). Monte-Carlo simulation of unipolar diffusion charging for spherical and non-spherical particles. *Journal of Aerosol Science*, 35(6), 707-730. doi: <http://dx.doi.org/10.1016/j.jaerosci.2003.11.010>
- Biswas, P., Wu, C.Y. (2005). Nanoparticles and the environment. [Research Support, Non-U S Gov't
- Research Support, U S Gov't, Non-P H S
- Review]. *J Air Waste Manag Assoc*, 55(6), 708-746.
- Bordado, J.C., Gomes, J.F., Albuquerque, P.C. (2012). Exposure to airborne ultrafine particles from cooking in Portuguese homes. *J Air Waste Manag Assoc*, 62(10), 1116-1126.
- Borm, P.J.A., Robbins, D., Haubold, S., Kuhlbusch, T., Fissan, H., Donaldson, K., Schins, R., Stone, V., Kreyling, W., Lademann, J., Krutmann, J., Warheit, D., Oberdorster, E. (2006). The potential risks of nanomaterials: a review carried out for ECETOC. *Particle and Fibre Toxicology*, 3, 11-11. doi: 10.1186/1743-8977-3-11
- Bozlaker, A., Prospero, J.M., Fraser, M.P., Chellam, S. (2013). Quantifying the Contribution of Long-Range Saharan Dust Transport on Particulate Matter Concentrations in Houston, Texas, Using Detailed Elemental Analysis. *Environmental Science & Technology*, 47(18), 10179-10187. doi: 10.1021/es4015663

- Braniš, M., Šafránek, J. (2011). Characterization of coarse particulate matter in school gyms. [Research Support, Non-U S Gov't]. *Environ Res*, 111(4), 485-491.
- Brines, M., Dall'Osto, M., Beddows, D.C.S., Harrison, R.M., Gómez-Moreno, F., Núñez, L., Artíñano, B., Costabile, F., Gobbi, G.P., Salimi, F., Morawska, L., Sioutas, C., Querol, X. (2015). Traffic and nucleation events as main sources of ultrafine particles in high-insolation developed world cities. *Atmos. Chem. Phys.*, 15(10), 5929-5945. doi: 10.5194/acp-15-5929-2015
- Brouwer, D. (2010). Exposure to manufactured nanoparticles in different workplaces. *Toxicology*, 269(2-3), 120-127.
- Brouwer, D., Berges, M., Virji, M.A., Fransman, W., Bello, D., Hodson, L., Gabriel, S., Tielemans, E. (2012). Harmonization of measurement strategies for exposure to manufactured nano-objects; report of a workshop. [Comment Research Support, Non-U S Gov't]. *Ann Occup Hyg*, 56(1), 1-9.
- Brouwer, D., van Duuren-Stuurman, B., Berges, M., Jankowska, E., Bard, D., Mark, D. (2009). From workplace air measurement results toward estimates of exposure? Development of a strategy to assess exposure to manufactured nano-objects. *J Nanopart Res*, 11(8), 1867-1881. doi: 10.1007/s11051-009-9772-1
- Brouwer, D.H. (2012). Control Banding Approaches for Nanomaterials. *Annals of Occupational Hygiene*, 56(5), 506-514.
- BSI. (2010). (BSI PD 6699-3:2010) Nanotechnologies—part 3: guide to assessing airborne exposure in occupational settings relevant to nanomaterials. London, UK: British Standards Institution.
- Buonanno, G., Fuoco, F.C., Morawska, L., Stabile, L. (2013a). Airborne particle concentrations at schools measured at different spatial scales. *Atmospheric Environment*, 67, 38-45. doi: <http://dx.doi.org/10.1016/j.atmosenv.2012.10.048>
- Buonanno, G., Morawska, L., Stabile, L. (2011). Exposure to welding particles in automotive plants. *Journal of Aerosol Science*, 42(5), 295-304. doi: <http://dx.doi.org/10.1016/j.jaerosci.2011.02.003>
- Buonanno, G., Morawska, L., Stabile, L., Viola, A. (2010). Exposure to particle number, surface area and PM concentrations in pizzerias. *Atmospheric Environment*, 44(32), 3963-3969. doi: <http://dx.doi.org/10.1016/j.atmosenv.2010.07.002>
- Buonanno, G., Stabile, L., Morawska, L., Russi, A. (2013b). Children exposure assessment to ultrafine particles and black carbon: The role of transport and cooking activities. *Atmospheric Environment*, 79(0), 53-58. doi: <http://dx.doi.org/10.1016/j.atmosenv.2013.06.041>
- Burkart, J., Steiner, G., Reischl, G., Moshhammer, H., Neuberger, M., Hitzemberger, R. (2010). Characterizing the performance of two optical particle counters (Grimm OPC1.108 and OPC1.109) under urban aerosol conditions. *Journal of Aerosol Science*, 41(10), 953-962. doi: <http://dx.doi.org/10.1016/j.jaerosci.2010.07.007>
- Charron, A., Harrison, R.M. (2003). Primary particle formation from vehicle emissions during exhaust dilution in the roadside atmosphere. *Atmospheric Environment*, 37(29), 4109-4119. doi: [http://dx.doi.org/10.1016/S1352-2310\(03\)00510-7](http://dx.doi.org/10.1016/S1352-2310(03)00510-7)
- Chen, D.R., Pui, D.Y.H., Hummes, D., Fissan, H., Quant, F.R., Sem, G.J. (1998). Design and evaluation of a nanometer aerosol differential mobility analyzer (Nano-DMA). *Journal of Aerosol Science*, 29(5-6), 497-509. doi: [http://dx.doi.org/10.1016/S0021-8502\(97\)10018-0](http://dx.doi.org/10.1016/S0021-8502(97)10018-0)
- Chen, T., Yan, J., Li, Y. (2014). Genotoxicity of titanium dioxide nanoparticles. *Journal of Food and Drug Analysis*, 22(1), 95-104. doi: <http://dx.doi.org/10.1016/j.jfda.2014.01.008>

- Chinchón, J.S., Querol, X., Fernández-Turiel, J.L., López-Soler, A. (1991). Environmental impact of mineral transformations undergone during coal combustion. *Environ Geol Water Sci*, 18(1), 11-15. doi: 10.1007/bf01704573
- Choi, H.S., Ashitate, Y., Lee, J.H., Kim, S.H., Matsui, A., Insin, N., Bawendi, M.G., Semmler-Behnke, M., Frangioni, J.V., Tsuda, A. (2010). Rapid Translocation of Nanoparticles from the Lung Airspaces to the Body. *Nature biotechnology*, 28(12), 1300-1303. doi: 10.1038/nbt.1696
- COM. (2011). *Commission recommendation of 18 October 2011 on the definition of nanomaterial (Text with EEA relevance) (2011/696/EU)*. Retrieved from <http://eur-lex.europa.eu/LexUriServ/LexUriServ.do?uri=OJ:L:2011:275:0038:0040:en:PDF>.
- COM. (2012). *SWD(2012) 288 final. Types and uses of nanomaterials, including safety aspects*. EUROPEAN COMMISSION Retrieved from http://ec.europa.eu/health/nanotechnology/docs/swd_2012_288_en.pdf.
- Cornelissen, R., Jongeneelen, F., van Broekhuizen, P., van Broekhuizen, F. (2011). Guidance working safely with nanomaterials and products, the guide for employers and employees. Document 1113. Amsterdam, The Netherlands: IVAM.
- Costabile, F., Birmili, W., Klose, S., Tuch, T., Wehner, B., Wiedensohler, A., Franck, U., König, K., Sonntag, A. (2009). Spatio-temporal variability and principal components of the particle number size distribution in an urban atmosphere. *Atmos. Chem. Phys.*, 9(9), 3163-3195. doi: 10.5194/acp-9-3163-2009
- Cusack, M., Pérez, N., Pey, J., Wiedensohler, A., Alastuey, A., Querol, X. (2013). Variability of sub-micrometer particle number size distributions and concentrations in the Western Mediterranean regional background. *Tellus B; Vol 65 (2013)*.
- Dahm, M.M., Evans, D.E., Schubauer-Berigan, M.K., Birch, M.E., Deddens, J.A. (2013). Occupational exposure assessment in carbon nanotube and nanofiber primary and secondary manufacturers: mobile direct-reading sampling. *Ann Occup Hyg*, 57(3), 328-344.
- Dahm, M.M., Evans, D.E., Schubauer-Berigan, M.K., Birch, M.E., Fernback, J.E. (2012). Occupational exposure assessment in carbon nanotube and nanofiber primary and secondary manufacturers. [Research Support, Non-U S Gov't]. *Ann Occup Hyg*, 56(5), 542-556.
- de Francisco, I., Lennikov, V.V., Bea, J.A., Vegas, A., Carda, J.B., de la Fuente, G.F. (2011). In-situ laser synthesis of rare earth aluminate coatings in the system Ln-Al-O (Ln = Y, Gd). *Sol State Sci*, 13(9), 1813-1819. doi: <http://dx.doi.org/10.1016/j.solidstatesciences.2011.07.013>
- de la Fuente, G.F. (2013). Laser applications in industry. China University of Geosciences Wuhan, 12 November 2013.
- Dekati. (2010). Electrical Low Pressure Impactor - ELPI, from http://www.exisab.com/Docs/ELPI_training/ELPITheory2010.pdf
- Demou, E., Peter, P., Hellweg, S. (2008a). Exposure to manufactured nanostructured particles in an industrial pilot plant. *Ann Occup Hyg*, 52(8), 695-706.
- Demou, E., Peter, P., Hellweg, S. (2008b). Exposure to Manufactured Nanostructured Particles in an Industrial Pilot Plant. *Annals of Occupational Hygiene*, 52(8), 695-706. doi: 10.1093/annhyg/men058
- Dixkens, J., Fissan, H. (1999). Development of an Electrostatic Precipitator for Off-Line Particle Analysis. *Aerosol Science and Technology*, 30(5), 438-453. doi: 10.1080/027868299304480
- Dockery, D.W., Pope, C.A., 3rd, Xu, X., Spengler, J.D., Ware, J.H., Fay, M.E., Ferris, B.G., Jr., Speizer, F.E. (1993). An association between air pollution and mortality in six U.S. cities. [Research Support, Non-U S Gov't
- Research Support, U S Gov't, Non-P H S
- Research Support, U S Gov't, P H S]. *N Engl J Med*, 329(24), 1753-1759.

- Donaldson, K., Aitken, R., Tran, L., Stone, V., Duffin, R., Forrest, G., Alexander, A. (2006). Carbon Nanotubes: A Review of Their Properties in Relation to Pulmonary Toxicology and Workplace Safety. *Toxicological Sciences*, 92(1), 5-22. doi: 10.1093/toxsci/kfj130
- Donaldson, K., Poland, C.A. (2012). Inhaled nanoparticles and lung cancer - what we can learn from conventional particle toxicology. [Research Support, Non-U S Gov't Review]. *Swiss Med Wkly*, 19(142), 13547.
- Donaldson, K., Seaton, A. (2012). A short history of the toxicology of inhaled particles. [journal article]. *Particle and Fibre Toxicology*, 9(1), 1-12. doi: 10.1186/1743-8977-9-13
- Donaldson, K., Stone, V., Clouter, A., Renwick, L., MacNee, W. (2001). Ultrafine particles. *Occupational and Environmental Medicine*, 58(3), 211-216.
- Donaldson, K., Tran, L., Jimenez, L., Duffin, R., Newby, D., Mills, N., MacNee, W., Stone, V. (2005). Combustion-derived nanoparticles: A review of their toxicology following inhalation exposure. *Particle and Fibre Toxicology*, 2(1), 10.
- Dorizas, P.V., Assimakopoulos, M.-N., Helmis, C., Santamouris, M. (2015). An integrated evaluation study of the ventilation rate, the exposure and the indoor air quality in naturally ventilated classrooms in the Mediterranean region during spring. *Science of The Total Environment*, 502, 557-570. doi: <http://dx.doi.org/10.1016/j.scitotenv.2014.09.060>
- Drexler, K.E. (1986). *Engines of creation: The Coming Era of Nanotechnology*: Anchor Press/Doubleday.
- EC. (1998). *Council Directive 98/24/EC of 7 April 1998 on the protection of the health and safety of workers from the risks related to chemical agents at work (fourteenth individual Directive within the meaning of Article 16(1) of Directive 89/391/EEC)*. OJ L 131, 5.5.1998, p. 11.: Retrieved from <http://eur-lex.europa.eu/LexUriServ/LexUriServ.do?uri=OJ:L:1998:131:0011:0023:EN:P DF>.
- EC. (2004). *Directive 2004/107/EC of the European Parliament and of the Council of 15 December 2004 relating to arsenic, cadmium, mercury, nickel and polycyclic aromatic hydrocarbons in ambient air*. Retrieved from <http://eur-lex.europa.eu/LexUriServ/LexUriServ.do?uri=OJ:L:2005:023:0003:0016:EN:P DF>.
- EC. (2008). *Directive 2008/50/EC of the European Parliament and of the Council of 21 May 2008 on ambient air quality and cleaner air for Europe* Retrieved from <http://eur-lex.europa.eu/legal-content/EN/TXT/PDF/?uri=CELEX:32008L0050&from=en>.
- ECHA. (2015a). Information on chemicals. Registered substances <http://echa.europa.eu/information-on-chemicals/registered-substances> (sited 14.04.2015).
- ECHA. (2015b). Topical Scientific Workshop: Regulatory Challenges in the Risk Assessment of Nanomaterials. Reference: ECHA-15-R-11-EN. Helsinki, Finland: European Chemicals Agency.
- Elder, A., Gelein, R., Silva, V., Feikert, T., Opanashuk, L., Carter, J., Potter, R., Maynard, A., Ito, Y., Finkelstein, J., Oberdörster, G. (2006). Translocation of Inhaled Ultrafine Manganese Oxide Particles to the Central Nervous System. *Environmental Health Perspectives*, 114(8), 1172-1178. doi: 10.1289/ehp.9030
- Estepa, C., Fuente, G.F.d.I. (2006). P 200600560.
- EU-OSHA. (2009). *Workplace Exposure to Nanomaterials*. Bilbao, Spain: European Agency for Safety and Health at Work.
- Evans, D.E., Heitbrink, W.A., Slavin, T.J., Peters, T.M. (2008). Ultrafine and respirable particles in an automotive grey iron foundry. [Research Support, Non-U S Gov't]. *Ann Occup Hyg*, 52(1), 9-21.

- Evans, D.E., Ku, B.K., Birch, M.E., Dunn, K.H. (2010). Aerosol Monitoring during Carbon Nanofiber Production: Mobile Direct-Reading Sampling. *Annals of Occupational Hygiene*, 54(5), 514-531. doi: 10.1093/annhyg/meq015
- Falck, G.C.M., Lindberg, H.K., Suhonen, S., Vippola, M., Vanhala, E., Catalán, J., Savolainen, K., Norppa, H. (2009). Genotoxic effects of nanosized and fine TiO₂. *Human & Experimental Toxicology*, 28(6-7), 339-352.
- Fauchais, P., Heberlein, J.V.R., Boulos, M. (2013). *Thermal Spray Fundamentals. From powder to part*. SPRINGER.
- Feynman, R. (1959). There's plenty of room at the bottom: an invitation to enter a new field of physics. In H.D.E. Gilbert (Ed.), *Miniaturization*. Reinhold, New York.
- Fierz, M. (2010). miniDiSC Application Note #11: Errors Due to the Size Distribution Shape, from <http://fierz.ch/minidisc/pdf/miniDiSCApplicationNote11.pdf>
- Fierz, M., Houle, C., Steigmeier, P., Burtscher, H. (2011). Design, Calibration, and Field Performance of a Miniature Diffusion Size Classifier. *Aerosol Sci Technol*, 45(1), 1-10. doi: 10.1080/02786826.2010.516283
- Fierz, M., Keller, A., Burtscher, H. (2009). Charge-based personal aerosol samplers. *Inhal Toxicol*, 1, 30-34.
- Fissan, H., Helsper, C., Thielen, H.J. (1983). Determination of particle size distribution by means of an electrostatic classifier. *J Aerosol Sci*, 14, 354-357.
- Fissan, H., Hummes, D., Stratmann, F., Büscher, P., Neumann, S., Pui, D.Y.H., Chen, D. (1996). Experimental Comparison of Four Differential Mobility Analyzers for Nanometer Aerosol Measurements. *Aerosol Science and Technology*, 24(1), 1-13. doi: 10.1080/02786829608965347
- Fissan, H., Pöcher, A., Neumann, S., Boulaud, D., Pourprix, M. (1998). Analytical and empirical transfer functions of a simplified spectromètre de mobilité électrique circulaire (SMEC) for nano particles. *Journal of Aerosol Science*, 29(3), 289-293. doi: [http://dx.doi.org/10.1016/S0021-8502\(97\)10014-3](http://dx.doi.org/10.1016/S0021-8502(97)10014-3)
- Fonseca, A.S., Maragkidou, A., Viana, M., Querol, X., Hämeri, K., de Francisco, I., Estepa, C., Borrell, C., Lennikov, V., de la Fuente, G.F. (2016). Process-generated nanoparticles from ceramic tile sintering: Emissions, exposure and environmental release. *Science of The Total Environment*. doi: <http://dx.doi.org/10.1016/j.scitotenv.2016.01.106>
- Fonseca, A.S., Viana, M., Querol, X., Moreno, N., de Francisco, I., Estepa, C., de la Fuente, G.F. (2015a). Ultrafine and nanoparticle formation and emission mechanisms during laser processing of ceramic materials. *Journal of Aerosol Science*, 88, 48-57. doi: <http://dx.doi.org/10.1016/j.jaerosci.2015.05.013>
- Fonseca, A.S., Viana, M., Querol, X., Moreno, N., Francisco, I., Estepa, C., Fuente, G.F. (2015b). Workplace Exposure to Process-Generated Ultrafine and Nanoparticles in Ceramic Processes Using Laser Technology *The Handbook of Environmental Chemistry* (pp. 1-21). Berlin, Heidelberg: Springer Berlin Heidelberg.
- Fonseca, A.S., Viitanen, A.K., Koivisto, A.J., Kangas, A., Huhtiniemi, M., Hussein, T., Vanhala, E., Viana, M., Querol, X., Hameri, K. (2015c). Characterization of exposure to carbon nanotubes in an industrial setting. [Research Support, Non-U S Gov't]. *Ann Occup Hyg*, 59(5), 586-599.
- Friedrichs, S., Schulte, J. (2007). Environmental, health and safety aspects of nanotechnology—implications for the R&D in (small) companies. *Science and Technology of Advanced Materials*, 8(1-2), 12-18. doi: <http://dx.doi.org/10.1016/j.stam.2006.11.020>
- Fromme, H., Twardella, D., Dietrich, S., Heitmann, D., Schierl, R., Liebl, B., Rüdén, H. (2007). Particulate matter in the indoor air of classrooms—exploratory results from Munich and surrounding area. *Atmospheric Environment*, 41(4), 854-866. doi: <http://dx.doi.org/10.1016/j.atmosenv.2006.08.053>
- Fuchs, N.A. (1963). On the stationary charge distribution on aerosol particles in a bipolar ionic atmosphere. *Geofisica Pura e Applicata*, 56(1), 185-193. doi: 10.1007/bf01993343

- Fujitani, Y., Kobayashi, T., Arashidani, K., Kunugita, N., Suemura, K. (2008). Measurement of the physical properties of aerosols in a fullerene factory for inhalation exposure assessment. [Research Support, Non-U S Gov't]. *J Occup Environ Hyg*, 5(6), 380-389.
- GAO. (2014). NANOMANUFACTURING: emergence and Implications for U.S. Competitiveness, the Environment, and Human Health. GAO-14-181SP: United States Government Accountability Office.
- Géhin, E., Ramalho, O., Kirchner, S. (2008). Size distribution and emission rate measurement of fine and ultrafine particle from indoor human activities. *Atmospheric Environment*, 42(35), 8341-8352. doi: <http://dx.doi.org/10.1016/j.atmosenv.2008.07.021>
- Geiser, M., Kreyling, W.G. (2010). Deposition and biokinetics of inhaled nanoparticles. [Research Support, N I H , Extramural Research Support, Non-U S Gov't Review]. *Part Fibre Toxicol*, 7(2), 1743-8977.
- Gieré, R., Querol, X. (2010). Solid Particulate Matter in the Atmosphere. *Elements*, 6(4), 215-222. doi: 10.2113/gselements.6.4.215
- Gillies, J.A., Gertler, A.W. (2000). Comparison and Evaluation of Chemically Speciated Mobile Source PM_{2.5} Particulate Matter Profiles. *Journal of the Air & Waste Management Association*, 50(8), 1459-1480. doi: 10.1080/10473289.2000.10464186
- Göhler, D., Stintz, M., Hillemann, L., Vorbau, M. (2010). Characterization of Nanoparticle Release from Surface Coatings by the Simulation of a Sanding Process. *Annals of Occupational Hygiene*, 54(6), 615-624. doi: 10.1093/annhyg/meq053
- Gomes, J.F., Albuquerque, P.C., Miranda, R.M., Vieira, M.T. (2012). Determination of airborne nanoparticles from welding operations. [Comparative Study Research Support, Non-U S Gov't]. *J Toxicol Environ Health A*, 75(13-15), 747-755.
- Gómez-Moreno, F.J., Alonso, E., Artíñano, B., Juncal-Bello, V., Iglesias-Samitier, S., Piñeiro Iglesias, M., Mahía, P.L., Pérez, N., Pey, J., Ripoll, A., Alastuey, A., de la Morena, B.A., García, M.I., Rodríguez, S., Sorribas, M., Titos, G., Lyamani, H., Alados-Arboledas, L., Latorre, E., Tritscher, T., Bischof, O.F. (2015). Intercomparisons of Mobility Size Spectrometers and Condensation Particle Counters in the Frame of the Spanish Atmospheric Observational Aerosol Network. *Aerosol Science and Technology*, 49(9), 777-785. doi: 10.1080/02786826.2015.1074656
- Gomez, V., Irusta, S., Balas, F., Navascues, N., Santamaria, J. (2014a). Unintended emission of nanoparticle aerosols during common laboratory handling operations. *Journal of Hazardous Materials*, 279, 75-84. doi: <http://dx.doi.org/10.1016/j.jhazmat.2014.06.064>
- Gomez, V., Irusta, S., Balas, F., Santamaria, J. (2013). Intense generation of respirable metal nanoparticles from a low-power soldering unit. [Research Support, Non-U S Gov't]. *J Hazard Mater*, 257, 84-89.
- Gomez, V., Levin, M., Saber, A.T., Irusta, S., Dal Maso, M., Hanoi, R., Santamaria, J., Jensen, K.A., Wallin, H., Koponen, I.K. (2014b). Comparison of dust release from epoxy and paint nanocomposites and conventional products during sanding and sawing. [Comparative Study Research Support, Non-U S Gov't]. *Ann Occup Hyg*, 58(8), 983-994.
- Gramsch, E., Gidhagen, L., Wahlin, P., Oyola, P., Moreno, F. (2009). Predominance of soot-mode ultrafine particles in Santiago de Chile: Possible sources. *Atmospheric Environment*, 43(14), 2260-2267. doi: <http://dx.doi.org/10.1016/j.atmosenv.2009.01.047>
- Grimm, H., Eatough, D.J. (2009). Aerosol Measurement: The Use of Optical Light Scattering for the Determination of Particulate Size Distribution, and Particulate Mass, Including the Semi-Volatile Fraction. *Journal of the Air &*

- Waste Management Association*, 59(1), 101-107. doi: 10.3155/1047-3289.59.1.101
- Guichard, Y., Schmit, J., Darne, C., Gaté, L., Goutet, M., Rousset, D., Rastoix, O., Wrobel, R., Witschger, O., Martin, A., Fierro, V., Binet, S. (2012). Cytotoxicity and Genotoxicity of Nanosized and Microsized Titanium Dioxide and Iron Oxide Particles in Syrian Hamster Embryo Cells. *Annals of Occupational Hygiene*, 56(5), 631-644.
- Guo, N.L., Wan, Y.-W., Denvir, J., Porter, D.W., Pacurari, M., Wolfarth, M.G., Castranova, V., Qian, Y. (2012). Multi-walled carbon nanotube-induced gene signatures in the mouse lung: potential predictive value for human lung cancer risk and prognosis. *Journal of toxicology and environmental health. Part A*, 75(18), 1129-1153. doi: 10.1080/15287394.2012.699852
- Gutiérrez Mora, F., Domínguez-Rodríguez, A., Lennikov, V.V., de la Fuente, G.F. (2009). Influence of Thermal Effects Produced by Laser Treatment on the Tribological Behavior of Porcelain Ceramic Tiles. *Key Engineering Materials*, 423, 41-46.
- Ham, S., Yoon, C., Lee, E., Lee, K., Park, D., Chung, E., Kim, P., Lee, B. (2012). Task-based exposure assessment of nanoparticles in the workplace. [journal article]. *J Nanopart Res*, 14(9), 1-17. doi: 10.1007/s11051-012-1126-8
- Hameri, K., Lahde, T., Hussein, T., Koivisto, J., Savolainen, K. (2009). Facing the key workplace challenge: assessing and preventing exposure to nanoparticles at source. *Inhal Toxicol*, 1, 17-24.
- Handy, R.D., Shaw, B.J. (2007). Toxic effects of nanoparticles and nanomaterials: Implications for public health, risk assessment and the public perception of nanotechnology. *Health, Risk & Society*, 9(2), 125-144. doi: 10.1080/13698570701306807
- Hansen, S.F. (2009). *Regulation and Risk Assessment of Nanomaterials – Too Little, Too Late? (PhD Thesis)*. Technical University of Denmark Lyngby, Denmark.
- Harrison, R.M., van Grieken, R., E (1998). *Atmospheric Particles. IUPAC Series on Analytical and Physical Chemistry of Environmental Systems*: John Wiley & Sons.
- Harrison, R.M., Yin, J. (2000). Particulate matter in the atmosphere: which particle properties are important for its effects on health? *Science of The Total Environment*, 249(1-3), 85-101. doi: [http://dx.doi.org/10.1016/S0048-9697\(99\)00513-6](http://dx.doi.org/10.1016/S0048-9697(99)00513-6)
- He, C., Morawska, L., Taplin, L. (2007). Particle Emission Characteristics of Office Printers. *Environmental Science & Technology*, 41(17), 6039-6045. doi: 10.1021/es063049z
- Heal, M.R., Kumar, P., Harrison, R.M. (2012). Particles, air quality, policy and health. [10.1039/C2CS35076A]. *Chemical Society Reviews*, 41(19), 6606-6630. doi: 10.1039/c2cs35076a
- Heim, M., Mullins, B.J., Umhauer, H., Kasper, G. (2008). Performance evaluation of three optical particle counters with an efficient “multimodal” calibration method. *Journal of Aerosol Science*, 39(12), 1019-1031. doi: <http://dx.doi.org/10.1016/j.jaerosci.2008.07.006>
- Heitbrink, W.A., Evans, D.E., Ku, B.K., Maynard, A.D., Slavin, T.J., Peters, T.M. (2008). Relationships Among Particle Number, Surface Area, and Respirable Mass Concentrations in Automotive Engine Manufacturing. *Journal of Occupational and Environmental Hygiene*, 6(1), 19-31. doi: 10.1080/15459620802530096
- Hering, S.V., Flagan, R.C., Friedlander, S.K. (1978). Design and evaluation of new low-pressure impactor. I. *Environmental Science & Technology*, 12(6), 667-673. doi: 10.1021/es60142a004
- Hering, S.V., Stolzenburg, M.R., Quant, F.R., Oberreit, D.R., Keady, P.B. (2005). A Laminar-Flow, Water-Based Condensation Particle Counter (WCPC). *Aerosol Science and Technology*, 39(7), 659-672. doi: 10.1080/02786820500182123

- Hermann, M., Wehner, B., Bischof, O., Han, H.S., Krinke, T., Liu, W., Zerrath, A., Wiedensohler, A. (2007). Particle counting efficiencies of new TSI condensation particle counters. *Journal of Aerosol Science*, 38(6), 674-682. doi: <http://dx.doi.org/10.1016/j.jaerosci.2007.05.001>
- Hillamo, R.E., Kauppinen, E.I. (1991). On the Performance of the Berner Low Pressure Impactor. *Aerosol Science and Technology*, 14(1), 33-47. doi: 10.1080/02786829108959469
- Hinds, W.C. (1999). *Aerosol technology: properties, behavior, and measurement of airborne particles*: Wiley.
- Hirano, S. (2009). A current overview of health effect research on nanoparticles. *Environmental Health and Preventive Medicine*, 14(4), 223-225. doi: 10.1007/s12199-008-0064-7
- Höck, J., Hofmann, H., Krug, H., Lorenz, C., Limbach, L., Nowack, B., Riediker, M., Schirmer, K., Som, C., Stark, W., Studer, C., von Götz, N., Wengert, S., Wick, P. (2008). Precautionary Matrix for Synthetic Nanomaterials. Federal Office for Public Health and Federal Office for the Environment. Berne.
- Hoet, P.H., Bruske-Hohlfeld, I., Salata, O.V. (2004). Nanoparticles - known and unknown health risks. [Journal article]. *J Nanobiotechnology*, 2(1), 12.
- Hoppel, W.A. (1978). Determination of the aerosol size distribution from the mobility distribution of the charged fraction of aerosols. *Journal of Aerosol Science*, 9(1), 41-54. doi: [http://dx.doi.org/10.1016/0021-8502\(78\)90062-9](http://dx.doi.org/10.1016/0021-8502(78)90062-9)
- Hristozov, D.R., Gottardo, S., Critto, A., Marcomini, A. (2012). Risk assessment of engineered nanomaterials: a review of available data and approaches from a regulatory perspective. *Nanotoxicology*, 6(8), 880-898. doi: 10.3109/17435390.2011.626534
- Hussein, T., Hämeri, K., Heikkinen, M.S.A., Kulmala, M. (2005). Indoor and outdoor particle size characterization at a family house in Espoo–Finland. *Atmospheric Environment*, 39(20), 3697-3709. doi: <http://dx.doi.org/10.1016/j.atmosenv.2005.03.011>
- IARC. (2010). The International Agency for Research on Cancer. IARC monographs on the evaluation of carcinogenic risks to humans: carbon black, titanium dioxide, and talc. Vol. 93. Lyon, France: World Health Organization, International Agency for Research on Cancer. <http://monographs.iarc.fr/ENG/Monographs/vol93/index.php>
- ICRP. (1994). Human Respiratory Tract Model for Radiological Protection. ICRP Publication 66. Ann. ICRP 24 (1-3). International Commission on Radiological Protection.
- IFA. (2009). Technical Information - Nanoparticles at the workplace: <http://www.dguv.de/ifa/Fachinfos/Nanopartikel-am-Arbeitsplatz/index-2.jsp>
- Isaxon, C., Gudmundsson, A., Nordin, E.Z., Lönnblad, L., Dahl, A., Wieslander, G., Bohgard, M., Wierzbicka, A. (2015). Contribution of indoor-generated particles to residential exposure. *Atmospheric Environment*, 106, 458-466. doi: <http://dx.doi.org/10.1016/j.atmosenv.2014.07.053>
- ISO. (2015). ISO/TS 80004-1:2015, Nanotechnologies - Vocabulary - Part 1: Core terms: International Organization for Standardization.
- Janssen, N.A.H., Gerlofs-Nijland, M.E., Lanki, T., Salonen, R.O., Cassee, F., Hoek, G., Fischer, P., Brunekreef, B., Krzyzanowski, M. (2012). Health effects of black carbon *WHO Regional Office for Europe*.
- Järvinen, A., Aitomaa, M., Rostedt, A., Keskinen, J., Yli-Ojanperä, J. (2014). Calibration of the new electrical low pressure impactor (ELPI+). *Journal of Aerosol Science*, 69, 150-159. doi: <http://dx.doi.org/10.1016/j.jaerosci.2013.12.006>
- Jensen, A.C.Ø., Levin, M., Koivisto, A.J., Kling, K.I., Saber, A.T., Koponen, I.K. (2015). Exposure Assessment of Particulate Matter from Abrasive Treatment of Carbon and Glass Fibre-Reinforced Epoxy-Composites: Two Case Studies. *Aerosol and Air Quality Research*, 15(5), 1906-1916

- doi: 10.4209/aaqr.2015.02.0086
- Jeong, C.-H., Evans, G.J. (2009). Inter-Comparison of a Fast Mobility Particle Sizer and a Scanning Mobility Particle Sizer Incorporating an Ultrafine Water-Based Condensation Particle Counter. *Aerosol Science and Technology*, 43(4), 364-373. doi: 10.1080/02786820802662939
- Jung, H., Kittelson, D.B. (2005). Characterization of Aerosol Surface Instruments in Transition Regime. *Aerosol Science and Technology*, 39(9), 902-911. doi: 10.1080/02786820500295701
- Kaluza, S., Balderhaar, J., Orthen, B., Honnert, B., Jankowska, E., Pietrowski, P., Rosell, M., Tanarro, C., Tejedor, J., Zugasti, A. (2009). Literature Review - Workplace exposure to nanoparticles. European Agency for Safety and Health at Work (EU-OSHA), Spain.
- Kaminski, H., Beyer, M., Fissan, H., Asbach, C., Kuhlbusch, T.A.J. (2015). Measurements of Nanoscale TiO₂ and Al₂O₃ in Industrial Workplace Environments - Methodology and Results. *Aerosol and Air Quality Research*, 15(1), 129-141. doi: 10.4209/aaqr.2014.03.0065
- Kaminski, H., Kuhlbusch, T.A.J., Rath, S., Götz, U., Sprenger, M., Wels, D., Polloczek, J., Bachmann, V., Dziurawicz, N., Kiesling, H.-J., Schwegelshohn, A., Monz, C., Dahmann, D., Asbach, C. (2013). Comparability of mobility particle sizers and diffusion chargers. *Journal of Aerosol Science*, 57(0), 156-178. doi: <http://dx.doi.org/10.1016/j.jaerosci.2012.10.008>
- Karagulian, F., Belis, C.A., Dora, C.F.C., Prüss-Ustün, A.M., Bonjour, S., Adair-Rohani, H., Amann, M. (2015). Contributions to cities' ambient particulate matter (PM): A systematic review of local source contributions at global level. *Atmospheric Environment*, 120, 475-483. doi: <http://dx.doi.org/10.1016/j.atmosenv.2015.08.087>
- Karlsson, H.L., Gustafsson, J., Cronholm, P., Möller, L. (2009). Size-dependent toxicity of metal oxide particles—A comparison between nano- and micrometer size. *Toxicology Letters*, 188(2), 112-118. doi: <http://dx.doi.org/10.1016/j.toxlet.2009.03.014>
- Kearney, J., Wallace, L., MacNeill, M., Héroux, M.-E., Kindzierski, W., Wheeler, A. (2014). Residential infiltration of fine and ultrafine particles in Edmonton. *Atmospheric Environment*, 94, 793-805. doi: <http://dx.doi.org/10.1016/j.atmosenv.2014.05.020>
- Kearney, J., Wallace, L., MacNeill, M., Xu, X., VanRyswyk, K., You, H., Kulka, R., Wheeler, A.J. (2011). Residential indoor and outdoor ultrafine particles in Windsor, Ontario. *Atmospheric Environment*, 45(40), 7583-7593. doi: <http://dx.doi.org/10.1016/j.atmosenv.2010.11.002>
- Kerminen, V.-M., Pakkanen, T.A., Mäkelä, T., Hillamo, R.E., Sillanpää, M., Rönkkö, T., Virtanen, A., Keskinen, J., Pirjola, L., Hussein, T., Hämeri, K. (2007). Development of particle number size distribution near a major road in Helsinki during an episodic inversion situation. *Atmospheric Environment*, 41(8), 1759-1767. doi: <http://dx.doi.org/10.1016/j.atmosenv.2006.10.026>
- Keskinen, J., Pietarinen, K., Lehtimäki, M. (1992). Electrical low pressure impactor. *J Aerosol Sci*, 23, 353–360.
- Kim, B., Kim, H., Yu, I.J. (2014). Assessment of Nanoparticle Exposure in Nanosilica Handling Process: Including Characteristics of Nanoparticles Leaking from a Vacuum Cleaner. *Industrial Health*, 52(2), 152-162. doi: 10.2486/indhealth.2013-0087
- Kim, K.-H., Kabir, E., Kabir, S. (2015). A review on the human health impact of airborne particulate matter. *Environment International*, 74, 136-143. doi: <http://dx.doi.org/10.1016/j.envint.2014.10.005>
- Klepeis, N.E., Nelson, W.C., Ott, W.R., Robinson, J.P., Tsang, A.M., Switzer, P., Behar, J.V., Hern, S.C., Engelmann, W.H. (2001). The National Human Activity Pattern Survey (NHAPS): a resource for assessing exposure to environmental pollutants. [Research Support, Non-U S Gov't

- Research Support, U S Gov't, Non-P H S]. *J Expo Anal Environ Epidemiol*, 11(3), 231-252.
- Kling, K.I., Levin, M., Jensen, A.C.Ø., Jensen, K.A., Koponen, I.K. (2016). Size-Resolved Characterization of Particles and Fibers Released during Abrasion of Fiber-Reinforced Composite in a Workplace Influenced by Ambient Background Sources *Aerosol and Air Quality Research*, 16, 11-24. doi: 10.4209/aaqr.2015.05.0295
- Knutson, E.O., Whitby, K.T. (1975). Aerosol classification by electric mobility: apparatus, theory, and applications. *Journal of Aerosol Science*, 6(6), 443-451. doi: [http://dx.doi.org/10.1016/0021-8502\(75\)90060-9](http://dx.doi.org/10.1016/0021-8502(75)90060-9)
- Koivisto, A.J. (2013). *Source specific risk assessment of indoor aerosol particles*. PhD, University of Helsinki, Helsinki, Finland.
- Koivisto, A.J., Hussein, T., Niemelä, R., Tuomi, T., Hämeri, K. (2010). Impact of particle emissions of new laser printers on modeled office room. *Atmospheric Environment*, 44(17), 2140-2146. doi: <http://dx.doi.org/10.1016/j.atmosenv.2010.02.023>
- Koivisto, A.J., Lyrranen, J., Auvinen, A., Vanhala, E., Hameri, K., Tuomi, T., Jokiniemi, J. (2012). Industrial worker exposure to airborne particles during the packing of pigment and nanoscale titanium dioxide. [Comparative Study Research Support, Non-U S Gov't]. *Inhal Toxicol*, 24(12), 839-849.
- Koivisto, A.J., Palomaki, J.E., Viitanen, A.K., Siivola, K.M., Koponen, I.K., Yu, M., Kanerva, T.S., Norppa, H., Alenius, H.T., Hussein, T., Savolainen, K.M., Hameri, K.J. (2014). Range-finding risk assessment of inhalation exposure to nanodiamonds in a laboratory environment. [Research Support, Non-U S Gov't]. *Int J Environ Res Public Health*, 11(5), 5382-5402.
- Koponen, I.K., Asmi, A., Keronen, P., Puhto, K., Kulmala, M. (2001). Indoor air measurement campaign in Helsinki, Finland 1999 – the effect of outdoor air pollution on indoor air. *Atmospheric Environment*, 35(8), 1465-1477. doi: [http://dx.doi.org/10.1016/S1352-2310\(00\)00338-1](http://dx.doi.org/10.1016/S1352-2310(00)00338-1)
- Koponen, I.K., Jensen, K.A., Schneider, T. (2009). Sanding dust from nanoparticle-containing paints: Physical characterisation. *Journal of Physics: Conference Series*, 151(1), 012048.
- Koponen, I.K., Koivisto, A.J., Jensen, K.A. (2015). Worker Exposure and High Time-Resolution Analyses of Process-Related Submicrometre Particle Concentrations at Mixing Stations in Two Paint Factories. [Research Support, Non-U S Gov't]. *Ann Occup Hyg*, 59(6), 749-763.
- Kousaka, Y., Okuyama, K., Adachi, M. (1985). Determination of Particle Size Distribution of Ultra-Fine Aerosols Using a Differential Mobility Analyzer. *Aerosol Science and Technology*, 4(2), 209-225. doi: 10.1080/02786828508959049
- Kreyling, W.G., Semmler-Behnke, M., Seitz, J., Scymczak, W., Wenk, A., Mayer, P., Takenaka, S., Oberdorster, G. (2009). Size dependence of the translocation of inhaled iridium and carbon nanoparticle aggregates from the lung of rats to the blood and secondary target organs. [Research Support, N I H , Extramural Research Support, Non-U S Gov't]. *Inhal Toxicol*, 1, 55-60.
- Kreyling, W.G., Semmler, M., Erbe, F., Mayer, P., Takenaka, S., Schulz, H., Oberdorster, G., Ziesenis, A. (2002). Translocation of ultrafine insoluble iridium particles from lung epithelium to extrapulmonary organs is size dependent but very low. [Research Support, Non-U S Gov't Research Support, U S Gov't, Non-P H S]. *J Toxicol Environ Health A*, 65(20), 1513-1530.
- Krug, H.F., Klug, P. (2010). Impact of Nanotechnological Developments on the Environment *Nanotechnology*: Wiley-VCH Verlag GmbH & Co. KGaA.
- Kubelová, L., Vodička, P., Schwarz, J., Cusack, M., Makeš, O., Ondráček, J., Ždímal, V. (2015). A study of summer and winter highly time-resolved submicron

- aerosol composition measured at a suburban site in Prague. *Atmospheric Environment*, 118, 45-57. doi: <http://dx.doi.org/10.1016/j.atmosenv.2015.07.030>
- Kuhlbusch, T., Asbach, C., Fissan, H., Gohler, D., Stintz, M. (2011a). Nanoparticle exposure at nanotechnology workplaces: A review. *Particle and Fibre Toxicology*, 8(1), 22.
- Kuhlbusch, T.A., Fissan, H. (2006). Particle characteristics in the reactor and pelletizing areas of carbon black production. [Research Support, Non-U S Gov't]. *J Occup Environ Hyg*, 3(10), 558-567.
- Kuhlbusch, T.A.J., Asbach, C., Fissan, H., Göhler, D., Stintz, M. (2011b). Nanoparticle exposure at nanotechnology workplaces: A review. *Particle and Fibre Toxicology*, 8, 22-22. doi: 10.1186/1743-8977-8-22
- Kuhlbusch, T.A.J., Fissan, H., Asbach, C. (2009). Nanotechnologies and Environmental Risks. In I. Linkov & J. Steevens (Eds.), *Nanomaterials: Risks and Benefits* (pp. 233-243). Dordrecht: Springer Netherlands.
- Kulmala, M. (2003). How Particles Nucleate and Grow. *Science*, 302(5647), 1000-1001. doi: 10.1126/science.1090848
- Kulmala, M., Kerminen, V.-M. (2008). On the formation and growth of atmospheric nanoparticles. *Atmospheric Research*, 90(2-4), 132-150. doi: <http://dx.doi.org/10.1016/j.atmosres.2008.01.005>
- Kulmala, M., Vehkamäki, H., Petäjä, T., Dal Maso, M., Lauri, A., Kerminen, V.M., Birmili, W., McMurry, P.H. (2004). Formation and growth rates of ultrafine atmospheric particles: a review of observations. *Journal of Aerosol Science*, 35(2), 143-176. doi: <http://dx.doi.org/10.1016/j.jaerosci.2003.10.003>
- Kumar, P., Fennell, P., Britter, R. (2008). Effect of wind direction and speed on the dispersion of nucleation and accumulation mode particles in an urban street canyon. *Science of The Total Environment*, 402(1), 82-94. doi: <http://dx.doi.org/10.1016/j.scitotenv.2008.04.032>
- Kumar, P., Mulheron, M., Som, C. (2012). Release of ultrafine particles from three simulated building processes. [journal article]. *J Nanopart Res*, 14(4), 1-14. doi: 10.1007/s11051-012-0771-2
- Lahoz, R., de la Fuente, G.F., Pedra, J.M., Carda, J.B. (2011). Laser Engraving of Ceramic Tiles. *Int J Appl Ceram Technol*, 8(5), 1208-1217. doi: 10.1111/j.1744-7402.2010.02566.x
- Larrea, A., de la Fuente, G.F., Merino, R.I., Orera, V.M. (2002). ZrO₂-Al₂O₃ eutectic plates produced by laser zone melting. *Journal of the European Ceramic Society*, 22(2), 191-198. doi: [http://dx.doi.org/10.1016/S0955-2219\(01\)00279-5](http://dx.doi.org/10.1016/S0955-2219(01)00279-5)
- Lee, J.H., Ahn, K., Kim, S.M., Jeon, K.S., Lee, J.S., Yu, I.J. (2012). Continuous 3-day exposure assessment of workplace manufacturing silver nanoparticles. [journal article]. *J Nanopart Res*, 14(9), 1-10. doi: 10.1007/s11051-012-1134-8
- Lelieveld, J., Evans, J.S., Fnais, M., Giannadaki, D., Pozzer, A. (2015). The contribution of outdoor air pollution sources to premature mortality on a global scale. [Letter]. *Nature*, 525(7569), 367-371. doi: 10.1038/nature15371
- Lennikov, V.V., de Francisco, I., Bea, J.A., Estepa, L.C., de la Fuente, G.F. (2010). Influencia de los efectos termicos inducidos por el tratamiento con laser CO₂ en la microestructura de baldosas ceramicas. *Actas del XII Congreso Tratermat. Ed. R.Rodriguez y J.A.Garcia. AIN ISBN: 978-84-693-6946-3.*, 373-379.
- Lennikov, V.V., Kazin, P.E., Tretyakov, Y.D., de la Fuente, G.F. (2004). Laser Zone Melting and Texture Formation in MgO-doped Bi₂O₃Sr_{1.93}Ca_{1.07}Cu_{2.05}O_{8+δ}. *Zeitschrift für anorganische und allgemeine Chemie*, 630(13-14), 2337-2342. doi: 10.1002/zaac.200400311
- Lennikov, V.V., Pedra, J.M., Gómez, J.J., de la Fuente, G.F., Carda, J.B. (2007). In situ synthesis of composite MTiO₃-Al₂O₃ coatings via laser zone melting. *Solid State Sciences*, 9(5), 404-409. doi: <http://dx.doi.org/10.1016/j.solidstatesciences.2007.03.013>

- Leskinen, J., Joutsensaari, J., Lyyränen, J., Koivisto, J., Ruusunen, J., Järvelä, M., Tuomi, T., Hämeri, K., Auvinen, A., Jokiniemi, J. (2012). Comparison of nanoparticle measurement instruments for occupational health applications. *J Nanopart Res*, 14(2), 1-16. doi: 10.1007/s11051-012-0718-7
- Levin, M., Gudmundsson, A., Pagels, J.H., Fierz, M., Mølhav, K., Löndahl, J., Jensen, K.A., Koponen, I.K. (2015). Limitations in the Use of Unipolar Charging for Electrical Mobility Sizing Instruments: A Study of the Fast Mobility Particle Sizer. *Aerosol Science and Technology*, 49(8), 556-565. doi: 10.1080/02786826.2015.1052039
- Li, C., Liu, S., Zhu, Y. (2010). Determining Ultrafine Particle Collection Efficiency in a Nanometer Aerosol Sampler. *Aerosol Science and Technology*, 44(11), 1027-1041. doi: 10.1080/02786826.2010.508761
- Lim, S.S., Vos, T., Flaxman, A.D., Danaei, G., Shibuya, K., Adair-Rohani, H., Amann, M., Anderson, H.R., Andrews, K.G., Aryee, M., Atkinson, C., Bacchus, L.J., Bahalim, A.N., Balakrishnan, K., Balmes, J., Barker-Collo, S., Baxter, A., Bell, M.L., Blore, J.D., Blyth, F., Bonner, C., Borges, G., Bourne, R., Boussinesq, M., Brauer, M., Brooks, P., Bruce, N.G., Brunekreef, B., Bryan-Hancock, C., Bucello, C., Buchbinder, R., Bull, F., Burnett, R.T., Byers, T.E., Calabria, B., Carapetis, J., Carnahan, E., Chafe, Z., Charlson, F., Chen, H., Chen, J.S., Cheng, A.T., Child, J.C., Cohen, A., Colson, K.E., Cowie, B.C., Darby, S., Darling, S., Davis, A., Degenhardt, L., Dentener, F., Des Jarlais, D.C., Devries, K., Dherani, M., Ding, E.L., Dorsey, E.R., Driscoll, T., Edmond, K., Ali, S.E., Engell, R.E., Erwin, P.J., Fahimi, S., Falder, G., Farzadfar, F., Ferrari, A., Finucane, M.M., Flaxman, S., Fowkes, F.G., Freedman, G., Freeman, M.K., Gakidou, E., Ghosh, S., Giovannucci, E., Gmel, G., Graham, K., Grainger, R., Grant, B., Gunnell, D., Gutierrez, H.R., Hall, W., Hoek, H.W., Hogan, A., Hosgood, H.D., 3rd, Hoy, D., Hu, H., Hubbell, B.J., Hutchings, S.J., Ibeanusi, S.E., Jacklyn, G.L., Jasrasaria, R., Jonas, J.B., Kan, H., Kanis, J.A., Kassebaum, N., Kawakami, N., Khang, Y.H., Khatibzadeh, S., Khoo, J.P., Kok, C., Laden, F., Lalloo, R., Lan, Q., Lathlean, T., Leasher, J.L., Leigh, J., Li, Y., Lin, J.K., Lipshultz, S.E., London, S., Lozano, R., Lu, Y., Mak, J., Malekzadeh, R., Mallinger, L., Marcenes, W., March, L., Marks, R., Martin, R., McGale, P., McGrath, J., Mehta, S., Mensah, G.A., Merriman, T.R., Micha, R., Michaud, C., Mishra, V., Mohd Hanafiah, K., Mokdad, A.A., Morawska, L., Mozaffarian, D., Murphy, T., Naghavi, M., Neal, B., Nelson, P.K., Nolla, J.M., Norman, R., Olives, C., Omer, S.B., Orchard, J., Osborne, R., Ostro, B., Page, A., Pandey, K.D., Parry, C.D., Passmore, E., Patra, J., Pearce, N., Pelizzari, P.M., Petzold, M., Phillips, M.R., Pope, D., Pope, C.A., 3rd, Powles, J., Rao, M., Razavi, H., Rehfuss, E.A., Rehm, J.T., Ritz, B., Rivara, F.P., Roberts, T., Robinson, C., Rodriguez-Portales, J.A., Romieu, I., Room, R., Rosenfeld, L.C., Roy, A., Rushton, L., Salomon, J.A., Sampson, U., Sanchez-Riera, L., Sanman, E., Sapkota, A., Seedat, S., Shi, P., Shield, K., Shivakoti, R., Singh, G.M., Sleet, D.A., Smith, E., Smith, K.R., Stapelberg, N.J., Steenland, K., Stockl, H., Stovner, L.J., Straif, K., Straney, L., Thurston, G.D., Tran, J.H., Van Dingenen, R., van Donkelaar, A., Veerman, J.L., Vijayakumar, L., Weintraub, R., Weissman, M.M., White, R.A., Whiteford, H., Wiersma, S.T., Wilkinson, J.D., Williams, H.C., Williams, W., Wilson, N., Woolf, A.D., Yip, P., Zielinski, J.M., Lopez, A.D., Murray, C.J., Ezzati, M., AlMazroa, M.A., Memish, Z.A. (2012). A comparative risk assessment of burden of disease and injury attributable to 67 risk factors and risk factor clusters in 21 regions, 1990-2010: a systematic analysis for the Global Burden of Disease Study 2010. [Research Support, N I H , Extramural
Research Support, N I H , Intramural
Research Support, Non-U S Gov't]. *Lancet*, 380(9859), 2224-2260.
- Lingard, J.J., Agus, E.L., Young, D.T., Andrews, G.E., Tomlin, A.S. (2006). Observations of urban airborne particle number concentrations during rush-

- hour conditions: analysis of the number based size distributions and modal parameters. [Research Support, Non-U S Gov't]. *J Environ Monit*, 8(12), 1203-1218.
- Liu, B.Y.H., Pui, D.Y.H. (1974). A submicron aerosol standard and the primary, absolute calibration of the condensation nuclei counter. *Journal of Colloid and Interface Science*, 47(1), 155-171. doi: [http://dx.doi.org/10.1016/0021-9797\(74\)90090-3](http://dx.doi.org/10.1016/0021-9797(74)90090-3)
- Long, C.M., Sarnat, J.A. (2004). Indoor-Outdoor Relationships and Infiltration Behavior of Elemental Components of Outdoor PM_{2.5} for Boston-Area Homes. *Aerosol Science and Technology*, 38(sup2), 91-104. doi: 10.1080/027868290502281
- MacNeill, M., Wallace, L., Kearney, J., Allen, R.W., Van Ryswyk, K., Judek, S., Xu, X., Wheeler, A. (2012). Factors influencing variability in the infiltration of PM_{2.5} mass and its components. *Atmospheric Environment*, 61, 518-532. doi: <http://dx.doi.org/10.1016/j.atmosenv.2012.07.005>
- Marple, V., Olson, B., Romay, F., Hudak, G., Geerts, S.M., Lundgren, D. (2014). Second Generation Micro-Orifice Uniform Deposit Impactor, 120 MOUDI-II: Design, Evaluation, and Application to Long-Term Ambient Sampling. *Aerosol Science and Technology*, 48(4), 427-433. doi: 10.1080/02786826.2014.884274
- Marple, V.A., Rubow, K.L., Behm, S.M. (1991). A Microorifice Uniform Deposit Impactor (MOUDI): Description, Calibration, and Use. *Aerosol Science and Technology*, 14(4), 434-446. doi: 10.1080/02786829108959504
- Matson, U., Ekberg, L.E., Afshari, A. (2004). Measurement of Ultrafine Particles: A Comparison of Two Handheld Condensation Particle Counters. *Aerosol Science and Technology*, 38(5), 487-495. doi: 10.1080/02786820490462200
- Matti Maricq, M. (2007). Chemical characterization of particulate emissions from diesel engines: A review. *Journal of Aerosol Science*, 38(11), 1079-1118. doi: <http://dx.doi.org/10.1016/j.jaerosci.2007.08.001>
- Maynard, A., Kuempel, E. (2005). Airborne Nanostructured Particles and Occupational Health. *J Nanopart Res*, 7(6), 587-614. doi: 10.1007/s11051-005-6770-9
- Maynard, A.D., Aitken, R.J. (2007). Assessing exposure to airborne nanomaterials: Current abilities and future requirements. *Nanotoxicology*, 1(1), 26-41. doi: 10.1080/17435390701314720
- Maynard, A.D., Aitken, R.J., Butz, T., Colvin, V., Donaldson, K., Oberdorster, G., Philbert, M.A., Ryan, J., Seaton, A., Stone, V., Tinkle, S.S., Tran, L., Walker, N.J., Warheit, D.B. (2006). Safe handling of nanotechnology. [10.1038/444267a]. *Nature*, 444(7117), 267-269.
- Maynard, A.D., Baron, P.A., Foley, M., Shvedova, A.A., Kisin, E.R., Castranova, V. (2004). Exposure to carbon nanotube material: aerosol release during the handling of unrefined single-walled carbon nanotube material. [Research Support, U S Gov't, P H S]. *J Toxicol Environ Health A*, 67(1), 87-107.
- Mazzuckelli, L.F., Methner, M.M., Birch, M.E., Evans, D.E., Ku, B.-K., Crouch, K., Hoover, M.D. (2007). Identification and Characterization of Potential Sources of Worker Exposure to Carbon Nanofibers During Polymer Composite Laboratory Operations. *Journal of Occupational and Environmental Hygiene*, 4(12), D125-D130. doi: 10.1080/15459620701683871
- McGarry, P., Morawska, L., He, C., Jayaratne, R., Falk, M., Tran, Q., Wang, H. (2011). Exposure to particles from laser printers operating within office workplaces. [Research Support, Non-U S Gov't]. *Environ Sci Technol*, 45(15), 6444-6452.
- McMurry, P.H. (2000). A review of atmospheric aerosol measurements. *Atmospheric Environment*, 34(12-14), 1959-1999. doi: [http://dx.doi.org/10.1016/S1352-2310\(99\)00455-0](http://dx.doi.org/10.1016/S1352-2310(99)00455-0)
- Medved, A., Dorman, F., Kaufman, S.L., Pöcher, A. (2000). A New Corona-based Charger for Aerosol Particles. *J Aerosol Sci*, 31, S616-S661.

- Mészáros, E. (1999). *Fundamentals of Atmospheric Aerosol Chemistry*. Akadémiai Kiadó.
- Methner, M., Hodson, L., Geraci, C. (2010). Nanoparticle emission assessment technique (NEAT) for the identification and measurement of potential inhalation exposure to engineered nanomaterials--part A. *J Occup Environ Hyg*, 7(3), 127-132.
- Methner, M.M. (2008). Engineering case reports. Effectiveness of local exhaust ventilation (LEV) in controlling engineered nanomaterial emissions during reactor cleanout operations. *J Occup Environ Hyg*, 5(6), 15459620802059393.
- Methner, M.M. (2010). Effectiveness of a custom-fitted flange and local exhaust ventilation (LEV) system in controlling the release of nanoscale metal oxide particulates during reactor cleanout operations. *Int J Occup Environ Health*, 16(4), 475-487.
- Methner, M.M., Birch, M.E., Evans, D.E., Ku, B.K., Crouch, K., Hoover, M.D. (2007). Identification and characterization of potential sources of worker exposure to carbon nanofibers during polymer composite laboratory operations. *J Occup Environ Hyg*, 4(12), D125-130.
- Misra, C., Singh, M., Shen, S., Sioutas, C., Hall, P.M. (2002). Development and evaluation of a personal cascade impactor sampler (PCIS). *Journal of Aerosol Science*, 33(7), 1027-1047. doi: [http://dx.doi.org/10.1016/S0021-8502\(02\)00055-1](http://dx.doi.org/10.1016/S0021-8502(02)00055-1)
- Monsé, C., Monz, C., Dahmann, D., Asbach, C., Stahlmecke, B., Lichtenstein, N., Buchwald, K.-E., Merget, R., Bünger, J., Brüning, T. (2014). Development and Evaluation of a Nanoparticle Generator for Human Inhalation Studies with Airborne Zinc Oxide. *Aerosol Science and Technology*, 48(4), 418-426. doi: 10.1080/02786826.2014.883064
- Mora, M., Diez, J.C., Lopez-Gascon, C.I., Martinez, E., de la Fuente, G.F. (2003). Laser textured Bi-2212 in planar geometries. *Applied Superconductivity, IEEE Transactions on*, 13(2), 3188-3191. doi: 10.1109/tasc.2003.812192
- Morawska, L., He, C., Johnson, G., Guo, H., Uhde, E., Ayoko, G. (2009a). Ultrafine Particles in Indoor Air of a School: Possible Role of Secondary Organic Aerosols. *Environmental Science & Technology*, 43(24), 9103-9109. doi: 10.1021/es902471a
- Morawska, L., Wang, H., Ristovski, Z., Jayaratne, E.R., Johnson, G., Cheung, H.C., Ling, X., He, C. (2009b). JEM spotlight: Environmental monitoring of airborne nanoparticles. [Review]. *J Environ Monit*, 11(10), 1758-1773.
- Murphy, F.A., Poland, C.A., Duffin, R., Al Jamal, K.T., Ali-Boucetta, H., Nunes, A. (2011). Length-dependent retention of carbon nanotubes in the pleural space of mice initiates sustained inflammation and progressive fibrosis on the parietal pleura. *Am J Pathol*, 178. doi: 10.1016/j.ajpath.2011.02.040
- Nel, A. (2005). Atmosphere. Air pollution-related illness: effects of particles. [Research Support, U S Gov't, Non-P H S
- Research Support, U S Gov't, P H S]. *Science*, 308(5723), 804-806.
- NIOSH. (2011). Occupational Exposure to Titanium Dioxide, Current Intelligence Bulletin 63, April 2011. <http://www.cdc.gov/niosh/docs/2011-160/pdfs/2011-160.pdf>.
- NIOSH. (2013). Occupational exposure to carbon nanotubes and nanofibers, Current Intelligence Bulletin 65, Publication No. 2013-145 (pp. 1-184). Cincinnati: National Institute for Occupational Safety and Health, Department of Health and Human Services.
- Nurkiewicz, T.R., Porter, D.W., Hubbs, A.F., Cumpston, J.L., Chen, B.T., Frazer, D.G., Castranova, V. (2008). Nanoparticle inhalation augments particle-dependent systemic microvascular dysfunction. *Part Fibre Toxicol*, 5(1), 1743-8977.
- Nurkiewicz, T.R., Porter, D.W., Hubbs, A.F., Stone, S., Chen, B.T., Frazer, D.G., Boegehold, M.A., Castranova, V. (2009). Pulmonary Nanoparticle Exposure

- Disrupts Systemic Microvascular Nitric Oxide Signaling. *Toxicological Sciences*, 110(1), 191-203. doi: 10.1093/toxsci/kfp051
- Oberdörster, G. (2001). Pulmonary effects of inhaled ultrafine particles. *Int Arch Occup Environ Health*, 74(1), 1-8.
- Oberdörster, G. (2010). Safety assessment for nanotechnology and nanomedicine: concepts of nanotoxicology. [Research Support, N I H , Extramural
- Research Support, U S Gov't, Non-P H S]. *J Intern Med*, 267(1), 89-105.
- Oberdorster, G., Oberdorster, E., Oberdorster, J. (2005). Nanotoxicology: an emerging discipline evolving from studies of ultrafine particles. [Research Support, N I H , Extramural
- Research Support, U S Gov't, Non-P H S
- Research Support, U S Gov't, P H S
- Review]. *Environ Health Perspect*, 113(7), 823-839.
- Oberdörster, G., Oberdörster, E., Oberdörster, J. (2005). Nanotoxicology: An Emerging Discipline Evolving from Studies of Ultrafine Particles. *Environmental Health Perspectives*, 113(7), 823-839. doi: 10.1289/ehp.7339
- Oberdorster, G., Sharp, Z., Atudorei, V., Elder, A., Gelein, R., Kreyling, W., Cox, C. (2004). Translocation of inhaled ultrafine particles to the brain. [Comparative Study
- Research Support, U S Gov't, Non-P H S
- Research Support, U S Gov't, P H S]. *Inhal Toxicol*, 16(6-7), 437-445.
- Oberdorster, G., Sharp, Z., Atudorei, V., Elder, A., Gelein, R., Lunts, A., Kreyling, W., Cox, C. (2002). Extrapulmonary translocation of ultrafine carbon particles following whole-body inhalation exposure of rats. [Research Support, U S Gov't, Non-P H S
- Research Support, U S Gov't, P H S]. *J Toxicol Environ Health A*, 65(20), 1531-1543.
- Oberdörster, G., Sharp, Z., Atudorei, V., Elder, A., Gelein, R., Lunts, A., Kreyling, W., Cox, C. (2002). Extrapulmonary translocation of ultrafine carbon particles following whole-body inhalation exposure of rats. [Research Support, U S Gov't, Non-P H S
- Research Support, U S Gov't, P H S]. *J Toxicol Environ Health A*, 65(20), 1531-1543.
- Oberdorster, G., Stone, V., Donaldson, K. (2007). Toxicology of nanoparticles: A historical perspective. *Nanotoxicology*, 1. doi: 10.1080/17435390701314761
- Ono-Ogasawara, M., Serita, F., Takaya, M. (2009). Distinguishing nanomaterial particles from background airborne particulate matter for quantitative exposure assessment. [journal article]. *J Nanopart Res*, 11(7), 1651-1659. doi: 10.1007/s11051-009-9703-1
- OSHA. (2006). *29 CFR 1910.1000. Z-3 Table*.
- Ostraat, M., Engel, S., Swain, K.A., Kuhlbusch, T.A.J., Asbach, C. (2015). Harmonized Tiered Approach to Measure and Assess the Potential Exposure to Airborne Emissions of Engineered Nano-Objects and their Agglomerates and Aggregates at Workplaces *Series on the Safety of Manufactured Nanomaterials No. 55 - ENV/JM/MONO(2015)19*. Paris (France): OECD Environment, Health and Safety Publications.
- Paik, S.Y., Zalk, D.M., Swuste, P. (2008). Application of a Pilot Control Banding Tool for Risk Level Assessment and Control of Nanoparticle Exposures. *Annals of Occupational Hygiene*, 52(6), 419-428.
- Park, J., Kwak, B.K., Bae, E., Lee, J., Kim, Y., Choi, K., Yi, J. (2009). Characterization of exposure to silver nanoparticles in a manufacturing facility. [journal article]. *J Nanopart Res*, 11(7), 1705-1712. doi: 10.1007/s11051-009-9725-8
- Park, J.Y., Ramachandran, G., Raynor, P.C., Eberly, L.E., Olson, G., Jr. (2010). Comparing exposure zones by different exposure metrics using statistical parameters: contrast and precision. [Evaluation Studies

- Research Support, Non-U S Gov't]. *Ann Occup Hyg*, 54(7), 799-812.
- Peters, A., Wichmann, H.E., Tuch, T., Heinrich, J., Heyder, J. (1997a). Respiratory effects are associated with the number of ultrafine particles. [Research Support, Non-U S Gov't]. *Am J Respir Crit Care Med*, 155(4), 1376-1383.
- Peters, A., Wichmann, H.E., Tuch, T., Heinrich, J., Heyder, J. (1997b). Respiratory effects are associated with the number of ultrafine particles. *American journal of respiratory and critical care medicine*, 155(4), 1376-1383. doi: 10.1164/ajrccm.155.4.9105082
- Peters, T.M., Elzey, S., Johnson, R., Park, H., Grassian, V.H., Maher, T., O'Shaughnessy, P. (2009). Airborne monitoring to distinguish engineered nanomaterials from incidental particles for environmental health and safety. *J Occup Environ Hyg*, 6(2), 73-81.
- Peters, T.M., Ott, D., O'Shaughnessy, P.T. (2006). Comparison of the Grimm 1.108 and 1.109 portable aerosol spectrometer to the TSI 3321 aerodynamic particle sizer for dry particles. [Comparative Study Evaluation Studies]. *Ann Occup Hyg*, 50(8), 843-850.
- Pey, J. (2007). *Caracterización físico-química de los aerosoles atmosféricos en el Mediterráneo Occidental*. Universitat Politècnica de Catalunya.
- Pfefferkorn, F.E., Bello, D., Haddad, G., Park, J.-Y., Powell, M., McCarthy, J., Bunker, K.L., Fehrenbacher, A., Jeon, Y., Virji, M.A., Gruetzmacher, G., Hoover, M.D. (2010). Characterization of Exposures to Airborne Nanoscale Particles During Friction Stir Welding of Aluminum. *Annals of Occupational Hygiene*, 54(5), 486-503. doi: 10.1093/annhyg/meq037
- Pietrojusti, A., Magrini, A. (2014). Engineered nanoparticles at the workplace: current knowledge about workers' risk. *Occupational Medicine*, 64(5), 319-330.
- Plitzko, S. (2009). Workplace exposure to engineered nanoparticles. *Inhal Toxicol*, 1, 25-29.
- Poland, C.A., Duffin, R., Kinloch, I., Maynard, A., Wallace, W.A., Seaton, A. (2008). Carbon nanotubes introduced into the abdominal cavity of mice show asbestos-like pathogenicity in a pilot study. *Nat Nanotechnol*, 3. doi: 10.1038/nnano.2008.111
- Politis, M., Pilinis, C., Lekkas, T.D. (2008). Ultrafine Particles (UFP) and Health Effects. Dangerous. Like no Other PM? Review And Analysis. *Global NEST J.*, 10, 439-452.
- Preining, O., Berner, A. (1979). Aerosol Measurements in the Submicron Size Range. *EPA report, EPA-600/2-79-105*. Washington, DC: EPA.
- Price, H.D., Stahlmecke, B., Arthur, R., Kaminski, H., Lindermann, J., Däuber, E., Asbach, C., Kuhlbusch, T.A.J., BéruBé, K.A., Jones, T.P. (2014). Comparison of instruments for particle number size distribution measurements in air quality monitoring. *Journal of Aerosol Science*, 76(0), 48-55. doi: <http://dx.doi.org/10.1016/j.jaerosci.2014.05.001>
- Qi, C., Asbach, C., Shin, W.G., Fissan, H., Pui, D.Y.H. (2009). The Effect of Particle Pre-Existing Charge on Unipolar Charging and Its Implication on Electrical Aerosol Measurements. *Aerosol Science and Technology*, 43(3), 232-240. doi: 10.1080/02786820802587912
- Querol, X., Alastuey, A., Rodríguez, S., Plana, F., Ruiz, C.R., Cots, N., Massagué, G., Puig, O. (2001). PM10 and PM2.5 source apportionment in the Barcelona Metropolitan Area, Catalonia, Spain. *Atmos Environ*, 35, 6407-6419.
- Ramachandran, G., Ostraat, M., Evans, D.E., Methner, M.M., O'Shaughnessy, P., D'Arcy, J., Geraci, C.L., Stevenson, E., Maynard, A., Rickabaugh, K. (2011). A strategy for assessing workplace exposures to nanomaterials. *J Occup Environ Hyg*, 8(11), 673-685.
- Reche, C., Querol, X., Alastuey, A., Viana, M., Pey, J., Moreno, T., Rodríguez, S., González, Y., Fernández-Camacho, R., de la Rosa, J., Dall'Osto, M., Prévôt, A.S.H., Hueglin, C., Harrison, R.M., Quincey, P. (2011). New considerations for PM, Black Carbon and particle number concentration for air quality

- monitoring across different European cities. *Atmos. Chem. Phys.*, 11(13), 6207-6227. doi: 10.5194/acp-11-6207-2011
- Reche, C., Viana, M., Brines, M., Perez, N., Beddows, D., Alastuey, A., Querol, X. (2015). Determinants of aerosol lung-deposited surface area variation in an urban environment. [Research Support, Non-U S Gov't]. *Sci Total Environ*, 517, 38-47.
- Reche, C., Viana, M., Rivas, I., Bouso, L., Alvarez-Pedrerol, M., Alastuey, A., Sunyer, J., Querol, X. (2014). Outdoor and indoor UFP in primary schools across Barcelona. [Research Support, Non-U S Gov't]. *Sci Total Environ*, 493, 943-953.
- Riediker, M., Ostiguy, C., Triolet, J., Troisfontaine, P., Vernez, D., Bourdel, G., Thieriet, N., Cad, #xe8, ne, A. (2012). Development of a Control Banding Tool for Nanomaterials. *Journal of Nanomaterials*, 2012, 8. doi: 10.1155/2012/879671
- Rivas, I., Donaire-Gonzalez, D., Bouso, L., Esnaola, M., Pandolfi, M., de Castro, M., Viana, M., Alvarez-Pedrerol, M., Nieuwenhuijsen, M., Alastuey, A., Sunyer, J., Querol, X. (2015). Spatiotemporally resolved black carbon concentration, schoolchildren's exposure and dose in Barcelona. [Journal article]. *Indoor Air*, 27(10), 12214.
- Rivas, I., Viana, M., Moreno, T., Pandolfi, M., Amato, F., Reche, C., Bouso, L., Alvarez-Pedrerol, M., Alastuey, A., Sunyer, J., Querol, X. (2014). Child exposure to indoor and outdoor air pollutants in schools in Barcelona, Spain. [Research Support, Non-U S Gov't]. *Environ Int*, 69, 200-212.
- Rodríguez, S., Van Dingenen, R., Putaud, J.-P., Martins-Dos Santos, S., Roselli, D. (2005). Nucleation and growth of new particles in the rural atmosphere of Northern Italy—relationship to air quality monitoring. *Atmospheric Environment*, 39(36), 6734-6746. doi: <http://dx.doi.org/10.1016/j.atmosenv.2005.07.036>
- Rogak, S.N., Flagan, R.C., Nguyen, H.V. (1993). The Mobility and Structure of Aerosol Agglomerates. *Aerosol Science and Technology*, 18(1), 25-47. doi: 10.1080/02786829308959582
- Rossi, E.M., Pylkkanen, L., Koivisto, A.J., Vippola, M., Jensen, K.A., Miettinen, M., Sirola, K., Nykasenoja, H., Karisola, P., Stjernvall, T., Vanhala, E., Kiilunen, M., Pasanen, P., Mäkinen, M., Hameri, K., Joutsensaari, J., Tuomi, T., Jokiniemi, J., Wolff, H., Savolainen, K., Matikainen, S., Alenius, H. (2010). Airway exposure to silica-coated TiO₂ nanoparticles induces pulmonary neutrophilia in mice. [Research Support, Non-U S Gov't]. *Toxicol Sci*, 113(2), 422-433.
- Rubahn, H.-G. (1999). *Laser Applications in Surface Science and Technology*. New York: John Wiley & Sons.
- Sakamoto, Y., Nakae, D., Fukumori, N., Tayama, K., Maekawa, A., Imai, K., Hirose, A., Nishimura, T., Ohashi, N., Ogata, A. (2009). Induction of mesothelioma by a single intrascrotal administration of multi-wall carbon nanotube in intact male Fischer 344 rats. [Research Support, Non-U S Gov't]. *J Toxicol Sci*, 34(1), 65-76.
- Salma, I., Fűri, P., Németh, Z., Balásházy, I., Hofmann, W., Farkas, Á. (2015). Lung burden and deposition distribution of inhaled atmospheric urban ultrafine particles as the first step in their health risk assessment. *Atmospheric Environment*, 104, 39-49. doi: <http://dx.doi.org/10.1016/j.atmosenv.2014.12.060>
- Savolainen, K., Alenius, H., Norppa, H., Pylkkänen, L., Tuomi, T., Kasper, G. (2010). Risk assessment of engineered nanomaterials and nanotechnologies—A review. *Toxicology*, 269(2-3), 92-104. doi: <http://dx.doi.org/10.1016/j.tox.2010.01.013>
- Savolainen, K., Backman, U., Brouwer, D., Fadeel, B., Fernandes, T., Kuhlbusch, T., Landsiedel, R., Lynch, I., Pylkkanen, L. (2013). Nanosafety in Europe 2015—

- 2025: Towards Safe and Sustainable Nanomaterials and Nanotechnology Innovations, Finnish Institute of Occupational Health
- Schmoll, L.H., Elzey, S., Grassian, V.H., O'Shaughnessy, P.T. (2009). Nanoparticle aerosol generation methods from bulk powders for inhalation exposure studies. *Nanotoxicol*, 3(4), 265-275. doi: doi:10.3109/17435390903121931
- Schneider, T., Brouwer, D.H., Koponen, I.K., Jensen, K.A., Fransman, W., Van Duuren-Stuurman, B., Van Tongeren, M., Tielemans, E. (2011). Conceptual model for assessment of inhalation exposure to manufactured nanoparticles. [Research Support, Non-U S Gov't]. *J Expo Sci Environ Epidemiol*, 21(5), 450-463.
- Schulte, P.A., Murashov, V., Zumwalde, R., Kuempel, E.D., Geraci, C.L. (2010). Occupational exposure limits for nanomaterials: state of the art. [journal article]. *J Nanopart Res*, 12(6), 1971-1987. doi: 10.1007/s11051-010-0008-1
- Seaton, A., MacNee, W., Donaldson, K., Godden, D. (1995). Particulate air pollution and acute health effects. *Lancet*, 345(8943), 176-178.
- Seinfeld, J.H., Pandis, S.N. (2006). *Atmospheric Chemistry and Physics: From Air Pollution to Climate Change, 2nd Edition*: Wiley.
- Seipenbusch, M., Binder, A., Kasper, G. (2008). Temporal Evolution of Nanoparticle Aerosols in Workplace Exposure. *Annals of Occupational Hygiene*, 52(8), 707-716. doi: 10.1093/annhyg/men067
- SER. (2012). Provisional nano reference values for engineered nanomaterials, Advisory Report 12/01, Sociaal Economische Raad, Den Haag.
- Shvedova, A.A., Kapralov, A.A., Feng, W.H., Kisin, E.R., Murray, A.R., Mercer, R.R., St Croix, C.M., Lang, M.A., Watkins, S.C., Konduru, N.V., Allen, B.L., Conroy, J., Kotchey, G.P., Mohamed, B.M., Meade, A.D., Volkov, Y., Star, A., Fadeel, B., Kagan, V.E. (2012). Impaired clearance and enhanced pulmonary inflammatory/fibrotic response to carbon nanotubes in myeloperoxidase-deficient mice. [Research Support, N I H , Extramural Research Support, Non-U S Gov't Research Support, U S Gov't, Non-P H S]
- Research Support, U S Gov't, P H S]. *PLoS One*, 7(3), 30.
- Shvedova, A.A., Kisin, E.R., Murray, A.R., Johnson, V.J., Gorelik, O., Arepalli, S. (2008). Inhalation versus aspiration of single walled carbon nanotubes in C57/Bl6 mice: Inflammation, fibrosis, oxidative stress and mutagenesis. *Am J Physiol Lung Cell Mol Physiol*, 295. doi: 10.1152/ajplung.90287.2008
- Sorensen, C.M. (2001). Light Scattering by Fractal Aggregates: A Review. *Aerosol Science and Technology*, 35(2), 648-687. doi: 10.1080/02786820117868
- Stabile, L., Cauda, E., Marini, S., Buonanno, G. (2014). Metrological Assessment of a Portable Analyzer for Monitoring the Particle Size Distribution of Ultrafine Particles. *Annals of Occupational Hygiene*, 58(7), 860-876.
- Stelson, A.W., Seinfeld, J.H. (1982). Relative humidity and temperature dependence of the ammonium nitrate dissociation constant. *Atmospheric Environment (1967)*, 16(5), 983-992. doi: [http://dx.doi.org/10.1016/0004-6981\(82\)90184-6](http://dx.doi.org/10.1016/0004-6981(82)90184-6)
- Streets, D.G., Devane, M.K., Lu, Z., Bond, T.C., Sunderland, E.M., Jacob, D.J. (2011). All-Time Releases of Mercury to the Atmosphere from Human Activities. *Environmental Science & Technology*, 45(24), 10485-10491. doi: 10.1021/es202765m
- Szymczak, W., Menzel, N., Keck, L. (2007). Emission of ultrafine copper particles by universal motors controlled by phase angle modulation. *Journal of Aerosol Science*, 38(5), 520-531. doi: <http://dx.doi.org/10.1016/j.jaerosci.2007.03.002>
- Takagi, A., Hirose, A., Nishimura, T., Fukumori, N., Ogata, A., Ohashi, N., Kitajima, S., Kanno, J. (2008). Induction of mesothelioma in p53+/- mouse by intraperitoneal application of multi-wall carbon nanotube. [Research Support, Non-U S Gov't]. *J Toxicol Sci*, 33(1), 105-116.
- Talbot, N., Kubelova, L., Makes, O., Cusack, M., Ondracek, J., Vodička, P., Schwarz, J., Zdimal, V. (2016). Outdoor and indoor aerosol size, number, mass and

- compositional dynamics at an urban background site during warm season. *Atmospheric Environment*, 131, 171-184. doi: <http://dx.doi.org/10.1016/j.atmosenv.2016.01.055>
- Tammet, H., Mirme, A., Tamm, E. (2002). Electrical aerosol spectrometer of Tartu University. *Atmospheric Research*, 62(3-4), 315-324. doi: [http://dx.doi.org/10.1016/S0169-8095\(02\)00017-0](http://dx.doi.org/10.1016/S0169-8095(02)00017-0)
- Taniguchi, N. (1974). On the basic concept of nano-technology. *Proc. Intl. Conf. Prod. Eng.*, Tokyo, Part II, 18-23.
- ten Brink, H.M., Plomp, A., Spoelstra, H., van de Vate, J.F. (1983). A high-resolution electrical mobility aerosol spectrometer (MAS). *Journal of Aerosol Science*, 14(5), 589-597. doi: [http://dx.doi.org/10.1016/0021-8502\(83\)90064-2](http://dx.doi.org/10.1016/0021-8502(83)90064-2)
- Tritscher, T., Beeston, M., Zerrath, A.F., Elzey, S., Krinke, T.J., Filimundi, E., Bischof, O.F. (2013). NanoScan SMPS – A Novel, Portable Nanoparticle Sizing and Counting Instrument. *Journal of Physics: Conference Series*, 429(1), 012061.
- Tsai, C.-J., Huang, C.-Y., Chen, S.-C., Ho, C.-E., Huang, C.-H., Chen, C.-W., Chang, C.-P., Tsai, S.-J., Ellenbecker, M.J. (2011). Exposure assessment of nano-sized and respirable particles at different workplaces. [journal article]. *J Nanopart Res*, 13(9), 4161-4172. doi: 10.1007/s11051-011-0361-8
- Tsai, S.-J., Ada, E., Isaacs, J.A., Ellenbecker, M.J. (2008). Airborne nanoparticle exposures associated with the manual handling of nanoalumina and nanosilver in fume hoods. [journal article]. *J Nanopart Res*, 11(1), 147-161. doi: 10.1007/s11051-008-9459-z
- TSI. (2007). Hand-held Condensation Particle Counter Model 3007, from http://www.tsi.com/uploadedFiles/Product_Information/Literature/Spec_Sheet_s/3007_1930032.pdf
- TSI. (2012a). Nano water-based condensation particle counter (N-WCPC) Model 3788, from http://www.tsi.com/uploadedFiles/Site_Root/Products/Literature/Spec_Sheet_s/3788_A4_5001341_web.pdf
- TSI. (2012b). NanoScan SMPS Nanoparticle Sizer Model 3910. P/N 5001412 Rev B (A4). USA: TSI Incorporated.
- TSI. (2013a). DUSTTRAK™ DRX AEROSOL MONITOR MODEL 8533/8534/8533EP, from http://www.tsi.com/uploadedFiles/Site_Root/Products/Literature/Manuals/8533-8534-DustTrak_DRX-6001898-web.pdf
- TSI. (2013b). Nanometer Aerosol Sampler Model 3089, from http://www.tsi.com/uploadedFiles/Site_Root/Products/Literature/Spec_Sheet_s/3089.pdf
- TSI. (2015). Choosing the right CPC for your application. APPLICATION NOTE CPC-002 (US). *APPLICATION NOTE CPC-002 (US)*, from http://www.tsi.com/uploadedFiles/Site_Root/Products/Literature/Application_Notes/CPC-002-appnote.pdf
- Tsuda, H., Xu, J., Sakai, Y., Futakuchi, M., Fukamachi, K. (2009). Toxicology of engineered nanomaterials - a review of carcinogenic potential. [Research Support, Non-U S Gov't Review]. *Asian Pac J Cancer Prev*, 10(6), 975-980.
- van Broekhuizen, P. (2012). *Nano Matters: Building Blocks for a Precautionary Approach*. PhD thesis. Available at: www.ivam.uva.nl/?nanomatters.
- van Broekhuizen, P., Broekhuizen, F., Cornelissen, R., Reijnders, L. (2011). Use of nanomaterials in the European construction industry and some occupational health aspects thereof. [journal article]. *J Nanopart Res*, 13(2), 447-462. doi: 10.1007/s11051-010-0195-9
- van Broekhuizen, P., Broekhuizen, F., Cornelissen, R., Reijnders, L. (2012a). Workplace exposure to nanoparticles and the application of provisional nanoreference values in times of uncertain risks. [journal article]. *J Nanopart Res*, 14(4), 1-25. doi: 10.1007/s11051-012-0770-3

- van Broekhuizen, P., van Veelen, W.I.M., Streekstra, W.-H., Schulte, P., Reijnders, L. (2012b). Exposure Limits for Nanoparticles: Report of an International Workshop on Nano Reference Values. *Annals of Occupational Hygiene*, 56(5), 515-524.
- Van Duuren-Stuurman, B., Vink, S.R., Verbist, K.J., Heussen, H.G., Brouwer, D.H., Kroese, D.E., Van Niftrik, M.F., Tielemans, E., Fransman, W. (2012a). Stoffenmanager Nano version 1.0: a web-based tool for risk prioritization of airborne manufactured nano objects. [Research Support, Non-U S Gov't]. *Ann Occup Hyg*, 56(5), 525-541.
- Van Duuren-Stuurman, B., Vink, S.R., Verbist, K.J.M., Heussen, H.G.A., Brouwer, D.H., Kroese, D.E.D., Van Niftrik, M.F.J., Tielemans, E., Fransman, W. (2012b). Stoffenmanager Nano Version 1.0: A Web-Based Tool for Risk Prioritization of Airborne Manufactured Nano Objects. *Annals of Occupational Hygiene*, 56(5), 525-541.
- Vaquero, C., Gelarza, N., Ipiña, J.L.L.d., Gutierrez-Cañas, C., Múgica, I., Aragón, G., Jaen, M., Pina, R., Larraza, I., Esteban-Cubillo, A., Thompson, D., Pui, D.Y.H. (2015). Occupational exposure to nano-TiO₂ in the life cycle steps of new depollutant mortars used in construction. *Journal of Physics: Conference Series*, 617(1), 012006.
- Viana, M., Diez, S., Reche, C. (2011). Indoor and outdoor sources and infiltration processes of PM₁ and black carbon in an urban environment. *Atmospheric Environment*, 45(35), 6359-6367. doi: <http://dx.doi.org/10.1016/j.atmosenv.2011.08.044>
- Viana, M., Rivas, I., Querol, X., Alastuey, A., Sunyer, J., Álvarez-Pedrerol, M., Bouso, L., Sioutas, C. (2014). Indoor/outdoor relationships and mass closure of quasi-ultrafine, accumulation and coarse particles in Barcelona schools. *Atmos. Chem. Phys.*, 14(9), 4459-4472. doi: 10.5194/acp-14-4459-2014
- Vodička, P., Schwarz, J., Ždímal, V. (2013). Analysis of one year's OC/EC data at a Prague suburban site with 2-h time resolution. *Atmospheric Environment*, 77, 865-872. doi: <http://dx.doi.org/10.1016/j.atmosenv.2013.06.013>
- Voliotis, A., Bezantakos, S., Giamarelou, M., Valenti, M., Kumar, P., Biskos, G. (2014). Nanoparticle emissions from traditional pottery manufacturing. [Research Support, Non-U S Gov't]. *Environ Sci Process Impacts*, 16(6), 1489-1494.
- Wagstrom, K.M., Pandis, S.N. (2011). Contribution of long range transport to local fine particulate matter concerns. *Atmospheric Environment*, 45(16), 2730-2735. doi: <http://dx.doi.org/10.1016/j.atmosenv.2011.02.040>
- Wake, D., Mark, D., Northage, C. (2002). Ultrafine Aerosols in the Workplace. *Annals of Occupational Hygiene*, 46(suppl 1), 235-238.
- Wang, S.C., Flagan, R.C. (1989). Scanning electrical mobility spectrometer. *Journal of Aerosol Science*, 20(8), 1485-1488. doi: [http://dx.doi.org/10.1016/0021-8502\(89\)90868-9](http://dx.doi.org/10.1016/0021-8502(89)90868-9)
- Wang, S.C., Flagan, R.C. (1990). Scanning Electrical Mobility Spectrometer. *Aerosol Science and Technology*, 13(2), 230-240. doi: 10.1080/02786829008959441
- Wang, X., Chancellor, G., Evenstad, J., Farnsworth, J.E., Hase, A., Olson, G.M., Sreenath, A., Agarwal, J.K. (2009). A Novel Optical Instrument for Estimating Size Segregated Aerosol Mass Concentration in Real Time. *Aerosol Science and Technology*, 43(9), 939-950. doi: 10.1080/02786820903045141
- Warneck, P. (1988). *Chemistry of the Natural Atmosphere*: Academic Press.
- Watson, J.G., Chow, J.C., Sodeman, D.A., Lowenthal, D.H., Chang, M.C.O., Park, K., Wang, X. (2011). Comparison of four scanning mobility particle sizers at the Fresno Supersite. *Particuology*, 9(3), 204-209. doi: <http://dx.doi.org/10.1016/j.partic.2011.03.002>
- Wehner, B., Birmili, W., Gnauk, T., Wiedensohler, A. (2002). Particle number size distributions in a street canyon and their transformation into the urban-air background: measurements and a simple model study. *Atmospheric*

- Environment*, 36(13), 2215-2223. doi: [http://dx.doi.org/10.1016/S1352-2310\(02\)00174-7](http://dx.doi.org/10.1016/S1352-2310(02)00174-7)
- Weichenthal, S. (2012). Selected physiological effects of ultrafine particles in acute cardiovascular morbidity. [Review]. *Environ Res*, 115, 26-36.
- Weschler, C.J. (2011). Chemistry in indoor environments: 20 years of research. [Review]. *Indoor Air*, 21(3), 205-218.
- WHO. (2013). Nanotechnology and human health: Scientific evidence and risk governance. Report of the WHO expert meeting 10–11 December 2012, Bonn, Germany: Copenhagen, World Health Organization Regional Office for Europe.
- WHO. (2015). *List of classifications, Volumes 1-114*. Retrieved from <http://monographs.iarc.fr/ENG/Classification/index.php>.
- Wiedensohler, A., Birmili, W., Nowak, A., Sonntag, A., Weinhold, K., Merkel, M., Wehner, B., Tuch, T., Pfeifer, S., Fiebig, M., Fjåraa, A.M., Asmi, E., Sellegri, K., Depuy, R., Venzac, H., Villani, P., Laj, P., Aalto, P., Ogren, J.A., Swietlicki, E., Williams, P., Roldin, P., Quincey, P., Hüglin, C., Fierz-Schmidhauser, R., Gysel, M., Weingartner, E., Riccobono, F., Santos, S., Gruning, C., Faloon, K., Beddows, D., Harrison, R., Monahan, C., Jennings, S.G., O'Dowd, C.D., Marinoni, A., Horn, H.G., Keck, L., Jiang, J., Scheckman, J., McMurry, P.H., Deng, Z., Zhao, C.S., Moerman, M., Henzing, B., de Leeuw, G., Löschau, G., Bastian, S. (2012). Mobility particle size spectrometers: harmonization of technical standards and data structure to facilitate high quality long-term observations of atmospheric particle number size distributions. *Atmos. Meas. Tech.*, 5(3), 657-685. doi: 10.5194/amt-5-657-2012
- Wiedensohler, A., Orsini, D., Covert, D.S., Coffmann, D., Cantrell, W., Havlicek, M., Brechtel, F.J., Russell, L.M., Weber, R.J., Gras, J., Hudson, J.G., Litchy, M. (1997). Intercomparison Study of the Size-Dependent Counting Efficiency of 26 Condensation Particle Counters. *Aerosol Science and Technology*, 27(2), 224-242. doi: 10.1080/02786829708965469
- Wijnhoven, S., Dekkers, S., Kooi, M., Jongeneel, R., de Jong, W. (2011). Nanomaterials in consumer products : Update of products on the European market in 2010: Rijksinstituut voor Volksgezondheid en Milieu RIVM.
- Winklmayr, W., Reischl, G.P., Lindner, A.O., Berner, A. (1991). A new electromobility spectrometer for the measurement of aerosol size distributions in the size range from 1 to 1000 nm. *Journal of Aerosol Science*, 22(3), 289-296. doi: [http://dx.doi.org/10.1016/S0021-8502\(05\)80007-2](http://dx.doi.org/10.1016/S0021-8502(05)80007-2)
- Witschger, O., Bihan, O., Reynier, M., Durand, C., Marchetto, A., Zimmermann, E., Charpentier, D. (2012). Préconisation en matière de caractérisation et d'exposition des potentiels d'émission et d'exposition professionnelle aux aérosols lors d'opérations nanomatériaux
- Wohlleben, W., Brill, S., Meier, M.W., Mertler, M., Cox, G., Hirth, S., von Vacano, B., Strauss, V., Treumann, S., Wiench, K., Ma-Hock, L., Landsiedel, R. (2011). On the lifecycle of nanocomposites: comparing released fragments and their in-vivo hazards from three release mechanisms and four nanocomposites. [Comparative Study]. *Small*, 7(16), 2384-2395.
- Yamada, M., Takaya, M., Ogura, I. (2015). Performance evaluation of newly developed portable aerosol sizers used for nanomaterial aerosol measurements. *Ind Health*, 53(6), 511-516.
- Yeganeh, B., Kull, C.M., Hull, M.S., Marr, L.C. (2008). Characterization of Airborne Particles During Production of Carbonaceous Nanomaterials. *Environmental Science & Technology*, 42(12), 4600-4606. doi: 10.1021/es703043c
- Yokel, R.A., MacPhail, R.C. (2011). Engineered nanomaterials: exposures, hazards, and risk prevention. *Journal of Occupational Medicine and Toxicology (London, England)*, 6, 7-7. doi: 10.1186/1745-6673-6-7
- Zalk, D.M., Paik, S.Y., Swuste, P. (2009). Evaluating the Control Banding Nanotool: a qualitative risk assessment method for controlling nanoparticle exposures.

- [journal article]. *J Nanopart Res*, 11(7), 1685-1704. doi: 10.1007/s11051-009-9678-y
- Zhang, Q., Gangupomu, R.H., Ramirez, D., Zhu, Y. (2010). Measurement of ultrafine particles and other air pollutants emitted by cooking activities. [Research Support, U S Gov't, Non-P H S]. *Int J Environ Res Public Health*, 7(4), 1744-1759.
- Zhang, S.-H., Akutsu, Y., Russell, L.M., Flagan, R.C., Seinfeld, J.H. (1995). Radial Differential Mobility Analyzer. *Aerosol Science and Technology*, 23(3), 357-372. doi: 10.1080/02786829508965320
- Zhang, Y., Leu, Y.-R., Aitken, R.J., Riediker, M. (2015). Inventory of Engineered Nanoparticle-Containing Consumer Products Available in the Singapore Retail Market and Likelihood of Release into the Aquatic Environment. *International Journal of Environmental Research and Public Health*, 12(8), 8717-8743. doi: 10.3390/ijerph120808717
- Zhu, Y., Hinds, W.C., Kim, S., Shen, S., Sioutas, C. (2002). Study of ultrafine particles near a major highway with heavy-duty diesel traffic. *Atmospheric Environment*, 36(27), 4323-4335. doi: [http://dx.doi.org/10.1016/S1352-2310\(02\)00354-0](http://dx.doi.org/10.1016/S1352-2310(02)00354-0)
- Zimmer, A.T., Maynard, A.D. (2002). Investigation of the aerosols produced by a high-speed, hand-held grinder using various substrates. *Ann Occup Hyg*, 46(8), 663-672.
- Zimmerman, N., Godri Pollitt, K.J., Jeong, C.-H., Wang, J.M., Jung, T., Cooper, J.M., Wallace, J.S., Evans, G.J. (2014). Comparison of three nanoparticle sizing instruments: The influence of particle morphology. *Atmospheric Environment*, 86, 140-147. doi: <http://dx.doi.org/10.1016/j.atmosenv.2013.12.023>
- Zimmerman, N., Jeong, C.-H., Wang, J.M., Ramos, M., Wallace, J.S., Evans, G.J. (2015). A source-independent empirical correction procedure for the fast mobility and engine exhaust particle sizers. *Atmospheric Environment*, 100, 178-184. doi: <http://dx.doi.org/10.1016/j.atmosenv.2014.10.054>

ANNEX A: LIST OF ABBREVIATIONS, ACRONYMS AND SYMBOLS

The following tables describe the significance of various abbreviations, acronyms and symbols used throughout the Thesis.

Abbreviation/Acronym	Description
ACGIH	American Conference of Governmental Industrial Hygienists
BLPI	Berner low-pressure impactor
CNF	Carbon nanofibers
CNT	Carbon nanotubes
CPC	Condensation particle counters
DC	Diffusion chargers
DiSCmini	Diffusion Size Classifier Miniature
DMA	Differential mobility analyser
DNEL	Derived no-effect level
EC	European Commission
EDX	Energy dispersive X-ray
EEA	European Environment Agency
ELPI	Electrical low pressure impactors
ENP	Engineered nanoparticles
EU	European Union
HEPA	High efficiency particulate air filter
IARC	International Agency for Research on Cancer
IC	Ion chromatography
ICP-AES	Inductively coupled plasma by atomic emission spectrometry
ICP-MS	Inductively coupled plasma by mass spectrometry
ICRP	International Commission on Radiological Protection
IFA	German Institute for Occupational Safety and Health of the German Social Accident Insurance
ITC	Institute for Ceramic Technology
KET	Key enabling technologies
LEV	Local exhaust ventilation
LOAEL	Lowest observed adverse effect level
Moudi	Micro-orifice uniform deposit impactor
MWCNT	Multi-walled carbon nanotubes
N/A	Not applicable
nano-BLPI	Nano-Berner low-pressure impactor
Nano-Moudi	Nano-Micro-orifice uniform deposit impactor

NAS	Nanometer aerosol sampler
N-ENP	Non-engineered nanoparticles
NIOSH	National Institute for Occupational Safety and Health
NRV	Nano reference values
N-WCPC	Nano-Water-based condensation particle counters
OEL	Occupational exposure limits
OPC	Optical particle counter
OPS	Optical particle sizer
OSHA	Occupational Safety and Health Administration
PCIS	Personal cascade impactor sampler
PEL	Permissible exposure
PGNP	Process-generated nanoparticles
PM	Particulate matter
PM₁₀	Respirable particles
PPE	Personal protective equipment
PTFE	Polytetrafluoroethylene filters
rDMA	Radial differential mobility analyser
REL	Recommended exposure limit
SEM	Scanning electron microscopy
SER	Social and Economic Council of the Netherlands
SI	International System of Units
SMPS	Scanning mobility particle sizers
SMPS-L	Scanning mobility particle sizer with a long DMA
SMPS-N	Scanning mobility particle sizer with a nano DMA
SWCNT	Single-walled carbon nanotubes
TEM	Transmission electron microscopy
TLV	Threshold limit value
TWA	Time weighted average
UCPC	Ultrafine butanol condensation particle counter
ULPA	Ultra-low penetration air filters
WCPC	Water-based condensation particle counters

Symbol	Description	Unit
---------------	--------------------	-------------

<i>t</i>	Time duration of the activity	min
<i>WA</i>	Measured particle concentrations at the breathing zone or emission source during the work activity	$\mu\text{g m}^{-3}$, cm^{-3} or $\mu\text{m}^2 \text{cm}^{-3}$
<i>BG</i>	Average background registered concentrations	$\mu\text{g m}^{-3}$, cm^{-3} or $\mu\text{m}^2 \text{cm}^{-3}$
<i>BZ</i>	Measured background corrected particle concentration in the breathing zone	$\mu\text{g m}^{-3}$, cm^{-3} or $\mu\text{m}^2 \text{cm}^{-3}$
σ	Standard deviation	nm, $\mu\text{g m}^{-3}$, cm^{-3} , $\mu\text{m}^2 \text{cm}^{-3}$
D_p	Particle diameter	μm or nm
<i>N</i>	Total particle number concentration	cm^{-3}
<i>M</i>	Total particle mass concentration	$\mu\text{g m}^{-3}$
<i>PSD</i>	Particle size distribution	$\mu\text{g m}^{-3}$, cm^{-3} or $\mu\text{m}^2 \text{cm}^{-3}$
<i>LDSA</i>	Lung deposited surface area concentration	$\mu\text{m}^2 \text{cm}^{-3}$
<i>SA</i>	Surface area concentration	$\mu\text{m}^2 \text{cm}^{-3}$
$PM_1, PM_{2.5}, PM_4, PM_{10}$	Particle mass concentration for particles < 1, 2.5, 4 and 10 μm , respectively	$\mu\text{g m}^{-3}$
<i>n</i>	Total number of measurements	-

Chemical abbreviation	Description	Chemical abbreviation	Description
Ag	Silver	Nd	Neodymium
Al	Aluminium	NH ₃	Ammonia
Al ₂ O ₃	Aluminium oxide	NH ₄ ⁺	Ammonium
As	Arsenic	NH ₄ Cl	Ammonium chloride
Au	Gold	NH ₄ NO ₃	Ammonium nitrate
Na	Sodium	Ni	Nickel
Ba	Barium	NO ₃ ⁻	Nitrate
Bi	Bismuth	NO _x	Nitrogen oxides
Ca	Calcium	P	Phosphorus
CaSO ₄	Anhydrite	Pb	Lead
Cd	Cadmium	Pr	Praseodymium
Ce	Cerium	Rb	Rubidium
CO	Carbon monoxide	S	Sulfur
Co	Cobalt	Sb	Antimony
Cr	Chromium	Sc	Scandium
Cs	Cesium	Se	Selenium
Cu	Copper	SiO ₂	Silicon dioxide
DEHS	Di-ethyl-hexyl-sebacate	Sn	Tin
Fe	Iron	SO ₂	Sulfur dioxide
Fe ₂ O ₃	Hematite	SO ₄ ²⁻	Sulphate
Ga	Gallium	Sr	Strontium
Gd	Gadolinium	Ta	Tantalum
Ge	Germanium	Th	Thorium
H ₂ SO ₄	Sulfuric acid	Ti	Titanium
HClO ₄	Perchloric acid	TiO ₂	Titanium dioxide
HF	Hydrofluoric acid	Tl	Thallium
Hf	Hafnium	U	Uranium
HNO ₃	Nitric acid	V	Vanadium
K	Potassium	VOCs	Volatile organic compounds
La	Lanthanum	W	Tungsten
Li	Lithium	Y	Yttrium
Mg	Magnesium	Zn	Zinc
Mn	Manganese	ZnO	Zinc oxide
Mo	Molybdenum	Zr	Zirconium
NaCl	Sodium chloride		
Nb	Niobium		

